CRANFIELD UNIVERSITY

Kevin Mullaney

The fabrication of micro-tapered optical fibres for sensing applications

Centre for Engineering Photonics,
School of Aerospace, Transport and Manufacturing.

PhD Thesis

Supervisors: Professor Ralph Tatam and Professor Stephen James
November 2016

CRANFIELD UNIVERSITY

Centre for Engineering Photonics,
School of Aerospace, Transport and Manufacturing
PhD Thesis
2016

Kevin Mullaney

The fabrication of micro-tapered optical fibres for sensing applications.

Supervisors: Professor Ralph Tatam and Professor Stephen James

November 2016

This thesis is submitted in partial fulfilment of the requirements for the degree of Doctor of Philosophy

ABSTRACT

This thesis describes the processes used to manufacture optical fibre tapers and tapered long period gratings (TLPGs) using a CO_2 laser. A semi-automated system for fabricating adiabatic and non-adiabatic tapers with repeatable physical dimensions has been developed. The tapers had waist diameters which were reproducible to within ± 0.5 μm. This system has also been used to fabricate TLPGs with periods ranging from 378 μm to 650 μm.

Novel techniques to monitor the process of fabricating tapers were also explored. These techniques included; monitoring the transmission of the fibre using a spectrophotometer, using an in-line fibre Bragg grating (FBG) to measure the strain experienced by the optical fibre and the use of a near infra-red (NIR) camera to aid fibre alignment and laser power optimisation. The spectrophotometer allowed the optical properties of the tapers to be tailored for specific applications and the FBG provided strain data for process optimisation. The use of a NIR camera and an FBG as an in-line strain sensor are a novel use of these devices in a fibre tapering process.

Tapers were also thin-film coated using sputtering techniques to form surface plasmon resonance sensors and their refractive index sensitivity was measured. A novel protein sensor based on gold nanoparticles deposited on a fibre taper is also reported, together with a lossy mode resonance taper sensor.

The TLPGs which were fabricated, comprised of between 6 to 18 periods. The refractive index sensitivity of a 6 period TPLG was measured and was 372 nm/ RI. Their resonance bands had twice the bandwidth and exhibited a higher extinction, compared to UV-written long period gratings of a similar number of periods.

ACKNOWLEDGEMENTS

I would like to thank my supervisors, Professor Stephen James and Professor Ralph Tatam for their help, guidance and support for the duration of the PhD. They always gave professional guidance and provided constructive recommendations which helped me in the course of my work.

I would like to express my appreciation to all the people in the department who have helped me in the course of my studies. I would like to express my appreciation to Dr. Ricardo Correia and Dr. Edmond Chehura who always offered freely their expertise with various experiments and FBG technology. I would also like to express my appreciation to both Dr. Divya Tiwari and Dr. Sergiy Korposh (University of Nottingham) for allowing me to include some of their experimental work, using tapers I fabricated within this thesis. I am also grateful to the professional support from Steve Staines in fabricating many of the mechanical and electronic components used in my experiments. Invariably, he always gave me back more than I originally requested.

Finally, I would like to thank my family and friends for their unwavering support.

TABLE OF CONTENTS

LIST OF FIGURES

LIST OF TABLES

1 Introduction

1.1 Background

Optical fibres are widely used for telecommunications and optical sensing applications. In the telecommunication arena, light signals can be transmitted with low loss along optical fibres for many kilometres by utilizing the refractive index differential of the layers within the fibre to confine the light in the fibre core. In certain optical sensing applications, the physical dimensions of the fibre are locally perturbed so allowing the transmitted light to interact with the surrounding environment and hence be modified by its optical properties. The modified transmitted light can then be analysed to provide information on changes in the surrounding environment. A typical example might be the measurement of the refractive index of the surrounding medium, however they have also been used for biosensing [1, 2] and chemical sensing [3]. Other applications have included; medical diagnostics [4], environmental monitoring [5] and monitoring magnetic fields [6].

The light propagating through the core of an optical fibre can be forced to interact with the surrounding medium by removing the cladding, by either etching or tapering the fibre. Chandani *et al.* in 2007 [7] describes a sensor where the fibre cross-section has been etched to a D-shaped profile and Kieu *et al.* in 2006 [8] describes a bi-conical fibre taper sensor. In a bi-conical fibre taper, the single mode fibre (SMF) diameter reduces over a short distance to form a taper waist. The fibre diameter then increases back to its original diameter after the waist, as shown in figures 1 and 2 (a, b).

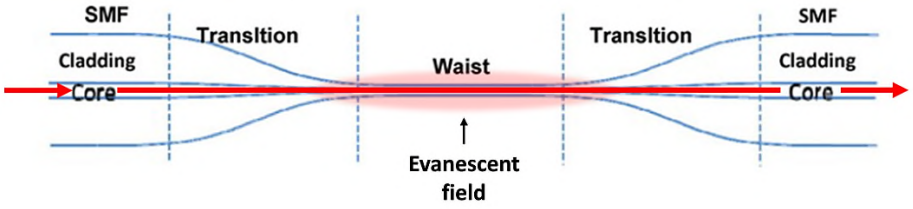

Figure 1: Schematic of a tapered optical fibre.

The taper is formed by locally heating a short section of fibre to its melting point while stretching it. Tapering the fibre is more advantageous over etching as the interaction of the transmitted light with the surrounding medium is more controllable.

As the light propagates along the fibre in the non-tapered region, its energy is confined within the fibre core. However, when the light travels along the smaller diameter taper waist, the evanescent field of the propagating mode is no longer confined and extends into the surrounding environment for a distance [9] of typically ~ 0.5 μm, figure 1. The properties of the light propagating in the tapered section of the optical fibre are then sensitive to the local optical properties outside the fibre. This feature forms the basis for the use of a fibre taper as an optical sensor.

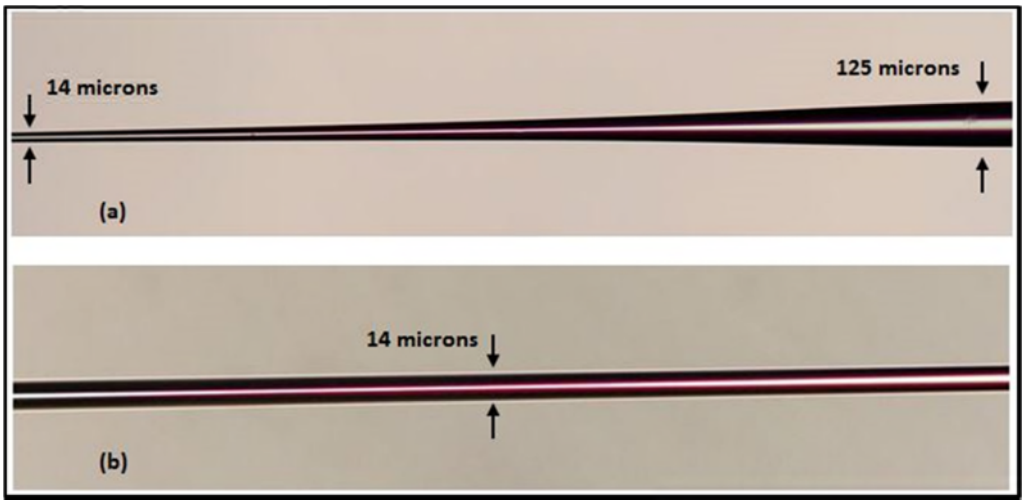

Figure 2: (a) A micrograph of a typical tapered fibre. The un-tapered fibre is 125 μm in diameter and (b) the taper waist is 14 μm in diameter .

Another type of sensor which is sensitive to the medium surrounding a fibre, is a long period grating (LPG). These devices [11] consist of a periodic modulation of the core refractive index, which results in discrete wavelength bands being coupled into the fibre cladding, producing resonance bands in the transmission spectrum. The spectral features of these bands are sensitive to the optical properties of the medium in the immediate vicinity of the grating. The lengths of these devices are typically 20-30 mm, the longer devices typically exhibit increased refractive index sensitivity over shorter devices [12].

The heat source employed during taper fabrication is usually either a flame [13] or a carbon dioxide (CO_2) laser [14, 15, 16] which produces radiation at 10.6 μm. The use of a CO_2 laser has a number of advantages over a flame. The heated-zone properties can be controlled in a repeatable fashion and the use of a laser avoids the production of air turbulence, present when using a flame, which can influence the shape and uniformity of the diameter of the tapered region [16].

This thesis is focussed primarily on the development of an optical system and associated processes for the fabrication of optical fibre tapers using a CO_2 laser. The system has also been used to fabricate long period gratings in optical fibres by using CO_2 laser radiation to create periodic micro-tapers along the fibre.

Tapers produced from this work have been used as novel protein sensors by the University of Nottingham and as an ammonia sensor within Cranfield University.

For the University of Nottingham, 90 tapers with an optimised geometry were supplied to Dr Korposh and his team, who then undertook the subsequent coating deposition and the subsequent analysis. The outcome was the development of a novel protein sensor which could detect levels of streptavidin (SV) below 2.5 nM.

Within Cranfield University, adiabatic tapers with an optimised geometry were supplied to Dr Tiwari, who then undertook the deposition of a specialised functional coating and the subsequent analysis. The outcome of this work was the development of an ammonia sensor, which was effective at sensing ammonia within the range; 0.6 -10 ppm.

1.2 Aims and objectives

The aims of this thesis are to develop the capability to fabricate optical tapers as a repeatable process and to develop the techniques for making tapered long period gratings for use as optical sensors. The tapered fibres and gratings are to be made using a CO_2 laser-based system. The objectives required to achieve the above aims are:

i. The development of a CO_2 fibre tapering system with a level of automation such that single tapers with waists of ≥ 5 μm and lengths of > 10 mm can be made with reproducible optical properties and geometry.
ii. To explore the use of monitoring techniques to develop processes which are optimized for their application. The techniques which are investigated, are: thermal imaging of the heated fibre using a near infrared (NIR) camera, monitoring the visible and NIR spectrum of the light transmitted though the taper using a spectrophotometer and the use of an in-line fibre Bragg grating (FBG) as a strain sensor during the tapering process.
iii. Adapting the system for tapering fibres such that periodic micro-tapers can be produced, so forming a tapered long period grating (TLPG).
iv. Develop and optimize the process for making TLPGs to enhance their capability as a compact optical sensor.

The aspects of this thesis which are novel are:

i. The use of an NIR camera for both fibre and system alignment and as a tool to determine the optimal laser power during the tapering process.
ii. The use of an FBG as an in-line fibre strain sensor during the tapering process. This allows the onset of fibre breakage to be identified when fabricating small diameter tapers (< 8μm) and confirms the fibre is at the melting temperature prior to stretching the fibre.
iii. The optimization of micro-taper geometry such that compact tapered long period gratings can be fabricated.

1.3 Thesis organisation

This thesis comprises of eight chapters. Chapter one introduces the concept of tapers and long period gratings in optical fibres and describes the objectives of this thesis and the areas of novelty. Chapter two reviews the different techniques for fabricating tapers using a CO_2 laser. It also reviews the various fabrication techniques for making TLPGs.

Chapter three summarises the theory of optical tapers and long period fibre gratings. Chapter four describes the experimental arrangement that has been developed to fabricate optical fibre tapers and chapter five provides detailed process descriptions for making tapers and TLPGs. Chapter six provides a summary of the experimental work that was undertaken on tapers and the results achieved of using these devices as protein and ammonia sensors. Chapter seven provides a summary of the experimental work that was undertaken on TLPGs and the results achieved. Finally, chapter eight discusses the results and makes recommendations for future work on these topics.

1.4 References

[1] M. I. Zibaii, A. Kazemi, H. Latifi, M. K. Azar, S. M. Hosseini and M. H. Ghezelaiagh, "Measuring bacterial growth by refractive index tapered fiber optic biosensor," *J. Photochem. and Photobiol. B: Biol.*, Vol. 101, No. 3, pp. 313–320, 2010.

[2] M. I. Zibaii, H. Latifi, E. Ghanati, M. Gholami and S. M. Hosseini, "Label free detection of DNA hybridization by refractive index tapered fiber biosensor", Biophotonics: Photonic Solutions for better Health Care 11, *Proc. SPIE*, Vol. 7715, 1–9, 2010.

[3] R. Jarzebinska, C. S. Cheung, S. W. James and R. P. Tatam, "Response of the transmission spectrum of tapered optical fibres to the deposition of a nanostructured coating," *Meas. Sci. Technol.*, Vol. 20, No. 3, pp. 1–6, 2009.

[4] D. J. Oh, J. H. Jung, J. Y. Kang and S. H. Lee, "A disposable polymer waveguide lab-on-a-chip for real-time detection of protein C using evanescent wave," *2010 IEEE Sensors Conf.*, pp. 1605–1608, 2010.

[5] R. Jarzebinska, S. Korposh, S. James, W. Batty, R. Tatam and S.W. Lee, "Optical gas sensor fabrication based on porphyrin-anchored electrostatic self-assembly onto tapered optical fibers," *Anal. Lett.*, Vol. 45, No. 10, pp. 1297–1309, 2012.

[6] A. Layeghi, H. Latifi and O. Frazão, "Magnetic field sensor based on non-adiabatic tapered optical fiber with magnetic fluid," *IEEE Photonics Technol. Lett.*, Vol. 26, No. 19, pp. 1904–1907, 2014.

[7] S. M. Chandani and N. A. F. Jaeger, "Optical fiber-based liquid level sensor," *Opt. Eng.*, Vol. 46, No. 11, pp. 114401–07, 2007.

[8] K. Q. Kieu and M. Mansuripur, "Bi-conical fiber taper sensors," *IEEE Photonics Technol. Lett.*, Vol. 18, No. 21, pp. 2239–2241, 2006.

[9] G. Brambilla, F. Xu, P. Horak, Y. Jung, F. Koizumi, N. P. Sessions, E. Koukharenko, X. Feng, G. S. Murugan, J. S. Wilkinson and D. J. Richardson, "Optical

fiber nanowires and microwires: fabrication and applications," *Adv. Opt. Photonics*, Vol. 1, No. 1, p. 107, 2009.

[10] Y. Tian, W. Wang, N. Wu, X. Zou, and X. Wang, "Tapered optical fiber sensor for label-free detection of biomolecules," *Sensors*, Vol. 11, No. 4, pp. 3780–3790, 2011.

[11] A. M. Vengsarkar, P. J. Lemaire, J. B. Judkins, V. Bhatia, T. Erdogan and J. E. Sipe, "Long period fiber gratings as band-rejection filters," Light. Technology, Vol. 14, No. 1, pp. 58–65, 1996.

[12] H. Tsuda and K. Urabe, "Characterization of long-period grating refractive index sensors and their applications," *Sensors (Switzerland)*, Vol. 9, No. 6, pp. 4559–4571, 2009.

[13] J. Villatoro, D. Monzón-Hernández, E. Mejía and D. Monzo, "Fabrication and modelling of uniform-waist single-mode tapered optical fiber sensors.," *Appl. Opt.*, Vol. 42, No. 13, pp. 2278 –2283, 2003.

[14] F. Bayle and J. P. Meunier, "Efficient fabrication of fused-fiber bi-conical taper structures by a scanned CO_2 laser beam technique," *Appl. Opt.*, Vol. 44, No. 30, pp. 6402–11, 2005.

[15] J. M. Ward, D. G. O'Shea, B. J. Shortt, M. J. Morrissey, K. Deasy and S. G. Nic Chormaic, "Heat-and-pull rig for fiber taper fabrication," *Rev. Sci. Instrum.*, Vol. 77, No. 8, p. 083105, 2006.

[16] T. E. Dimmick, G. Kakarantzas, T. A. Birks and P. St. J. Russell, "Carbon dioxide laser fabrication of fused-fiber couplers and tapers," *Appl. Opt.*, Vol. 38, No. 33, p. 6845, 1999.

2 Tapered optical fibres

2.1 Introduction

Tapered optical fibres have applications in telecommunications as directional couplers [1] and can also be used as sensing devices in a wide range of bio-medical and chemical applications [2, 3, 4]. A tapered fibre is fabricated by heating locally a short section of optical fibre while stretching it. This results in a length of fibre that has a narrow waist. In the region of the taper waist, the evanescent field of the propagating mode extends into the medium around the fibre, so allowing the interaction of light with the surrounding medium. The light transmitted by a tapered optical fibre is sensitive to changes in the refractive index of the medium within the vicinity of the taper waist and this feature forms the basis for the use of tapers in evanescent wave spectroscopy [5, 6].

Tapered optical fibres have been used for a number of different sensing applications. For example; they have been used to monitor in real-time the growth of *Escherichia coli* in an aqueous medium [2], for the detection of label free single stranded DNA in real time [7], for Raman spectroscopic sensing [8], as gas sensors [4] and as a magnetic field sensor [9]. Tapers have also been used to couple light to a microsphere so allowing wavelength selective fibre lasers [10] to be made for environmental sensing applications. The optical tapers used in these systems typically have waist diameters of < 25 μm and had overall lengths of between 2 and 25 mm [11, 12, 13, 14].

For biological and chemical sensing applications, taper waist diameters of 5-20 μm tend to be used [3, 4, 7]. The minimum waist diameter is usually ~ 5 μm, as tapers below this waist diameter are fragile to handle during experimental trials and are easily broken.

Another type of optical fibre device which has developed significant interest is the long period grating [15]. A long period grating (LPG) consists of a periodic perturbation of the properties of a fibre. These properties are usually the refractive index of the core (figure 3) but in certain instances [17] the fibre diameter is also modulated (see figure 4). They can have periods (Λ) ranging typically between 100 μm and 700 μm and lengths from 2 to 30 mm. The periodic perturbation interacts with the core mode,

allowing the coupling of power to the cladding modes at specific wavelengths where the phase matching condition is satisfied. This modal coupling creates a series of attenuation bands in the transmission spectrum of the optical fibre [15].

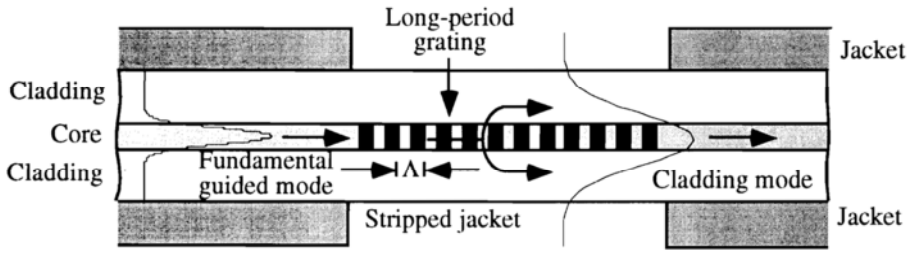

Figure 3: Coupling of the guided mode to the cladding modes in a long period grating. The symbol Λ, represents the periodicity of the refractive index modulation of the core [17].

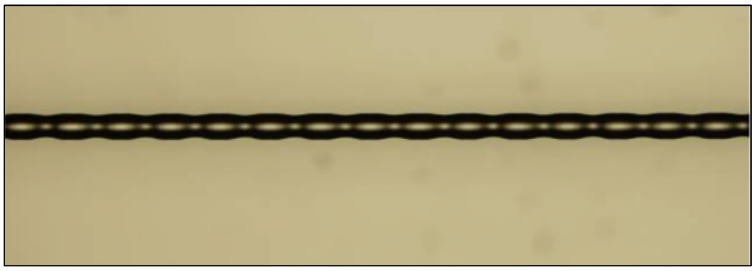

Figure 4: A periodic structure fabricated in fibre using a CO_2 laser. This structure contains 20 tapered sections spaced 200 μm apart [21].

While LPGs were developed primarily as devices for optical communications [15], where they have been used as band rejection filters, gain equalizers, fibre couplers and dispersion compensators [16], they also found applications in the field of optical sensing [17, 18]. LPGs can be fabricated by either ultra-violet (UV) irradiation or the periodic application of heat over a sub-millimetre length of the fibre. The heat source can be produced by either CO_2 laser radiation, arc discharge or resistive heating. The use of a CO_2 laser is attractive as this technique is more flexible, is repeatable and produces less contamination on the fibre surface than some of the other techniques.

In TLPGs, the fibre geometry is usually perturbed by periodically micro-tapering the fibre. This is usually achieved by locally heating and stretching the fibre. For this type of device [19, 20, 21, 22, 23] the micro-taper waist diameter is typically between 70 μm and 120 μm.

In general terms, UV written LPGs have only the core index modulated by the incident radiation whereas CO_2 written LPGs have both the core and cladding index modulated and in addition can also be modulated by physically tapering the fibre.

This chapter has two main themes; the first is the provision of a review of the various methods that have been reported for tapering optical fibres, concentrating on CO_2 laser based heating techniques with a view to identifying what has been done by other research groups so that an improved fabrication system can be developed. The second theme is to review the techniques for creating TLPGs, with the aim of assessing whether the CO_2 laser fabrication technique can be further improved and to propose a direction for future research activities in this area.

2.2 Tapered optical fibres

The two main heat sources employed to fabricate optical fibre tapers are gas flames [24, 25] and CO_2 lasers [11, 12, 13]. Other heat sources have also been used, though to a much lesser degree. Bobb *et al.* in 1990 [26] used a platinum furnace to make tapers and Musa *et al.* in 2011 [27] used the electric arc from a fusion splicer. However, both of these techniques are less flexible over the control over the length of the heating zone compared to CO_2 irradiation techniques or gas flames.

As discussed previously, the two main techniques for fabricating tapers employ either a gas flame or a CO_2 laser as the heat source. In the flame technique, the gas burner [28, 29, 30, 31] is either stationary or can move on an oscillating translation stage to give control over the length of the fibre heated zone. This allows tapers to be produced which are longer and thinner than if the flame is stationary and allows the shape of the taper transitions to be tailored to specific profiles. The latter is important as it critically determines the taper optical properties.

Using the travelling flame technique, Harun *et al.* in 2012 [32] fabricated taper waists with a diameter of 400 nm, using a flame width of 1 mm with automated motor control of the translation stages and a precision oxy-butane burner. The travelling flame technique also allows the possibility of producing asymmetric tapers in a controllable fashion. Baker *et al.* in 2010 [33] used this technique to produce asymmetric tapers and tapers of an arbitrary profile. Pricking *et al.* in 2010 [34] refined this technique further to produce taper waists with a sinusoidal diameter variation along the length of the waist.

The use of a CO_2 laser has a number of advantages over a flame. The heated zone properties can be controlled flexibly in a repeatable fashion down to a length of ~ 190 μm using a focussing lens [35]. This hot-zone length appears to be currently unattainable with the flame technique, where the shortest length reported is ~ 1 mm [32]. In addition, the use of a laser avoids the production of air turbulence and combustion contaminants, present when using a flame, that potentially can influence the shape, uniformity and cleanliness of the tapered region [13].

The various experimental approaches to tapering fibres using a CO_2 laser are reviewed in the following section.

2.2.1 CO_2 laser-fabricated tapered fibres

The first group who reported the tapering of optical fibres using a CO_2 laser was Yokota *et al.* in 1997 [36]. In their experimental arrangement, shown in figure 5 they used a CO_2 laser operating at 10.6 μm and a visible guide laser, operating at 633 nm. They used a laser power in the range 20-30 W, which was focussed using a circular ZnSe lens with a focal length of 50 mm. The laser beam was stationary and the spot size on the fibre was varied by defocussing the laser spot. The fibre was pulled in opposite directions by the use of two 10 g weights at either end of the fibre. This arrangement produced tapers with waist diameters of 38 μm and lengths of 4.1 mm. Subsequent researchers [12, 37, 38] refined the technique for making tapers by scanning the focussed spot along fibre and using translation stages to pull the fibre. This allowed

tapers to be fabricated with ~ 3.5 μm diameter waists and with low optical losses (0.1 - 0.3 dB).

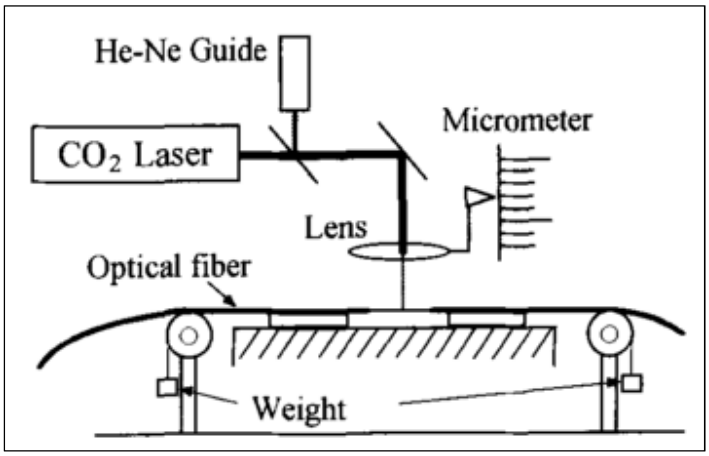

Figure 5: CO_2 laser taper rig [36].

The key elements of most laser-based taper rigs are:

i. CO_2 laser operating in a continuous wave (CW) mode.
ii. An alignment laser.
iii. A zinc selenide (ZnSe) focussing lens.
iv. A light delivery method.
v. Process control methodology.
vi. Process monitoring.

These elements are reviewed in the following sections.

2.2.1.1 CO_2 Laser

Previous researchers [10, 11, 14] have utilized lasers with maximum output powers ranging from 10 W to 35 W operating in CW mode. During the tapering process, the laser output is not maintained at a constant power as the fibre diameter decreases, but progressively increases during the pulling process to maintain the fibre temperature at the fibre softening point [12]. Figure 6 illustrates the laser power curve used by Ward *et*

al. in 2006 [12] during a typical fibre pulling process. The curve is typically a fourth order polynomial. Most researchers [2, 13, 39] have used this method of fibre temperature control rather than for example moving the lens, as otherwise the heating zone length would decrease as the focussed spot size changed.

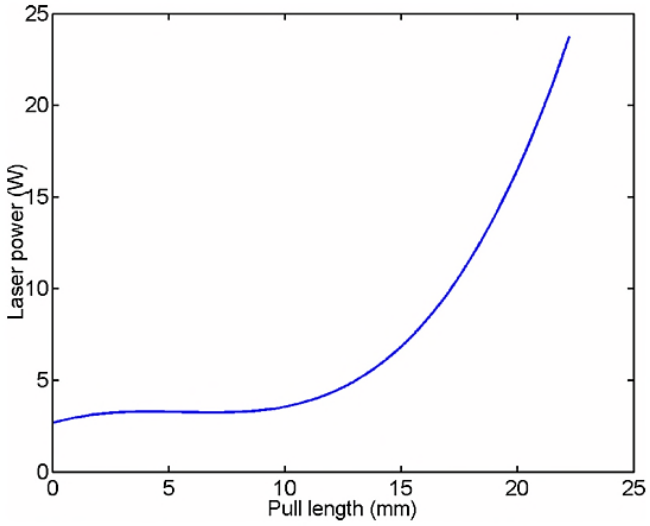

Figure 6: Power curve for a CO_2 laser for a taper pull length of 22 mm [12].

2.2.1.2 Alignment laser

The majority of research groups [2, 13, 39] have used a helium-neon (HeNe) laser to inject a visible light beam into the path of the invisible CO_2 beam to aid the alignment of the CO_2 laser to the fibre, as the CO_2 spot diameter is comparable in size to the diameter of the fibre (~ 125 μm). The choice of alignment laser is dictated by the optical transparency of the ZnSe focussing lens. HeNe lasers emit radiation at ~ 0.633 μm which is within the transparency window [35] of ZnSe (0.58 – 22 μm).

2.2.1.3 Focussing lens

Generally, a ZnSe lens is used to focus the laser beam to a small spot to heat the fibre. ZnSe is the preferred lens material as it is transparent both in the visible spectrum and at 10.6 μm. An alternative material would be Germanium, but this is opaque in the visible spectrum and thus negates the use of the HeNe alignment laser. Typical lens focal

lengths have ranged from 50 to 300 mm [13, 36]. A plano-convex cylindrical lens is the preferred [40] lens design as it produces a line focus which can be aligned along the longitudinal axis of the fibre.

Other approaches to the focussing of the laser onto the fibre have also been reported. Grellier in 2000 [14] used a single concave mirror and Vieko *et al.* in 2003 [41] used the combination of an angled mirror and concave mirror (both with holes) to heat the fibre equally around its circumference. The latter approach was particularly effective at improving the fabricated quality of scanning near-field optical probes.

2.2.1.4 Light delivery method

A scanning mirror attached to a galvanometer was used by Bayle *et al.* in 2005 [11] to vary the position of the focussed laser spot along the fibre. These researchers optimized the temperature uniformity over the scanned region of the fibre by adjusting the galvanometer scanning waveform and frequency, while observing the light intensity from the HeNe laser reflected from the fibre using a charge coupled device (CCD) camera. Li *et al.* in 2010 [42] extended this idea further, using two scanning mirrors to scan both along and across the fibre to give complete freedom in programming the scanning pattern along the fibre. This technique was useful in producing a relatively uniform temperature along the heating zone.

Sumetsky *et al.* in 2004 [40] enclosed the fibre in a sapphire tube to increase the fibre temperature so allowing taper waists with diameters of ~ 500 nm to be fabricated. The taper waist length produced was ~ 2 mm. These nano-tapers can be used to efficiently couple light to high Q micro-cavities. They were fabricated by indirectly heating the fibre by scanning the outside of the sapphire tube with the line focus from a cylindrical lens. The outside diameter of the tube was 0.9 mm and the inner diameter was 0.6 mm.

McAtamney *et al.* in 2005 [1] used a bespoke diffractive optical element (DOE) to produce a “top-hat” temperature profile along the fibre by modifying the Gaussian profile from the laser. However the optical performance of the tapers produced were not as optically efficient as a single scanning laser system in terms of transmission loss through the taper.

Later, Özcan *et al.* in 2007 [43] used a DOE as a beam splitter to heat the tapered fibre on two sides during the pulling process. The advantage of this technique was that the tapers produced were less elliptical (~ 0.5%) in cross section compared to using single-sided scanning of the fibre as for example described by Bayle *et al.* in 2005 [11]. The disadvantage of using a DOE is their intrinsic high insertion loss and so a higher power CO_2 laser is required as a consequence.

Wieduweilt *et al.* in 2013 [44] used a more energy efficient arrangement by using conventional beam splitters to produce two beams with focussed spherical spot sizes of 800 µm at the beam waists, arranged so they illuminated opposing sides of the fibre. These laser spots were then scanned along the fibre. This system produced taper waist diameters of 5-20 µm with taper lengths of 10 mm.

2.2.1.5 Process control methodology.

Most researchers have fabricated tapers using manual control of the laser and stages with some degree of automation gained by using a LabVIEW programming environment [10, 14]. However, the degree of the automation is unclear.

Aharoni *et al.* in 2012 [45] describe an optical fibre drawing rig and aspects of the control methodology that they developed are also applicable for use in tapering fibres. They used a long-wave filtered infra-red (IR) camera to provide fast, closed loop control of the laser by monitoring the temperature of the fibre. The LabVIEW program they developed adjusts automatically the pulling motor speed and laser power during the pulling process whilst maintaining a constant fibre temperature.

2.2.1.6 Process monitoring.

There have been limited reports in the literature of the use of systems to monitor the tapering process. Taper insertion loss has been measured [12, 14] during the process by coupling the output from a laser diode into the fibre and monitoring the transmitted power. Both of these groups were investigating low-loss adiabatic taper fabrication

techniques. They found that for adiabatic tapers, as the waist diameter decreases the light transmission remains relatively constant as shown in figure 7.

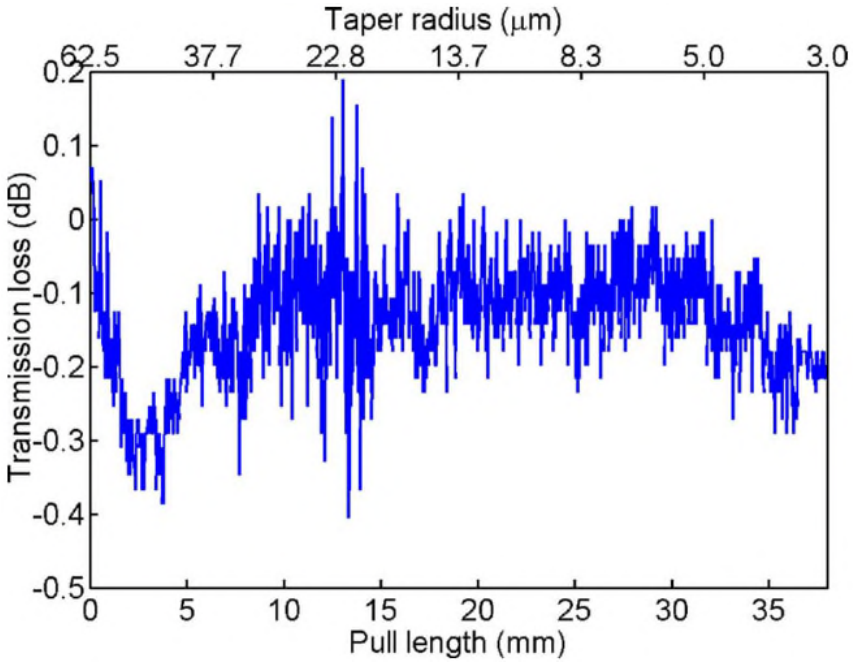

Figure 7: Transmission loss measurements for a 3 μm diameter taper with a 0.2 dB loss [12].

The force experienced by the fibre during the tapering process has been monitored using a load cell [14]. The data produced by the load cell was used to provide information to the operator so that the laser power could be adjusted manually during the process, with the objective of maintaining the fibre at the melting temperature. The method by which the load cell was incorporated into the system however caused the fibre to move perpendicular to the fibre axis during the stretching process. As a result, the shape of the taper was influenced, resulting in large variations in insertion loss between subsequent tapers.

As discussed in the previous section, Aharoni *et al.* in 2012 [45] monitored successfully the temperature of optical fibre pre-forms during a fibre drawing process using a long wave IR camera.

2.2.1.7 Summary

The optical fibre taper rig features discussed in the preceding paragraphs are summarized in table 1, together with the proposed taper rig features that will be used in this work. The rationale for the selection of the proposed features is discussed in chapter 4. To the best of my knowledge, there have been no reports of the inclusion of all of these features in one tapering system to date.

Table 1: Taper rig proposed process features

Number	Taper rig feature	Detail of taper rig feature cited in literature	Taper rig feature to be used in this project.
1	Laser power	10-30 W [11,14]	10 W initially, 25 W used later
2	Alignment laser	HeNe laser [2,13,39]	HeNe alignment laser
3	ZnSe focussing lens	50-300 mm focal length [13, 36]	Focal length of 190.5 mm initially used, 100 mm & 50 mm used later
4	ZnSe lens type	Spherical or cylindrical [13, 40]	Cylindrical lens
5	Scanning mirror	*Either*: no scan, scan in one plane, or scanning in two planes has been used [11,36, 42]	Scan in one plane only.
6	Power control method	Laser power adjusted manually by attempting to achieve constant incandescent emission using un-aided eye [12]	Pre-programmed power profiles derived using information gained from imaging the heated fibre using an NIR camera.
7	Fibre alignment.	HeNe laser [2,13,39]	NIR camera and HeNe laser
8	Fibre tension control	Load cell used by one group [14]	Fibre Bragg grating
9	Fibre translation.	*Either*: using weights or using linear translation stages [12, 36]	Rotational translation stages.
10	In-process optical assessment.	Laser diode and power meter [12,14]	Spectrophotometer and tungsten light source.

2.3 Micro-tapered long period gratings.

2.3.1 Introduction

Refractive index structures fabricated within the core of optical fibres using UV irradiation have been used for some years as wavelength selective components and sensors [46, 47, 48, 49]. As well as using UV radiation to induce a refractive index variation within the fibre core, it was also discovered [50] that the core index can be changed by heating the fibre up to ~ 1000 ^{0}C using a variety of heating methods [48], namely; CO_2 and CO laser irradiation, femto-second laser radiation and localised electrical discharges. The differing methods are listed and compared in section 2.3.2. The local refractive index variations in the fibre can be caused by a combination of:

i. Mechanical deformation of the fibre [51].
ii. Stress-optic effects due to the redistribution of glass elastic stresses induced in the fibre during the fibre drawing process [52, 53].
iii. Redistribution of the chemical composition of the glass due to thermo-induced diffusion of dopants in the core [54].

One of the key advantages of thermally induced gratings is their ability to retain their spectral properties at higher temperatures compared to UV written gratings. The spectral properties of UV written gratings start to degrade [50] at temperatures in excess of 200 ^{0}C whereas thermally formed gratings start to degrade at temperatures close to the melting temperature [48] of the fibre ~ 1000 ^{0}C. Gratings formed with UV irradiation are usually written in photo-sensitive fibre or hydrogen loaded fibre [47], whereas using thermal techniques, any type of silica fibre can be used [48].

If a UV written fibre grating is annealed at elevated temperatures, then the original spectrum disappears but a replica spectrum appears albeit at a much greatly reduced intensity and at a different wavelength because the average index of the grating has been reduced. These “two stage processed” gratings are referred to as “regenerated gratings”

[55, 56, 57]. An important property of regenerated gratings is that they are spectrally stable up to temperatures of ~ 1000 ^{0}C.

As well as their higher temperature resistance, another advantage of thermally generated gratings is that larger mode coupling coefficients can be achieved compared to UV-written gratings as the magnitude of the index modulation is greater [48, 50]. Spectral resonance bands of a given extinction coefficient can be produced with fewer grating periods [58] and so the overall grating length can be physically shorter than that of a UV-written grating with a comparable spectrum.

The reported disadvantages [48] of this technique are:

i. Higher spectral losses (~ 10 dB) caused by physical fibre deformation [20].
ii. Poor reproducibility of the spectral characteristics [48].
iii. Heat transfer between adjacent periods limiting the grating period to ~ 175 μm [59].

It was viewed that items (i) and (ii) can be optimized by appropriate process control. Item (iii) could potentially be resolved by using a short pulse length CO_2 laser, rather than using a laser functioning in either long pulse or CW mode. This would help to limit thermal diffusion between adjacent periods especially if this were combined with using a smaller spot size.

In the next section, the various methods for the fabrication of LPGs using non-UV techniques are reviewed, together with the proposed method for fabricating the CO_2 laser written TLPGs described within this thesis.

2.3.2 Review of non-UV fabrication processes for LPG fabrication

Over the last 20 years there has been significant research effort into the use of non-UV laser-based techniques to produce LPGs as these can be fabricated in any type of fibre as mentioned in the previous section. Poole *et al.* in 1994 [60] were the first to create periodic deformations in an optical fibre, producing resonance bands at ~ 1540 nm.

They used a single pulse from a CO_2 laser to ablate the fibre surface and then a subsequent arc discharge at these locations to create periodic micro-bends in the fibre via an annealing process. Attenuation levels of up to 24 dB were achieved at 1540 nm with a typical - 3dB bandwidth of 37 nm for the resonance bands. The length of this LPG was ~ 3.7 mm.

Following Poole`s initial work, a range of differing grating fabrication techniques to make these gratings have been investigated, namely:

i. CO_2 irradiation at 10.6 μm, but with no dimensional modifications to the fibre [17, 61, 62, 63, 64]. In this case, refractive index modulation of the fibre is achieved by a localised temperature increase causing residual stress relaxation in the fibre.
ii. CO irradiation at ~ 5.5 μm, but with no dimensional modifications to the fibre [50]. This laser wavelength was used as silica is more transparent at 5.5 μm compared to 10.6 μm and so the thermal gradient within the fibre is more uniform as the laser energy is absorbed over a greater distance.
iii. CO_2 irradiation, forming micro-tapered zones [20, 21, 22, 23].
iv. CO_2 irradiation followed by arc discharge to form micro-tapered zones [51].
v. Femto-second laser irradiation and a CO_2 technique to create sinusoidal modulated gratings [65].
vi. Using CO_2 irradiation to form micro-tapered zones along the 6 μm waist of a fibre taper [66].
vii. Arc-discharge, but with no fibre dimensional changes [67].
viii. Arc-discharge, forming micro-tapered zones [68, 69, 70].
ix. Resistive heating, forming micro-tapered zones [71].

A review of the various techniques for producing LPGs using a CO_2 laser was undertaken and a summary is provided in table 2. A similar review of the results achieved using arc discharge and resistive heating was also undertaken, this is provided

in table 3. Initial conclusions that can be drawn from these tables are discussed in the following sections.

2.3.2.1 CO_2 irradiated LPGs – no taper

Using CO_2 laser-based heating, it is possible to either locally modify the fibre refractive index only or to induce a geometrical taper *and* change the fibre refractive index. In both cases, both the cladding and core refractive indices are modified [22]. To modulate the refractive index of the optical fibre and not produce a taper, low power and short laser pulses are used and the fibre is not pulled during irradiation.

Using a CO_2 laser at low power to modulate the refractive index of the fibre only, can produce narrow resonance bands with low insertion losses (figure 8), especially if techniques are used to irradiate the fibre symmetrically [62,63] so avoiding the coupling to asymmetric cladding modes which can degrade the spectral characteristics (figure 9). Using a laser power of less than 5 W and short pulse lengths (< 450 ms) appears to give the best results. Liu *et al.* in 2011 [64], suggests that the asymmetric to symmetric cladding mode "switching mechanism" is driven by the timescale, peak power and size of the laser spot on the fibre. They also suggest that the theory of coupled modes may be adequate to describe UV generated LPGs, but for CO_2 irradiated LPGs, the cladding also undergoes an induced index change. This impacts on the overlap integral, and so the resonance wavelength positions and extinction levels predicted by the classical coupled mode model may be in error.

The smallest laser spot sizes that have been used are typically ~ 100 μm, producing gratings with periods of 175 μm [59]. The period dimension is limited as only a fraction of the spot size can heat the fibre to its melting point owing to its Gaussian intensity distribution (assuming the grating duty cycle is 50 %).

The smallest spot size attainable ~ 80 μm, is limited by the summation of aberration and diffraction effects caused by the optical focussing system [35]. The performance of the LPG shown in figure 8 is comparable to UV-written LPGs, with the added advantage of high temperature capability and high laser damage resistance. Accordingly, they have found applications as wavelength tuning elements in fibre lasers [59].

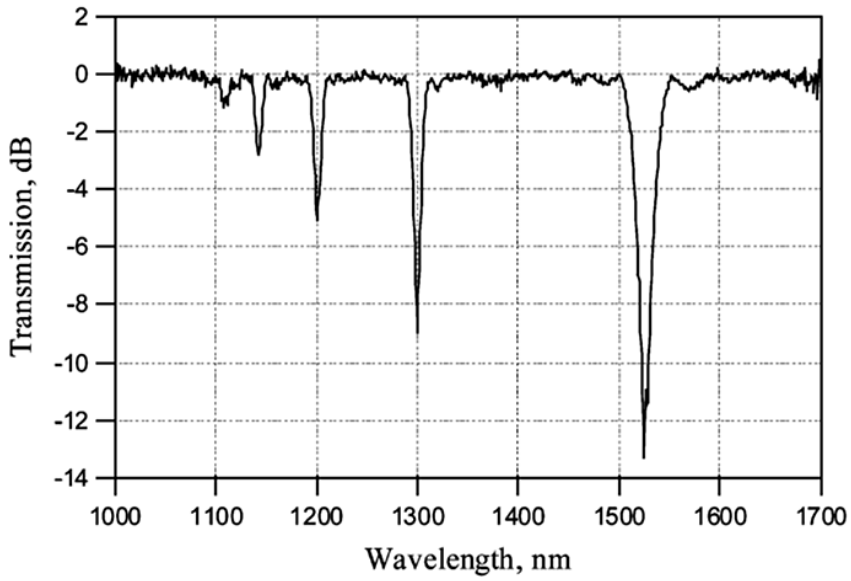

Figure 8: Transmission spectrum of a LPG fabricated with a reflector behind the fibre so producing symmetric cladding mode resonances. The fibre used was SMF-28 and the grating period was 370 μm [62].

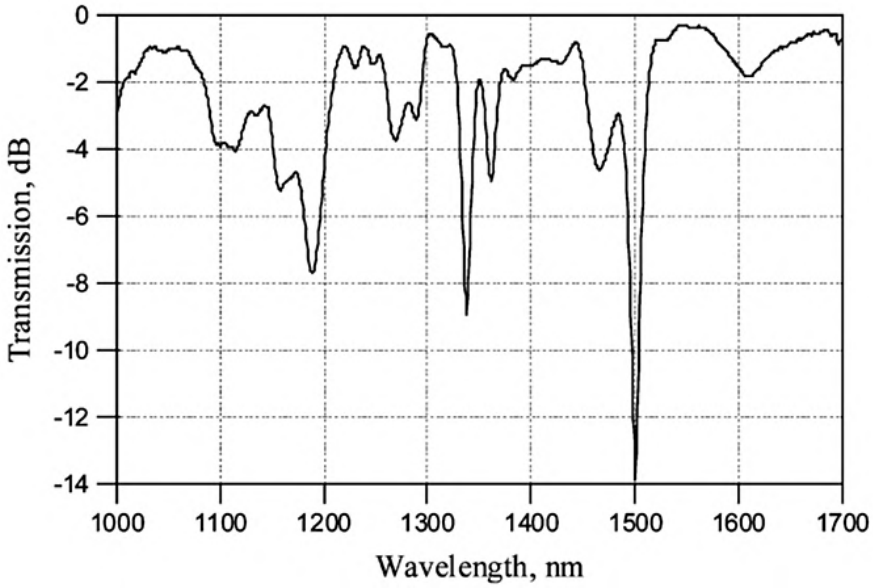

Figure 9: Transmission spectrum of a long period grating fabricated by heating one side of the fibre only, so producing asymmetric cladding mode resonances. The fibre used was SMF-28 and the grating period was 370 μm [62].

2.3.2.2 Tapered CO_2 irradiated LPGs

If the laser power is increased to 6-10 W and the fibre pulled during the irradiation process, then a micro-taper can be produced in addition to the modification of the index of the fibre as discussed in section 2.3.1. Tapered long period gratings (TLPGs) made using this technique [23, 72], tend to have higher insertion losses and wider bandwidth resonance bands as compared to those of CO_2 laser-written, non-tapered gratings. The magnitude of these properties appears to be driven largely by the parameters used in the fabrication process. It is believed that the increased bandwidth of the resonance bands is due to the higher coupling coefficients associated with these types of gratings, as the fibre is both index modulated and geometrically modulated by the taper. Compared to UV-written LPGs, TLPGs have the advantages that they can be compact (length < 5 mm), as compared to a typical length of 30 mm for UV-written LPGs and they are optically stable at higher temperatures.

The experimental configurations that have used to make TLPGs have typically used laser powers < 10 W, combined with fast shuttering to control the pulse length. A cylindrical ZnSe lens is the preferred focussing lens as it produces a line focus. The line focus is usually orientated perpendicular to the fibre as this arrangement makes the system tolerant of fibre displacements which are perpendicular to both the fibre and laser axes. Tensioning of the optical fibre during the process is achieved by either attaching a weight (~ 6g) to the fibre, or by pulling the fibre using linear translation stages. The impact of tensioning the fibre on the writing efficiency has been reported by Wang [22]. It was found that this parameter can produce conflicting results, depending on the magnitude of the tension used in a given scheme.

2.3.2.3 Tapered arc-discharge LPGs

As well as using laser irradiation to fabricate TLPGs, arc discharge techniques [68, 70] can also produce high quality TLPGs. The main mechanisms for the formation of arc-induced gratings as periodic structures are: glass densification, viscoelastic stress caused by taper drawing and geometric modulation (tapering) of the fibre [68].

TLPGs produced using this technique can exhibit low insertion losses (~ 1 dB) together with narrow resonance bands and high levels of extinction as shown in figure 10. To achieve these levels of performance the micro-tapers are made with repeatable geometrical taper profiles. The taper profiles were measured with a digital processing technique and were found to have an axial diameter error variation of less than ± 0.3 μm.

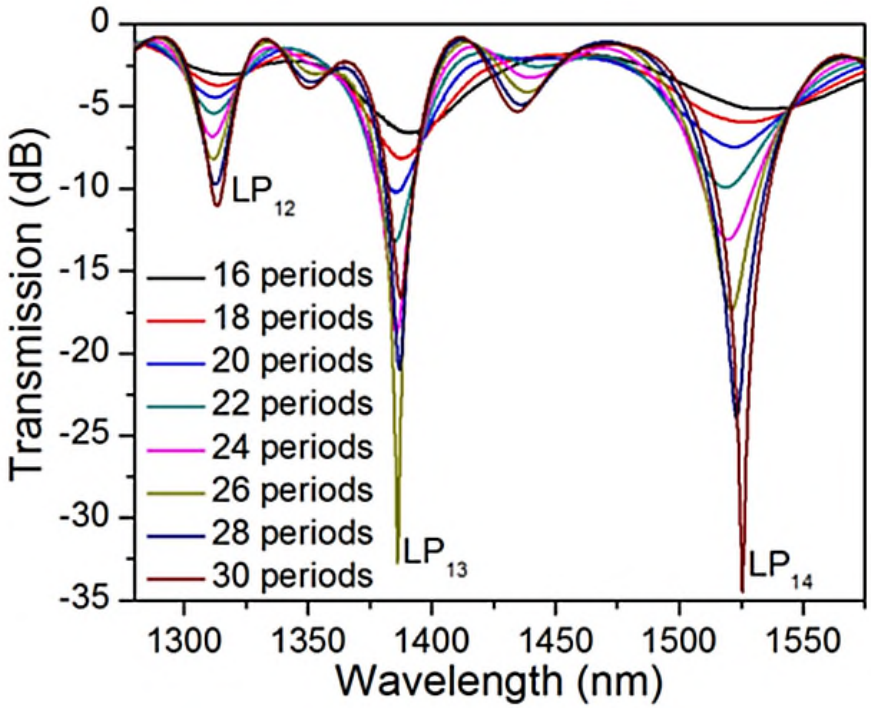

Figure 10: Transmission profile of a TLPG fabricated using a fusion splicer. The period was 650μm and the fibre was SMF-28 [70].

The spectral profiles, shown in figure 10, demonstrate that coupling to symmetric higher order modes can be achieved using micro-tapers. Because the coupling coefficient is large, the number of periods required to achieve a certain level of extinction is less than that for UV-written gratings of the same length. Typical taper waists achieved using this technique ranged from 110 – 120 μm and this may explain the lower insertion losses obtained with this technique compared to the CO_2 laser technique, as in the latter case, the typical waist diameters employed were all < 90 μm,

see table 2. Either a weight (~ 2 g) or rotation stages were used to pull the fibre in the arc discharge technique.

Ultra-short long period gratings (~ 1 mm) for use as high temperature sensors, have been fabricated by Nam *et al.* in 2005 [69] using the electric arc technique. Using only 2 periods, resonance bands were observed with an extinction of ~ 30 dB.

Table 2: Summary of CO_2 laser based techniques for fabricating long period gratings.

Reference	Fibre type	Taper / diam.- µm	Total length / mm	Period Spacing / µm	Period number	Tension method	Spot size / mm	Optics	Laser power	Wavelength band / nm	Pass band loss / dB	Peak width - nm / blocking - dB	Mode	Comments
Narayanan *et al.* 1997 [51]	Unknown	Yes, but assymetric	6	610	10	Relied on the stages	0.07	63.5 mm spherical	Unknown power, but short pulses.	1400-1600	0.3	48 / 23	Circular symmetric	This was a two stage process, laser to ablate one side and arc to deform core and claddining,core displaced.
Davis *et al.* 1998 [61]	SMF-28	No	19	480	40	3.9 g weight	0.145	Unknown	0.4 W / 270 ms pulse	1400-1600	3	5 .0 / 30	Circular symmetric	
Bouslamani *et al.* 2003 [20]	SMF-28	Yes / unknown	1.4	100	14	Relied on the stages	0.08	Spherical lens	Unknown power	1200-1600	10	8.0 / 40		
Grubsky *et al.* 2006 [62]	SMF-28	No	Unknown	357	Unkown	Unknown	0.1	Corner reflector & 50 mm cyclind.	6 W, 50 ms pulse.	1000-1700	~ 0.1	4.0 /13	Circular symmetric	
Little *et al.* 2006 [21]	SMF-28	Yes / 65	4	200	20	Relied on the stages	0.1	Spherical lens	Unknown power / CW mode	1400-1600	10.0 / 20		Circular asymmetric	Complex interference pattern
Kritzinger *et al.* 2009 [63]	PS1500	No	25	455	55	None	0.17	Concave mirror with a slit	1.15 W / 400 ms pulse	600-1600	< 0.5	5.0 / 10	Circular symmetric	Duty cycle 50/50. Fibre assembly translates to make periods.
Liu *et al.* 2011 [64]	SMF-28	No	18.75	625	30	10 g	0.12	Cylind.	2.7 W / 120 ms pulse	1200-1600	3	3.0 /30		
Wang *et al.* 2012 [74]	SMF-28	yes / 90 mcn	10	500	20	3.5 g	0.2	254 mm Cylind.	10.5 W	1500-1600	50	10.0 /20		Taper good quality, duty-cycle appears 50/50
Castro Alves *et al.* 2013 [23]	SMF-28	yes / 90 ?	30	350	85	40 g weight	0.15	50mm Cylind.	10 W	1400-1600	20	10.0 / 10		Tapers asymmetric - appears a low quality grating.

Table 3: Summary of thermal heating techniques used to fabricate long period gratings.

Reference	Fibre type	Fabrication method	Tapered / diam./µm	Total length/mm	Period Spacing/µm	Period number	Tension method	Wavelength band / nm	Pass band loss /dB	Peak width - nm / blocking - dB	Mode	Comments
Nam *et al.* 2005 [69]	SMF28	Arc discharge	Yes / 115	2	500	4	Weight	1200-1400	5	~ 10 / 30	Unknown	Shows impact of coupling on bandwidth and depth
Shao *et al.* 2008 [71]	SMF28	Resistive heating	Yes, 110	10	457	22	Relied on stages to pull	1200-1600	6	~ 10 / 30	Asymmetric circuler	Asymmetry is due to "C" shaped heating element.
Smietana *et al.* 2010 [67]	PS1250/1500	Arc discharge	No	20	350	57	< 2 g	1200-1600	1	~ 8 / 23	Symmetric circular	
Smietana *et al.* 2011 [68]	SMF28	Arc discharge	Yes, 120	37	345	108	2 g weight	1200-1600	1	~ 8 / 35	Symmetric circular	
Yin *et al.* 2014 [70]	SMF	Arc discharge	Yes / 115 / 450	19.65	550	30	Relied on stages to pull	1300-1550	1	~8 / 30	Symmetric circular	

2.3.2.4 Tapered resistively heated LPGs.

TLPGs have also been fabricated using resistive heating [71]. The non-uniform heating element employed however, created an asymmetric refractive index profile, so creating a significant polarisation dependant loss (PDL). Micro-tapers were formed by pulling the fibre in opposite directions using translation stages. The grating period was 457 μm and the diameter of the taper waists was 110 μm. The 22-period grating had a resonance band at 1566 nm with an extinction of ~ 30 dB.

In summary, high quality LPGs with defined resonance bands and low insertion losses have been fabricated to date using either:

a) Index modulation of the fibre using a CO_2 laser – without tapering.
b) Using arc discharge heating to both index modulate and geometrically taper the fibre.

The CO_2 technique for fabricating TLPGs could be further optimized so it has the same optical performance as arc-discharge techniques by ensuring that the taper geometry is repeatable and optimized to reduce optical insertion losses. Tapering is advantageous as it can realise physically shorter and temperature resistant LPGs. In addition, the CO_2 tapering process has advantages over arc-discharge techniques, as the spot-size can be reduced to 80 μm so allowing gratings with periods of less than 160 μm to be fabricated, whereas current fusion splicers are limited by the fixed dimensions of the electrodes which limits the period to a minimum of 221 μm [68]. The ability to fabricate gratings with periods less than 200 μm is important as it allows gratings to be fabricated with increased sensitivity [73] and allows for example [18] measurand sensitivities to be modified e.g. strain versus temperature. A laser spot size of 80 μm is the smallest diameter which can be typically achieved using a beam expanding telescope and an optimal focal length lens (see section 4.3.4).

2.4 Conclusions

A review of the CO_2 laser-based techniques for fabricating optical tapers has identified key elements of a system for making tapers. Aspects of the process for making tapers will be improved, these will include:

a) Pre-programmed power profiles to control the laser during the process. The laser process parameters will be determined experimentally.
b) The use of an NIR camera to aid fibre alignment and to aid (a) above.
c) The use of a fibre Bragg grating (FBG) to monitor the strain experienced by the optical fibre during the taper pulling process.
d) The development of a CO_2 fibre tapering system with a level of automation such that single tapers with waists of $\geq 5\mu m$ can be made with reproducible optical properties and geometry.

After a process is developed for fabricating single tapers it will then be adapted to fabricate TLPGs.

A review of the techniques for making TLPGs with a CO_2 laser has been undertaken. It was found that high quality LPGs with well-defined resonance bands and low insertion losses have been fabricated either using:

a) Index modulation of the fibre using a CO_2 laser – without micro-tapering.
b) Using arc discharge heating to both index modulate and geometrically micro-taper the fibre.

The CO_2 laser-based technique for fabricating micro-tapered LPGs will be further optimized so it has optical performance comparable with that of arc-discharge-based techniques in terms of the parameters of the resonance bands (table 3). The micro-taper geometry will be optimized in an attempt to reduce optical insertion losses below ~ 2

dB. The losses which are currently observed with CO_2 fabricated TLPGs are ~ 10 dB. The device geometry will also be further optimized to enhance their capability as a compact optical sensor.

2.5 References

[1] C. McAtamney, A. Cronin, R. Sherlock, G. M. O`Connor and T. J. Glynn, "Reproducible method for fabricating fused bi-conical tapered couplers using a CO_2 laser based process," *Proceedings of the Third International WLT - Conference on Lasers in Manufacturing 2005, Munich,* 2005, pp. 1–5.

[2] M. I. Zibaii, A. Kazemi, H. Latifi, M. K. Azar, S. M. Hosseini and M. H. Ghezelaiagh, "Measuring bacterial growth by refractive index tapered fiber optic biosensor," *J. Photochem. and Photobiol. B: Biol.*, Vol. 101, No. 3, pp. 313–320, 2010.

[3] R. Jarzebinska, C. S. Cheung, S. W. James and R. P. Tatam, "Response of the transmission spectrum of tapered optical fibres to the deposition of a nanostructured coating," *Meas. Sci. Technol.*, Vol. 20, No. 3, pp. 1–6, 2009.

[4] R. Jarzebinska, S. Korposh, S. James, W. Batty, R. P. Tatam and S.W. Lee, "Optical gas sensor fabrication based on porphyrin-anchored electrostatic self-assembly onto tapered optical fibers," *Analytical Lett.*, Vol. 45, No. 10, pp. 1297–1309, 2012.

[5] S. Lacroix, F. Gonthier, R. Black and J. Bures, "Tapered -fibre interferometric wavelength response - the achromatic fringe," *Opt. Lett.*, Vol. 13, No. 5, pp. 395–397, 1988.

[6] F. Gonthier, J. Lapierre, C. Veilleux, S. Lacroix and J. Bures, "Investigation of power oscillations along tapered monomode fibers.," *Appl. Opt.*, Vol. 26, No. 3, pp. 444–9, 1987.

[7] M. I. Zibaii, H. Latifi, E. Ghanati, M. Gholami and S. M. Hosseini, "Label free detection of DNA hybridization by refractive index tapered fiber biosensor", Bio-photonics: Photonic Solutions for better Health Care 11, *Proc. SPIE*, Vol. 7715, 1–9, 2010.

[8] P. S. Edwards, C. T. Janisch, B. Peng, J. Zhu, S. K. Ozdemir, L. Yang and Z. Liu, "Label-free particle sensing by fiber taper-based Raman spectroscopy," *IEEE Photonics Technol. Lett.*, Vol. 26, No. 20, pp. 2093–2096, 2014.

[9] A. Layeghi, H. Latifi and O. Frazão, “Magnetic field sensor based on non-adiabatic tapered optical fiber with magnetic fluid,” *IEEE Photonics Technol. Lett.*, Vol. 26, No. 19, pp. 1904–1907, 2014.

[10] S. Y. Chen, T. L. Yeo, W. Z. Zhao, T. Sun, K. T. V. Grattan, R. Lade, B. D. Powell, G. Foster-Turner and M. Osborne, “Development of multi-wavelength microsphere fibre laser system for potential sensor applications,” *Opt. Commun.*, Vol. 282, No. 3, pp. 401–405, 2009.

[11] F. Bayle and J.P. Meunier, “Efficient fabrication of fused-fiber bi-conical taper structures by a scanned CO_2 laser beam technique,” *Appl. Opt.*, Vol. 44, No. 30, pp. 6402–11, 2005.

[12] J. M. Ward, D. G. O’Shea, B. J. Shortt, M. J. Morrissey, K. Deasy and S. G. Nic Chormaic, “Heat-and-pull rig for fiber taper fabrication,” *Rev. Sci. Instrum.*, Vol. 77, No. 8, p. 083105, 2006.

[13] T. E. Dimmick, G. Kakarantzas, T. Birks, and P. St. J. Russell, “Carbon dioxide laser fabrication of fused-fiber couplers and tapers,” *Appl. Opt.*, Vol. 38, No. 33, p. 6845, 1999.

[14] A. J. C. Grellier, “Characterisation of optical fibre tapering using a CO_2 laser,” PhD thesis, University of Canterbury, 2000.

[15] A. M. Vengsarkar, P. J. Lemaire, J. B. Judkins, V. Bhatia, T. Erdogan and J. E. Sipe, “Long period fiber gratings as band-rejection filters,” *Light. Technology*, Vol. 14, No. 1, pp. 58–65, 1996.

[16] Y. Liu and K. S. Chiang, “Recent development on CO_2 laser written long-period fiber gratings”, Passive components and fiber-based devices V, *Proc. SPIE*, Vol. 7134, p. 713437 1–11, 2008.

[17] V. Bhatia, “Properties and sensing applications of long-period gratings”, PhD Thesis, Virginia Polytechnic Institute and State University, 1996.

[18] S. W. James and R. P. Tatam, “Optical fibre long-period grating sensors : characteristics and application,” *Meas. Sci. Technol.*, Vol. 14, pp. R49–R61, 2003.

[19] C. Narayanan, H. M. Presby and A. M. Vengsarkar, “Band-rejection fibre filter using periodic core deformation,” *Electron. Lett.*, Vol. 33, No. 4, pp. 280–281, 1997.

[20] H. Hamama, M. Ketata, Y. Bouslimani and O. Latry, “CO_2 laser beam based technique for producing optical fiber components”, Applications of photonic technology 6, *Proc. SPIE*, Vol. 5260, pp. 154–162, 2003.

[21] D. J. Little, G. D. Marshall and M. J. Withford, “Fabrication of periodic, resonant features in optical fibres using a CO_2 laser micro-tapering system,” 2nd *PICALO Conference Proceedings*, 2006, pp. 383–386.

[22] Y. Wang, “Review of long period fiber gratings written by CO_2 laser,” *J. Appl. Phys.*, Vol. 108, No. 8, p. 081101, 2010.

[23] D. Castro Alves, J. M. P. Coelho, M. Nespereira, F. Monteiro, M. Abreu and J. M. Rebordão, “Automation methodology for the development of LPFG using CO_2 laser radiation”, 8th Ibero-american Optics Meeting and 11th Latin American Meeting on Optics, Lasers and Applications, *Proc. SPIE*, Vol. 8785, p. 87854X 1–5, 2013.

[24] P. N. Moar, S. T. Huntington, J. Katsifolis, L. W. Cahill, A. Roberts and K. A. Nugent, “Fabrication, modelling, and direct evanescent field measurement of tapered optical fiber sensors,” *J. Appl. Phys.*, Vol. 85, No. 7, p. 3395, 1999.

[25] J. Villatoro, D. Monzón-Hernández, E. Mejía and D. Monzo, “Fabrication and modelling of uniform-waist single-mode tapered optical fiber sensors.,” *Appl. Opt.*, Vol. 42, No. 13, pp. 2278 –2283, 2003.

[26] L. C. Bobb, P. M. Shankar and H. D. Krumboltz, “Bending effects in biconically tapered single-mode fibers,” *J. Light. Technol.*, Vol. 8, No. 7, pp. 1084–1090, 1990.

[27] B. Musa, A. A. Rozi, A. S. M. Noor, A. Ismail and M. A. Mahdi, “Effect of fiber profile parameters on the transmission properties of the tapered optical fibers,” *2011 IEEE 2nd International Conference on Photonics*, Malaysia, 2011, pp. 1–4.

[28] K. Q. Kieu and M. Mansuripur, “Bi-conical fiber taper sensors,” *IEEE Photonics Technol. Lett.*, Vol. 18, No. 21, pp. 2239–2241, 2006.

[29] D. Maraldo, P. M. Shankar and R. Mutharasan, “Measuring bacterial growth by tapered fiber and changes in evanescent field.,” *Biosens. Bioelectron.*, Vol. 21, No. 7, pp. 1339–44, 2006.

[30] T. Martan, P. Honzátko, J. Kaňka and K. Novotný, “Workplace for manufacturing devices based on optical fiber tapers”, *15th Czech-Polish-Slovak Conference on Wave and Quantum Aspects of Contemporary Optics*, *Proc. SPIE*, Vol. 6609, 2007. p. 66090K 1–5.

[31] J. C. Graf, S. A. Teston, P. V. De Barba, J. Dallmannl, J. A. S. Limal, H. J. Kalinowski and A. S. Paterno, “Fiber taper rig using a simplified heat source and the flame-brush technique,” *International Microwave and Optoelectronics Conference*, Belem, 2009, pp. 621–624.

[32] S. W. Harun, K. S. Lim, C. K. Tio, K. Dimyati and H. Ahmad, “Theoretical analysis and fabrication of tapered fiber,” *Opt. - Int. J. Light Electron Opt.*, Vol. 124, No. 6, pp. 538–543, 2012.

[33] C. Baker and M. Rochette, “A generalized heat-brush approach for precise control of the waist profile in fiber tapers,” *Opt. Mater. Express*, Vol. 1, No. 6, pp. 1065–1076, 2011.

[34] S. Pricking and H. Giessen, “Tapering fibers with complex shape,” *Opt. Express*, Vol. 18, No. 4, pp. 3426–37, 2010.

[35] J. Ready, *Laser Institute of America, Handbook of Laser Materials Processing*, 2001.

[36] H. Yokota, E. Sugai and Y. Sasaki, “Optical irradiation method for fiber coupler fabrications,” *Opt. Rev.*, Vol. 4, No. 1, pp. 104–107, 1997.

[37] L. Zhang, L. Liu, Z. Cai, C. Ye and G. Wen, “Fabricating sub-wavelength fiber tapers using a CO_2 laser”, Passive components and fiber-based devices, *Proc. SPIE*, Vol. 5623, pp. 987–994, 2005.

[38] A. Pal, S. Y. Chen, R. Sen, T. Sun and K. T. V Grattan, “A high-Q low threshold thulium-doped silica microsphere laser in the 2 μm wavelength region designed for gas sensing applications,” *Laser Phys. Lett.*, Vol. 10, No. 8, p.p. 1-6, 2013.

[39] A. Malki, O. Latry, M. Ketata, F. Van Lauwe, L. Bachelot, P. Royer and V. Lauwe, “ Microlenses-fibers fabricated by melting-tapering process using CO_2 laser,” *OSJ/SPIE Conference on Optical Engineering for Sensing and Nanotechnology (ICOSN `99)*, Japan, 1999,Vol. 3740, pp. 432–437.

[40] M. Sumetsky, Y. Dulashko and A. Hale, “Fabrication and study of bent and coiled free silica nanowires: Self-coupling micro-loop optical interferometer,” *Opt. Express*, Vol. 12, No. 15, pp. 3521–31, 2004.

[41] V. P. Veiko, A. N. Kalachev, L. N. Kaporsky, S. A. Volkov and N. B. Voznesensky, “Laser technology of SNOM-tips fabrication: process, diagnostics, processing and testing”, *Laser processing of advanced materials and laser microtechnologies*, *Proc. SPIE*, Vol. 5121, pp. 164–174, 2003.

[42] M. Li, F. Pang, H. Guo, Y. Liu, N. Chen, Z. Chen and T. Wang, “Tapered optical fiber fabricated by high-frequency pulsed carbon dioxide laser”, *Advanced sensor systems and applications IV*, *Proc. SPIE*, Vol. 7853, pp. 78533E1–6, 2010.

[43] L. Ç. Özcan, V. Tréanton, F. Guay and R. Kashyap, “Highly symmetric optical fiber tapers fabricated with a CO_2 laser,” *IEEE Photonics Technol. Lett.*, Vol. 19, No. 9, pp. 656–658, 2007.

[44] T. Wieduwilt, K. Kirsch, J. Dellith, R. Willsch and H. Bartelt, “Optical fiber micro-taper with circular symmetric gold coating for sensor applications based on surface plasmon resonance,” *Plasmonics*, Vol. 8, No. 2, pp. 545–554, 2013.

[45] R. Aharoni, L. Bidani, M. Sinvani and Z. Zalevsky, “Initiatory concept of localized laser-based tapering rig for realization of in-fiber devices,” *Opt. Eng.*, Vol. 51, No. 7, pp. 1–8, 2012.

[46] K. O. Hill, B. Malo, K. A. Vineberg, F. Bilodeau, D. C. Johnson and I. Skinner, “Efficient mode conversion in telecommunication fibre using externally written gratings,” *Electron. Lett.*, Vol. 26, No. 16, p. 1270, 1990.

[47] K. O. Hill and G. Meltz, “Fiber Bragg grating technology fundamentals and overview,” *J. Light. Technol.*, Vol. 15, No. 8, pp. 1263–1276, 1997.

[48] S. A. Vasiliev and O. I. Medvedkov, “Long-period refractive index fiber gratings: properties, applications and fabrication Techniques”, *Advances in fiber optics*, *Proc. SPIE*, vol. 4083, pp. 212–223, 2000.

[49] G. Rego, “A review of refractometric sensors based on long period fibre gratings,” *The Scientific World Journal*, Vol. 2013, p.p. 1-14, 2013.

[50] E. M. Dianov, K. Karpov, M. V. Grekov, K. M. Golant, S. A. Vasiliev, O. I. Medvedkov and R. R. Khrapko, “Thermo-induced long-period fibre gratings,” *European conference on Optical Communications*, Edinburgh, UK, 1997, No. 448, pp. 53–56.

[51] C. Narayanan, H. M. Presby and A. M. Vengsarkar, “Band-rejection fiber filter using periodic core deformation,” *Electronics Letters*, pp. 280–281, 1997.

[52] M. Akiyama, K. Nishide, K. Shima, A. Wada and R. Yamauchi, “A novel long-period fiber grating using periodically released residual stress of pure-silica core fiber,” *Optical Fiber Communications*, San Jose, California, 1998, pp. 276–277.

[53] T. Enomoto, M. Shigehara, S. Ishikawa, T. Danzuka and H. Kanamori, “Long-period fiber grating in a pure silica core fiber written by residual stress relaxation,” *Optical Fiber Communications*, San Jose, California, 1998, pp. 277–278.

[54] K. Karpov, M. V. Grekov, E. M. Dianov, K. M. Golant, S. A. Vasiliev, R. R. Medvedkov and R. R. Khrapko, “Mode-field converters and long-period gratings fabricated by thermo-diffusion in nitrogen-doped silica-core fibers,” *Optical Fiber Communications*, San Jose, California, 1998, pp. 279–280.

[55] L. B. Melo, N. Ângelo, N. Aberto, C. Marques, J. Monteiro, G. Rego, P. Caldas and R. Nogueira, “Comparative study of different parameters of fibre Bragg gratings and long period gratings sensors for high temperature measurements”, *International conference on applications of optics and photonics*, 2011, *Proc. SPIE*, Vol. 8001, pp. 1–7.

[56] S. Bandyopadhyay, J. Canning, P. Biswas, R. Chakraborty and K. Dasgupta, "Regeneration of complex Bragg gratings", *20th International conference on optical fiber sensors, Proc. SPIE*, Vol. 7503, pp. 1–4, 2009.

[57] W. Liu, K. Cook and J. Canning, "Ultra high temperature regeneration of long period gratings (LPGs) in Boron co-doped Germanosilicate optical fibre," *Fifth Asia Pacific Optical sensors conference*, Jeju, Korea, 2015, Vol. 9655, p. 96552T–1/4.

[58] S. G. Kosinski and A. M. Vengsarkar, "Splicer based long period fiber gratings," *Optical Fiber Communications conference*, San Jose, California, 1998, pp. 278-279.

[59] P. Peterka, J. Maria and B. Dussardier, "Long-period fiber grating as wavelength selective element in double-clad Yb-doped fiber-ring lasers," *Laser Phys. Lett.*, Vol. 6, No. 10, pp. 732–736, 2009.

[60] C. D. Poole, H. M. Presby and J. P. Meester, "Two-mode fibre spatial-mode converter using periodic core deformation," *Electron. Lett.*, Vol. 30, No. 17, p. 1437, 1994.

[61] D. D. Davis, T. K. Gaylord, E. N. Glystis, S. G. Kosinski, S. C. Mettler and A. M. Vengsarkar, "Long-period fibre grating fabrication with focused CO_2 laser pulses," *Electron. Lett.*, Vol. 34, No. 3, pp. 302–303, 1998.

[62] V. Grubsky and J. Feinberg, "Fabrication of axially symmetric long-period gratings with a carbon dioxide Laser," *IEEE Photonics Technol. Lett.*, Vol. 18, No. 21, pp. 2296–2298, 2006.

[63] R. Kritzinger, D. Schmieder and A. Booysen, "Azimuthally symmetric long-period fibre grating fabrication with a TEM_{01} mode CO_2 laser," *Meas. Sci. Technol.*, Vol. 20, No. 3, pp. 1–8, 2009.

[64] X. Liu, M. Yan, L. Zhan, S. Luo, Z. Zhang and Y. Xia, "Controlling of symmetric and asymmetric mode coupling in long-period fiber gratings single-side induced by long-pulse CO_2 laser," *Opt. Commun.*, Vol. 284, No. 5, pp. 1232–1237, 2011.

[65] X. Fang, X. Y. He, C. R. Liao, M. Yang, D. N. Wang and Y. Wang, "A new method for sampled fiber Bragg grating fabrication by use of both femto-second laser and CO_2 laser.," *Opt. Express*, Vol. 18, No. 3, pp. 2646–54, 2010.

[66] H. Xuan, W. Jin and M. Zhang, "CO_2 laser induced long period gratings in optical microfibers.," *Opt. Express*, Vol. 17, No. 24, pp. 21882–90, 2009.

[67] M. Smietana, W. J. Bock and P. Mikulic, "Comparative study of long-period gratings written in a boron co-doped fiber by an electric arc and UV irradiation," *Meas. Sci. Technol.*, Vol. 21, No. 2, pp. 1-8, 2010.

[68] M. Smietana, W. J. Bock, P. Mikulic and J. Chen, "Increasing sensitivity of arc-induced long-period gratings—pushing the fabrication technique toward its limits," *Meas. Sci. Technol.*, Vol. 22, No. 1, pp. 1–6, 2011.

[69] S. Nam, C. Zhan, J. Lee, C. Hahn, K. Reichard, P. Ruffin, K. L. Deng and S. Yin, "Bend-insensitive ultra-short long-period gratings by the electric arc method and their applications to harsh environment sensing and communication.," *Opt. Express*, Vol. 13, No. 3, pp. 731–7, 2005.

[70] G. Yin, Y. Wang, C. Liao, J. Zhou, X. Zhong, G. Wang, B. Sun and J. He, "Long period fiber gratings inscribed by periodically tapering a fiber," *IEEE Photonics Technol. Lett.*, Vol. 26, No. 7, pp. 698–701, 2014.

[71] L.-Y. Shao, J. Zhao, X. Dong, H. Y. Tam, C. Lu and S. He, "Long-period grating fabricated using resistive filament heating", *19th International conference on optical fibre sensors*, *Proc. SPIE*, Perth, Australia, 2008, Vol. 7004, pp. 1–4.

[72] B. S. Wang and J. Stathis, "Technologies of fiber fusion and fused device fabrication for sensing applications," *Fiber optics sensing and applications VII, Proc. SPIE*, Vol. 7677, No. 2, pp. 1–6, 2010.

[73] R. Y. N. Wong, E. Chehura, S. E. Staines, S. W. James and R. P. Tatam, "Fabrication considerations for fiber optic long period gratings operating at the phase matching turning point," *Appl. Opt.*, Vol. 53, No. 21, pp. 4669–4674, 2014.

[74] P. Wang, G. Brambilla, M. Ding, L. Bo, Y. Semenova, Q. Wu and G. Farrell, “Refractive index sensing measurement based on periodically tapered small core single mode fibre,” *Proc. SPIE*, Vol. 8421, p. 84211S 1–4, 2012.

3 Tapered optical fibre theory

3.1 Introduction

This chapter describes the theory of tapered optical fibres and optical fibre long period gratings. The origins of the channelled spectrum that is observed in the transmission spectrum of a non-adiabatic taper are discussed. The theoretical model describing the fabrication of fibre tapers with an exponential transition zone profile is summarised. Later in this chapter, the theoretical background of UV and CO_2 written long period gratings (LPGs) is described, with the objective of explaining the spectral characteristics and properties of these devices. Finally, the use of CO_2 radiation to fabricate micro-tapered long period gratings is discussed.

3.2 Theory of optical fibres.

An optical fibre is a dielectric optical waveguide which typically has cylindrical symmetry [1]. If light is coupled into the core of the fibre at one end, it emerges from the remote end with low [2] power loss ~ 0.2 dB/km depending on the type of fibre used and the wavelength of the transmitted light. This property gives optical fibres the capability to transmit continuous light energy or for optical data transmission over significant distances. Figure 11 shows a generic optical fibre design with a core of high refractive index (n_{core}) surrounded by a lower index cladding (n_{clad}). The refractive index difference is such that light propagating within the fibre, which is incident at an angle greater than the critical angle (θ_c) on the core/cladding interface, is totally internally reflected and is thus confined to propagate within the core.

The critical angle θ_c is defined in equation (3-1) :

$$\theta_c = sin^{-1}\left[\frac{n_{clad}}{n_{core}}\right] \tag{3-1}$$

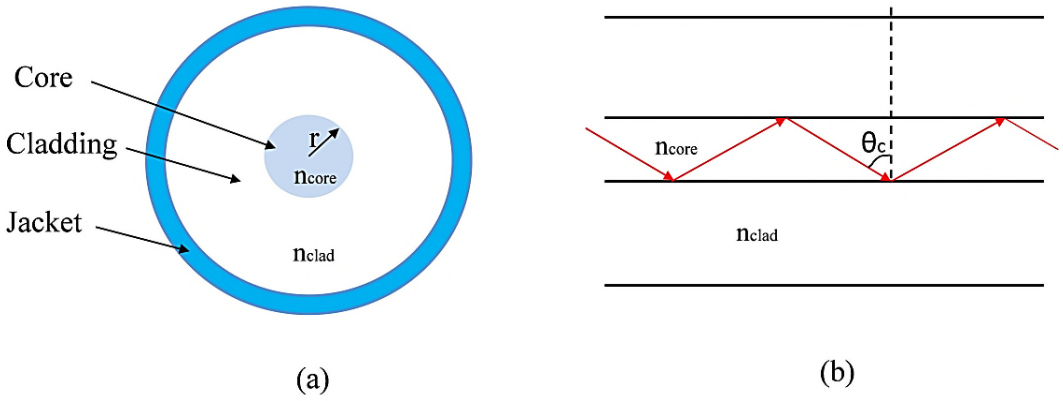

Figure 11: (a) Generic optical fibre design, (b) path of a light ray propagating at the geometric angle for total internal reflection.

This simple geometry would perhaps suggest that a continuous range of totally internally reflected rays inside the fibre structure is possible; in fact, the wave nature of light means that it must satisfy a self-interference condition in order to be trapped inside the optical waveguide. There are only a finite number of paths that satisfy this condition and these are analogous to the propagating electromagnetic modes of the structure. Optical fibres that can support a large number of modes (large core diameter and numerical aperture) can be analysed using geometrical optics, while optical fibres that support only a small number of modes must be characterised by solving Maxwell`s equations with the appropriate boundary conditions for the waveguide [1].

Optical fibres for communications applications can be either single-mode or multimode. In single-mode fibres, only one mode propagates along the core, which has a typical diameter of < 8 μm. Multi-mode fibres have core diameters > 50 μm and can support many hundreds of modes [3].

When light travels along a single-mode fibre it propagates along the core without undergoing reflection at the cladding/core interface. As well as modes being guided in the core, under specific circumstances light can escape the core and be coupled into modes that are supported by the waveguide formed by the cladding with the surrounding, lower refractive index, medium. These so called “cladding modes” are usually rapidly attenuated by the lossy cladding / jacket interface, if the jacket is present on the fibre.

When the light wave propagates along a single mode fibre, the mode field diameter is larger than the diameter of the core and extends into the cladding figure 12. This electric field propagates across the core / cladding boundary and is known as an evanescent wave [1].

.

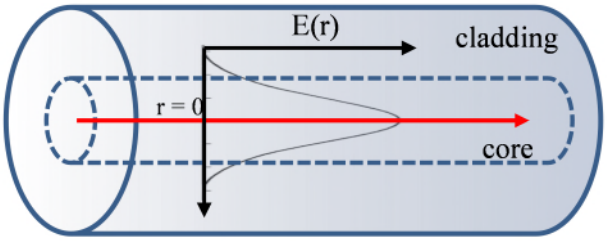

Figure 12: Modal field distribution in a single-mode fibre, r is the core radius; E(r) is the modal electric field.

A guided mode in the fibre propagates with an effective index n_{eff} = β/k where β is the mode propagation constant and k = 2π / λ is the free space propagation constant. The effective index (n_{eff}) lies between n_{core} and n_{clad} when the mode is confined to the core, but when it is propagating in the cladding, $n_{air} < n_{eff} < n_{clad}$. When n_{eff} is equal to the refractive index of the surrounding medium, the mode radiates into that medium. The refractive index of the buffer jacket of an optical fibre is similar to that of the cladding, which explains why these modes are attenuated in a short distance when they propagate along the fibre. If the jacket is removed, the cladding mode travels a greater distance, as the refractive index of air/vacuum is unity, however any contamination or bends in the fibre will attenuate the cladding modes also.

The number of allowed modes [4, 5] in a fibre is determined by the V-number defined in equation (3-2):

$$V = \frac{2\pi a}{\lambda} \sqrt{(n_{core}^2 - n_{clad}^2)} \qquad (3\text{-}2)$$

where λ is the wavelength, a is the core radius and n_{clad} and n_{core} are as defined earlier in this section. When V < 2.405, the fibre supports only the fundamental mode (LP_{01}) which is a radially symmetric mode.

We can define separate V-numbers for both core and cladding using equations (3-3 and 3-4):

$$V_{core} = \frac{2\pi a}{\lambda} \sqrt{(n_{core}^2 - n_{clad}^2)} \tag{3-3}$$

$$V_{clad} = \frac{2\pi R}{\lambda} \sqrt{(n_{clad}^2 - n_{air}^2)} \tag{3-4}$$

where R is the radius of the cladding.

For situations in which the light is guided by the core, the core-cladding index difference is typically small, with $n_{core} - n_{clad} < 0.03$. Under these circumstances, the weakly guiding condition, only one mode is propagated along the fibre core. Here the V- number is less than unity. If a fibre is tapered, the fibre diameter is reduced and the light escapes from the core. Under these circumstances, light is guided by the cladding and the surrounding medium is air and the index difference is accordingly much larger. Here V_{clad} is > 2.405 and many more modes can be supported within the cladding and so the taper waist behaves like a multi-mode fibre and the evanescent field extends into the medium around the taper waist.

3.3 Theory of optical tapers

When a single mode fibre is tapered by locally heating a short section of fibre and pulling axially in opposite directions, a narrow taper waist is formed that is surrounded by two transition zones (figure 13).

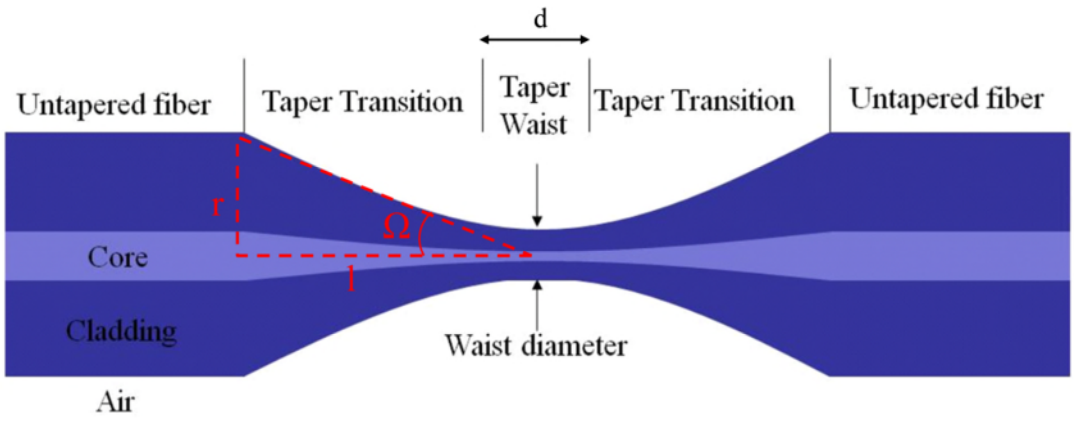

Figure 13: Cross-section of a taper and definition of the taper half-angle (Ω) and d [6].

As the taper diameter reduces, it reaches a diameter where the core mode to cladding mode transition [5, 7] occurs, where the V number of the core - cladding interface is given by equation (3-5):

$$V_{\text{core/clad}} \sim \sqrt{\frac{2}{\ln S}}\left(1 + \frac{0.26}{\ln S}\right)^{-0.5} \tag{3-5}$$

where S = cladding diameter / core diameter. For a typical single-mode fibre, the cladding mode transition [7] occurs at fibre diameter of ~ 40 µm. Here the propagating light wave ceases to be guided by the core and instead is guided by the air / cladding interface. In this region, the taper can behave like a multi-mode fibre, provided certain conditions are met. In the taper region, the effective V number is high (> 100), much greater than 2.405 and thus it can support many modes [8].

The taper angle (Ω) of the transition zones, shown in figure 13, is a key parameter in influencing the optical behaviour of a taper [9]. If the taper half angle (Ω) is less than ~ 5 x 10^{-3} radians, then the taper is referred to as adiabatic; when it exceeds ~ 5 x 10^{-3} radians it is termed a non-adiabatic taper [10, 11]. When the fundamental mode propagates through the transition zone of an adiabatic taper, the core electric field progressively increases into the cladding, until the core diameter reduces and then air-

cladding guiding of the propagating wave occurs. Because the taper angle is very small, energy coupling to higher order modes is minimized and light transmission through the taper is high. When the length of the transition zone is larger than the local coupling length between the fundamental mode and the higher order cladding modes then the power loss is small ~ 0.06 dB, as the fundamental mode of the fibre has coupled to the fundamental mode of the tapered region [12].

If a fibre is non-adiabatic, the taper transition zone is smaller than the coupling length between the fundamental mode and the high order cladding modes, and so significant coupling then occurs. Under these circumstances, the taper half angle is typically greater than ~5 x 10^{-3} radians. The light couples efficiently from the fundamental core mode to the first two or more modes of the taper waveguide (LP_{01}, $LP_{02\ etc.}$) as the light propagates in the taper waist region.

The different modes experience differing phase changes as they propagate along the taper. The phase difference between the modes depends on the both the refractive indices of the fibre and surrounding medium and the length of the taper. When the propagating modes are recombined at the second transition zone, interference between the single mode of the fibre and the two or more modes of the taper causes periodic oscillations (figure 14) in the transmission spectrum of the taper [11, 13, 14]. The modes are coupled into the single mode fibre after the second transition zone with a typical overall transmission loss of ~ 3dB [9].

When there are only two modes, the relative phase difference ($\Delta\ \varphi$) is given by equation (3-6):

$$\Delta\ \varphi = \Delta\beta . d \tag{3-6}$$

Where $\Delta\beta$ is the difference in propagation constants of the two modes and d is the length of the taper waist. If $\Delta\beta$ or d change then the phase difference will also change. This feature is the basis for the use of tapers as optical sensors, as the phase difference depends on the index of the fibre, the surrounding medium

and the interaction length [14].

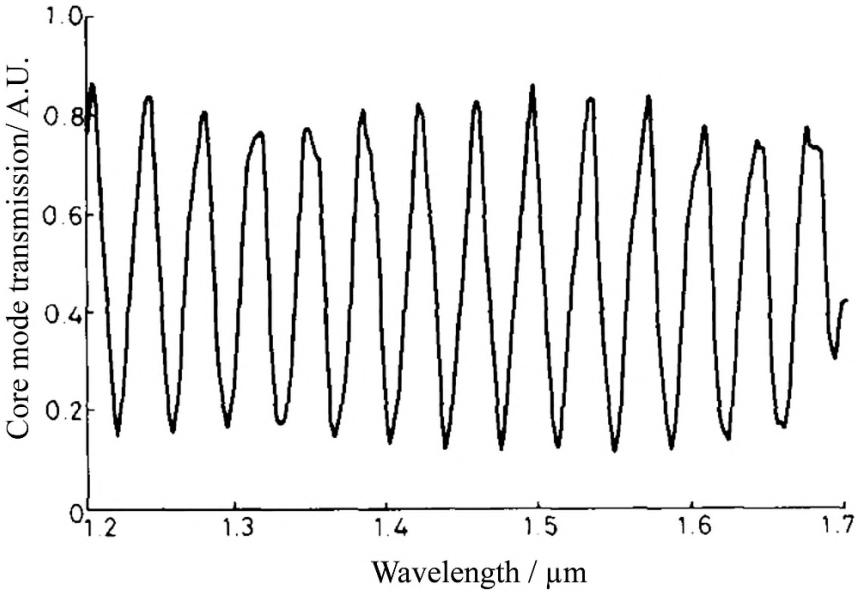

Figure 14: Experimental core-mode transmission of a bi-taper as a function of wavelength [13].

Using coupled mode theory, solutions to Maxwell`s equations allow the local fibre modes to be calculated assuming a core-cladding-air interface structure for the taper [7]. The effective mode indexes, $n_{eff} = \beta/k$, for a typical taper can be calculated and are shown in table 4 for the radially symmetric LP_{0n} modes. It is assumed the core/ cladding diameter ratio is constant. Cladding modes start to appear when the taper diameter is 33 μm and reduce in number as the fibre diameter decreases further until one mode (LP_{01}) remains.

Table 4: Effective mode indexes of fibre modes at selected diameters [7].

Fiber Diameter (μm)	LP_{01}	LP_{02}	LP_{03}	LP_{04}	LP_{05}	LP_{06}	LP_{07}	LP_{08}
125	1.45597							
33	1.45354	1.45310	1.45227	1.45105	1.44944	1.44744	1.44504	
25	1.45344	1.45265	1.45119	1.44905	1.44624	1.44275	1.43857	1.43370
20	1.45333	1.45208	1.44978	1.44643				
13	1.45292	1.44989	1.44441					
10	1.45244	1.44741						

3.4 Taper fabrication theory

The theory of the process of tapering a fibre has been described in detail by Harun *et al.* in 2012 [15] and Birks *et al.* in 1992 [16]. When a fibre is heated and pulled, it is assumed that the volume of the heated length of the fibre is conserved during the heating process. Birks *et al.* [16] present simple equations to describe the relationship between elongation profile, elongation distance and hot-zone length, where the hot-zone is the length of the fibre at the melting temperature. Their analysis is summarised in the following paragraphs.

The cylinders shown in figure 15 represent a fibre before and after heating and stretching. At time t, the heated fibre bounded by AB, has a hot-zone length of L and waist radius of r. After a short interval of time, δt, the heated fibre is stretched and the new length is $L+\delta x$ where δx is the increase in extension during the interval δt. The hot-zone length is changed to $L+\delta L$, in the same time, where δL may be negative, positive or zero. The radius of the heated fibre is $r+\delta r$, where δr is the change is waist radius. The volume at time t is the same as that at $t+\delta t$. The fibre length A`B` is still within the hot-zone and will be further stretched and narrowed. If the hot-zone length has a uniform temperature during the tapering process, Birks *et al.* have shown [16] that the taper radius profile has a decaying exponential profile with the following equation (3-7):

$$r\,(z) = r_0\, e^{-Z/L} \tag{3-7}$$

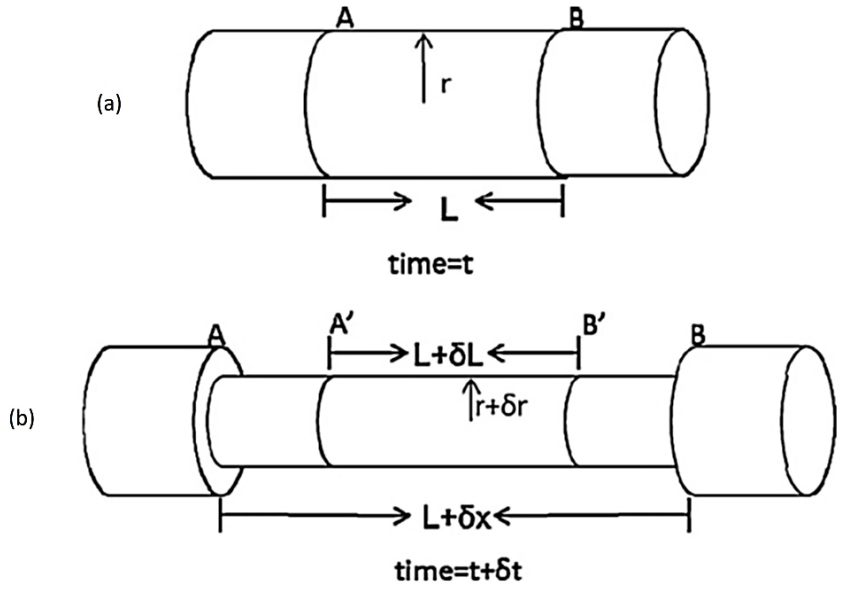

Figure 15: Cylinder illustrates a fibre (a) before heating and (b) after heating and stretching where the diameter of the fibre has been reduced where it was elongated [15].

Where r is the taper radius, r_0 is the initial taper radius, z is the pull length and L is the length of the hot-zone. The measured profile of a typical optical fibre taper is shown in figure 16 and matches closely the exponential function described in equation 3.7. This taper had a constant hot-zone length of 10 mm and the translation stages were moving with a velocity of 1.1 mm s^{-1}. Birks *et al.* also describes how to fabricate tapers with different taper profiles by varying the hot-zone length during the tapering process. Linear, concave and asymmetric taper profiles have all been described in the literature [15].

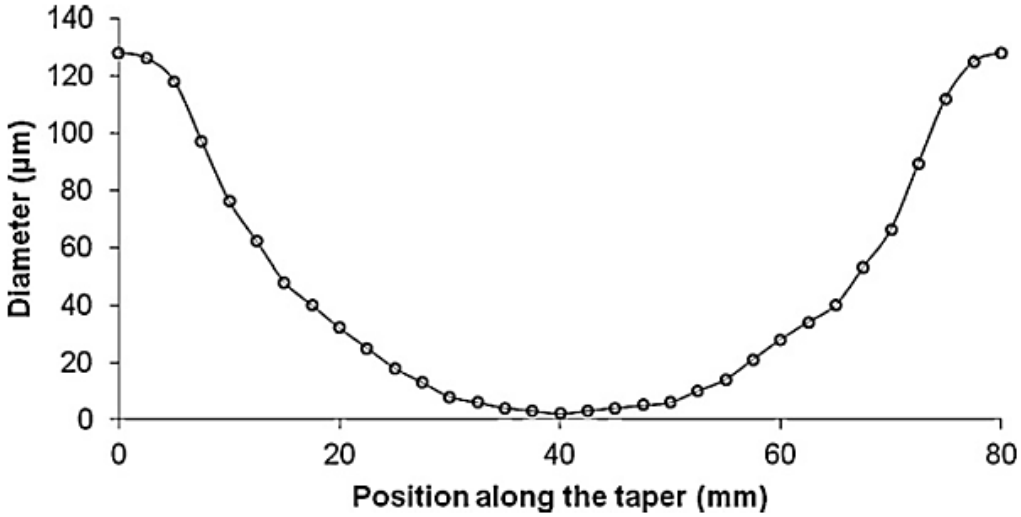

Figure 16: Tapered fibre with a exponential profile fabricated using a constant hot-zone length of 10 mm [15].

3.5 Theory of fibre gratings

3.5.1 Introduction

Fibre gratings have a range of applications in fibre-optic systems, including; optical sensing, fibre filters and fibre lasers. There are two main types of grating, depending on the length of the grating period. Fibre Bragg gratings (FBGs) have periods that are sub-micron and long period gratings (LPGs) typically have periods of hundreds of microns.

Fibre Bragg gratings are formed by the periodic modulation of the fibre core with UV radiation whereas LPGs can be formed with either UV or CO_2 radiation, thermal heating or mechanical deformation.

The objective of this section of the thesis is to provide a theoretical description of long period gratings, together with a description of their spectral characteristics. Firstly, fibre Bragg gratings are discussed followed by the theory of UV written long period gratings. Then a review of the CO_2 laser written long period gratings is given followed by the origins of the associated fibre index perturbation and finally a review of the theory of tapered long period gratings.

3.5.2 Fibre Bragg gratings

An FBG is a periodic refractive index structure and has been the subject of significant research [17, 18] over the years. FBGs can be fabricated by exposing the fibre core to an intense UV interference pattern. The interference pattern is often generated by using a phase mask [18] which is placed in front of the fibre. If the fibre core is photo-sensitive, the fibre core refractive index is perturbed locally by exposure to the periodic intensity pattern.

FBGs couple the forward propagating fundamental core mode to a mode with the opposite direction of propagation. This coupling occurs at a specific wavelength called the Bragg wavelength, which is dictated by the periodicity of the grating. As a result, at the Bragg wavelength (λ_B), a narrow band reflection occurs. The FBG behaves like a narrow band filter when used in transmission. The Bragg wavelength satisfies the following condition described in equation (3-8):

$$\lambda_B = 2\, n_{eff}^{core} \Lambda_{Br} \tag{3-8}$$

Where n_{eff}^{core}, is the effective index of the fundamental mode, Λ_{Br} is the grating period (~ 0.5 μm). The optical properties of FBGs, the various fabrication techniques and their range of applications have been described by a number of researchers [18, 19, 20].

3.5.3 UV written long period gratings

Long period gratings were first proposed by Vengsarkar *et al.* in 1996 [17]. They typically have periods (Λ_{LPG}) from 100 – 800 μm and couple the fundamental core mode with cladding modes propagating in the same direction. The attenuation of the cladding modes causes the spectral response of the fibre to contain a series of resonance bands at specific wavelengths. Each resonant band corresponds to the coupling to a different cladding mode. An example of a transmission spectrum of an LPG is shown in figure 17.

The resonance wavelength (λ_{LPG}) [20] for an LPG is described by equation (3-9):

$$\lambda_{LPG} = (n_{eff}^{co} - n_{eff}^{cl})\Lambda_{LPG} \quad \textbf{(3-9)}$$

Where n_{eff}^{co} is the effective index of the core mode and n_{eff}^{cl} is the effective index of a specific cladding mode. The resonance bands in the spectrum shown in figure 17 are sensitive to the period of the LPG, the refractive index of the medium surrounding the fibre, the length of the LPG and the immediate environment in terms of refractive index, temperature, strain and bend radius. Any changes in these parameters will change the period and/or the differential refractive index of the core and cladding modes. The phase matching condition (equation 3.9) for coupling to specific cladding modes is thus modified which results in changes to the resonant wavelengths. This property forms the basis for the use of LPGs as sensors.

The light coupled into the cladding mode is matched optically to the jacket and is attenuated by a combination of; radiation, fibre bending and contamination on the fibre surface causing light scattering. This causes the attenuation bands to appear in the transmission spectrum of the fibre. Whereas FBGs reflect light at their resonance wavelengths, LPGs couple to cladding modes which are then attenuated at specific wavelengths as defined by equation 3.9. Typical resonance wavelengths are illustrated in figure 17 for an LPG of period 570 μm in single-mode fibre [21].

Modelling the optical performance of an LPG requires the calculation of the refractive indices of the cladding and core modes, so allowing the wavelengths of the attenuation bands to be calculated [23, 24]. In order to determine the degree of coupling between the core and cladding modes, the wave equation for a 3-layer dielectric cylinder with a stepped radial index distribution can be solved [22], however other models have also be used [17]. The 3-layer model allows the electric fields for the core and cladding modes to be calculated.

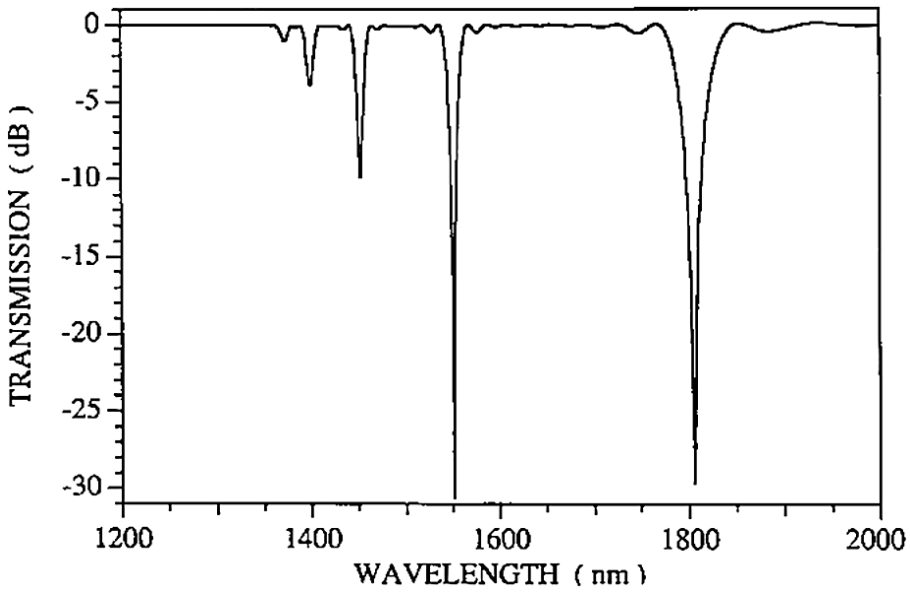

Figure 17: Theoretical spectra of an LPG designed to couple the LP_{01} core mode to the ν=5 cladding mode at 1550 nm, where ν is the cladding mode order number. The grating period is 570 μm [21].

Significant coupling from the core mode to cladding modes occurs when the overlap integral (η_{LPG}) between the electric field profiles of the modes is large. The integration region [20] is determined by the physical location of the index modulation created during the grating fabrication process. The overlap integral [20] is given in equation 3.10 and assumes that only the fibre core has been index modulated by the UV radiation:

$$\eta_{LPG} = \int_0^a E_{co}\, E_{cl}^{*} r\, dr \,/\, (\int_0^\infty \left| E_{co} \right|^2 \, r\, dr \int_0^\infty \left| E_{cl} \right|^2 \mathrm{r}\, dr)^{1/2} \qquad (3\text{-}10)$$

where E_{co} and E_{cl} are the electric field amplitudes of the core and cladding modes respectively and r is the radial coordinate. The calculated local intensity profiles [22] of the first four cladding modes (ν=1, 2, 3, 4) are shown in figure 18. The low order *even* modes contain little light in the fibre core, whereas the low-order *odd* modes have a peak localised in the core. As a consequence, the coupling between the low order even modes and the LP_{01} core mode of the fibre is very weak.

The variation in coupling between the LP_{01} core mode and the cladding modes for a typical fibre is shown in figure 19 [22]. Figure 19 also shows the coupling between the lowest order even modes and the core mode is very weak compared to that of the odd modes and in addition explains the progressive increase in resonance band attenuation as the wavelength increases as observed in figure 17. Equation 3.10 indicates that the modes (LP_{0n}) which are excited, are circularly symmetric about the fibre axis.

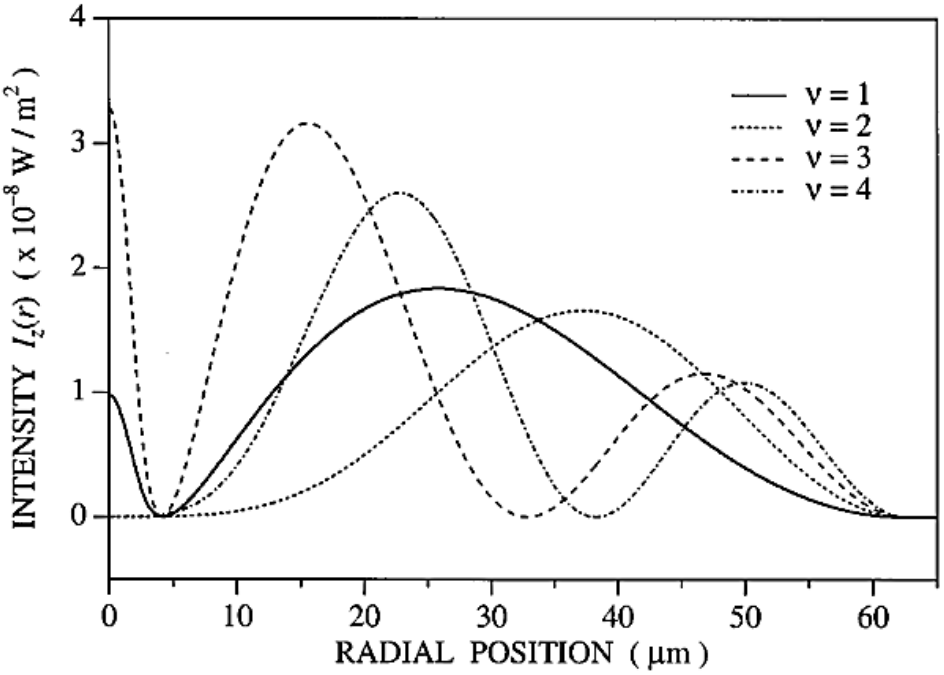

Figure 18: Plots of the mode intensity as a function of radius for the first order cladding modes in a fibre. All modes are circularly symmetric and are normalized to 1 W power [22].

Figure 20 shows the dependence of the coupling wavelength, for cladding modes 2-8, as a function of grating period. These graphs were calculated using the 3-layer cylindrical waveguide model of a fibre shown in figure 11, using MATLAB software within Cranfield University [25]. The fibre modelled had a cut-off wavelength of 650 nm. The parameters used for modelling the optical fibre are detailed in table 5.

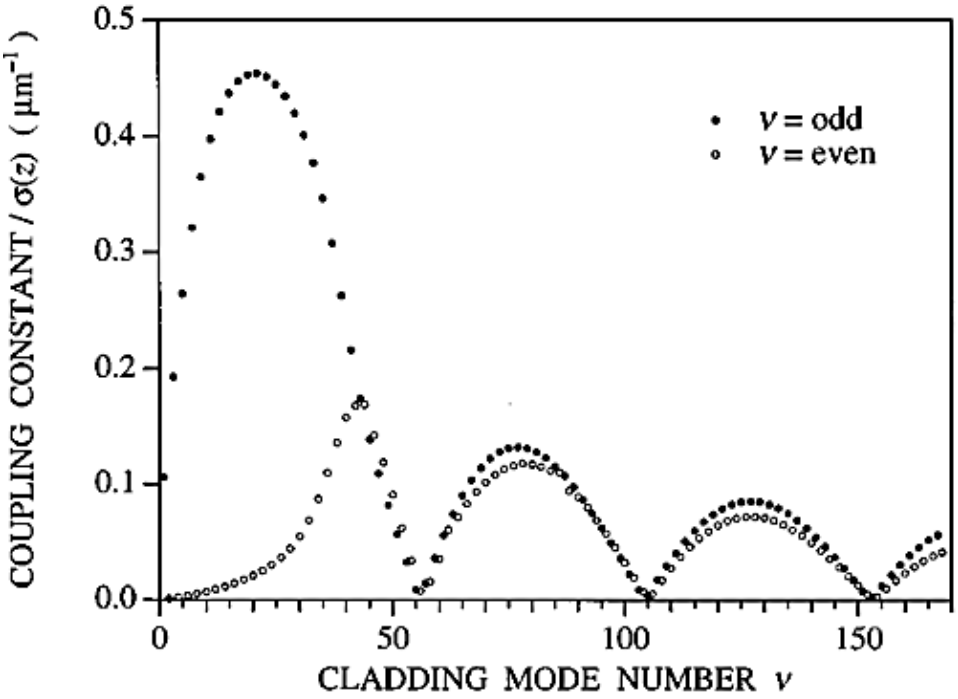

Figure 19: Coupling constant divided by σ(z) for the 168 first order cladding modes in a fibre, showing odd and even modes separately [22].

Table 5: Parameters used for modelling optical fibre, based on values of Fibercore PM750 fibre.

Core radius (r_{core})	2.2 μm
Cladding radius (r_{clad})	62.6 μm
Core refractive index (n_{core})	1.4583
Cladding refractive index (n_{clad})	1.4533
Ambient refractive index	1.0

The LPG resonance band minimum [20] transmission value (T), is given by equation (3-11):

$$T = 1 - sin^2(k_{LPG}\, L) \tag{3-11}$$

where k_{LPG} is the coupling coefficient and L is the length of the grating. The depth of the minima is proportional to the length of the grating and the magnitude of the coupling coefficient.

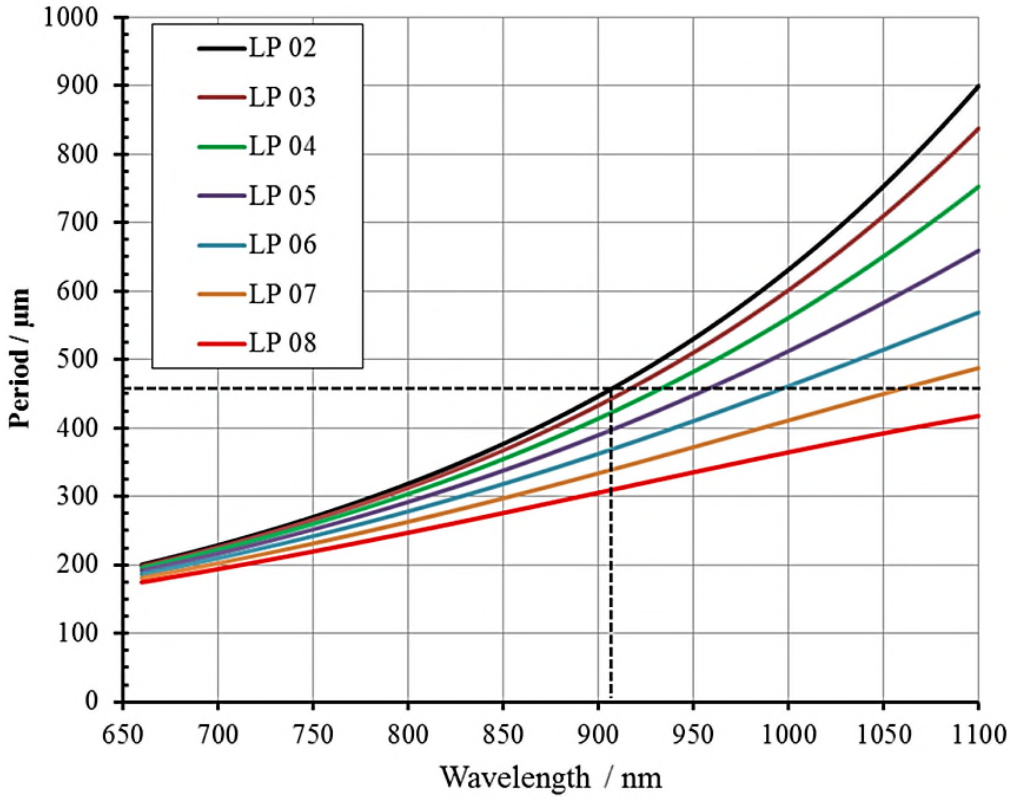

Figure 20: Plot of the resonant wavelength as a function of LPG period for coupling between the guided core mode and cladding modes of order 2-8, assuming the fibre cut-off wavelength is 650 nm. If the period is ~ 450 µm, the LP_{02} mode wavelength is ~ 907 nm (shown by dashed line).

The coupling coefficient [20] is measure of the overlap between the mode fields of the core and cladding and is given in equation 3-12:

$$k_{LPG} = \pi \Delta n_{mod} \eta_{LPG} / \lambda_{LPG} \tag{3-12}$$

where Δn_{mod} is the induced refractive index change in the core.

The full spectral width [20] of the first resonance peak is described by equation (3-13):

$$\Delta\lambda_{LPG,0} = 2\alpha_{BRF}\lambda_{LPG}\frac{\Lambda_{LPG}}{L}\left[1 - \left(\frac{k_{LPG}\,L}{\pi}\right)^2\right]^{1/2} \quad (3\text{-}13)$$

where α_{BRF} is the bandwidth refinement factor, which has value near unity.

As well as the depth of the attenuation bands being strongly influenced by the refractive index change (Δn_{mod}) via the coupling coefficient, the bandwidth of the attenuation bands is also influenced.

3.5.4 Review CO_2 laser written long period gratings

As discussed in section 2.3, there are a variety of techniques for fabricating LPGs using thermal radiation to change the fibre properties. The two techniques that employ CO_2 laser irradiation are given below:

i. CO_2 irradiation, but with no dimensional modifications to the fibre [26, 27,28 ,29].
ii. CO_2 irradiation, forming micro-tapered zones [30, 31, 32, 33].

Details of the experimental systems used to fabricate these LPGs outlined were given in table 2 (section 2.3).

3.5.5 Origins of index perturbation in CO_2 written LPGs.

The previous section (3.5.3) describes the theory of LPGs which are written using UV irradiation of the fibre core. UV irradiation of the fibre core causes a permanent positive refractive index change of between 10^{-3} to 10^{-5} if the core has been doped with Ge [17] to enhance the photo-sensitive effect. The refractive index change in the core is associated with the formation of Ge-related glass defects [34].

Fibres with higher photosensitivity (5.9 x 10^{-3}) have also been created by hydrogen loading [35] the core or doping the core with boron and germanium (3 x10^{-3}) [36]. The magnitude of the refractive index change also depends on factors such as the UV irradiation fluence and any fibre pre-processing which has occurred. From a LPG modelling perspective, the refractive index change in the core is assumed [22] to be uniform along the length of the grating and the refractive index of the cladding is assumed to be unchanged.

When a silica fibre is irradiated by the output from a CO_2 laser at a wavelength of 10.6 µm, the physical mechanisms that induce refractive index changes are substantially different from those associated with UV irradiation. The reststrahlen reflectance [37] of silica is ~ 12% at 10.6 µm, and so most of the incident laser energy is absorbed by the fibre within a distance of 10-20 µm, as the material optical absorption coefficient is high at this wavelength. The absorbed energy then propagates through the fibre from the cladding to the central core by thermal conduction and creates a temperature gradient across the fibre to a level depending on the laser energy fluence and timespan [38].

As discussed in section 3.5.4, CO_2 laser fabrication of LPGs can result in either periodic index modulation of the fibre with *no dimensional changes* to the fibre or periodic micro-tapering of the fibre depending on the technique used. These two options are discussed in the following sections (3.5.5.1 & 2), together with their associated effects on the fibre refractive index.

3.5.5.1 CO_2 LPG – no fibre dimensional change

Using this technique, the fibre is translated periodically along the fibre axis and irradiated at each location by the beam from a CO_2 laser. When the fibre temperature is greater than its melting or fictive temperature [26], the fibre melts, but there is no modification to the diameter or geometry of the fibre as the fibre is not under any axial strain.

One of the mechanisms changing the refractive index of the fibre during this process, is the relaxation of intrinsic stress within the fibre core. During the fibre drawing process, stresses are induced in the fibre which subsequently relax, when the fibre is heated

above its fictive temperature by CO_2 laser irradiation [40]. Stresses in the fibre change the fibre refractive index via the stress-optic effect. Stress relaxation causes the index to decrease on heating, The magnitude of the decrease [41] depends on the fibre type, fibre drawing process, laser power density at the fibre and whether the fibre is hydrogenated. In Ge or Ge-Bo doped fibres, stress relaxation is the dominant index modulation mechanism. For example, a refractive index change of -7.2×10^{-4} has been reported [40] for Corning SMF-28 single mode fibre.

Changes in the glass structure causing glass densification [40] is the dominant physical mechanism for CO_2 laser irradiation induced refractive index changes in commercial boron-doped single mode fibre. The refractive index change under these circumstances tends to increase, but the magnitude is dependent on the annealing temperature of the fibre during the drawing process [40].

Davis *et al.* in 1998 [26] measured the cladding and core radial refractive indices using transverse interferometry (see figure 21). Under CO_2 irradiation, the positive refractive index change due to residual stress relief and/or densification was 3×10^{-4} and both the cladding and core indices were increased. The index increase was greatest towards the side of the fibre which is closest to the laser. This is a common effect in CO_2 induced LPGs and is caused by the laser energy being strongly absorbed on the incident side of the fibre causing a thermal gradient across the fibre.

The fibre has a high absorption coefficient at 10.6 μm and so most of the energy is absorbed in the first 10-20 μm of the fibre cladding. There are a number of techniques for correcting this index asymmetry optically and these are discussed in sections 2.2.1 and 2.3.2.1.

3.5.5.2 CO_2 tapered long period gratings

When TLPGs are fabricated, during the irradiation process, the fibre is axially tensioned using either mechanical stages or weights, so forming a locally tapered region once the fictive temperature [40, 41] of the fibre has been exceeded. Under these conditions, viscoelastic strains can be frozen into the fibre when is cooled below its fictive temperature under tension. These strains can have a significant impact on the

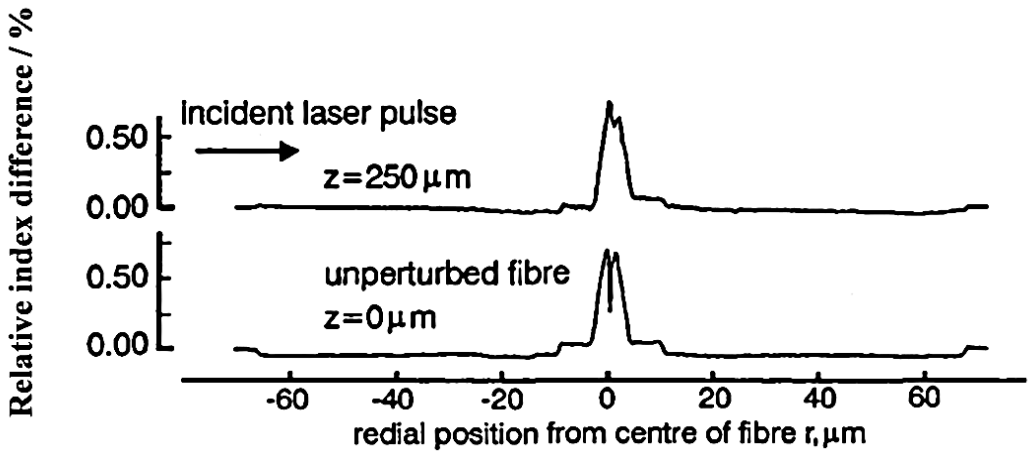

Figure 21: Radial relative index profiles in non-H_2-loaded fibre gratings at positions z along the fibre axis [26].

refractive index profile of the fibre, greater than those related to the elasto-optic effect [38, 40, 41]. This results in a large decrease in the fibre index, typically $> 10^{-3}$. If the fibre cross-sectional area is also reduced (i.e. tapered), then the index change is even more pronounced. Using these techniques, Yablon *et al.* in 2004 [41] used this effect to create a high performance all-fibre beam expander, increasing the fibre mode field diameter to in excess of 40 μm compared to 8 μm for an untreated fibre. The majority of the fibre index change occurs in the cladding [41], as shown in figure 22.

A summary of the typical refractive index changes that can be produced using UV and CO_2 irradiation is given in table 6.

The refractive index changes associated with CO_2 laser LPGs produce transmission spectra that are different from those of UV generated LPGs. The resonance attenuations bands are more attenuating for a given number of periods and the spectral bandwidth of the individual bands are wider than UV generated LPGs. This is due to a combination of the increased refractive index differential typically observed with these gratings coupled with the cladding index changes (table 6).

Table 6: Typical changes in fibre refractive indices under different irradiation conditions.

Fabrication technique	Physical mechanism	Refractive index change		Comments
		Total cladding change Δn	Total core change Δn	
UV laser [18]	Photo-sensitive effect	0	10^{-4}	Refractive index change in core only
CO_2 laser [26,38]	Residual elastic stress & glass densification	$3x10^{-4}$	$< 3x10^{-4}$	Positive index change, asymmetric changes in cladding, if irradiation is single sided.
CO_2 laser and fibre tension [38,40,41]	Residual elastic stress, glass densification & frozen visco-elastic stress	$> -3\ x10^{-3}$	$-1x\ 10^{-3}$	Negative index change in cladding. Symmetric change.

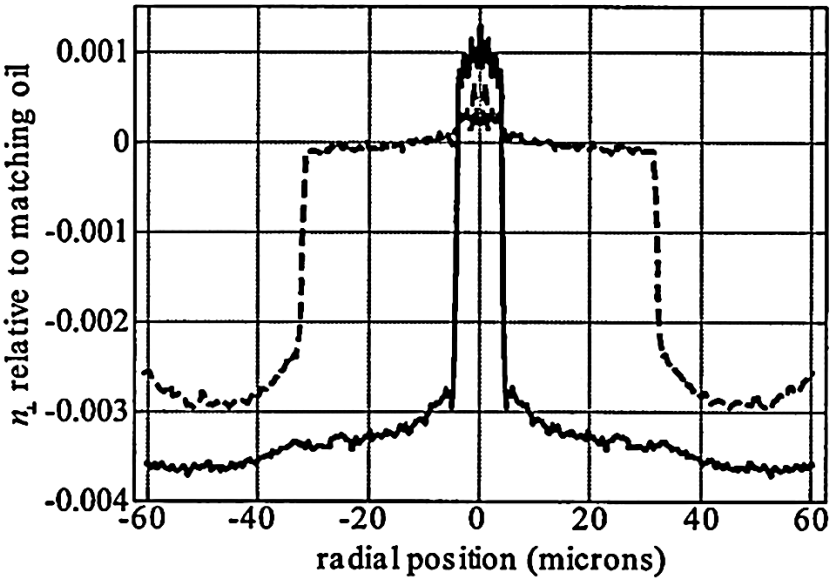

Figure 22: As drawn (solid line) fibre and the refractive index profile (dashed line) for one type of fibre beam expander. Note the large refractive index change occurring in the large cross-sectional area cladding regions compared to the fibre core [41].

3.5.6 Theory of tapered long period gratings

The theory of UV written LPGs summarised earlier needs to be extended to describe the case of TLPGs. Limited research has been undertaken to date on this subject area [22, 42, 43, 44]. However, the current status of the work is summarised in the following paragraphs.

For TLPGs, the resonant wavelength [22, 42] can be obtained from the phase matching condition as given by equations 3-14 to 3-16:

$$(\beta_{co} + \sigma_{co-co}) - (\beta_{vj}^{clad} + \sigma_{vj-vj}) = \frac{\pi}{\Lambda} \tag{3-14}$$

$$\sigma_{co-co}(z) = \frac{\omega\varepsilon_0 n}{2} \overline{\delta n(z)} \iint dxdy\delta n(x,y)\, \vec{E}_{co}(x,y)\vec{E}_{co}(x,y) \tag{3-15}$$

$$\sigma_{vj-vj}(z) = \frac{\omega\varepsilon_0 n}{2} \overline{\delta n(z)} \iint dxdy\delta n(x,y)\, \vec{E}_{vj}(x,y)\vec{E}_{vj}(x,y) \tag{3-16}$$

Where β_{co} and β_{vj}^{clad} are the propagation constants of the core mode and *vj* cladding mode respectively, Λ is the grating period, and σ_{co-co} and σ_{vj-vj} are the D.C. (period averaged) self –coupling coefficients of the core mode and the *vj* cladding mode, respectively. In equations 3-15 and 3-16, $\Delta\varepsilon(x,y,z) \equiv 2n\delta n$ is used, where $\delta n(x,y,z) = \delta n(z)\, \delta n(x,y)$. As $\delta n \ll n$, $\delta n(x,y,z)$ cannot be assumed uniform [42] across the entire cross-section of the fibre.

If we further define [42] the effective index perturbation for both core mode and cladding mode by equations 3-17 and 3-18,

$$\delta n_{co}^{eff}(x,y) = \frac{\iint dxdy\delta n(x,y)\,\vec{E}_{co-co}(x,y)\;\vec{E}_{co-co}(x,y)}{\iint dxdy\,E_{co-co}(x,y)\;\vec{E}_{co-co}(x,y)} \quad (3\text{-}17)$$

$$\delta n_{vj}^{eff}(x,y) = \frac{\iint dxdy\delta n(x,y)\,\vec{E}_{vj-vj}(x,y)\;\vec{E}_{vj-vj}(x,y)}{\iint dxdy\,\vec{E}_{vj-vj}(x,y)\;\vec{E}_{vj-vj}(x,y)} \quad (3\text{-}18)$$

The TLPG resonant wavelength can be expressed by equation 3-19.

$$\lambda_{max} = [\,(n_{eff,co}\,(\lambda_{max}) - (n_{eff,cl}^{n}\,(\lambda_{max}) + \overline{\delta n(z)}\,(\delta n_{co}^{eff} - \delta n_{vj}^{eff})\,]\,\Lambda \quad (3\text{-}19)$$

In equation 3-19, the relative effective index perturbation between the core and cladding mode, $\delta n_{co}^{eff} - \delta n_{vj}^{eff}$, can have different values depending on the method of grating fabrication. For UV- written LPGs, $\delta n_{co}^{eff} \gg \delta n_{vj}^{eff}$, since the refractive index perturbation is only in the core. For a TLPG, experimental results [42] suggest $\delta n_{co}^{eff} = \delta n_{vj}^{eff}$, as the resonant wavelength does not shift with increased index modulation.

3.6 Conclusions

This chapter describes the theory of tapered optical fibres and their fabrication. It describes the origin of the interference pattern which is observed in the transmission spectrum of a non-adiabatic taper and then summarises the features of adiabatic tapers. Following this, the theory for fabricating tapers with a transition zone profile which has an exponential shape is provided.

Later in the chapter the theoretical background of long period gratings (LPGs) was described with the objective of modelling the spectral characteristics and properties of these devices. Existing LPG models are accurate at predicting the performance of gratings where the core index alone is modified, however limited work has been undertaken to predict the performance of TLPGs fabricated using CO_2 lasers. In this case, the models are more complex due to the addition of a number of different index modulation envelopes that vary with and are perpendicular to, the fibre axis.

3.7 References

[1] A. W. Snyder and J. Love, *Optical Waveguide Theory*, Chapman and Hall, 1983.

[2] L. Ma, K. Tsujikawa, N. Hanzawa and F. Yamamoto, "Design of optical power delivery network based on power limitation of standard single-mode fiber at a wavelength of 1550 nm," *Appl. Opt.*, Vol. 54, No. 12, pp. 3720–3724, 2015.

[3] M. Bass, *Handbook of Optics,* Vol. 2, *Devices, Measurements and Properties*, 1995.

[4] F. K. Fatemi, S. Ravets, J. E. Hoffman, G. Beadie, S. L. Rolston and L. A. Orozco, "Higher order mode propagation in ultra-thin optical fibers for atom traps", *Complex light and optical forces VII*, *Proc. SPIE*, Vol. 8637, pp. 1–7, 2013.

[5] D. Grobnic, S. J. Mihailov, H. Ding and C. W. Smelser, "Bragg grating evanescent field sensor made in bi-conical tapered fiber with femtosecond IR Radiation," *IEEE Photonics Technol. Lett.*, Vol. 18, No. 1, pp. 160–162, 2006.

[6] Y. Tian, W. Wang, N. Wu, X. Zou and X. Wang, "Tapered optical fiber sensor for label-free detection of biomolecules," *Sensors*, Vol. 11, No. 4, pp. 3780–3790, 2011.

[7] A. J. Fielding, K. Edinger and C. C. Davis, "Experimental observation of mode evolution in single-mode tapered optical fibers," *J. Light. Technol.*, Vol. 17, No. 9, pp. 1649–1656, 1999.

[8] L. C. Bobb, P. M. Shankar and H. D. Krumboltz, "Bending effects in biconically tapered single-mode fibers," *J. Light. Technol.*, Vol. 8, No. 7, pp. 1084–1090, 1990.

[9] B. Musa, A. A. Rozi, A. S. M. Noor, A. Ismail and M. A. Mahdi, "Effect of fiber profile parameters on the transmission properties of the tapered optical fibers," *IEEE 2nd International conference on Photonics*, Malaysia, 2011, pp. 1–4.

[10] K. Q. Kieu and M. Mansuripur, "Biconical fiber taper sensors," *IEEE Photonics Technology Lett.*, Vol. 18, No. 21, pp. 2239–2241, 2006.

[11] J. D. Love, W. M. Henry, W. J. Stewart, R. J. Black, S. Lacroix and F. Gonthier, "Tapered single-mode fibres and devices, Part 1 : Adiabaticity criteria," *IEE Proc.*, Vol. 138, No. 5, pp. 343–354, 1991.

[12] C. McAtamney, A. Cronin, R. Sherlock, G. M. O`Connor and T. J. Glynn, "Reproducible method for fabricating fused biconical tapered couplers using a CO_2 laser based process," *Proceedings of the Third International WLT- Conference on Lasers in Manufacturing 2005,Germany,* 2005, pp. 1–5.

[13] R. Black, S. Lacroix, F. Gonthier, and J. D. Love, "Part 2 : Experimental and theoretical quantification," *IEE Proc.*, Vol. 138, No. 5, pp. 355–364, 1991.

[14] G. Cohoon, C. Boyter, M. Errico, K. Vandervoort and E. Salik, "Enhancing the sensitivity of bi-conical tapered fiber sensors with multiple passes through the taper," *Opt. Eng.*, Vol. 49, No. 3, p. 034401, 2010.

[15] S. W. Harun, K. S. Lim, C. K. Tio, K. Dimyati and H. Ahmad, "Theoretical analysis and fabrication of tapered fiber," *Opt. - Int. J. Light Electron Opt.*, Vol. 124, No. 6, pp. 538–543, 2012.

[16] T. A. Birks and Y. W. Li, "The shape of fiber tapers," *J. Light. Technol.*, Vol. 10, No. 4, pp. 432–438, 1992.

[17] A. M. Vengsarkar, P. J. Lemaire, J. B. Judkins, V. Bhatia, T. Erdogan and J. E. Sipe, "Long period fiber gratings as band-rejection filters," *J. Light. Technol.*, Vol. 14, No. 1, pp. 58–65, 1996.

[18] K. O. Hill and G. Meltz, "Fiber Bragg grating technology fundamentals and overview," *J. Light. Technol.*, Vol. 15, No. 8, pp. 1263–1276, 1997.

[19] K. T. V. Grattan and T. Sun, "Fiber optic sensor technology: an overview," *Sensors Actuators A Phys.*, Vol. 82, No. 1–3, pp. 40–61, 2000.

[20] S. A. Vasil'ev, O. I. Medvedkov, I. G. Korolev, A S. Bozhkov, A. S. Kurkov and E. M. Dianov, "Fibre gratings and their applications," *Quantum Electron.*, Vol. 35, No. 12, pp. 1085–1103, 2005.

[21] T. Erdogan, "Fiber grating spectra," *J. Light. Technol.*, Vol. 15, No. 8, pp. 1277–1294, 1997.

[22] T. Erdogan, "Cladding-mode resonances in short and long-period fiber grating filters," *J. Opt. Soc. Am.*, Vol. 14, No. 8, pp. 1760-1773, 1997.

[23] S. W. James and R. P. Tatam, "Optical fibre long-period grating sensors : characteristics and application," *Meas. Sci. Technol.*, Vol. 14, pp. R49–R61, 2003.

[24] V. Bhatia, "Properties and Sensing Applications of Long-Period Gratings," PhD Thesis, Virginia Polytechnic Institute and State University, 1996.

[25] S.W. James, Cranfield University, *Personal communication*, Feb. 2014.

[26] D. D. Davis, T. K. Gaylord, E. N. Glystis, S. G. Kosinski, S. C. Mettler and A. M. Vengsarkar, "Long-period fibre grating fabrication with focused CO_2 laser pulses," *Electron. Lett.*, Vol. 34, No. 3, pp. 302–303, 1998.

[27] V. Grubsky and J. Feinberg, "Fabrication of axially symmetric long-period gratings with a carbon dioxide laser," *IEEE Photonics Technol. Lett.*, Vol. 18, No. 21, pp. 2296–2298, 2006.

[28] R. Kritzinger, D. Schmieder and A. Booysen, "Azimuthally symmetric long-period fibre grating fabrication with a TEM_{01}-mode CO_2 laser," *Meas. Sci. Technol.*, Vol. 20, No. 3, 2009.

[29] X. Liu, M. Yan, L. Zhan, S. Luo, Z. Zhang and Y. Xia, "Controlling of symmetric and asymmetric mode coupling in long-period fiber gratings single-side induced by long-pulse CO_2 laser," *Opt. Commun.*, Vol. 284, No. 5, pp. 1232–1237, 2011.

[30] H. Hamama, M. Ketata, Y. Bouslimani and O. Latry, "CO_2 laser beam based technique for producing optical fiber components", *Applications of photonic technology 6, Proc. SPIE*, Vol. 5260, pp. 154–162, 2003.

[31] D. J. Little, G. D. Marshall and M. J. Withford, "Fabrication of periodic , resonant features in optical fibres using a CO_2 laser micro-tapering system," 2nd *PICALO*, 2006, pp. 383–386.

[32] P. Wang, G. Brambilla, M. Ding, L. Bo, Y. Semenova, Q. Wu and G. Farrell, "Refractive index sensing measurement based on periodically tapered small core single-mode fibre", *22nd Optical Fiber Sensor conference*, Beijing, China, 2012, *Proc. SPIE*, Vol. 8421, pp.1–4.

[33] D. Castro Alves, J. M. P. Coelho, M. Nespereira, F. Monteiro, M. Abreu, and J. M. Rebordão, "Automation methodology for the development of LPFG using CO_2 laser radiation", *8th Ibero-american optics meeting and 11th Latin American Meeting on optics, lasers and applications*, Porto, Portugal , *Proc. SPIE*, Vol. 8785, p. 87854X 1–5, 2013.

[34] H. Hosono, K. Kawamura, N. Ueda, H. Kawazoe, S. Fujitsu and N. Matsunami, "Formation and photo-bleaching of 5 eV bands in ion-implanted SiO_2:Ge and SiO_2 glasses for photosensitive materials," *J. Phys. Condens. Matter*, Vol. 7, No. 26, pp. L343–L350, 1995.

[35] P. J. Lemaire, R. M. Atkins, V. Mizrahi and W. A. Reed, "High pressure H_2 loading as a technique for achieving ultra-high UV photosensitivity and thermal sensitivity in GeO_2 doped optical fibres," *Electron. Lett.*, Vol. 29, No. 13, pp. 1191–1193, 1993.

[36] D. L. Williams, B. J. Ainslie, J. R. Armitage, R. Kashyap and R. Campbell, "Enhanced UV photosensitivity in boron co-doped germanosilicate fibres," *Electron. Lett.*, Vol. 29, No. 1, pp. 45–47,1993.

[37] J. D. Rancourt, *Optical Thin Films: User Handbook*, SPIE, 1996.

[38] Y. Wang, "Review of long period fiber gratings written by CO_2 laser," *J. Appl. Phys.*, Vol. 108, No. 8, p.p. 1-37, 2010.

[39] L. Drozin, P. Fonjallaz and L. Stensland, "Long-period fibre gratings written by CO_2 exposure of H_2-loaded, standard fibres," *Electron. Lett.*, Vol. 36, No. 8, pp. 742–743, 2000.

[40] A. D. Yablon, M. F. Yan, P. Wisk, F. V. Di Marcello, J. W. Fleming, W. A. Reed, E. M. Monberg, D. J. Di Giovanni, J. Jasapara and M. E. Lines, "Refractive index

perturbations in optical fibers resulting from frozen-in viscoelasticity," *Appl. Phys. Lett.*, Vol. 84, No. 1, pp. 19–21, 2000.

[41] A. D. Yablon, M. F. Yan, D. J. Di Giovanni, M. E. Lines, S. L. Jones, D. N. Ridgway, G. A. Sandels, I. A. White, P. Wisk, F. V. DiMarcello, E. M. Monberg and J. Jasapara, "Frozen-in viscoelasticity for novel beam expanders and high-power connectors," *J. Light. Technol.*, Vol. 22, No. 1, pp. 16–23, 2004.

[42] S. Nam, C. Zhan, J. Lee, C. Hahn, K. Reichard, P. Ruffin, K. L. Deng and S. Yin, "Bend-insensitive ultra-short long-period gratings by the electric arc method and their applications to harsh environment sensing and communication," *Opt. Express*, Vol. 13, No. 3, pp. 731–7, 2005.

[43] L. Jin, W. Jin and J. Ju, "Understanding the mode coupling process in a strong long period grating", *Fourth European workshop on optical fibre sensors*, Porto, Portugal, *Proc. SPIE*, Vol. 7653, pp. 76530U 1–4, 2010.

[44] L.-Y. Shao, J. Zhao, X. Dong, H. Y. Tam, C. Lu and S. He, "Long-period grating fabricated using resistive filament heating," *19th International conference on optical fibre sensors*, Perth, Australia, *Proc. SPIE*, Vol. 7004, p. 70044K 1–4, 2008.

4 Experimental system

4.1 Introduction

This chapter describes the experimental arrangement which was used for tapering optical fibres. The various components which make up the system are discussed, together with the control methodology.

The experimental arrangement has evolved over a two-year period as improvements were progressively implemented. For clarity, only the optimized system is described in the following sections.

4.2 Concept optical design

The concept optical design of the fibre tapering rig was developed following a review of the systems that previous researchers have developed to taper fibres [1-7]. Within table 7, the first two columns summarize the components and control methods that have been used by previous researchers and the final column identifies the features which were included within the taper system developed during this work.

The components that were initially used were selected from items that were available within the Engineering Photonics Department at Cranfield University. At an early stage it was decided that an IR camera should be used both to aid the optimization of the fibre temperature distribution and to aid the alignment of the fibre within the focal plane of the laser focussing system. An in-line fibre Bragg grating was chosen for the measurement of the strain applied to the fibre during the tapering process, as previous reports have shown that the incorporation of a load cell into the system can result in misalignment of the optical fibre, which influences the shape of the tapers produced. A charge coupled device (CCD) spectrophotometer and a tungsten light source were used to facilitate the measurement of the transmission spectrum of the optical fibre over the wavelength range 500 - 1150 nm. This allowed the tapering process to be terminated when the desired fibre transmission spectrum was achieved during the process. A

schematic of the conceptual optical design of the optical fibre tapering rig is shown in figure 23, together with the co-ordinate plane definition.

Table 7: Taper rig process features

Number	Taper rig feature	Detail of taper rig feature cited in literature	Taper rig feature to be used in this project.
1	Laser power	10-30 W [2,5]	10 W initially, 25 W used later.
2	Alignment laser	HeNe laser [3,4,8]	HeNe alignment laser
3	ZnSe focussing lens	50-300 mm focal length [1,3]	190.5 mm initially, 100 mm used later.
4	ZnSe lens type	Spherical or cylindrical [3,9]	Cylindrical
5	Scanning mirror	*Either*: no scan, scan in one plane, or scanning in two planes has been used [1,5,7]	Scan in one plane only.
6	Power control method	Laser power adjusted manually by attempting to achieve constant incandescent emission using un-aided eye [6].	Pre-programmed power profiles derived using information gained from imaging the heated fibre using an NIR camera.
7	Fibre alignment.	HeNe laser [3,4,8]	NIR camera and HeNe laser
8	Fibre tension control	Load cell used by one group [10]	Fibre Bragg grating
9	Fibre translation.	*Either*: using weights or using linear translation stages [1,6]	Rotational translation stages.
10	In-process optical assessment.	Laser diode and power meter [6,10]	Spectrophotometer and tungsten light source.

The experimental layout is shown in figure 24. The output from the CO_2 laser was used to heat the fibre and ZnSe optical elements were used for power tapping and injecting the HeNe alignment laser into the path of the CO_2 laser beam. The galvanometer-mounted mirror was driven with a triangular waveform to provide uniform illumination along the section of fibre to be tapered. A cylindrical ZnSe lens was used to produce a

focussed line along the x-plane. A cylindrical lens was chosen over a spherical lens as it produces an elliptically shaped focussed spot, which is more efficient for scanning along the narrow fibre. The major axis of the elliptical spot was aligned parallel with the fibre axis and the minor axis was perpendicular to the fibre axis.

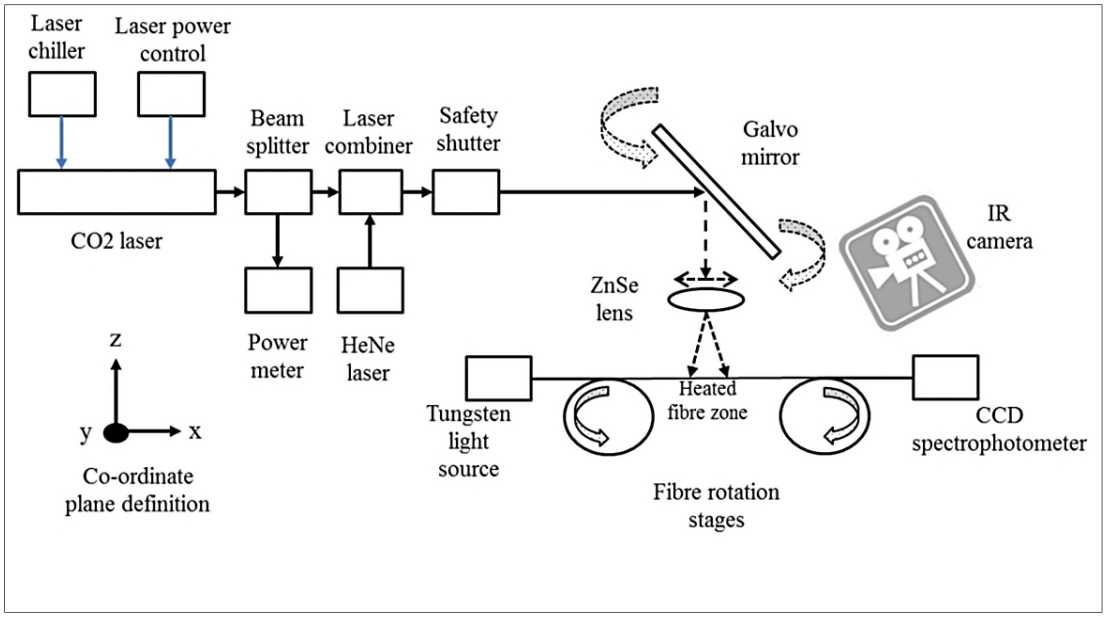

Figure 23: Conceptual design of the tapering rig.

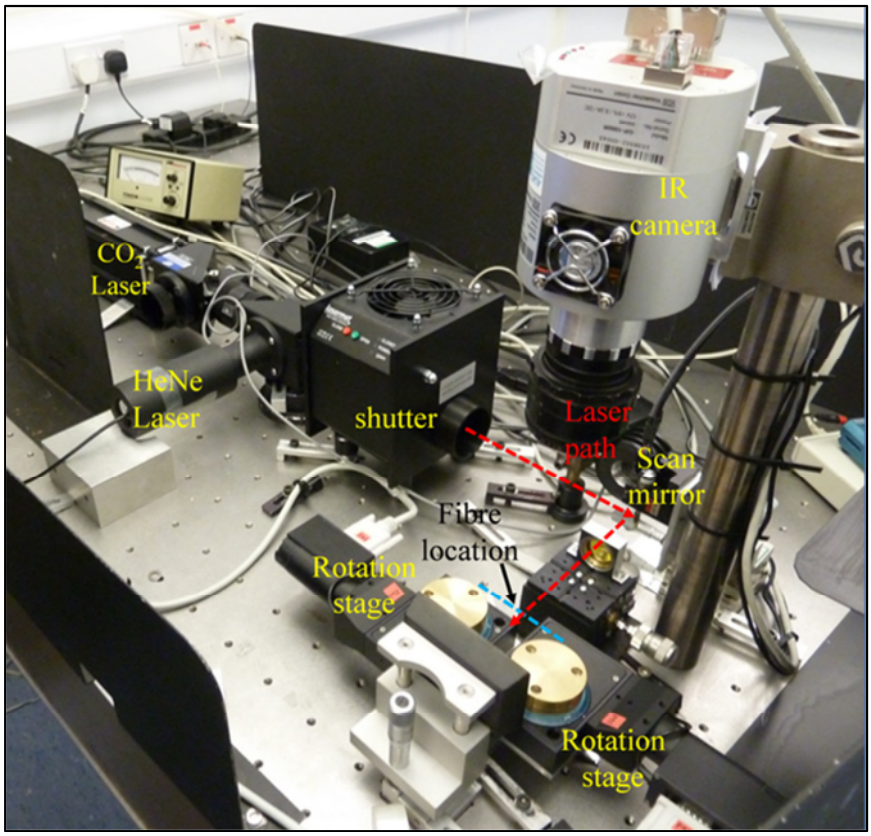

Figure 24: Experimental layout of the taper rig.

4.3 Optical component review

4.3.1 CO_2 Laser

The CO_2 laser used in the initial stages of this research was a Synrad 48-1 laser, which has a specified typical output power of 10 W. As the development of the system progressed, it was identified that a higher power laser was required, as the minimum taper waist diameter that could be fabricated was limited to 20 μm, using the 10 W laser. Below this diameter, the fibre would break as the fibre solidified due to insufficient laser power. To resolve this issue, a Synrad 48-2 laser was purchased. This laser has a maximum output power of typically 25 W and also has improved power stability. The summary specifications for both lasers are given in table 8. To improve

the power stability of both lasers, the cooling water was provided by a Termotek P1020 chiller operating at a temperature of 18 ± 0.1 ^{0} C. Before the laser was operated, the cooling water was circulating for at least one hour. The rationale for these specific parameter values is discussed in section 5.2.1.

To control the laser output power, two pulse-width modulated (PWM) signals were generated in a TTL format. The first signal was a constant "tickle signal" that initiates the CO_2 laser plasma at low powers. This is a square wave with a repetition rate of 5 kHz and a pulse width or time duration of 1.0 µs.

Table 8: CO_2 laser - Summary specifications [11].

Characteristics	**Model – Synrad 48-1**	**Model – Synrad 48-2**
Typical power output	10 W	25 W
Wavelength	10.2 to 10.8 microns	10.2 to 10.8 microns
Beam diameter/divergence	3.5mm/ 4mR	3.5mm/ 4mR
Mode	TEM_{00} , 95% purity, M^2 <1.2	TEM_{00} , 95% purity, M^2 <1.2
Polarisation	Linear – vertical 50:1	Linear – vertical 50:1
Power control	Pulse width modulation – to 20 kHz.	Pulse width modulation – to 20 kHz.
Power stability from cold start	± 10 %	± 5 %
Cooling water (18-23 ^{0}C)	1.9 L min.$^{-1}$	3.0 L min.$^{-1}$

The second signal is also a square wave, with a repetition rate of 10 kHz but with a duration that is adjustable from 1.0 µs to 0.1 ms. The second signal provides the power control for the laser. A pulse duration of 1.0 µs (this equates to a 0% duty cycle), results in zero power being emitted from the laser, while a long pulse duration of 0.1 ms (100% duty cycle), produces 100% of the available laser power. These two signals were generated using LabVIEW software in conjunction with a National Instruments USB-6251 data acquisition module. Examples of typical waveforms are shown in figures 25 and 26.

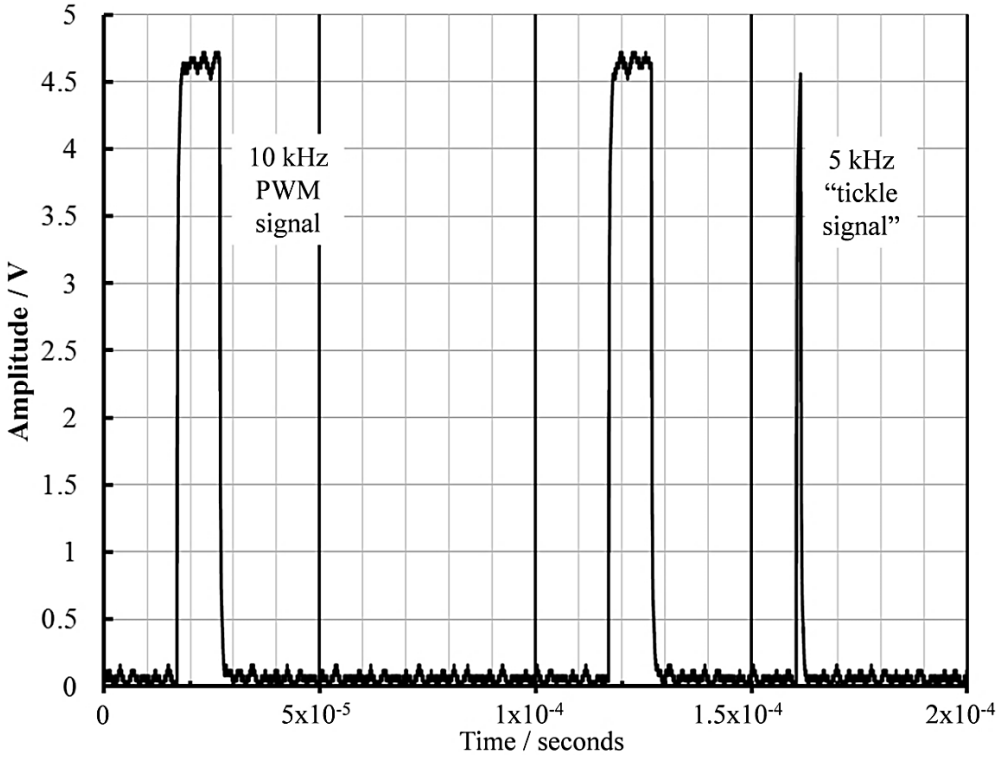

Figure 25: Pulse width modulation (PWM) and "tickle signal" driving waveforms at a 10 % duty cycle. This corresponds to a laser power of 2.4 W at the laser-combiner.

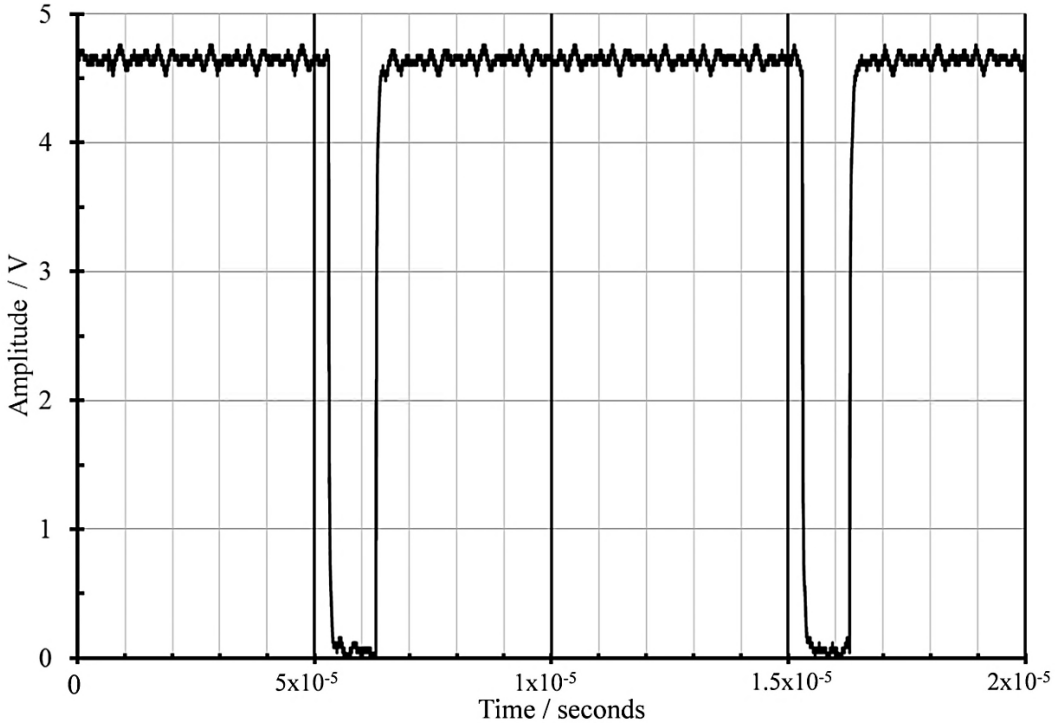

Figure 26: Pulse width modulation (PWM) driving waveform at a 90 % duty cycle. This corresponds to a laser power of 19.3 W at the laser-combiner.

The output power of the Synrad 48-2 laser as a function of duty cycle is shown in figure 27. The solid curve represents the power measured at the scanning mirror and the dashed curve represents the power output from the beam-splitter (B/S) tap. The power meter used to make these measurements was a PM 5100 (Molectron) which has an accuracy of ± 3%.

The laser beam profile changes to circular/ near Gaussian shape at a distance of 0.6 m from the laser exit window [11].The quoted [11] M^2 for this laser is < 1.2, whereas for a perfect [12] Gaussian beam, $M^2 = 1$. To ensure an optimal focussed spot size, the focussing optics were located greater than 0.6 m from the laser.

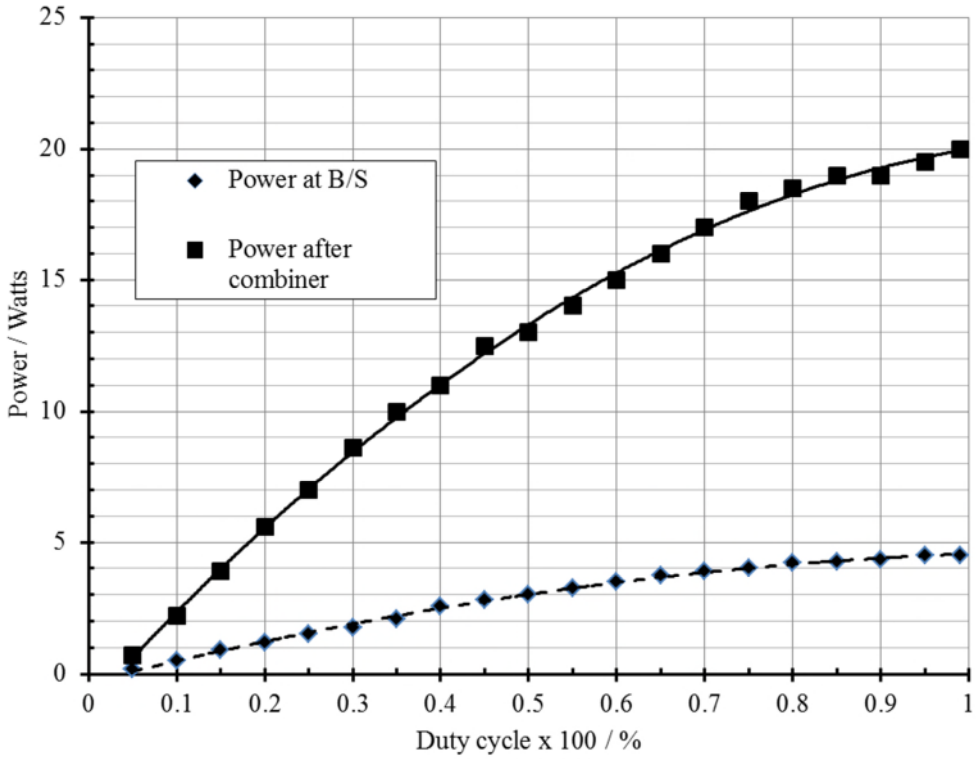

Figure 27: Synrad 48-2 laser power versus duty cycle at a PWM frequency of 10 kHz.

4.3.2 HeNe laser

To assist in the alignment of the CO_2 laser beam with respect to the optical fibre, a low power (1mW) HeNe alignment laser was injected into the main beam path using the

beam combiner described in section 4.3.3.2. This was aligned such that it was coaxial with the CO_2 beam. The method used to align the beams is described in appendix C of this thesis.

4.3.3 Beam sampling optics

4.3.3.1 Beam splitter

The output from the laser is transmitted through a beam-splitter, which samples the total beam, allowing the laser power to be monitored during the tapering process. The beam-splitter used was a TBU25 manufactured by ULO Optics. It comprises of a ZnSe window inclined at ~ 45 degrees to the beam axis. As the optical specification for this component was unknown, the split ratio of the beam splitter was measured experimentally. The beam-splitter was tested in isolation by measuring the power at the exit ports and the split ratio was found to be 83:17. The first number is the percentage transmitted light and the second number is the light reflected to the sampling port. Minimal optical absorption was detected in this component at 10.6 μm. The laser damage threshold is rated at 1.4 kW/cm^2, so it was adequate for this application.

4.3.3.2 Laser combiner

The primary output from the beam-splitter passes through a laser combiner, where the output of the HeNe laser is injected. After the laser combiner, the HeNe beam co-propagates with the CO_2 laser beam. The combiner used was a TBU25 component with an unknown coating on the angled ZnSe internal window surfaces. As the optical specification for this component was unknown, the transmission of the combiner was measured experimentally. The light transmitted at a wavelength of 10.6 μm was measured to be 92 %. The reflective surface on one of the window faces ensures that an adequate level of 633 nm laser light is reflected in the same direction as the transmitted 10.6 μm laser light. The laser damage threshold is rated at 1.4 kW/cm^2, so it was adequate for this application.

4.3.4 Focussing lens

A ZnSe plano-convex cylindrical lens was used to focus the output from the CO_2 laser to an elliptical spot. The lens was supplied by II-VI Infrared Optics and is an anti-reflection coated component which has a laser damage threshold of > 1.4 kW/cm^2.

An elliptical spot is preferred over a circular spot as the major axis of the ellipse can be aligned parallel to the fibre when the elliptical spot is swept by the scanning mirror in the x-plane. The selection of the focal length of the lens is crucial for tapering fibres as it determines both the focused power density at the fibre, and hence fibre temperature, and the positional tolerance on the placement of the fibre within the focussed spot.

The lens used initially, acquired before the start of this work, had a focal length of 190.5 mm. Subsequently, a lens of 50 mm focal length was trialled. It was found however, that the use of a 50 mm lens placed tight tolerances on the positional location of the fibre in the y and z planes. It was difficult to meet these tolerances in practice as the fibre invariably translates in x, y, z space due to thermal expansion during heating. It was found that a lens of focal length 100 mm in the optimized experimental arrangement described in section 4.2 gave the required flux density to repeatedly taper optical fibres to waist diameters of ~ 5 μm, while not placing stringent demands on the physical positioning of the fibre within the focussed beam.

To calculate the theoretical spot-size [12] of a Gaussian beam, equation (4-1) was used:

$$\mathrm{d} = \frac{4M^2\lambda f}{\pi D} \tag{4-1}$$

Where: f is the lens effective focal length

D is the input beam diameter at the lens

d is the diameter of the focussed spot

λ is the wavelength of the laser

M^2 is the beam quality factor of the laser derived from the laser data sheet

The calculated spot sizes are given in table 9.

Table 9: Focussed spot dimensions and depth of focus for various lens focal lengths

Focal length / mm	**Minor axis distance* / µm**	**Major axis distance* / mm**	**Depth of focus / mm**
190.5	765	3.5	± 25.2
100.0	388	3.5	± 6.94
50.0	190	3.5	± 1.74

Note: (*) this refers to the $1/e^2$ value.

ZnSe has refractive indices of 2.4028 at 10.6 µm and 2.6 at 0.633 µm [12]. As a result the focussed spot size for the HeNe alignment laser will be different and occur at a shorter focal length than for the CO_2 laser beam.

The unjacketed optical fibre has a diameter of ~ 125 µm, and the use of a lens of focal length 190.5 mm will produce a system more tolerant of fibre positional errors in the y-plane, compared to the 50 mm lens, where the margin is only ± 33 µm. However, the laser energy density within the focussed spot is much higher when using shorter focal length lenses. If an even smaller spot size is required, then a beam expanding telescope [12] can be used to increase D in equation (4-1).

The calculated depth of focus for each of the three lenses is also given in table 9. The definition of depth of focus used here *"is an increase in the beam diameter by 5 %"*. The equation [12] used to calculate this parameter (4-2), is given below:

$$\text{depth of focus} = \frac{2\lambda}{\pi}\left(\frac{2F}{D}\right)^2 \qquad (4\text{-}2)$$

Where the terms are as defined for equation 4.1.

The use of the 100 mm focal length ZnSe cylindrical lens allowed the required laser flux density to be produced at the fibre and, together with the beam waist and Rayleigh range, provided acceptable tolerances on the alignment requirements in the x, y and z planes (figure 23). The use of a lens of a shorter focal length (e.g. 50 mm), was found to impact on the tolerances required in the mechanical aspects of the fabrication system. For example, a smaller depth of focus would result in a significant variation in the laser flux density at the fibre during the tapering process as the fibre can bow in the z-direction, particularly if the rate at which the fibre is pulled is slower than the rate of increase of length due to thermal expansion. In the y-direction, the use of a shorter focal length lens reduces the beam width, reducing the tolerance on the location of the central axis of the fibre relative to the centre of the beam along its short elliptical axis. Conversely, if the lens focal length was too long for a given laser power, then the focussed spot was too large, reducing the flux density available to heat the fibre to produce smaller diameter tapers.

4.3.5 Near infrared camera

A Vosskuhler NIR-300P near infrared camera was used to image the heated fibre. This camera has a spectral response from 900-1700 nm and has an active area of 9.6 mm x 7.68 mm. It comprises of 320 x 256 pixels with an individual pixel size of 30 x 30 μm. The focussing optic used with this camera was a Helios 44-2 camera lens. It has a F/2-16 aperture size with a focal length of 58 mm. The objective lens of the camera was located 100 mm from the fibre viewing in the y-direction. The InGaAs detector in the camera was shielded from any scattered 10.6 μm radiation by the glass camera lenses which have a transmission window in the range 0.4 μm to ~ 3.0 μm and are opaque at 10.6 μm.

As the spectral response of the NIR camera is 900 -1700 nm, it is sensitive to the black-body thermal emission spectra from the heated fibre. The camera spectral response and calculated Planck radiated power curves for a range of temperatures near the fibre melting point of 1183 K are given in figure 28. The black body emission curves were calculated for a range of temperatures [13] using equation 4-3.

$$\rho = \frac{2hc^2}{\lambda^5} \frac{1}{e^{\frac{h\nu}{kT}} - 1} \quad (4\text{-}3)$$

Where: Planck's constant, h= 6.63 x 10^{-34} J s

Speed of light, c = 3.0 x 10^{8} ms^{-1}

Wavelength of radiation, λ= m

Frequency of radiation, ν= c / λ

Boltzmann constant, k= 1.38 x 10^{-23} JK^{-1}

Blackbody temperature, T= K

Thus the camera can detect the emitted blackbody radiation once the fibre temperature exceeds ~ 773 K and with increasing sensitivity up to and beyond the melting point of the fibre. In figure 29, the calculated camera responsivity [14] as a function of temperature is shown.

It was not possible to measure the actual fibre temperature at this stage of the work, as this requires accurate data on the fibre emissivity, which is a function of temperature. In addition, the reduction of the fibre diameter and hence radiant area during the tapering process complicates further the fibre temperature measurement.

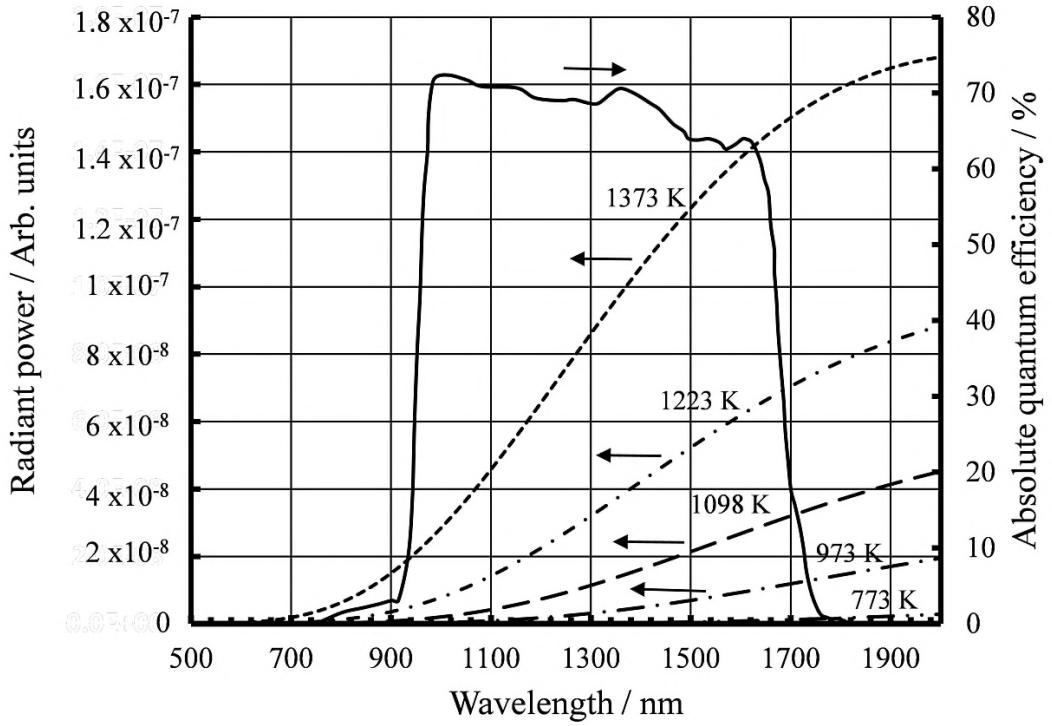

Figure 28: Spectral response of NIR-300P camera (solid curve) and calculated Planck radiated power curves (dashed curves) as a function of temperature.

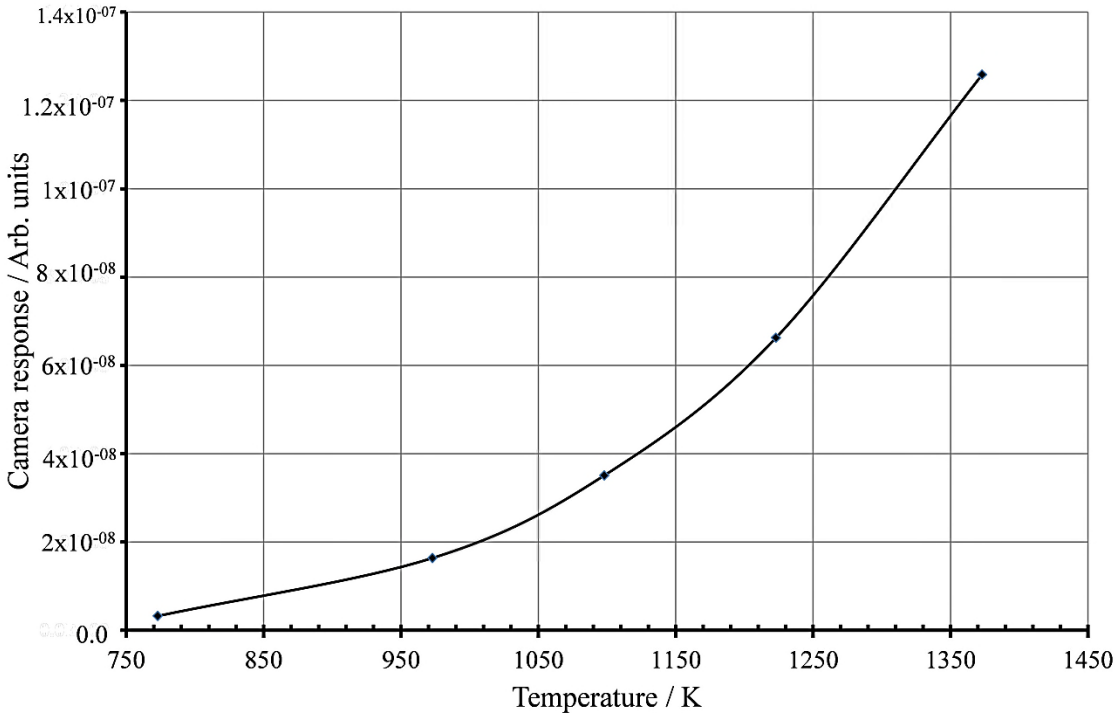

Figure 29: Theoretical NIR-300P camera responsivity as a function of black body emission temperature.

4.3.6 Spectrophotometer

The optical transmission of the fibre was measured during the taper process with an Ocean optics, CCD spectrophotometer (S2000) and a tungsten light source (HL-2000). The spectrophotometer had a spectral range of 530-1100 nm with a spectral resolution of ~ 1.0 nm.

4.4 Opto-mechanical components

4.4.1 Safety shutter

For laser safety, a shutter (LS-10-12, supplied by Lasermet) was included in the beam path, with the associated laser warning signage and door access interlocks. A shutter rated to 10 W was initially used, however when the laser was later upgraded, a 100 W variant was used (LS-100-12).

4.4.2 Galvonometer mirror

The galvanometer mounted mirror was a Cambridge Technology 6210 component. This was selected due to its compact size and its frequency response. The original scanner mirror was designed for low power, visible-wavelength applications, so the mirror was replaced with CO_2 laser-specific variant. This mirror provides high reflectivity at 0.633 µm and 10.6 µm, coupled with a laser damage threshold of 1 kW/cm^2 (average power) over a ± 15.0 degrees angular incidence range. The mirror was mounted so that it rotated about the y-axis, as shown in figure 23. The dimensions of the mirror used were ~ 13 mm x 9.7 mm, thus the scanning system could accommodate a 3.5 mm diameter beam incident at 45^0. The combined transmission loss associated with the scanning mirror and ZnSe cylindrical lens is 2.3%. The system energy loss associated with laser light travelling from the laser to the lens focal plane is 25.4%, with most energy being lost in the beam-splitters.

The mirror was driven with a 100 Hz triangular waveform to provide uniform illumination along the section of fibre to be tapered. A triangular waveform was found to give improved uniformity compared to a sinusoidal driving waveform, as it provided

a constant mirror velocity over the driving cycle. The 100 Hz frequency was found to be the optimum trade-off between mirror motion linearity, which decreased with increasing frequency, and mirror speed, as the sweep of the laser beam along the fibre was fast enough to ensure the fibre did not have time to cool between successive passes of the beam.

4.4.3 Fibre rotation stages and mount

Two rotary stages were used to support and stretch the fibre. The rotary stages were modified with 50 mm diameter brass capstans, which were inscribed with precision v-grooves around the capstan circumference. These grooves ensured reproducible fibre placement in the focal plane of the CO_2 laser. The stages are fixed to a plate whose height was adjustable in the y-axis (figure 23) using a micro-meter with an accuracy of 10 μm.

A steel plate was positioned immediately behind the fibre, acting as both a beam dump and an optical screen. The surface was lightly sand-blasted to produce a non-specular surface. The experimental set-up for the PI Instrumente M-60.DG rotation stages is shown in figure 30.

These rotation stages were used in the optimized taper system as they allow the option of variable velocity control, so allowing tapers to be made with bespoke taper profiles. A summary of the performance of the rotation stages is given in table 10. When tapers were fabricated using this system, the tangential velocity of both stages was set to 61 μm s^{-1}. As the stages rotate in opposite directions when pulling the fibre, the net fibre pulling rate is 122 μm s^{-1}. The rationale for selecting these specific values is discussed in section 5.2.6.

Table 10: Specifications for the M-60.DG stages

Stage Parameter	Value
Min. incremental motion	0.16 μm
Backlash	5 μm
Unidirectional repeatability	1.25 μm
Maximum speed	16 deg. s^{-1}

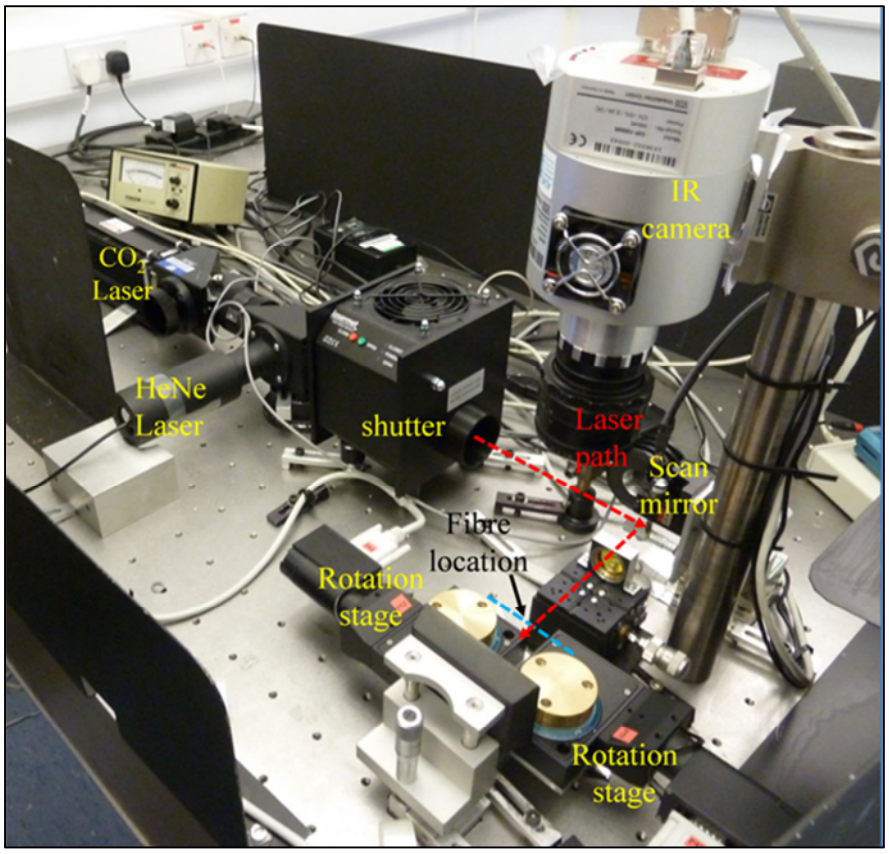

Figure 30: Experimental arrangement of rotation stages.

4.5 Computer control methodology

This section describes how the various components of the taper rig were controlled via a personal computer and provides a schematic of the electrical interconnections. The components described in sections 4.3 and 4.4 were controlled using a combination of LabVIEW, a graphical programming language and the software interfaces which were supplied with the components. The laser and galvanometer mirror scanner were controlled via LabVIEW, the rotation stages were controlled by PIMikroMove and the Ocean Optics spectrophotometer and NIR camera were driven by their own software. An overview of the capabilities of the software control is given below.

CO_2 Laser

The LabVIEW software used for control of the CO_2 laser generates two pulsed signals: the PWM signal and the "tickle signal". The frequency and duty cycle of both signals is variable, with the PWM signal controlling the output power of the laser. The PWM signal as a function of time, is fully programmable using the "arbitrary waveform function" within LabVIEW. The "tickle signal" maintains the laser plasma below lasing threshold and ensures that the laser functions reliably when operating at low power levels. The phase delay between the two laser control signals can also be adjusted.

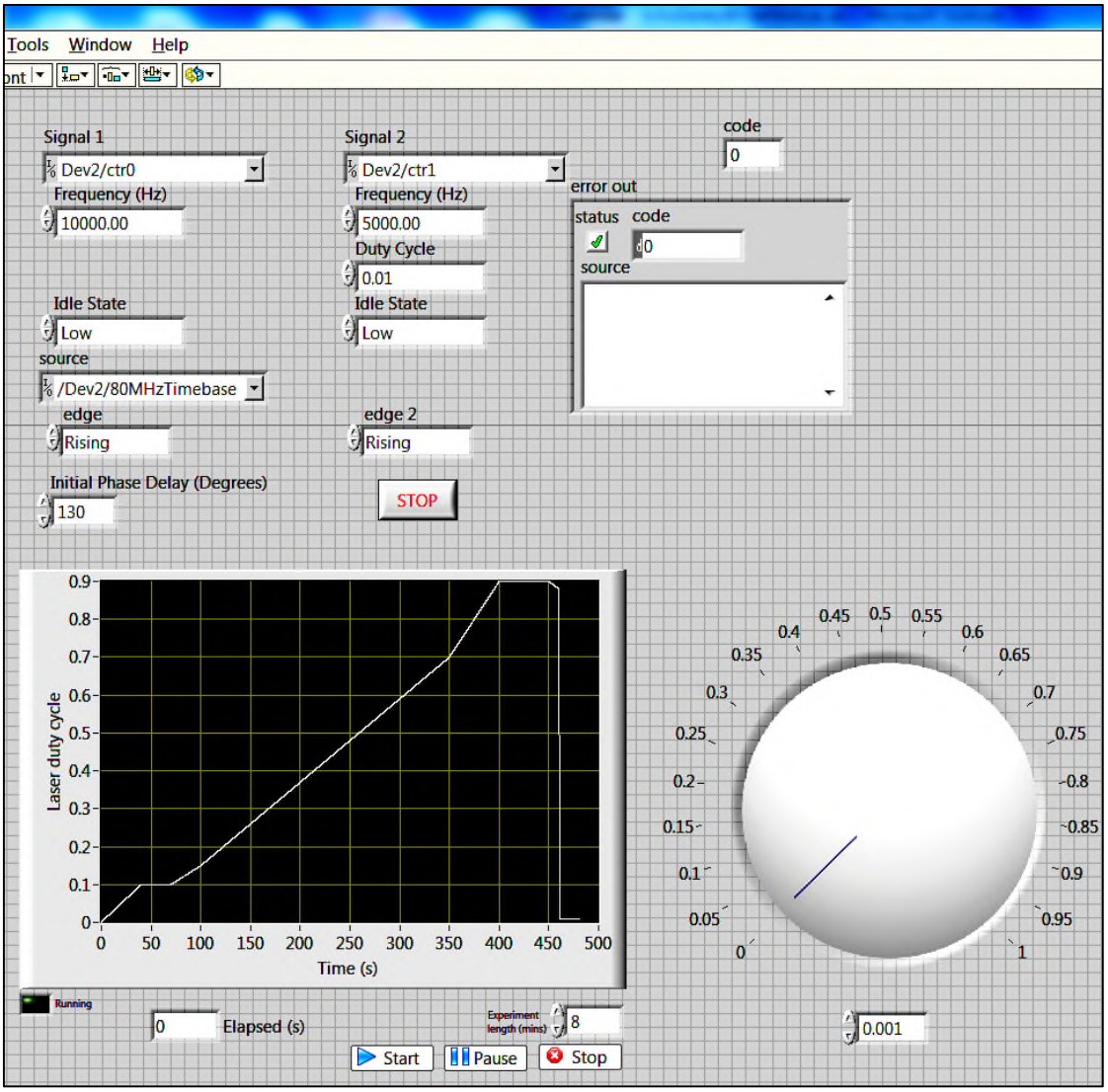

Figure 31: LabVIEW graphical user interface (GUI) for the CO_2 laser controller.

Different laser power profiles can be stored as separate '.lvm' files. As well as functioning in automatic mode, the CO_2 laser can also be operated in manual mode using the dial on the lower right of the laser control graphical user interface (GUI) shown in figure 31.

Galvonometer scanning mirror.

LabVIEW generates the waveform that drives the scanning mirror. The signal shape, amplitude and frequency are programmable from the scanning mirror GUI. A 100 Hz triangular waveform is used to rotate the mirror at a constant velocity about the y-axis. The LabVIEW code used for controlling both the CO_2 laser and scanning mirror are provided in appendices A and B of this thesis.

CCD spectrophotometer

The Ocean optics spectrophotometer is controlled using proprietary software. The CCD spectrophotometer and a tungsten-halogen light source are used to facilitate the measurement of the transmission spectrum of the optical fibre over the wavelength range 500 - 1150 nm, which allowed the tapering process to be terminated when the desired transmission spectrum is achieved.

PIMikroMove stages

The GUI for the rotation stages are shown in figure 32. The two rotation stages are controlled from this interface, allowing control of rotational velocity and direction.

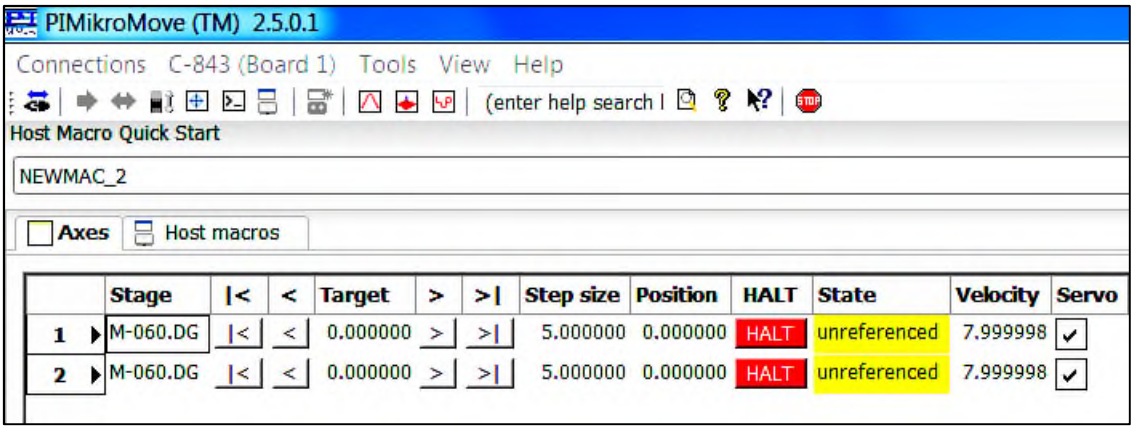

Figure 32: The graphical user interface for the rotation stages**.**

NIR Camera

The NIR camera is used to aid the alignment of the heated fibre within the focused laser spot and to observe both the thermal intensity distribution along the fibre and any displacement of the fibre ("bowing") during the tapering process.

An electrical schematic for the optical fibre tapering rig is shown in figure 33. The key components are controlled by a personal computer which houses the drive cards.

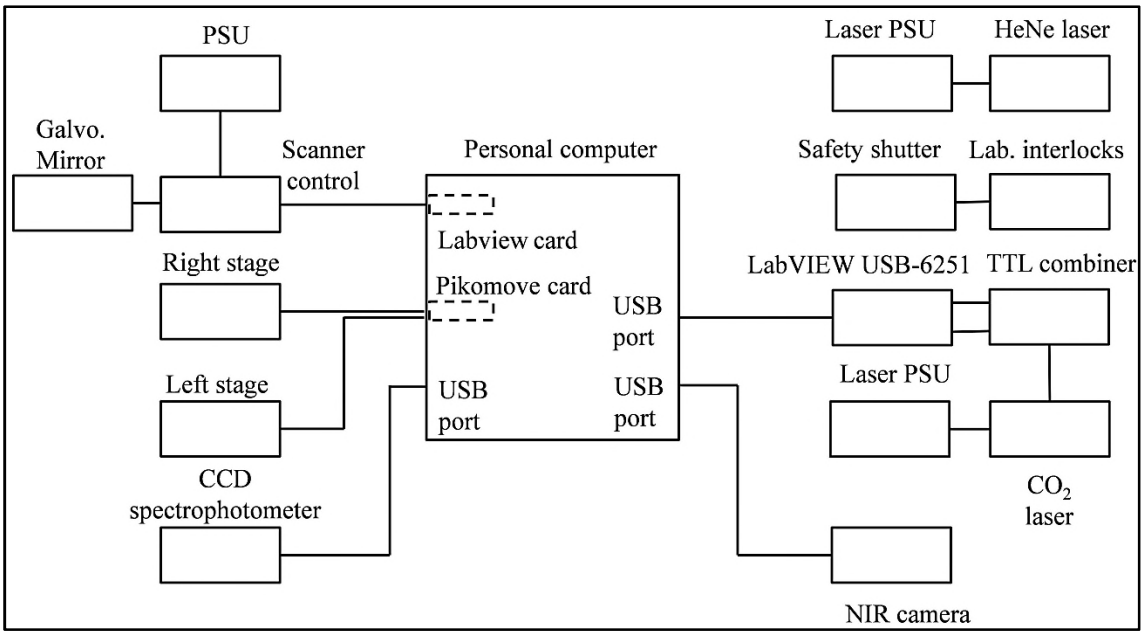

Figure 33: Electrical schematic for taper rig.

4.6 Conclusions

In this chapter, the experimental arrangement developed for tapering optical fibres is described. Detailed descriptions of the performance of each component comprising the system have been provided together with the control methodology and user interfaces.

The use of a NIR camera operating over 900-1700 nm for this application is novel and allows both the fibre to be accurately aligned to the focussed laser spot and allows observation of the heated fibre during the tapering process.

Future work could consider improving the degree of process automation. At present the timing of the rotation stages is controlled manually, it would be possible to operate these devices in a LabVIEW environment, so allowing process to be entirely automated for the operator.

4.7 References

[1] H. Yokota, E. Sugai and Y. Sasaki, "Optical irradiation method for fiber coupler fabrications," *Opt. Rev.*, Vol. 4, No. 1A, pp. 104–107, 1997.

[2] A. J. C. Grellier, N. K. Zayer and C. N. Pannell, "Heat transfer modelling in CO_2 laser processing of optical fibres," *Opt. Commun.*, Vol. 152, pp. 324–328, 1998.

[3] T. E. Dimmick, G. Kakarantzas, T. A. Birks and P. St. J. Russell, "Carbon dioxide laser fabrication of fused-fiber couplers and tapers," *Appl. Opt.*, Vol. 38, No. 33, p. 6845-6848, 1999.

[4] A. Malki, O. Latry, M. Ketata, F. Van Lauwe, L. Bachelot, P. Royer and V. Lauwe, "Microlenses-fibers fabricated by melting-tapering process using CO_2 laser, *Conference on Optical Engineering for Sensing and Nanotechnology*, Yokohama, Japan, 1999, Vol. 3740, pp. 432–437.

[5] F. Bayle and J. P. Meunier, "Efficient fabrication of fused-fiber biconical taper structures by a scanned CO_2 laser beam technique.," *Appl. Opt.*, Vol. 44, No. 30, pp. 6402–11, 2005.

[6] J. M. Ward, D. G. O'Shea, B. J. Shortt, M. J. Morrissey, K. Deasy and S. G. Nic Chormaic, "Heat-and-pull rig for fiber taper fabrication," *Rev. Sci. Instrum.*, Vol. 77, No. 8, p. 083105-1/6, 2006.

[7] M. Li, F. Pang, H. Guo, Y. Liu, N. Chen, Z. Chen and T. Wang, "Tapered optical fiber fabricated by high-frequency pulsed carbon dioxide laser," *Advanced sensors systems and applications IV, Proc. SPIE*, Vol. 7853, pp. 78533E1–6, 2010.

[8] M. I. Zibaii, A. Kazemi, H. Latifi, M. K. Azar, S. M. Hosseini and M. H. Ghezelaiagh, "Measuring bacterial growth by refractive index tapered fiber optic biosensor," *J. Photochem. Photobiol. B Biol.*, Vol. 101, No. 3, pp. 313–320, 2010.

[9] M. Sumetsky, Y. Dulashko and A. Hale, "Fabrication and study of bent and coiled free silica nanowires: Self-coupling microloop optical interferometer.," Opt. Express, Vol. 12, No. 15, pp. 3521–31, 2004.

[10] A. J. C. Grellier, “Characterisation of optical fibre tapering using a CO_2 laser”, PhD Thesis, University of Canterbury, 2000.

[11] “Series 48, Laser Operators Manual M Version”, Synrad Inc., 2011.

[12] J. Ready, Laser Institute of America Handbook of Laser Materials Processing, 2001.

[13] W. G. Rees, Physical Principles of Remote Sensing, Cambridge University Press, 2001.

[14] G. Vosskuhler, “NIR-300”, VDS Vosskuhler, 2010.

5 Process descriptions for tapering fibres

5.1 Introduction

This chapter summarises the optimized processes that have been developed for fabricating reproducibly, single tapers with waist diameters down to 5 μm and for making TLPGs. This taper waist diameter was chosen as the objective was to use the tapers for bio-chemical sensing applications [1, 2, 3] where typically waist diameters of 5-20 μm tend to be used. Tapers below a 5 μm waist diameter are very fragile to handle, during experimental trials. Summary process descriptions are provided for fabricating single tapers and TLPGs. In addition to summarising the processes, the origin for the various parameters that were used in the fabrication of these devices is also described in the following sections.

5.2 Method for tapering fibres

The experimental configuration used for tapering optical fibres is shown in figure 30 (section 4.4.3). A detailed description of the various components used is provided in chapter 4 of this thesis.

The key process steps for fabricating a taper are:

1) Switch on the laser water chiller – water temperature 18 ^{0}C.
2) Ensure that both lasers are aligned with the fibre in accordance with appendix C. Usually this step is only required if components in the optical system have been moved since the last alignment.
3) Prepare the fibre ends for connection to monitoring equipment and remove a 20 mm length of buffer jacket from the section of fibre to be tapered. Clean the stripped section of fibre using a lens tissue soaked in alcohol.
4) Attach the fibre to the rotation stages.
5) Switch on the galvanometer and apply a 100 Hz triangular waveform.

6) Switch on the HeNe laser. Adjust the height of the optical fibre relative to the laser beam using the translation stage on which the rotation stages are mounted, such that a symmetric diffraction pattern with uniform intensity, is observed on the metal plate behind the fibre.
7) Select the required laser power ramp profile on the LabVIEW GUI. Switch on the CO_2 laser.
8) Using NIR camera, adjust the position of the fibre relative to the centre of the CO_2 laser beam by adjusting the height of the rotation stages for the brightest image, while on the low power section of the power ramp profile.
9) Switch on the rotation stages, to start forming a taper.
10) After the required taper pulling time has elapsed, switch off the rotation stages and laser.
11) Remove tapered fibre from stages.

The specific steps which are of importance in producing reproducible tapers are discussed in the following sections.

5.2.1 Laser chiller – step 1.

The output power of the Synrad 48-1 laser was found to be sensitive to the temperature of the circulating cooling water. Experiments were undertaken at differing laser output powers and varying the chiller water temperature. The results are shown in figure 34. Operating the laser water chiller at a temperature of 18.0 ± 0.1 ^{0}C appears to optimise the power efficiency of the laser and produces the highest power. Operating the laser at water temperatures below 18 ^{0}C is undesirable, as moisture condensation occurs on the laser hardware, increasing the risk of component failure.

The laser chiller should be functioning one hour before it is used to produce tapers, to allow the laser to stabilize at 18 ^{0}C.

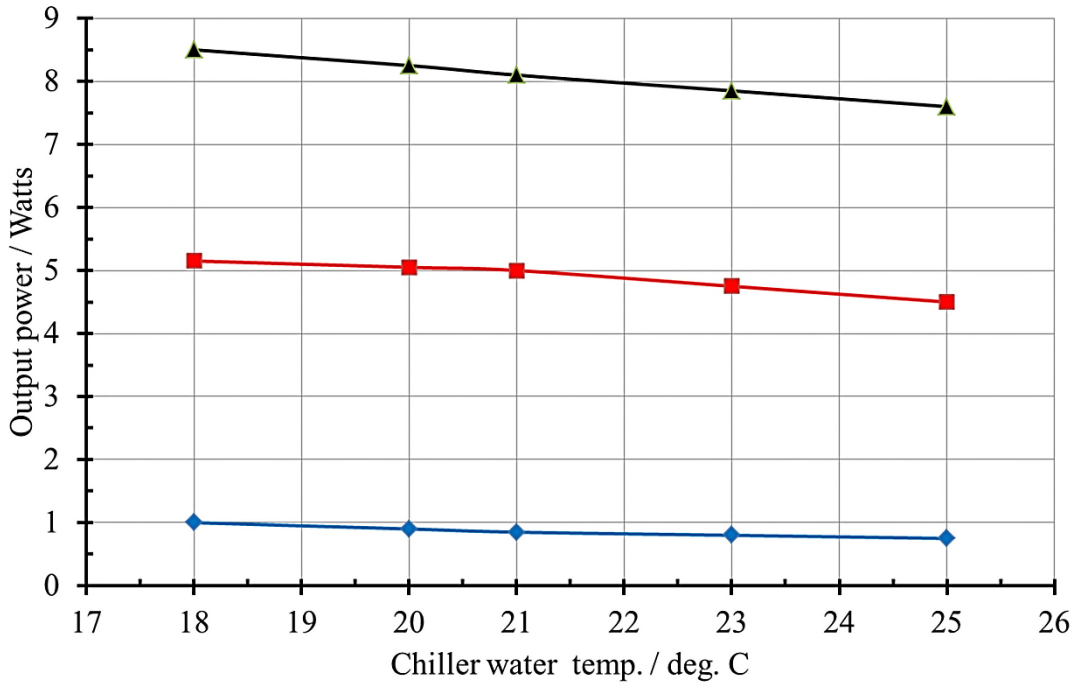

Figure 34: The CO_2 laser output power under three differing power levels when the chiller water temperature is changed (the measurement of power has a resolution of ± 3%).

Using a water chiller, instead of the laboratory cooling water supply, is required for the taper process as it improves the power stability of the laser. This is shown in figure 35 where the chiller water temperature is compared to the laboratory cooling water supply in terms of its effect on the power stability of the laser. The laser power stability using the chiller is ± 3.6 % compared to ± 9 % using laboratory cooling water.

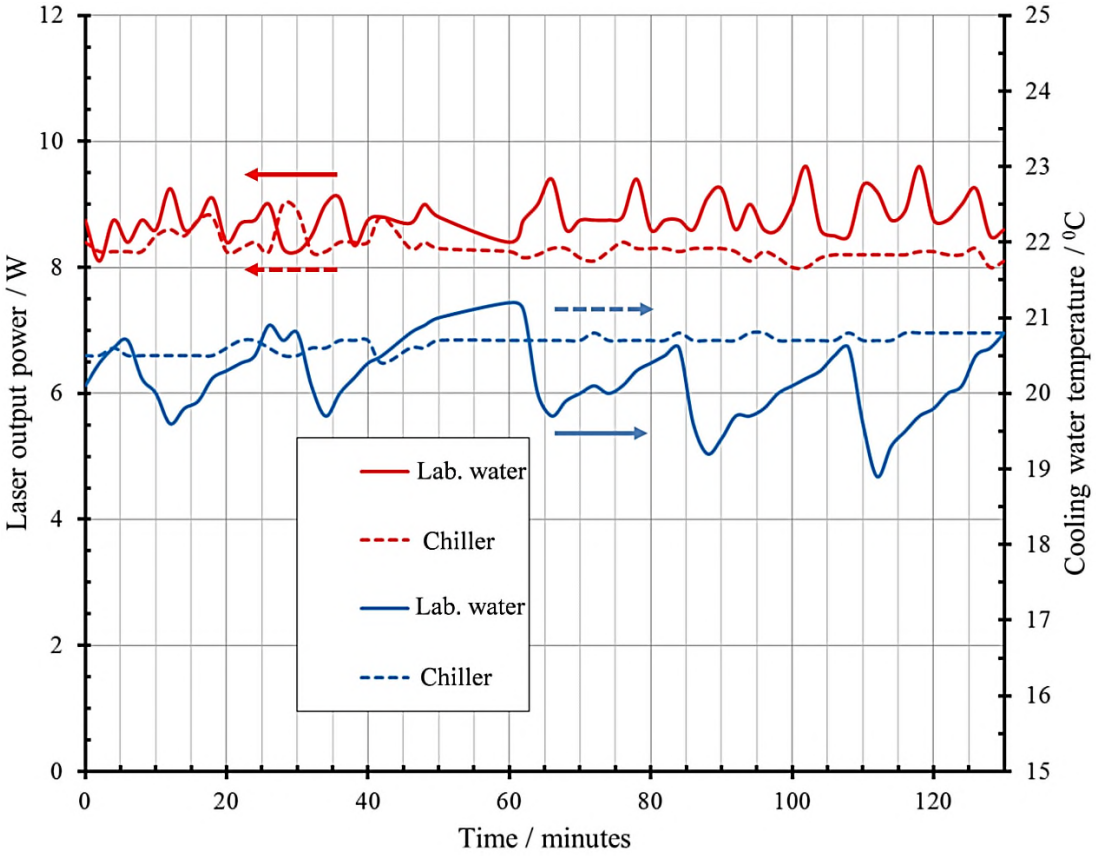

Figure 35: The Synrad-48.1 laser power variation achieved with laboratory water compared to chiller water (red curves). Temperature variation of laboratory water compared to chiller water, measured at the laser (blue curves).

5.2.2 Laser alignment – step 2

To obtain symmetric tapers with reproducible geometry, it was found that the alignment procedure described in appendix C should be used. The laser alignment procedure has the following aims:

a) To ensure that both the CO_2 and HeNe laser beams are coaxial with respect to each other and parallel to the optical table.
b) To ensure that the CO_2 beam centre is incident on the rotation axis of the galvanometer mirror.

c) To ensure that the ZnSe cylindrical lens is accurately aligned about the z-axis, so that when the mirror scans the beam along the fibre, the focussed spot travels parallel to the longitudinal axis of the fibre.

5.2.3 Fibre attachment to rotation stages – step 4

To obtain reproducible tapers it is important the fibre is placed in the focal plane of the scanning laser. To achieve this, a v-groove was machined into the brass capstans attached to the rotation stages. The groove width was 345 ± 15 μm and the depth was 172 ± 15 μm. The accuracy of the groove measurements was determined by the lathe tool which had an accuracy of ± 15 μm. These dimensions ensured the jacketed fibre (diam. ~ 245 μm) was both located in the groove and the outer surface was also proud of the capstan surface, so allowing adhesive tape to be used to hold it in position. The fibre is attached to the stage with a strip of 3M "Magic tape". This tape is preferred over other tapes as it was found to have a consistent adhesion between different tape reels. When the taper was completed, the "Magic tape" could also be more easily removed from the fibre without damaging the fibre, compared to "Sellotape", which is more adhesive.

5.2.4 Galvanometer mirror – step 5

As discussed in section 4.4.2, the mirror was driven with a 100 Hz triangular waveform. A triangular waveform was found to give improved fibre hot-zone uniformity compared to a sinusoidal driving waveform. This was determined qualitatively, by melting and cutting the frosted surface of an acrylic test-piece with the laser operating at an output power of 4 W. The acrylic used was Plexiglas GS, supplied by Rohm. The surfaces perpendicular to the frosted surface were polished so the laser cut profile could be viewed from the side of the test piece.

Figure 36 (a) shows the effect of scanning the laser beam with a 20 Hz sine wave function using a lens with a focal length of 190.5 mm. The length of the laser cut into the acrylic was 17 ± 0.25 mm and the width was 760 ± 30 μm. The latter dimension confirms that the equation used to predict the focussed spot size is quite accurate

(section 4.3.3). The twin peaks shown in figure 36 (a) are expected, as the dwell time of the laser beam on the acrylic test-piece increases around the turning points of the sine wave function. Figure 36 (b) shows the effect of scanning the beam with a 20 Hz *triangular* waveform. The dimensions are typically the same as for the sine wave, however the cut profile is more uniform as the laser beam velocity along the fibre is uniform, making a triangular waveform more suitable for heating the optical fibre in a tapering configuration.

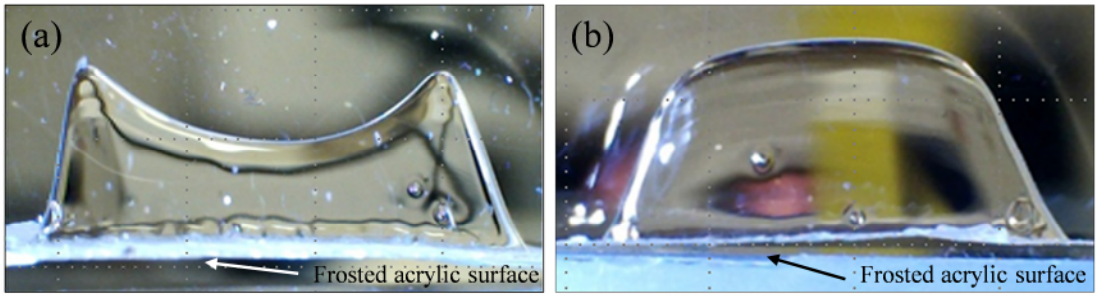

Figure 36: (a) The cut profile in an acrylic test piece when the laser is scanned with a 20 Hz sinusoidal waveform across the frosted surface of the acrylic. The length of the cut profile was 17 ± 0.25 mm. (b) The cut profile in an acrylic test piece when the laser is scanned with a 20 Hz triangular waveform. The length of the cut profile was 16.5 ± 0.25 mm,

The 100 Hz waveform frequency was selected for two reasons; mirror motion linearity decreases with increasing frequency and the sweep of the laser beam along the fibre was fast enough to ensure the fibre did not have time to cool between successive passes of the laser beam [4]. The effect of increasing the mirror driving frequency is shown in figure 37 (a) and (b). At 100 Hz the mirror motion replicates the driving waveform, whereas at 855 Hz the mirror motion is distorted at the waveform turning points. The mirror motion was determined by displaying the output of the optical transducer located within the mirror galvonometer.

If the mirror is stationary, the beam illuminating the fibre has an elliptical cross-section with a Gaussian profile, with a major axis length of 3.5 ± 0.25 mm and a minor axis length of 355 ± 30 μm. This was determined by measuring the laser cut in another acrylic test piece.

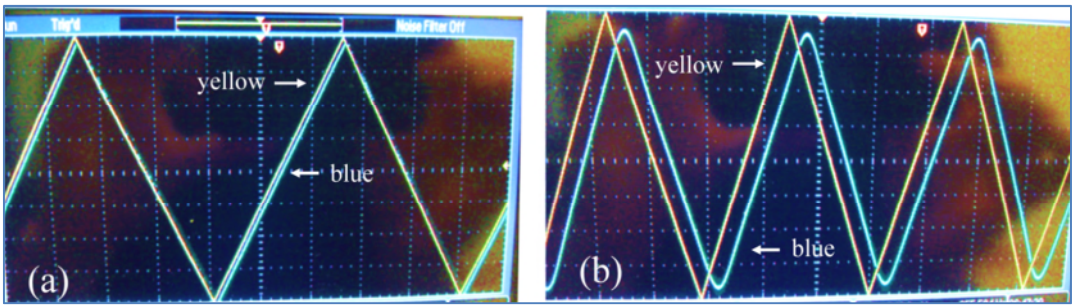

Figure 37: (a) The 100 Hz mirror driving signal (yellow curve) compared to the angular position of the mirror (blue curve) and (b), the 855 Hz mirror driving signal (yellow curve) compared to the angular position of the mirror (blue curve).

The ellipse minor axis is aligned so it is perpendicular the longitudinal axis of the fibre. When the mirror is activated, the amplitude of the triangular waveform determines the scan length along the fibre. Only the major axis length increases, due to reflection from the scanning mirror; the minor axis length is unchanged as shown in figure 38.

Changes in the laser scan length influences directly the overall length of the taper and the angle of the transition zones, as the length of the fibre that is physically softened is a fraction of the scan length (section 3.2). The diameter of the taper waist achieved is determined by the length of time for which the taper is stretched. Scan lengths of 4.5, 8 and 12.5 ± 0.25 mm were explored during this work (section 6.2). A scan length of 8 ± 0.25 mm, allows 5 ± 0.5 µm waist diameter tapers to be produced. If a scan length of 4.5 ± 0.25 mm is used, then non-adiabatic tapers of 15 ± 0.5 µm waist diameter are readily produced (section 3.4) with a high visibility channelled spectrum.

If adiabatic tapers are required, then the scan length should be increased to 12.5 mm to allow a greater volume of fibre to be melted. This allows the fabrication of tapers with less steep transition zones and longer taper waists.

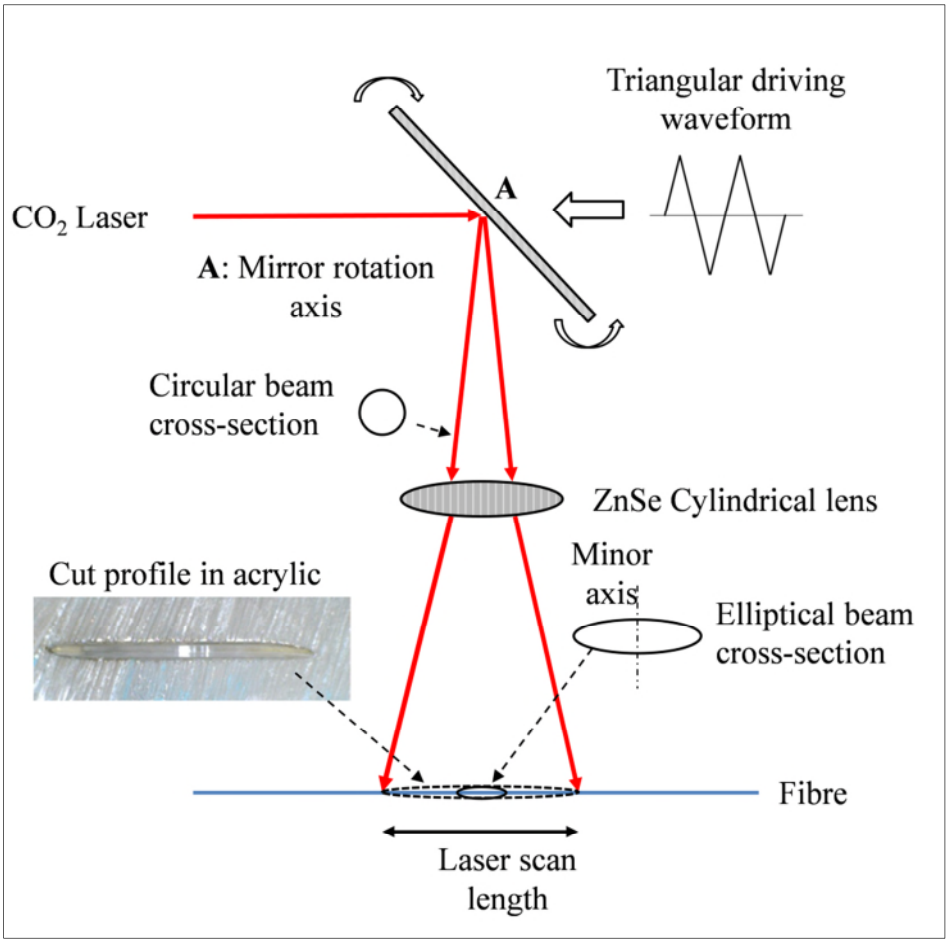

Figure 38: Schematic showing the scanning mechanism of the elliptical laser spot along the fibre.

Each scan length has an associated unique laser power ramp profile. If a scan length is required which is neither 4.5, 8 or 12.5 mm, then a new power ramp profile should be derived. The process for determining a power ramp profile is described in the following section.

5.2.5 Laser power ramp profile – steps 7, 8

A typical laser power ramp is shown in figure 39. The region AD is used to heat the fibre to its melting point. The region of constant power BC, provides the operator with a time window, during which the height of the rotation stages can be adjusted for maximum brightness of the heated fibre when observed with the NIR camera. This

adjustment ensures the fibre axis is placed at the peak of the laser intensity distribution from the CO_2 laser.

In figure 39, the rotation stages are switched on at point D once the softening point of the fibre has been reached. A taper can be produced within the region DF as the taper waist progressively reduces in diameter.

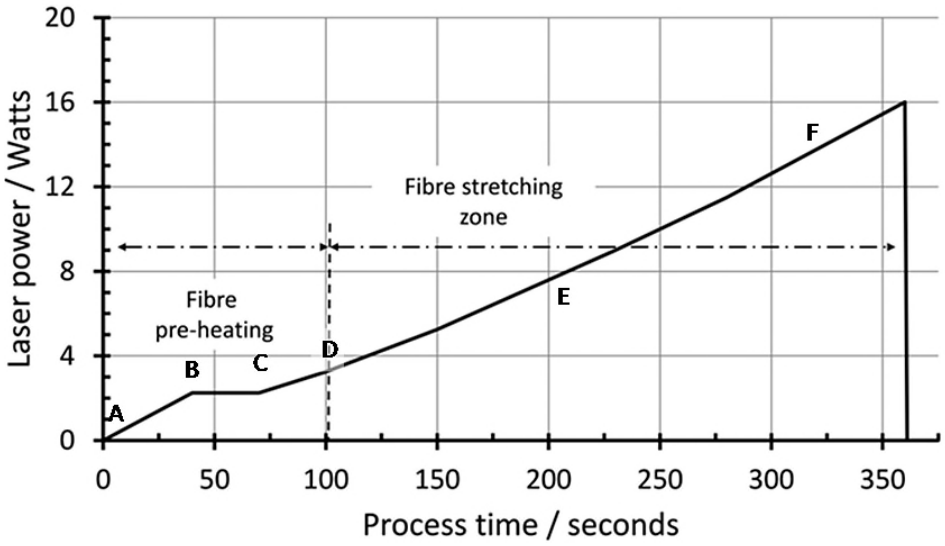

Figure 39: Programmed laser power profile used to heat the fibre when the scan length along the fibre is 8 mm. The region AD heats the fibre to its melting point at D, the region DF is the region over which the taper is pulled. The region BC is the time period over which the fibre is aligned to the minor axis of the scanning beam.

To maintain the fibre at the softening temperature while it is stretched, the laser power is progressively increased over the region DEF, this is because the minimum taper diameter which can be achieved is largely driven by the power of the laser [5, 6]. The energy absorbed by the fibre is a function of the volume of the fibre and therefore of the fibre radius squared. At the same time, the power dissipated by the fibre is a function of the surface area of the fibre, which falls linearly with radius. At a certain fibre radius, the radiated energy equals the absorbed energy and melting of the fibre is no longer possible [7]. Therefore the laser power must be increased as the waist diameter reduces, in order to maintain the taper at a temperature above its softening temperature.

To determine the melting or fictive temperature of the optical fibre, it was viewed with the NIR-300P camera (section 4.3.5) while the laser power was manually increased. In this instance, the fibre was not being stretched but was lightly tensioned between the two rotation stages. Figure 40 shows several NIR camera images under different conditions. Below a laser power of 3 W, the fibre is stationary in the camera field of view as the laser power increases and is observed as a faint image, as shown in figure 40 (a). This corresponds to the region ABC in figure 39.

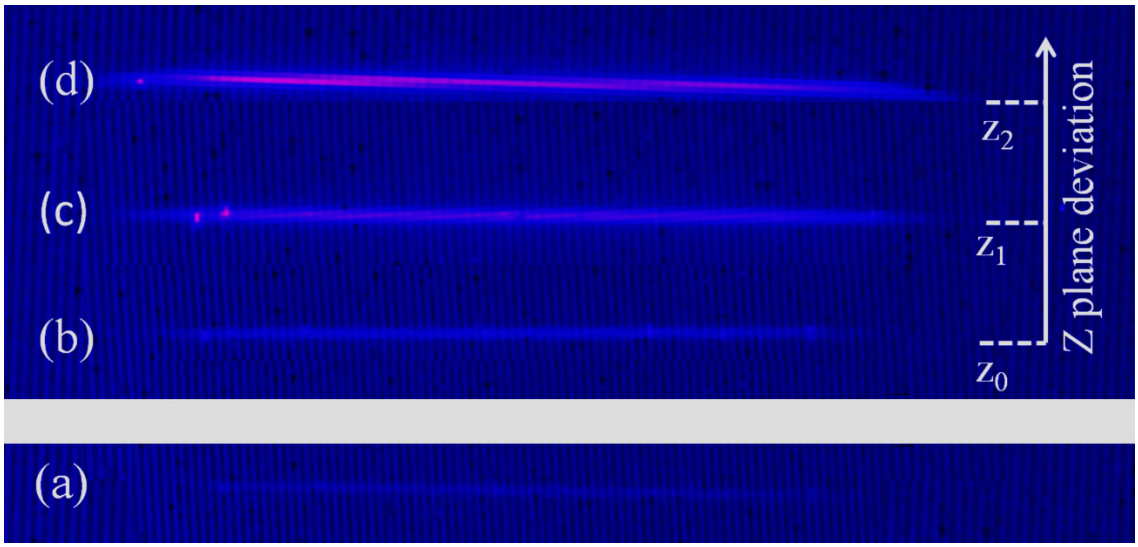

Figure 40: (a) The faint heated image of the fibre when viewed with the NIR camera at a power of 2.5 W. (b) Fibre image at a power of 3 W. (c) Fibre image at a power of 6 W, fibre has now moved from z_0 to z_1. (d) Fibre image at a power of 8 W. Fibre has now moved from z_1 to z_2 in the z-plane. A pseudo-colour scale was used on the camera.

At the fibre melting point, which occurs at a power of 3 W, figure 40 (b), the image is brighter than in figure (a) as the power has increased. This corresponds to point D in figure39.

As the laser power increases above 3 W (figure 40 c,d), the fibre image both becomes brighter and progressively displaces (~1.5 mm) across the camera field of view to z_1 and z_2 due to the fibre bowing between the rotation stages. The z plane is defined in figure

23, section 4.2. The fibre bows because the thermal expansion [8, 9] of the fibre is much greater above the fictive temperature of ~ 950 ^{0}C than it is below.

The rotation stages are then activated and the fibre displacement in the `z` direction decreases as a taper is formed. The laser power and elapsed time is noted when the fibre bowing in the z plane is minimized (at z_0). The fibre position (z_0) on the display monitor is identified using a marker. The laser power is increased again and the fibre displacement increases accordingly and the power and elapsed time is recorded again when the displacement is minimized after the rotation stages are activated. This process is repeated five times to produce data points (D_1-D_5) of laser power and time (figure 41).

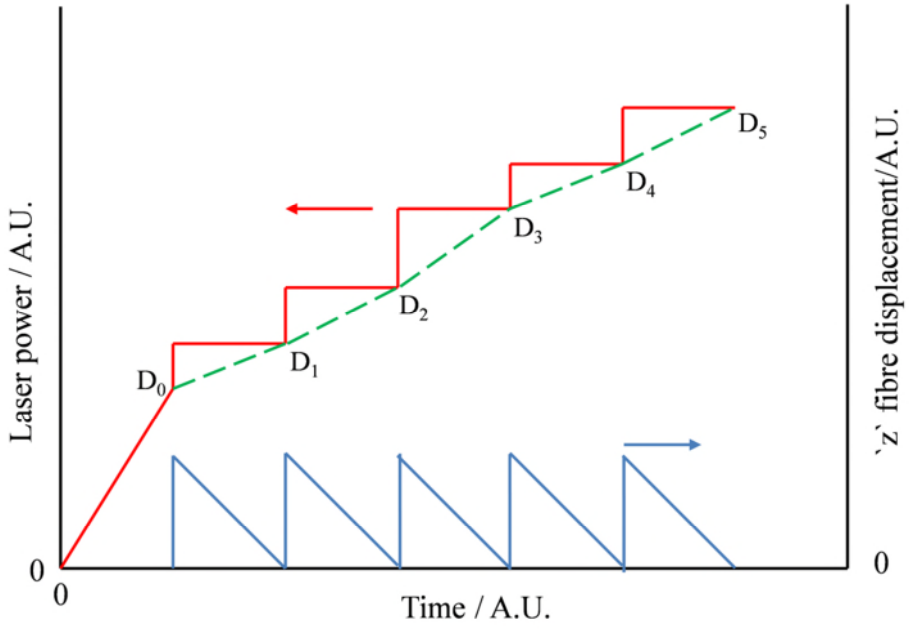

Figure 41: Schematic showing the derivation of the laser power ramp profile (green dashed line) by manually adjusting the laser power and observing the displacement of the fibre during the tapering process.

A polynomial curve was then fitted to the data points $D_{0\text{-}5}$ and the resultant laser power ramp profile is programmed using the 'arbitrary signal waveform profile module' in LabVIEW (figure 42). A taper was then pulled using this derived power ramp profile.

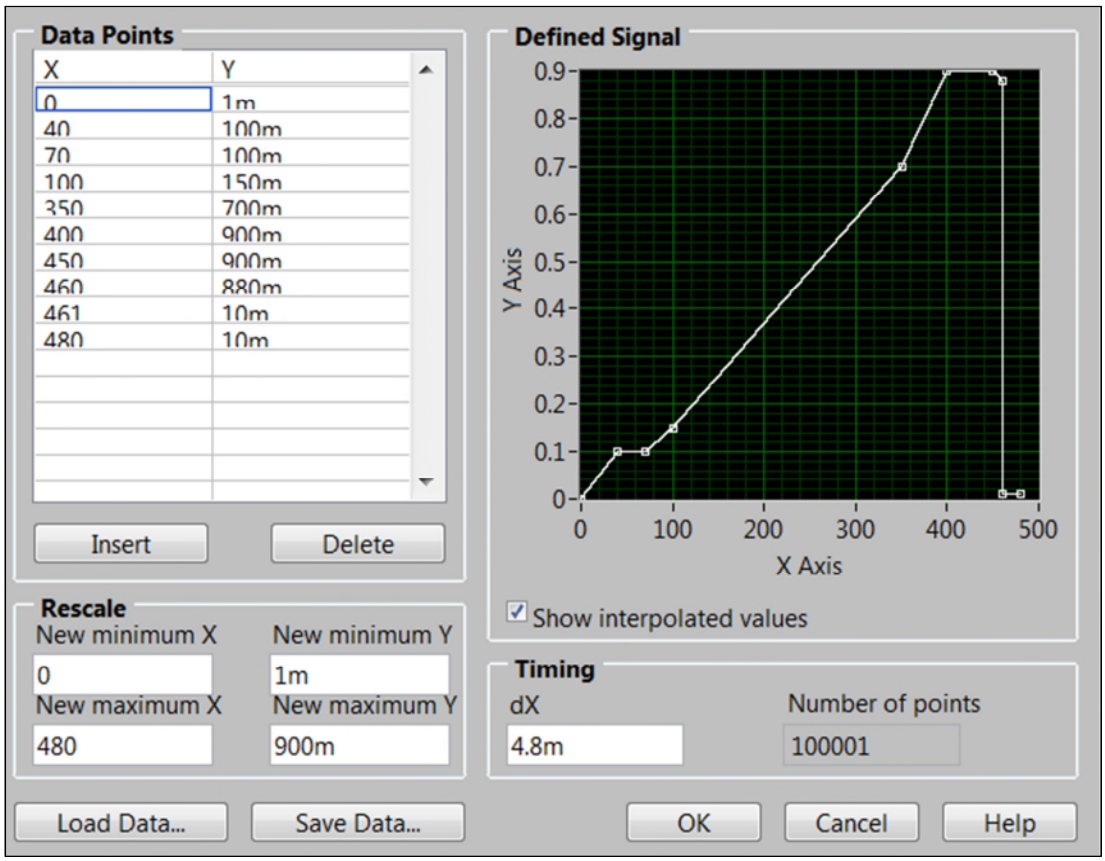

Figure 42: LabVIEW GUI for programming the laser power ramp profile as a function of time using the "arbitrary signal waveform module".

During the tapering process, the heated fibre should stationary when viewed with the NIR camera. This occurs when the fibre elongation rate matches the pulling rate of the stages and is practically observed when the fibre camera image is stationary and aligned with the marker on the computer monitor. If fibre motion is observed over a certain segment of the power curve, the laser power is adjusted and the ramp profile is locally corrected.

5.2.6 Stage rotation speed – step 9

As discussed in section 5.2.5, the fibre pulling rate should equal the fibre elongation rate, otherwise the fibre will either bow during the taper pull or break. Previous researchers [4, 5] have used fibre pull rates between 10 – 110 μm s^{-1}. This range was

used as a start point in this work, but the pull rate which was used in the final process was 61 μm s^{-1} . This value was chosen by undertaking a number of experiments and selecting the pull rate which gave a stationary image in the camera field of view whilst allowing the taper to be pulled over a ~ 3 minute timescale.

5.2.7 Process time – step 10

Tapers of a specific waist diameter can be fabricated using this system by generating a calibration curve, as shown in figure 43, and fitting an exponential function to the data points. The data points were generated by increasing the process time, whilst using the same power ramp profile and laser scan length, to fabricate a number of tapers with decreasing waist diameters.

With a scan length of 4.5 ± 0.25 mm, taper waist diameters of between 6 ± 0.5 μm and 50 ± 0.5 μm can be fabricated by simply selecting the process time from within the range 120 s to 215 s. Longer tapers can be fabricated by increasing the laser scan length and generating a new calibration curve.

Increasing the scan length to 12 ± 0.25 mm, decreases the taper angle and hence produces adiabatic tapers (section 3.3). Table 11 summarises the typical results which were achieved.

The scan lengths were determined by measuring the laser burn length on frosted acrylic test-pieces (section 5.2.4) when exposed to a laser power of 4 - 6 W. The measurements were made with a Vernier caliper.

The taper angle was measured by determining the local taper gradient as a function of longitudinal position along the taper. The local waist diameter was measured using an Olympus BX51 microscope at 1 ± 0.1 mm intervals along the tapered fibre.

The taper transmission loss was determined by measuring average fibre transmission over the wavelength interval 700-800 nm using the spectrophotometer described in section 4.3.6.

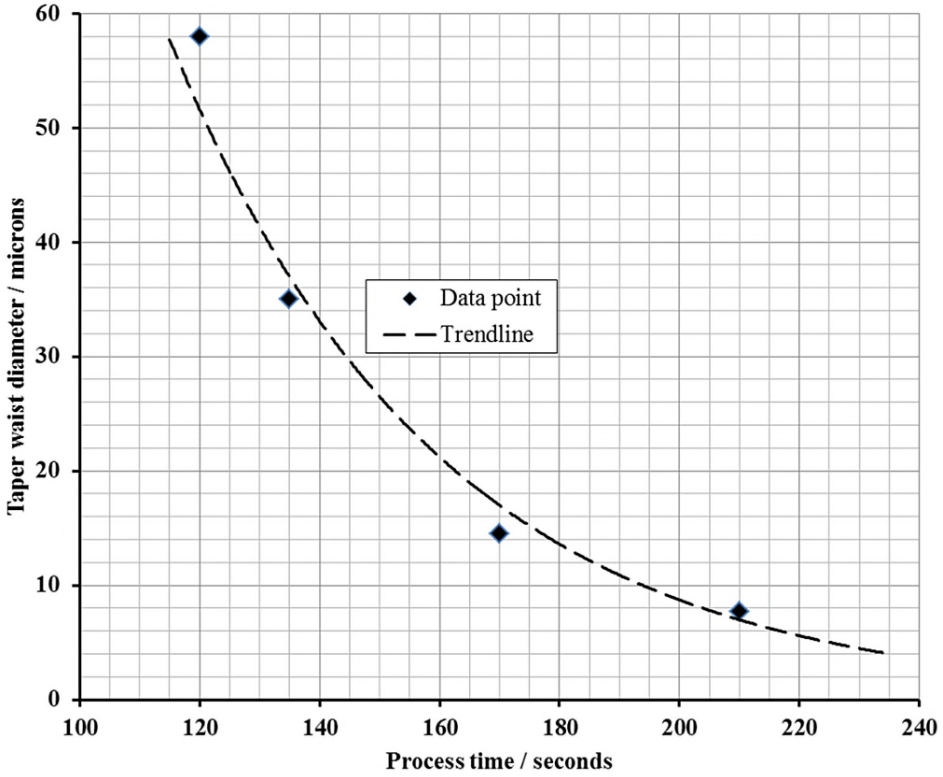

Figure 43: Taper calibration curve when the scan length is 4.5 mm. (The error on the data points is ± 0.5 μm. This error is associated with determining the edge of the fibre when using an Olympus BX51 microscope).

Table 11: Effect of scan length on taper properties.

Taper type	Scan length / mm	Taper angle / mrad.	Transmission loss / dB	Taper waist diameter / μm
Non-adiabatic	4.5 ± 0.25	12.4 ± 0.1	- 2.5 ± 0.04	14 ± 0.5
Non-adiabatic	8.0 ± 0.25	5.6 ± 0.1	- 1.07± 0.04	5 ± 0.5
Adiabatic	12.0 ± 0.25	2.8 ± 0.1	- 0.15 ± 0.04	25 ± 0.5

The taper waist diameter was measured using an Olympus BX51 microscope at 1 mm intervals along the tapered fibre.

5.3 Method for fabricating tapered long period gratings

This section describes the optimised process that has been developed for the fabrication of TLPGs. TLPGs consist of a number of micro-tapers, where adjacent micro-tapers are equally spaced along the optical fibre. Detailed instructions for fabricating TPLGs are given in appendix E of this thesis. To date, with the existing experimental system, TLPGs consisting of up to 18 micro-tapers have been fabricated. The micro-tapers had a length of ~ 190 μm with a pitch or periodicity of ~ 400 μm. The length of the taper was dictated by the minimum spot-size that could be produced using a lens of focal length 100 mm. The grating period was chosen with the aim of fabricating gratings with a 50% duty-cycle. The 50% duty cycle was chosen as previous researchers [10] have shown that this value produces attenuation bands with the greatest extinction for a given number of periods [10]. The experimental system used is shown in figure 44 and 45.

In addition to summarising the fabrication process, this section also describes the process parameters that are important in the formation of these devices.

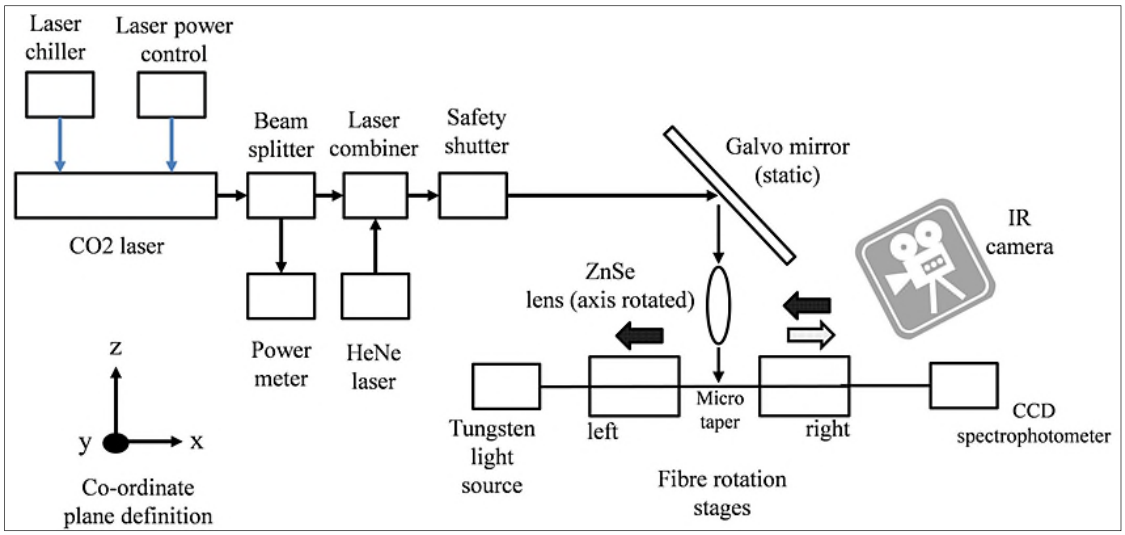

Figure 44: Schematic of the arrangement for fabricating TLPGs.

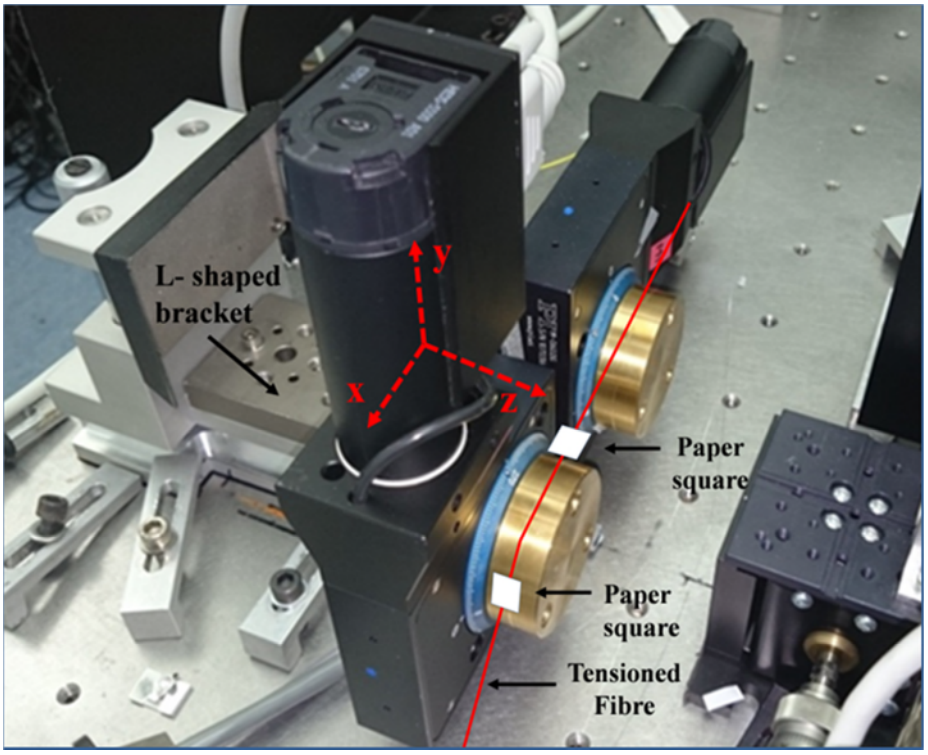

Figure 45: Experimental arrangement for fabricating TPLGs.

5.3.1 Method for fabricating TLPGs.

The experimental arrangement for fabricating TLPGs is different from that used to fabricate single tapers. The differences are summarised in table 12.

The galvanometer mirror is stationary for TLPG fabrication, as the objective is to produce micro-tapers. Using a stationary beam results in the hot-zone length being less than the micro-taper length of 190 μm and is determined by the thermal distribution within the minor axis focussed laser spot. Rotating the cylindrical focussing lens by 90^{0} ensures that the minor axis of the focussed elliptical spot impinges on the fibre.

When fabricating TLPGs, the rotation stages rotate about the z plane. This change was implemented as it allows the fibre to be placed unstrained across the stage v-grooves.

A weight was used to pre-tension the fibre to reduce the variability in the diameter of the first micro-taper compared to subsequent tapers produced later in the process. This

was implemented by attaching a 6 g weight to the right-hand end of the fibre so allowing the fibre to be attached to the stages with a repeatable tension.

Table 12: Differences in experimental arrangement.

Experimental feature	Tapers	TLPGs	Comments
1. Galvanometer mirror	Scanning during process	Stationary	
2. Cylindrical lens	Minor axis of elliptical focussed spot is perpendicular to fibre axis.	Minor axis of elliptical focussed spot is parallel to fibre axis.	This is achieved by rotating the lens by 90^0 about the z plane.
3. Rotation stage orientation	Rotate about the y plane	Rotate about the z plane.	This is achieved by mounting the rotation stages on an L-shaped bracket.
4. Fibre tensioning	Fibre is lightly tensioned by hand before attaching fibre to stages.	Fibre is pre-tensioned with a 6g weight before attaching fibre to stages.	
5. Fibre attachment method	Magic tape used.	Fibre attachment now ensures minimal stress is induced in the fibre during the attachment process to the stages.	This is achieved by using cards taped to the fibre to identify twisting about the fibre axis.

When producing micro-tapers it was found that any rotational twist in the fibre caused by the attachment method would physically deform the first taper when the fibre was heated above the fictive temperature. The formation of the 'kinked taper' resulted in a significant optical insertion loss. Two paper 'flags' (5 x 5 mm) attached to the fibre allowed any induced twist to be observed and corrected. The first 'flag' was located immediately after the left-hand stage and the second 'flag' was placed between the right-hand stage and the 6 g weight. The 'kinked taper' effect was not significant on single tapers as taper lengths are typically > 12 mm compared to ~ 190 μm for a typical micro-taper.

The key process steps for producing TLPGs are:

1) Switch on the laser water chiller – water temperature 18.0 ^{0}C.
2) Ensure that both lasers are aligned with the fibre in accordance with appendix C.
3) Prepare the fibre ends for connection to monitoring equipment and remove a 10 mm length of buffer jacket from the section of fibre to be tapered. Clean the stripped section of fibre using a lens tissue soaked in alcohol.
4) Attach the fibre to left-hand rotation stage. Attach the weight to right-hand fibre end. Attach 'paper flags' to fibre and ensure fibre is not stressed. Attach fibre to right-hand stage. Remove weight from fibre.
5) Switch on the HeNe laser. Adjust the position of the fibre relative to the laser beam using the translation stage on which the rotation stages are mounted, such that a symmetric diffraction pattern from the fibre is observed on the metal plate behind the fibre.
6) Select the required laser power ramp profile on the LabVIEW GUI. Switch on the CO_2 laser.
7) Switch on the rotation stages so forming a taper.
8) After typically 16 seconds switch off stages.
9) Calculate the position of the next micro-taper along the fibre and rotate the stages clock-wise.
10) Repeat steps 7- 9, depending on the number of micro-tapers required.
11) Switch off the CO_2 laser.
12) Remove TLPG from rotation stages.

The process steps which are important to fabricating TLPGs are discussed in the following sections.

5.3.2 Select required power ramp profile – step 6.

The laser power ramp profile used is illustrated in figure 46. The initial 50 s time period is used to pre-heat the laser. The power increase to 5.25 W is used to raise the fibre to the fictive temperature and allows a micro-taper to be produced. This power level and time-period were determined by producing a series of micro-tapers where the power level and pull time was varied and then measuring the taper profiles produced, using an Olympus BX51 microscope.

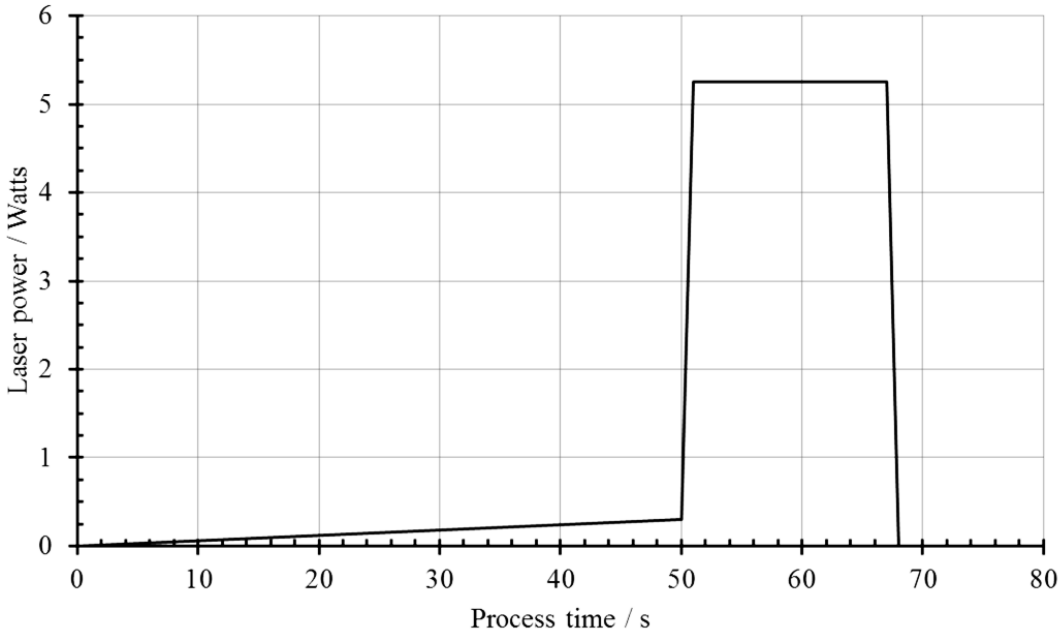

Figure 46: Laser power ramp for producing micro-tapers.

5.3.3 Switch on stages – step 7

The tangential velocity of the stages is ~ 6 μm s^{-1}. This value was chosen to allow the micro-taper to be pulled over a 16 s time period which is compatible with the operation of the stages as these were manually switched. If the velocity was much greater, then timing errors caused by the inherent variability in the timing of the manual operation of the stages would cause a consequent increased variability in micro-taper length.

5.3.4 Switch off stages – step 8

The stages are switched off after 16 s has elapsed. The time period of 16 s was chosen as it produces micro-tapers which have waist diameters of ~ 113 μm and an overall length of 190 μm. This diameter taper waist was found to give a low level of insertion loss (< 0.2 dB), within the transmission pass-band, for each individual micro-taper fabricated (section 6.4).

5.3.5 Calculate position of next micro-taper – step 9

This was achieved by using the rotation stage angular data to determine the taper length (T_L). The fibre translation distance (F_d) was then calculated so that the sum of $T_L + F_d$ was constant for a given periodic spacing (section 7.2.6).

5.4 Conclusions

The process for making tapers has been refined over an 18-month period after completing several hundred experimental trials and is now a reproducible process in the sense that tapers can be fabricated reproducibly with a waist diameter variation of less than ± 0.5 μm between tapers. The taper process could be automated further to simplify its use. The optical alignment of the CO_2 and HeNe lasers with respect to the optical fibre is described in appendix C of this thesis and the detailed process description for fabricating tapers is provided in appendix D.

The process for making TLPGs is also described and was developed over an eight month period. Fifty five TLPGs have been made to-date and further optimisation is required so that the devices approach the spectral performance of UV laser written LPGs. The detailed process description for fabricating TLPGs is provided in appendix E.

Further improvements to the process are required and are addressed in more detail in section 8.2 of this thesis. As a minimum however, the power stability of the laser needs to be improved, together with implementing a degree of automation, to reduce the timing errors which are inherent in any manual process where the time intervals of the process steps are comparatively short.

5.5 References

[1] M. I. Zibaii, H. Latifi, E. Ghanati, M. Gholami and S. M. Hosseini, "Label free detection of DNA hybridization by refractive index tapered fiber biosensor," *Proc. SPIE*, Vol. 7715, p. 77151Z 1–9, 2010.

[2] R. Jarzebinska, C. S. Cheung, S. W. James and R. P. Tatam, "Response of the transmission spectrum of tapered optical fibres to the deposition of a nanostructured coating," *Meas. Sci. Technol.*, Vol. 20, No. 3, pp. 1–6, 2009.

[3] R. Jarzebinska, S. Korposh, S. James, W. Batty, R. Tatam and S.-W. Lee, "Optical Gas Sensor Fabrication Based on Porphyrin-Anchored Electrostatic Self-Assembly onto Tapered Optical Fibers," *Anal. Lett.*, Vol. 45, pp. 1297–1309, 2012.

[4] F. Bayle and J.-P. Meunier, "Efficient fabrication of fused-fiber biconical taper structures by a scanned CO_2 laser beam technique.," *Appl. Opt.*, Vol. 44, No. 30, pp. 6402–11, 2005.

[5] J. M. Ward, D. G. O'Shea, B. J. Shortt, M. J. Morrissey, K. Deasy and S. G. Nic Chormaic, "Heat-and-pull rig for fiber taper fabrication," *Rev. Sci. Instrum.*, Vol. 77, No. 8, p. 083105-1/6, 2006.

[6] M. Sumetsky, Y. Dulashko and A. Hale, "Fabrication and study of bent and coiled free silica nanowires: self-coupling micro-loop optical interferometer.," *Opt. Express*, Vol. 12, No. 15, pp. 3521–31, 2004.

[7] A. J. C. Grellier, "Characterisation of optical fibre tapering using a CO_2 laser," PhD Thesis, University of Canterbury, 2000.

[8] A. D. Yablon, M. F. Yan, P. Wisk, F. V. DiMarcello, J. W. Fleming, W. A. Reed, E. M. Monberg, D. J. DiGiovanni, J. Jasapara and M. E. Lines, "Refractive index perturbations in optical fibers resulting from frozen-in viscoelasticity," *Appl. Phys. Lett.*, Vol. 84, No. 1, pp. 19–21, 2004.

[9] J.W. Fleming., "Sub-glass transition relaxation in optical fibers," *Opt. Fiber Commun. Conference*, Los Angeles, USA, 2004, TuB, TuB2.

[10] R. Y. N. Wong, E. Chehura, S. E. Staines, S. W. James and R. P. Tatam, “Fabrication considerations for fiber optic long period gratings operating at the phase matching turning point,” *Appl. Opt.*, Vol. 53, No. 21, pp. 4669–4674, 2014.

6 Taper Experimental Results

6.1 Introduction

The experimental results for the tapers which were fabricated are provided in this chapter. The aspects of this work which are novel are:

i. The use of a near infra-red (NIR) camera for both fibre and system alignment and as a tool to determine the optimal laser power during the tapering process.
ii. The use of a FBG as an in-line fibre strain sensor during the tapering process. This allowed the onset of fibre breakage to be identified when fabricating small diameter tapers (< 8μm) and also confirms the fibre is at the melting temperature when the fibre is initially stretched.

A range of coatings were also deposited onto tapers using both sputtering and layer- by - layer (L-b-L) deposition techniques. Using these differing techniques, surface plasmon resonance sensors and lossy mode resonance sensors were fabricated and the results are reported.

6.2 Single tapers - optical and geometrical properties

This section describes the results achieved using the optimized taper process and system for making tapers described in section 5.2.

A typical taper profile (taper A) produced by this system, under optimised alignment and power conditions, is shown in figure 47. The fibre diameter was measured using an Olympus BX51 microscope at 2 mm intervals. The taper was 34 ± 0.2 mm long and had an average waist diameter of 5.0 ± 0.5 μm. The transition zones were 11 ± 0.2 mm long. The taper half-angle was 5.6 ± 0.1 mrads and the fibre insertion loss was 1.07 ± 0.04 dB. The laser was scanned over a length of 8 ± 0.25 mm and the power was increased

from 3.8 W to 16 W as the fibre diameter slowly reduced. The programmed power profile used to fabricate this taper is shown in figure 48. During the time interval from 0 to 102 seconds the laser power is increased slowly to preheat the fibre. From 102 seconds the stages are activated and start stretching the fibre. The progressive power increase maintains the fibre at the softening temperature as the fibre diameter reduces.

The taper diameter profile can be predicted theoretically, using the "constant hot-zone model", described by Birks *et al.* in 1992 [1] and summarised in section 3.4. Birks *et al.* have shown that the taper radius profile has a decaying exponential profile with the following equation (6-1):

$$\mathrm{r}\,(\mathrm{z}) = r_0\, e^{-Z/L} \qquad (6\text{-}1)$$

Where r is the taper radius, r_0 is the initial fibre radius, Z is the pull length and L is the length of the fibre hot-zone.

Knowing the initial fibre radius and the taper diameter profile, L was varied until close agreement was achieved with the experimentally measured profile. Figure 47 also shows the diameter profile predicted by this model, assuming a constant hot-zone length of 4.5 mm. The length of the constant hot-zone was not experimentally measured as it requires the ability to be able to accurately measure fibre temperature near the softening temperature of ~ $1183\ ^0$ K [2]. The hot-zone length is less than the laser scan length as the temperature distribution along the fibre has a similar shape to the "optimal" profile shown in figure 49.

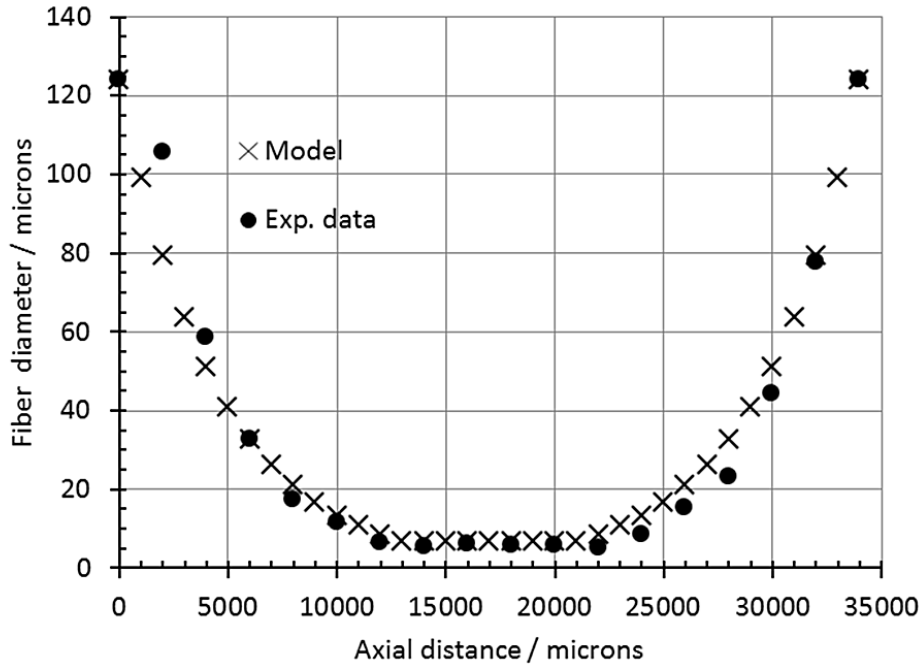

Figure 47: The profile of taper A, fabricated by scanning the laser output over a length of 8 mm and increasing the power from 3.8 W to 16 W. The uncertainties on the measured data points are smaller than the size of the graphed data points.

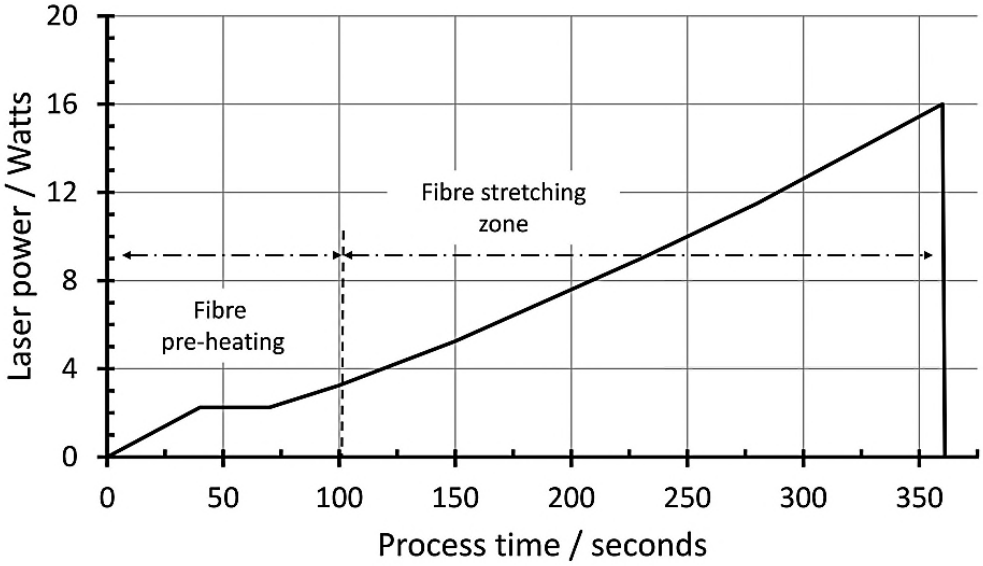

Figure 48: CO_2 laser power profile used to fabricate taper A.

The relative temperature distributions shown in figure 49 were measured using a FLIR Systems SC3000 thermal imaging camera operating over a wavelength range of 8 - 9 µm [3]. This camera uses a Stirling cooled quantum well infra-red photon (QWIP) detector operating at -200 ^{0}C. This detector is faster and more sensitive than micro-bolometers [4] The thermal accuracy of the camera is ± 2% and has a detector with 320 x 240 pixels. The camera objective had a field of view of 20^{0} and was located 0.42 ± 0.01 m from the fibre to be measured. This resulted in an instantaneous field of view of 0.45 x 0.45 mm at the fibre. The objective lens to fibre distance, was driven by the need to minimize scattered 10.6 µm laser radiation being incident on the detector, while still being able to image the fibre. The camera image frequency is 60 Hz.

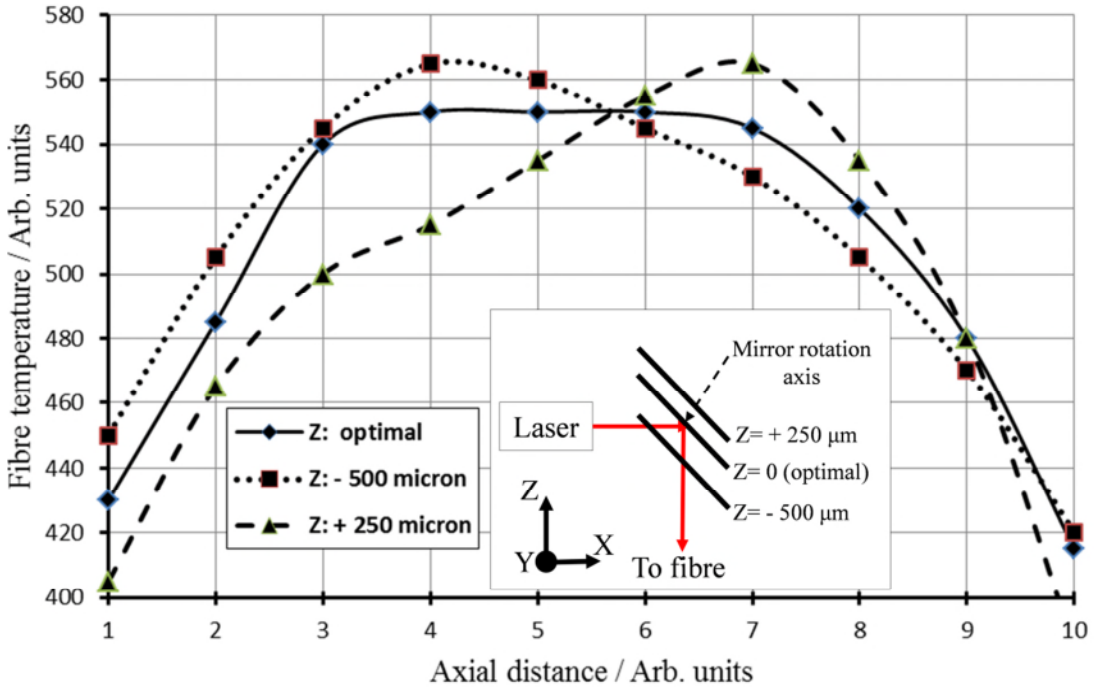

Figure 49: Relative temperature distribution along a heated fibre when the galvonometer mirror is displaced along the z axis from its optimal position. Measured using a FLIR Systems SC3000 IR camera.

This camera measures relative temperature only. To substantially improve its accuracy requires a knowledge of the emissivity of the fibre (which is a function of temperature

[4]) and the background environment in the immediate vicinity of the fibre. The emissivity value used for the measurements was 0.25.

The fibre was heated so that it was just below the fibre softening temperature (figure 50). The galvanometer-mounted mirror was then displaced along the z-axis by -250/+500 µm from its optimal position to explore the impact of changes in mirror alignment on the "optimal" temperature distribution. Figure 49 shows that displacing the mirror from its optimal location distorts the flat-topped temperature distribution and creates temperature distributions which are asymmetric.

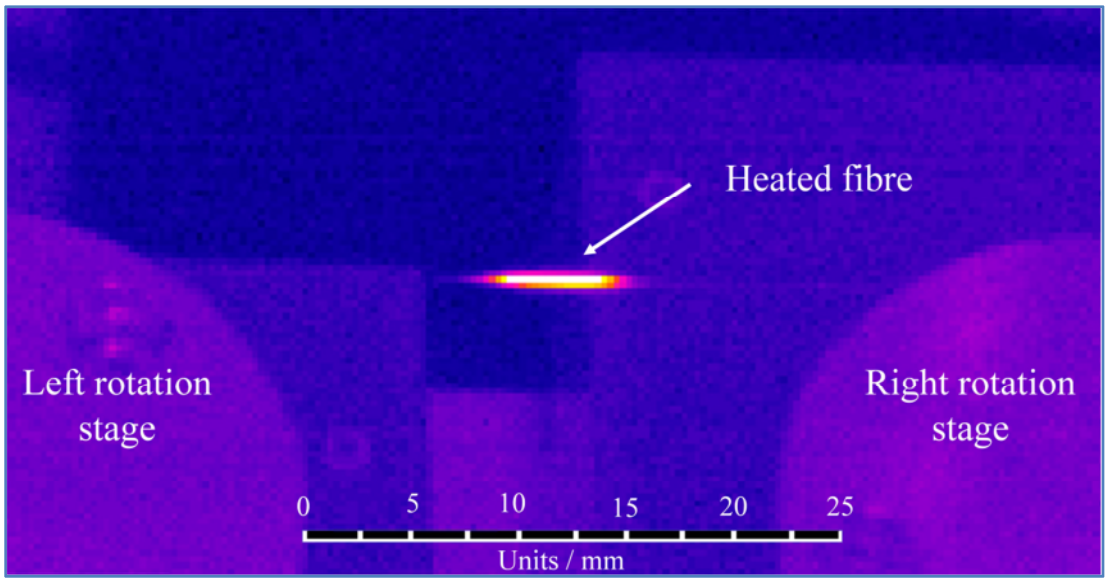

Figure 50: The thermal image from at fibre with a laser scan length of 8 ± 0.25 mm and an incident power of 3.5 W. The camera used to capture this image was a FLIR Systems SC3000. The spatial resolution was 0.45 x 0.45 mm. A pseudo-colour scale was used on the camera.

The results suggest that the mirror rotation axis needs to be aligned to the centre of the laser beam with an accuracy of significantly less than ± 250 µm.

The optical transmission of taper A is shown in figures 51 and 52. The channelled spectrum [5] starts to appear in the transmission spectrum once the taper waist diameter is less than < 40 µm, which corresponds to the cladding mode transition diameter discussed in section 3.3. Figure 52 shows the transmission of taper A, measured at a

wavelength of 800 nm using the Ocean Optics S2000 spectrophotometer and plotted as a function of time. This wavelength was chosen over shorter wavelengths to improve the visibility of the modulated fibre transmission characteristic. Modulation of the fibre transmission starts at pull times greater than 160 s for taper A.

To explore the impact of hot-zone length on taper optical properties, the laser scan length was reduced from 8 ± 0.25 mm to 4.5 ± 0.25 mm. The aim was to produce a taper with shorter transition zones and therefore an increased taper angle compared to taper A, with a corresponding increase in the visibility of the modulation of the fibre transmission.

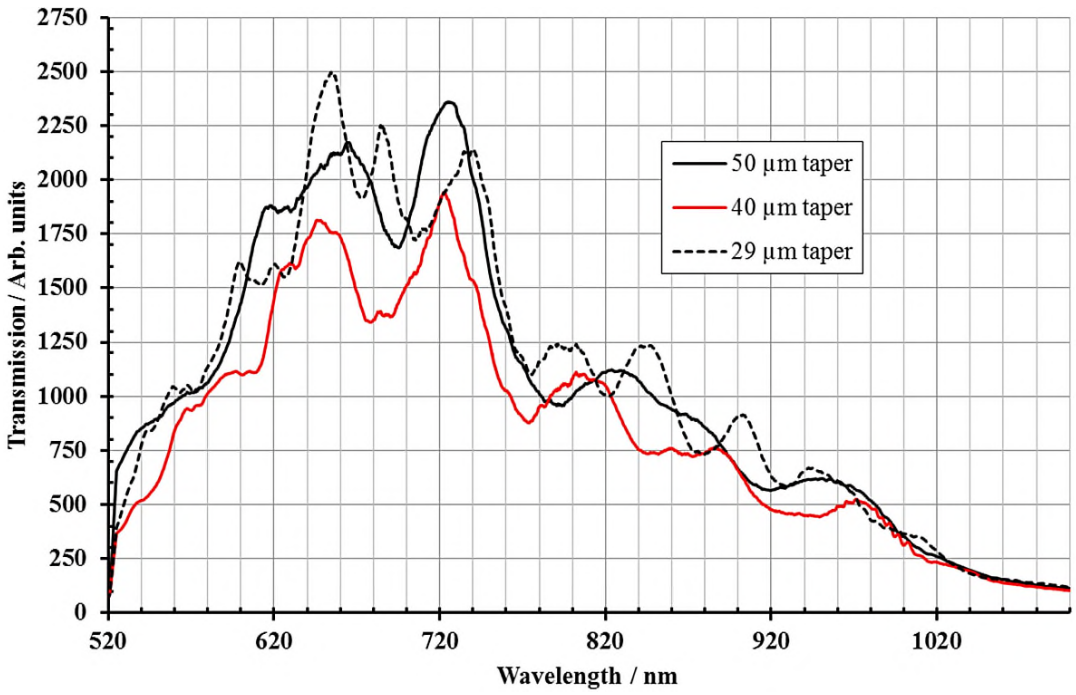

Figure 51: Optical transmission of taper A as the taper waist reduces from 50 to 29 microns. These curves were acquired at different times as the waist diameter progressively reduced.

This shorter taper (taper B) was fabricated using a lower power (figure 53) than was used for taper A. The taper angle is 12.4 ± 0.1 mrads with an associated transmission insertion loss of 2.50 ± 0.04 dB. Taper B is 11 ± 0.2 mm long, with an average waist diameter of 14.0 ± 0.5 µm. The transition zones were ~ 5 mm long. The profile of taper B, shown in figures 54 and 55, is in close agreement with the theoretical curve and has

an estimated theoretical constant hot-zone length of ~ 2.5 mm. The micrograph of taper B is representative of how a micrograph of taper A would appear.

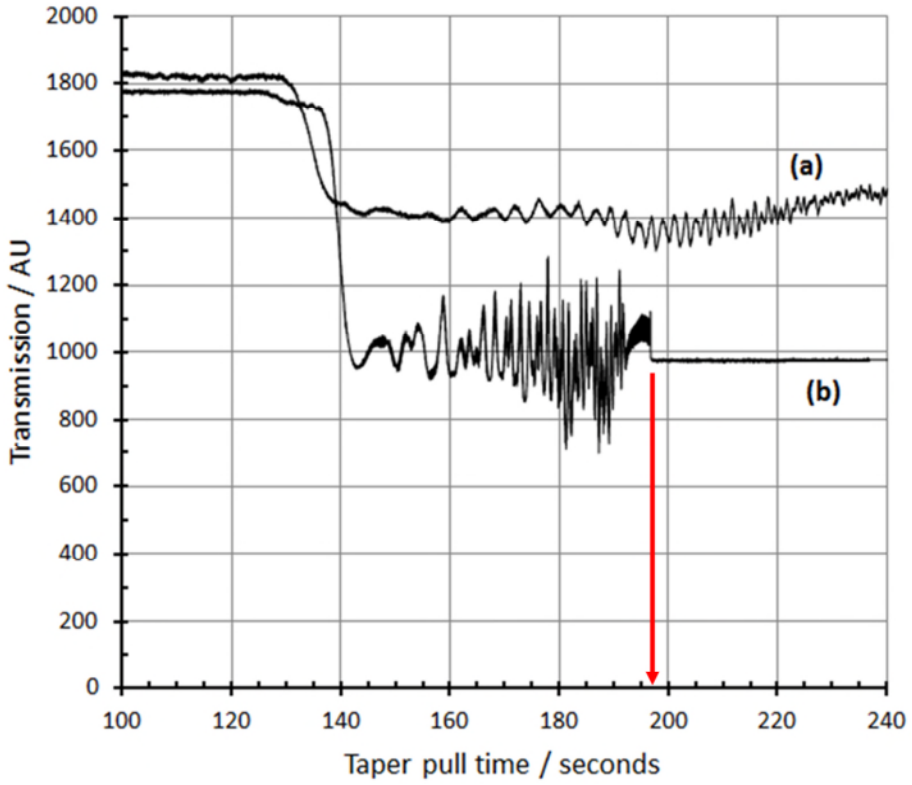

Figure 52: The transmitted power measured at one wavelength (800 nm) using the Ocean Optics S-2000 spectrophotometer, recorded while fabricating (a) taper A and (b) taper B. For taper B, the stages stop pulling the taper at ~ 195 s.

The optical transmission of taper B is shown in figures 52(b) and 56. Ten of these tapers were made, which had typical waist variations of ± 0.5 µm, indicating that the fabrication process was repeatable.

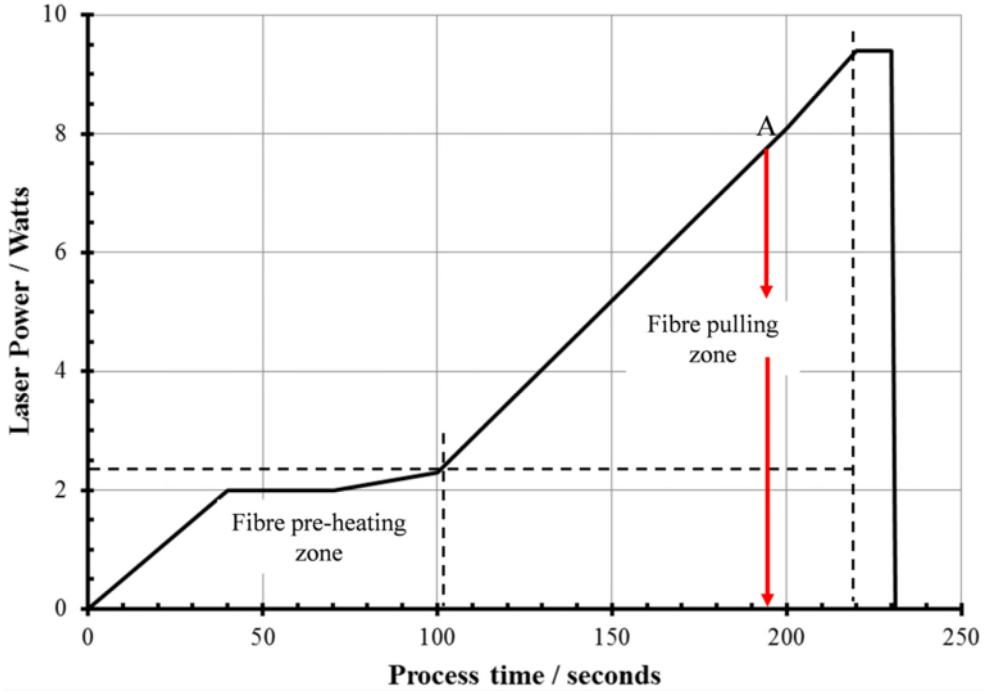

Figure 53: Laser power profile used to fabricate taper B. The laser was switched off at point A, after ~ 195 s had elapsed.

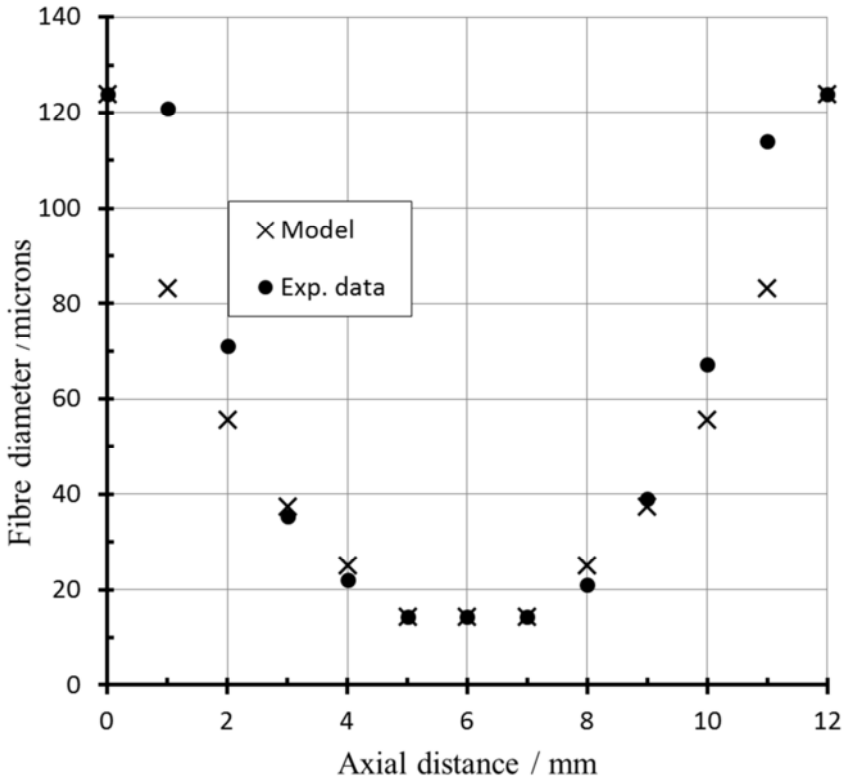

Figure 54: The profile of taper B, which was fabricated by scanning the CO_2 laser output over a length of 4.5 mm and increasing the power from ~ 2 W to ~ 7 W as the fibre diameter reduces.

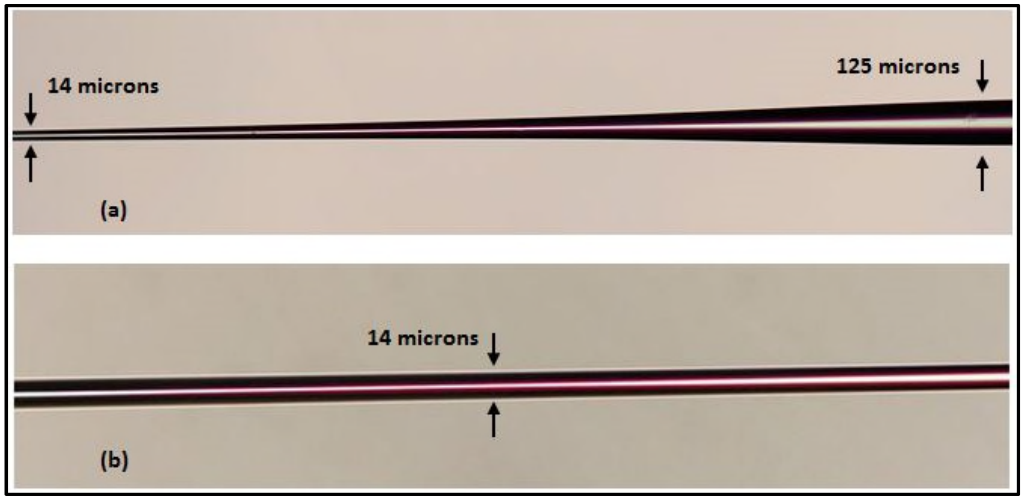

Figure 55: Micrographs of the tapered section and waist of taper B in (a) the tapered region and (b) the waist region. The length of this taper is 11 ± 0.2 mm.

The transmission of taper B starts to become modulated at pull times greater than 150 s, when the waist diameter is less than 25 μm. Taper B has a greater modulation visibility than for taper A, as the taper is more non-adiabatic due to the increased taper angle. In figure 56, the final transmission spectrum of taper B is shown at a waist diameter of ~ 14 μm.

Figure 57 shows the evolution of the channelled transmission spectrum that is characteristic of tapers with waist diameters of ~ 13 μm [5]. In the region of the taper waist, the light propagates at the air/cladding interface, as here the single-mode fibre converts to multi-mode fibre behaviour. The interference between the two (or more) modes of the taper at the second transition zone results in a characteristic channelled transmission spectrum, a manifestation of the different effective refractive indices of the modes in the tapered region. As the phase and period of the channelled spectrum changes in response to the reduction of the fibre diameter, the intensity measured at a fixed wavelength is modulated, as shown in figure 52 for a wavelength of 800 nm.

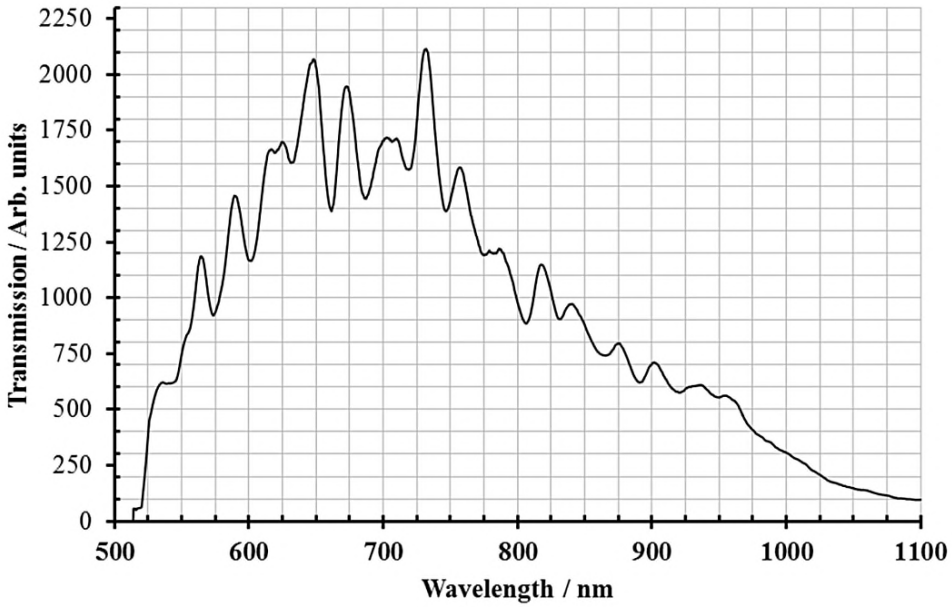

Figure 56: The optical transmission of taper B when the waist diameter is 14 µm.

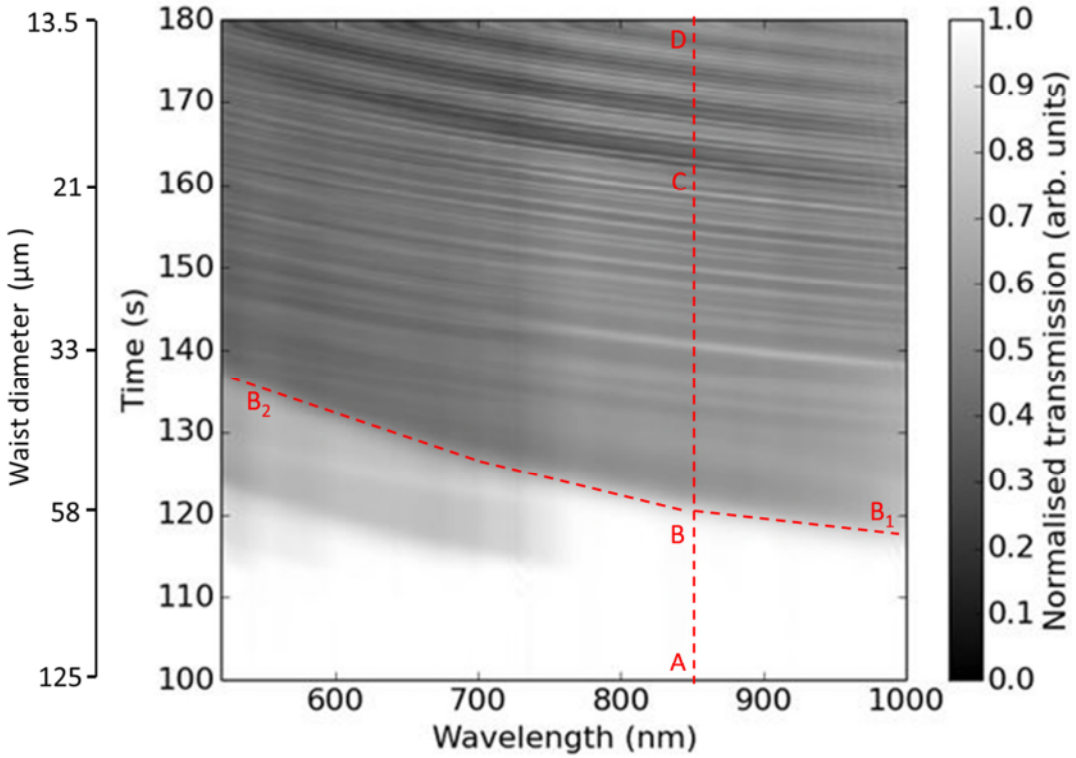

Figure 57: Evolution of the channelled spectrum during the fabrication of a non-adiabatic taper with a similar profile to that of taper B. The taper behaves as an adiabatic taper over the region AB and transforms to a non-adiabatic taper over the region BCD. Pronounced interference fringes are visible over the region CD and the guided mode to cladding mode transition diameter occurs along the locus B_2B B_1.

6.2.1 Adiabatic tapers

Tapers A and B described in section 6.2 are non-adiabatic as they have large taper angles (> 5.5 mrads) and have transmission losses exceeding 1.0 dB. For tapers to be classed as adiabatic, they should have low transmission losses (< 0.3 dB) and their taper angle should be sufficiently low so their profile follows the `adiabacity criterion` [6].

A taper can be made adiabatic by ensuring that the taper angle is sufficiently shallow (section 3.3). This is practically achieved by increasing the laser scan length from 8 mm to 12.0 ± 0.25 mm. This scan length ensures the taper angle will be adiabatic, together with having the required laser flux density to pull a longer taper, as the available laser flux density decreases as the scan length increases. Using this increased scan length, a taper with an average waist diameter of 25 ± 0.5 µm was fabricated. The transmission of this taper, designated taper C, is shown in figure 58 together with its taper profile in figure 59. The taper profile was measured using an Olympus BX51 microscope at 1 mm intervals

.

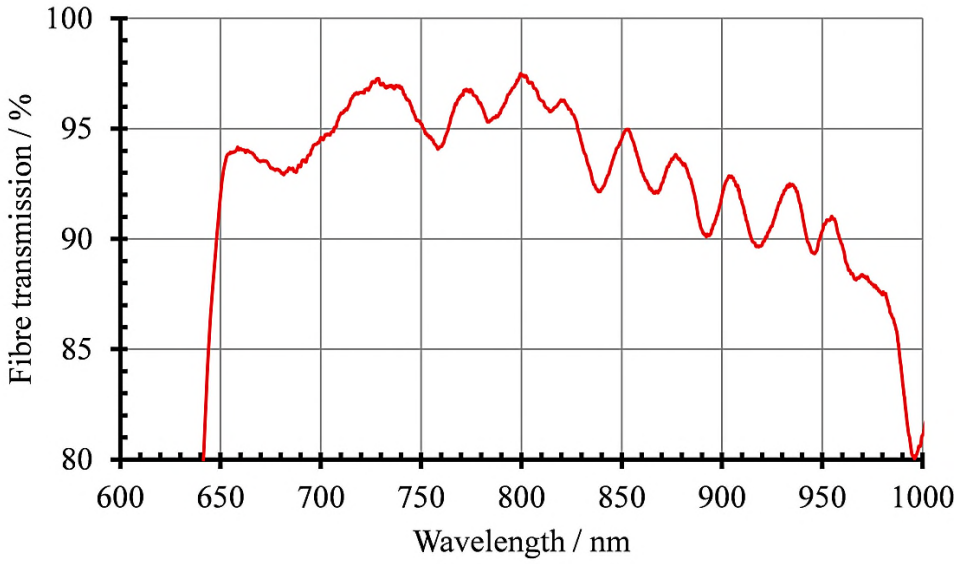

Figure 58: Transmission of an adiabatic taper C, fabricated using SM750 fibre. The waist diameter was 25 µm and the total length was 40 mm. The average insertion loss was 0.15 ± 0.4 dB over 700 - 800 nm.

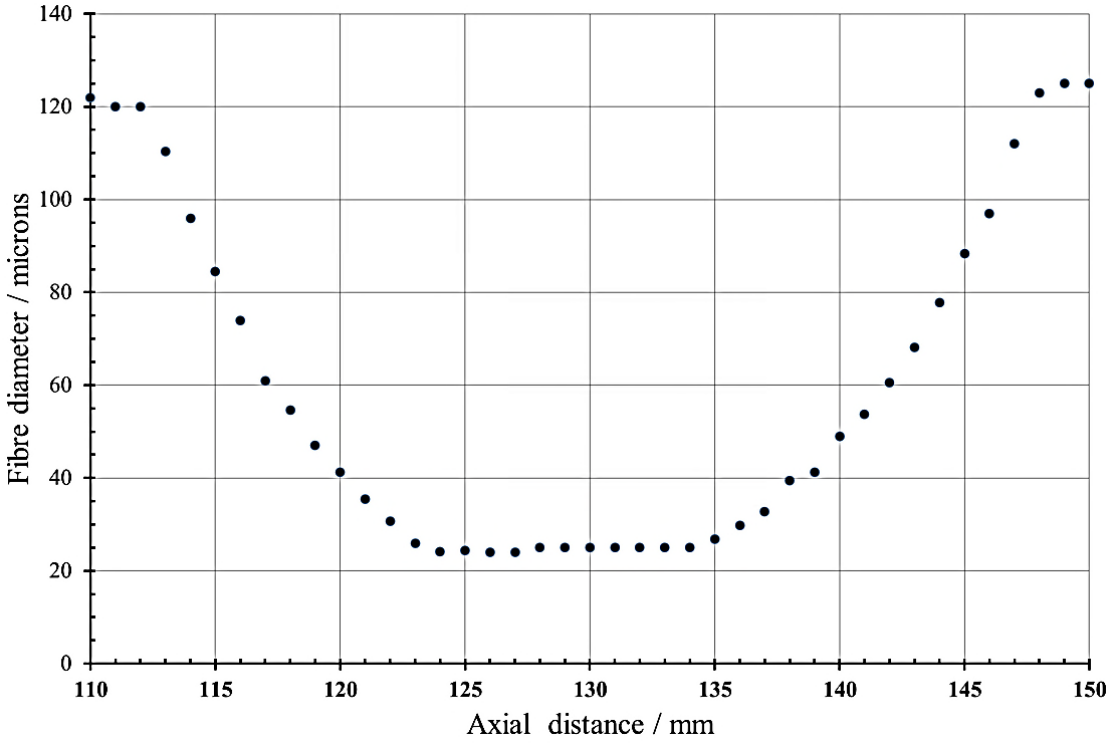

Figure 59: The profile of an adiabatic taper C, which was fabricated by scanning the laser output over a length of ~ 12 mm. The taper waist diameter was 25 μm, the fibre used was SM750.

A plot of the 'adiabacity criterion' is shown in figure 60, together with the taper angle profiles of tapers B and C. For a taper to be classed as adiabatic, the taper angle profile should be less than the 'adiabacity criterion' curve by approximately one decade [6].

Taper C meets the criterion as the taper angle curve lies below the green curve by one decade and the insertion loss is - 0.15 ± 0.04 dB, however taper B is non-adiabatic as it lies below the green curve by less than one decade and has an insertion loss of 2.5 ± 0.04 dB.

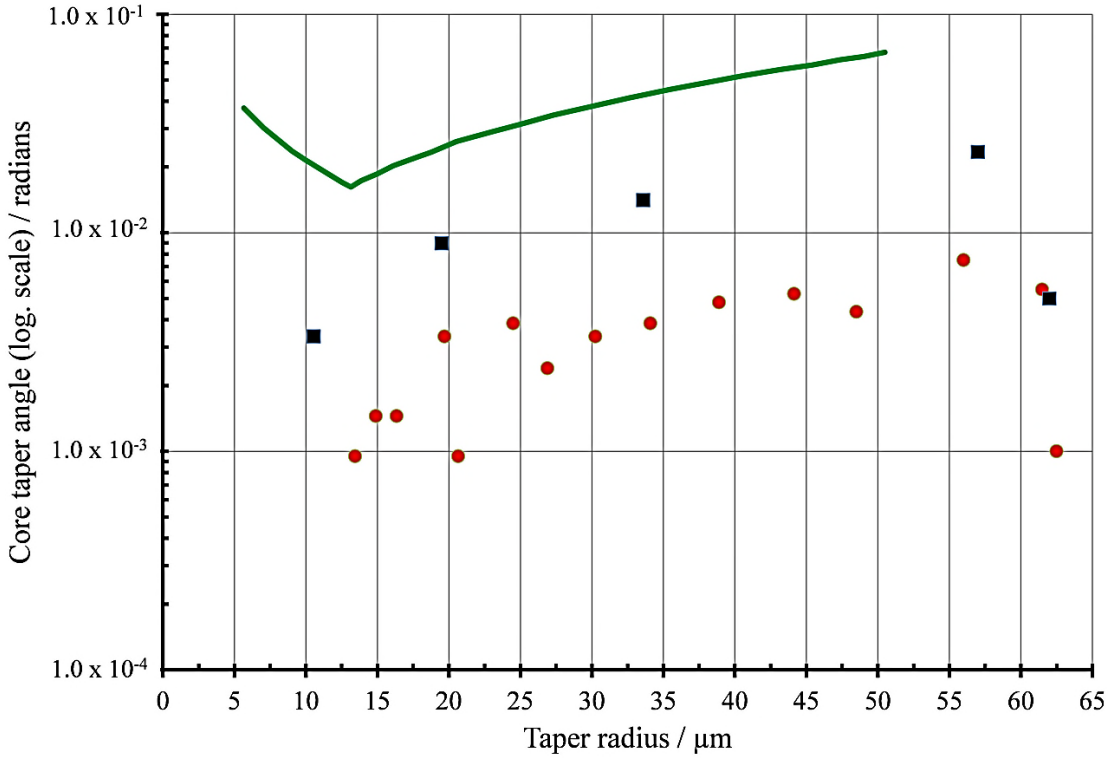

Figure 60: The taper angle for non-adiabatic taper B (black squares) and adiabatic taper C (red circles), compared to the 'adiabacity criterion' (green curve) from Ward *et al.* 2006 [6].

6.2.2 Asymmetric tapers

The tapers discussed in the section 6.2, had symmetric transition zones and a uniform diameter taper waist. However, many tapers produced during the early part of this work had asymmetric transition zones and exhibited non-uniform waist diameters as shown in figure 61. The taper profile was measured using an Olympus BX51 microscope at 1 mm intervals.

Asymmetric tapers typically have high transmission losses and exhibit a reduced, or a complete absence of the sinusoidal modulation of the transmission characteristic of the taper which make them unsuitable for use as optical sensors, however there other applications for them which are discussed in section 7.1.

It was viewed that asymmetric tapers may be caused by a non-uniform temperature distribution along the fibre coupled with other effects.

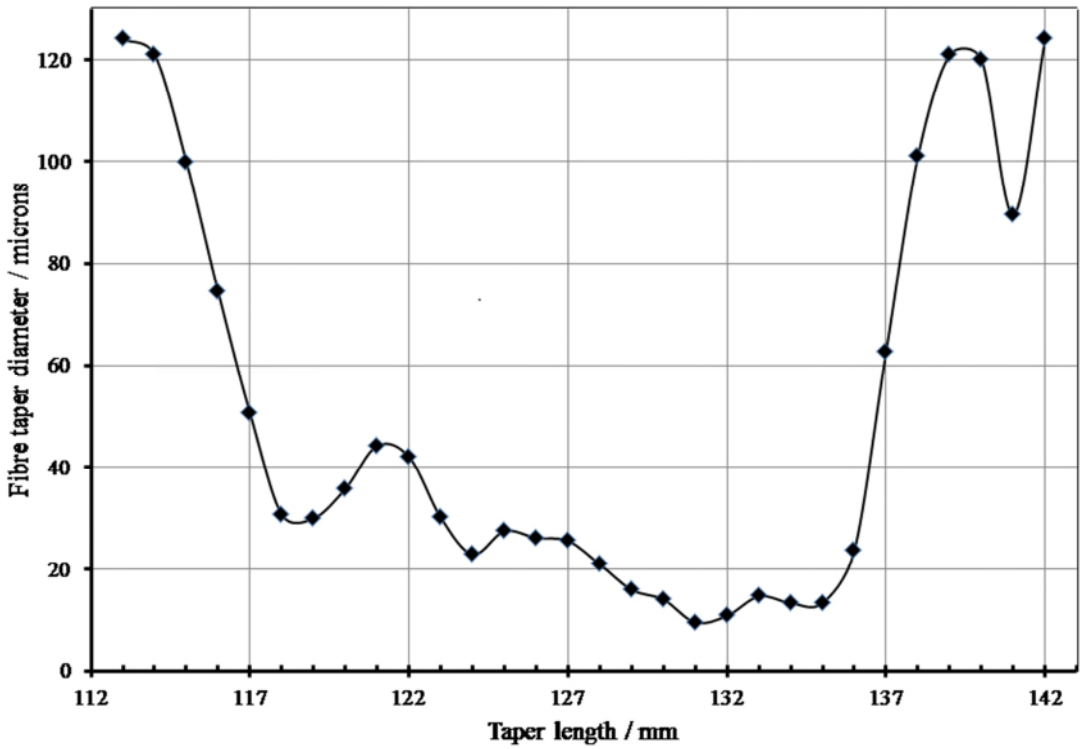

Figure 61: Asymmetric taper where the taper waist has poor uniformity along its length and asymmetric transition zones. The fibre was SMF-28.

To measure the relative temperature distribution along the fibre, a FLIR Systems SC 3000 infra-red camera was used as discussed in section 6.2. It was viewed that the alignment of the laser beam with respect to the rotation axis of the galvanometer mirror was important when producing symmetrical tapers. Figure 49 shows the relative temperature distribution along a fibre when the galvanometer-mounted mirror axis was displaced from the optimal position. This data was recorded using the SC 3000 camera (section 6.2) and figure 62 shows the resultant impact on taper symmetry when the mirror was misaligned, compared to a correctly aligned scanning mirror. The taper diameter profile was measured at 1.0 mm intervals using an Olympus BX51 microscope.

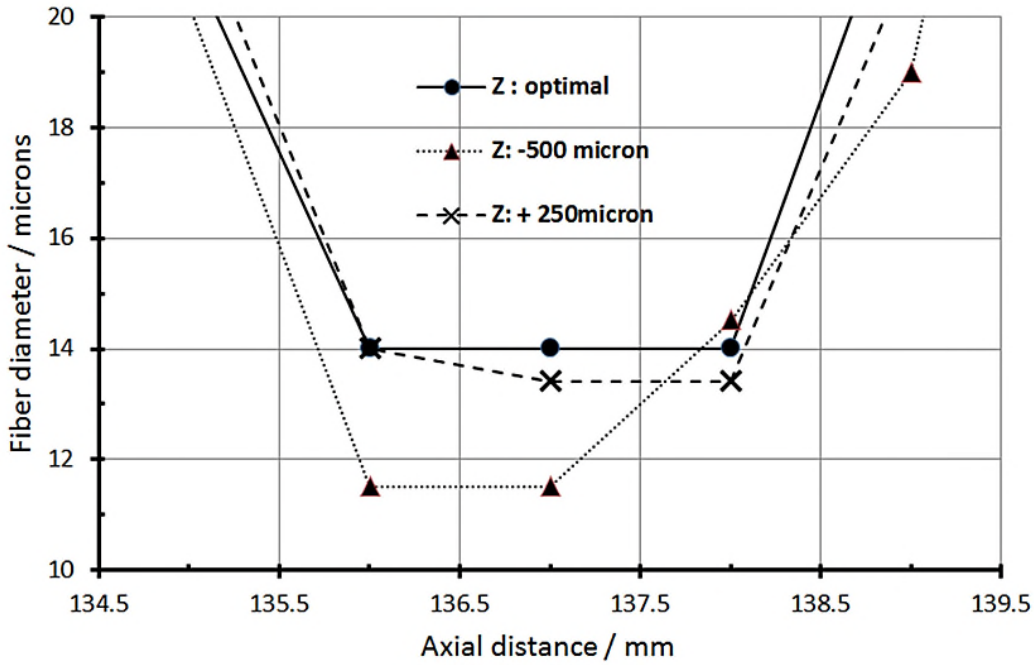

Figure 62: The effect of galvanometer mirror displacement on taper symmetry caused when the mirror is displaced in the z axis from its optimal position. The fibre used was SM750.The solid and dashed lines are a guide for the eye.

6.2.3 Taper strain measurements

Producing tapers with waist diameters of less than 8 µm can be difficult as the taper would occasionally break at the narrow taper waist. As the diameter of the fibre reduces below 8 µm, the fibre starts to solidify if the laser power is insufficient and breaks occur due to the increased tension exerted by the rotation stages. To overcome this problem, a method of monitoring fibre tension was required, with the objective of identifying the onset of solidification of the fibre.

After reviewing a number of options, it was decided that an FBG would be used as an in-line strain sensor. Grellier [7] in 2000 used a load cell to measure the strain applied to the fibre during tapering, but the technique used resulted in a perturbation in the positon of the fibre relative to the focal plane of the laser as the fibre tension varied. This caused the insertion loss of the tapers produced to vary unpredictably. The use of an FBG as an in-line intrinsic strain sensor allows this problem to be overcome. It is believed that this is the first time that an FBG has been used for this application.

The FBGs used in these experiments were fabricated in-house using hydrogen loaded single mode fibre (SMF-28) by Dr Ricardo Correia . They were written by UV exposure through a phase mask using an injection-seeded frequency-quadrupled Nd:YAG laser operating at a wavelength of 266 nm. Each FBG had a reflectivity of ~ 50 % at ~ 1530 nm and an estimated length of 6 mm. The FBG length is governed by the width of the slit in front of the phase mask. A SmartScan interrogator (Smartfibres Ltd) was used to monitor the FBG peak wavelength, and thus the strain experienced by the fibre, while it was being pulled during the tapering process. The Smartscan interrogator had a wavelength resolution of ± 0.1pm and had a spectral up-date rate of 250 Hz. During operation, the interrogator tracks the position of the reflection peak only, it does not record spectral changes to the shape of the FBG reflection band. A typical transmission of an FBG is shown in figure 63. The experimental arrangement is shown in figure 64.

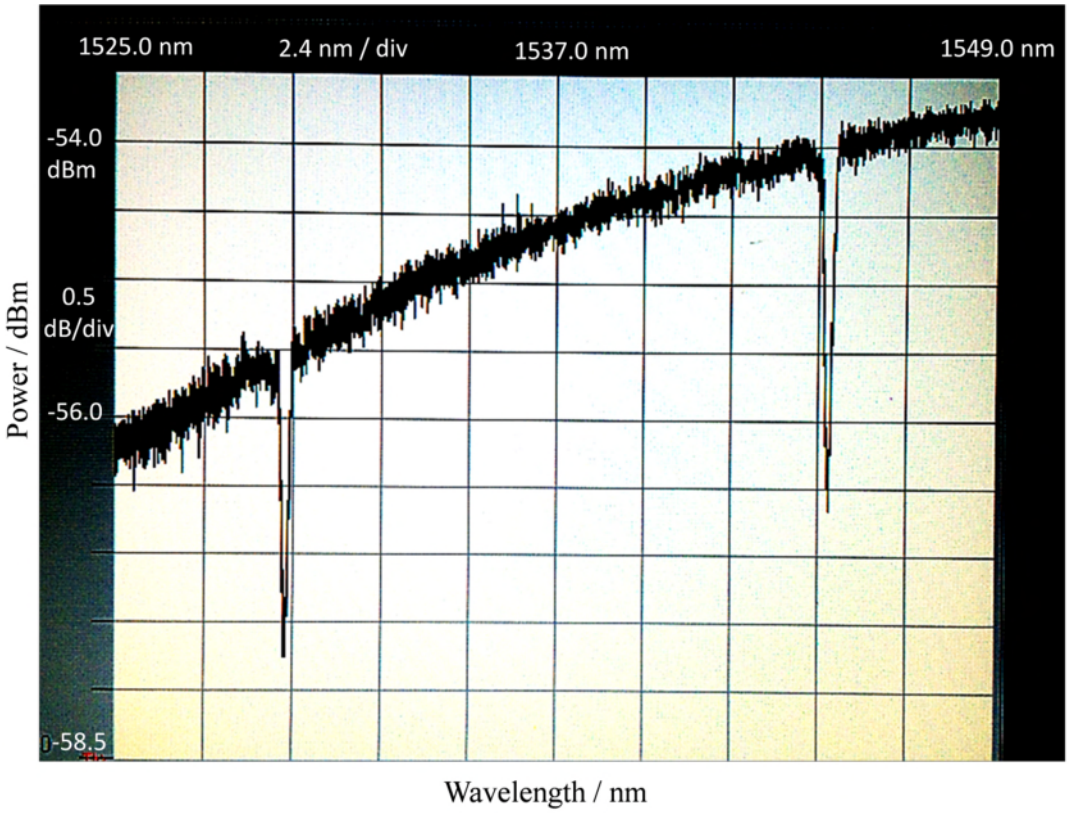

Figure 63: The screen shot of the transmission spectra of two FBGs. The measurement was taken with an optical spectrum analyser (Nettest 3651 HR 12) with a resolution of 0.02 nm.

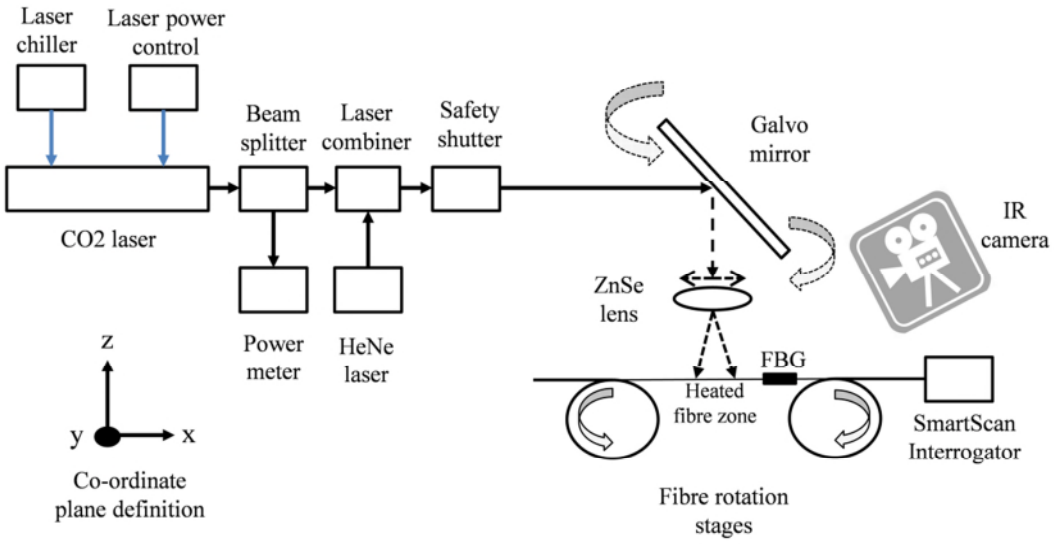

Figure 64: Schematic of the experimental arrangement used for measuring the strain experienced by the optical fibre during the tapering process.

The strain calibration of the FBG sensors was obtained by using an Instron mechanical test bench with the sensor mounted onto a 25 mm by 200 mm aluminium test plate with a thickness of 0.9 mm, attached using cyanoacrylate adhesive. To verify the performance of the calibration, a 2 mm gauge length resistive foil strain gauge (RFSG) (model 632-124 from RS components) was also mounted on the plate next to the FBG.

To measure the strain experienced by the fibre during the fabrication process, the FBG was located 12 mm from the laser heating zone to ensure that the strain measurements were not compromised by either heat conducted along the fibre or laser radiation scattered by the fibre. This distance was established by a series of experiments in which the fibre was heated to just below its melting point and the separation of the FBG was varied with respect to this heating zone while measuring the wavelength of the FBG reflection peak. The physical separation of the FBG from the laser focus where the FBG reflection peak did not change whilst the fibre was heated was used to determine the optimized separation between the laser heating zone and the FBG. Given the wavelength shift [8] of the FBG was ~ 10 pm / ^{0}C the temperature change of the fibre was calculated as the laser power was increased to just below its melting point. The results are shown in figure 65. In these experiments, the FBG was unstrained by fixing

one end of the fibre only and so any change in the FBG spectrum was due to thermal conduction along the fibre and not to a relaxation in tension due to softening of the fibre. A separate FBG was used a temperature reference and located on the rotation stage base-plate.

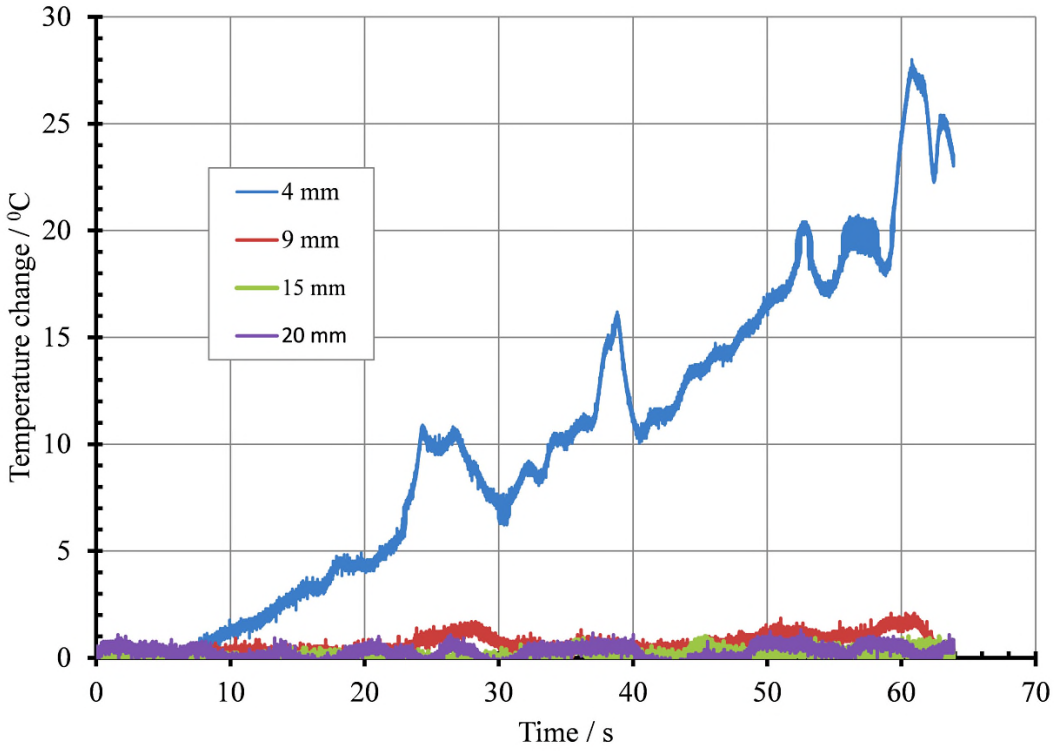

Figure 65: The temperature increase from ambient, measured by an FBG when the separation between the FBG and heating zone varies from 4 to 20 mm.

The strain measured by the FBG during taper fabrication is shown in figures 66 and 67, together with the measured variation in CO_2 laser power. The laser power fluctuations are likely to be caused by the laser mode-hopping. At 102 s, the fibre was stretched, resulting in an abrupt increase in the measured strain. As the laser power increases, the fibre starts to soften, resulting in a subsequent decrease in strain. As the fibre was then heated and pulled, no significant change in the strain was observed until 220 s had elapsed. At this time, the strain increases abruptly, as the laser intensity incident on the reduced-diameter fibre was insufficient to maintain the fibre at the softening

temperature and so the fibre solidifies. Just before this occurred (at 215 s), the laser power fluctuations and the measured strain vary in sympathy as the temperature of the fibre decreased and increased.

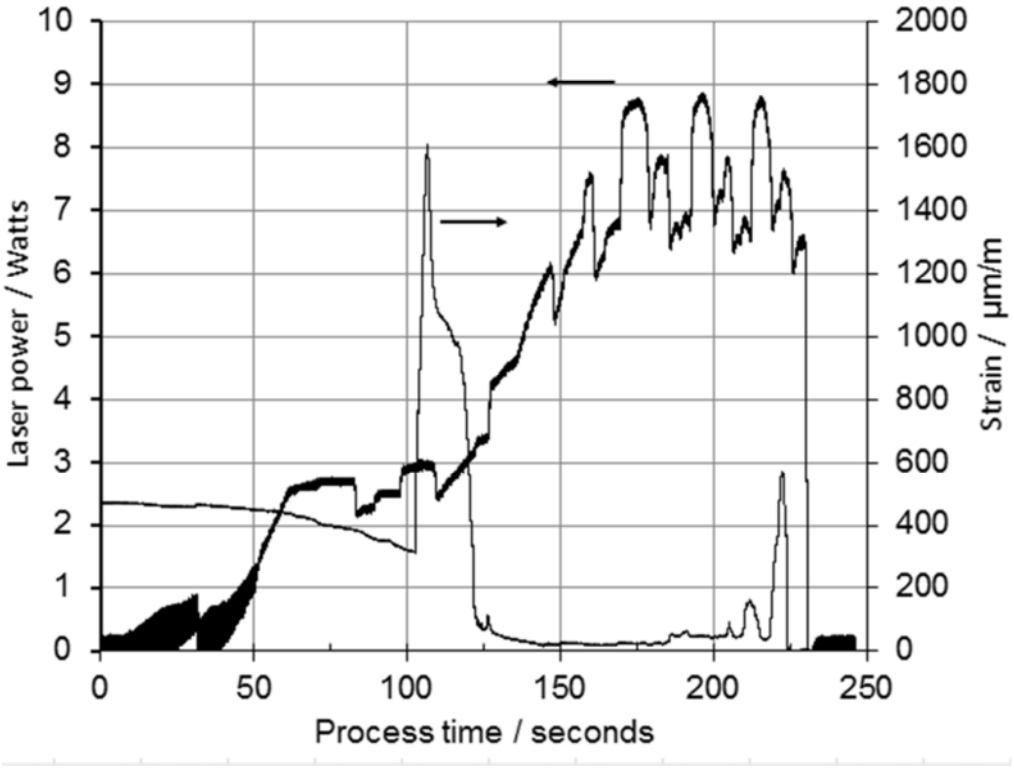

Figure 66: The strain measured by an FBG and laser power during the fabrication of a taper (no pre-heat).

At 224 s, the fibre broke, with a correspondingly abrupt reduction in strain. In this experiment, the laser had not been pre-heated prior to tapering the fibre. This caused the power instability observed from 175 s onwards.

Another experiment was undertaken with the laser pre-heated by operating it an output power of 10 W for 25 minutes before the tapering process started. The power profile then reverted to as shown in figure 66 (from 50 s onwards). The laser pre-heating means that the stages are activated at a different time (~ 65 s). The objective of the experiment was to see if pre-heating the laser would reduce the magnitude of the power variation due to mode hopping and to see what would be the consequent impact on taper strain.

The results are shown in figures 68 and 69. At 70 s, the fibre was stretched, resulting in an abrupt increase in the measured strain. As the laser power increases, the fibre starts to soften, resulting in a subsequent decrease in strain.

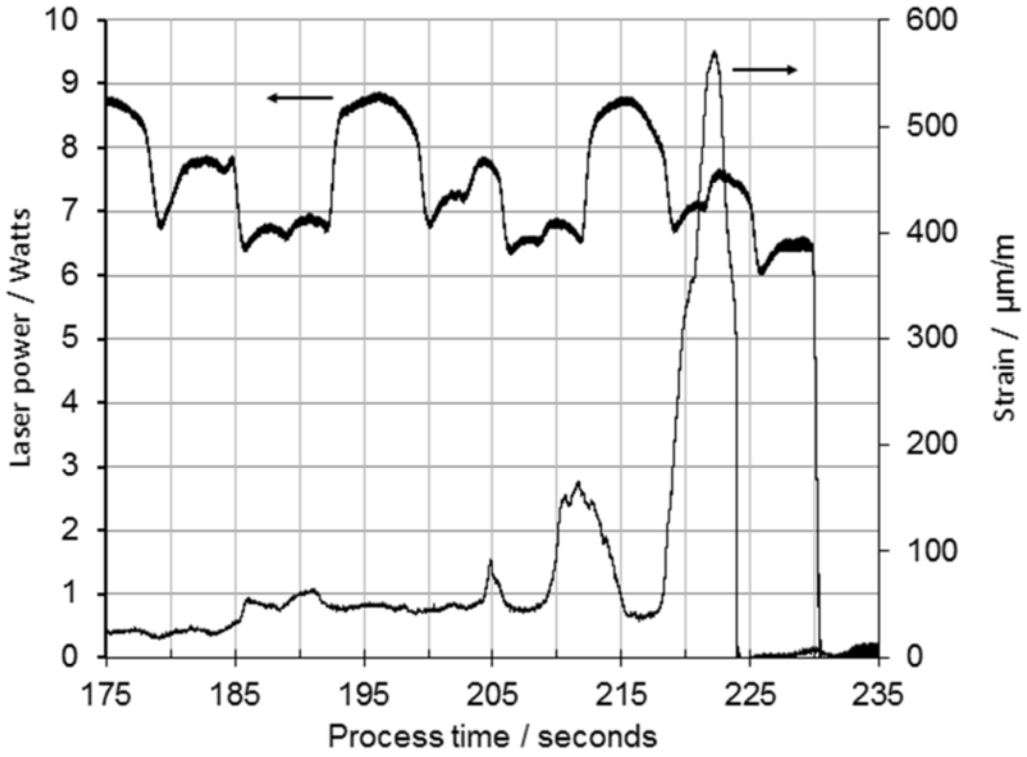

Figure 67: The strain measured by an FBG and laser power during the fabrication of a taper (no preheat). Expanded scale from 175 s.

The laser pre-heating caused the laser output power to be more stable over the region 100 - 200 s, which reduced the variation in the strain measured by the FBG.

FBGs have been used to measure strain during the stretching process and can be used to precisely time the onset of fibre pulling, optimizing the CO_2 laser power profile and identifying when fibre breakage is imminent. In this context, FBGs can be used for developing and optimizing the tapering process but not for routine taper production, as using FBGs increases fibre handling time and could reduce the mechanical integrity of the tapered fibre.

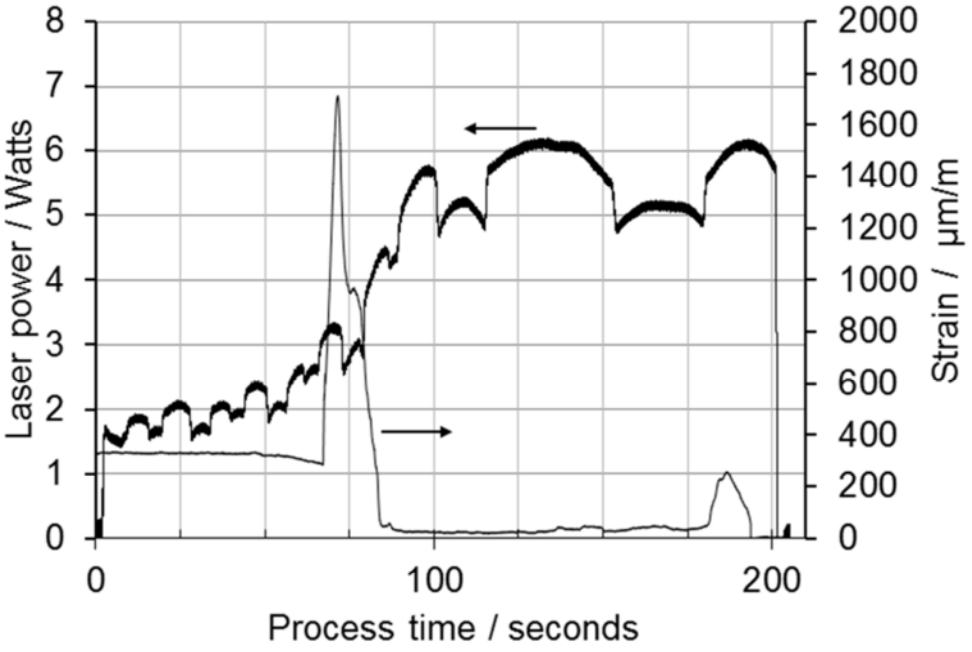

Figure 68: The strain measured by an FBG and the laser power during the fabrication of a taper (with preheat).

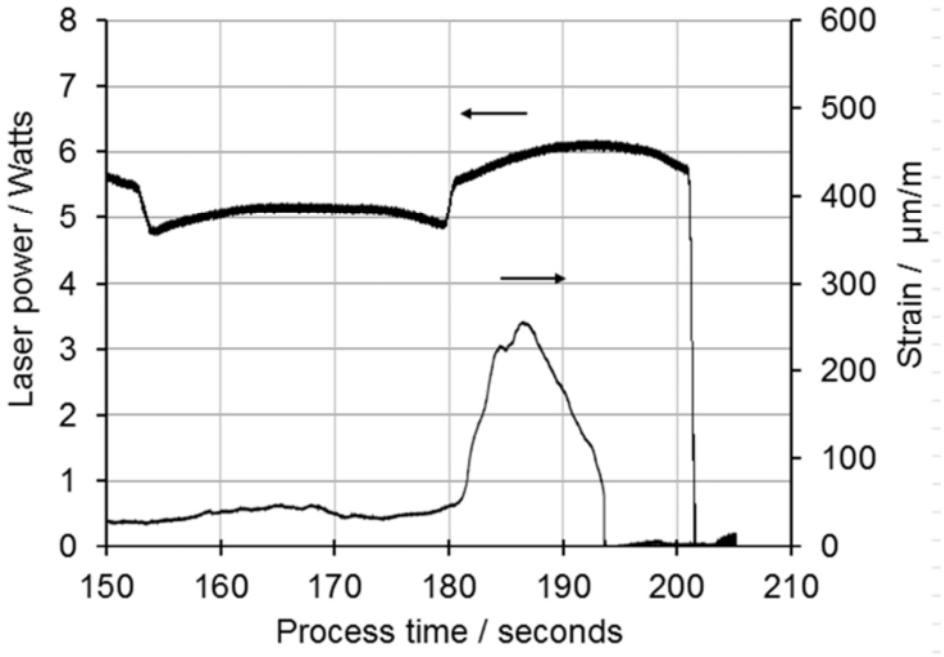

Figure 69: The strain measured by an FBG and the laser power during the fabrication of a taper (with preheat). Expanded scale from 150 s.

6.3 Coated optical tapers

6.3.1 Introduction

Optical fibre tapers can be used as optical sensors as they sensitive to the refractive index of the medium surrounding the taper waist. The sensitivity of an uncoated taper is typically ~ 10000 nm / RIU [9] where RIU is an acronym for “refractive index units”. The sensitivity of tapers to external refractive index changes can be further enhanced by depositing a metallic thin film coating on the taper waist so forming a surface plasmon resonance (SPR) sensor. Typical sensitivities of 11800 – 15000 nm / RIU have been achieved using this type of sensor [10, 11, 12, 13].

When a tapered fibre is used as an SPR sensor, the reduced cladding and core diameters in the taper region cause the evanescent wave to spread outside the fibre. If a metallic film is deposited on the surface of the waist, a surface plasmon wave can be excited in the metallic layer, when light incident at the cladding /metal layer interface just exceeds the critical angle for total internal reflection. These plasmon waves propagate along the interface between the metal layer and the surrounding medium. Due to the surface plasmon propagation, the fibre transmission spectrum contains a resonance minima at a specific wavelength. The central wavelength of the resonance minima shifts to longer wavelengths and deepens [14] if the refractive index of the medium surrounding the metallic layer increases (see figure 70). This forms the basis for their use as a high sensitivity optical sensor.

The optical properties of the resonance minima (wavelength, bandwidth and extinction) are determined by the interplay of waist diameter, transition geometry and thickness of the metallic layer. If gold is used as the sensing material, a layer thickness increase [11, 13], causes the minima to shift to longer wavelengths and decrease in extinction level as the evanescent wave is attenuated by the thicker gold film so reducing its ability to form a surface plasmon. The taper transition geometry [10] can also influence both the bandwidth of the resonance minima and the refractive index sensitivity with a sinusoidal shaped transition zones providing the greatest refractive index sensitivity

[15]. When the taper waist diameter decreases, the resonance bandwidth increases [16] and shifts to shorter wavelengths.

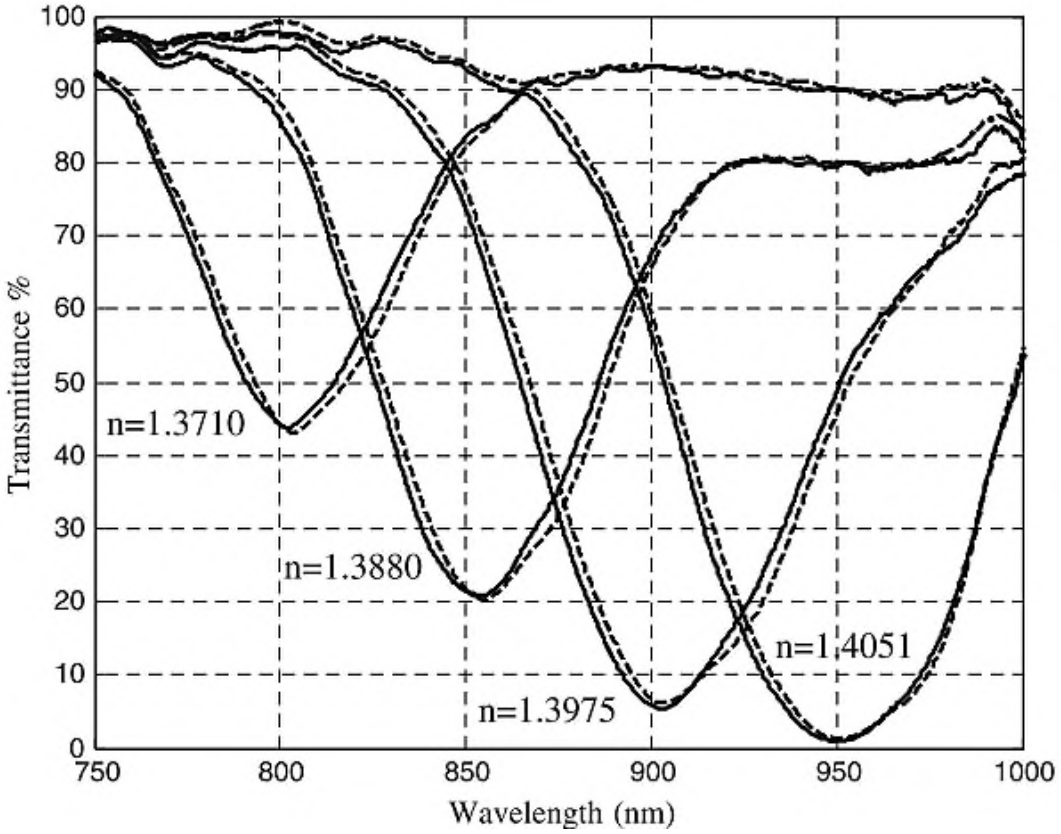

Figure 70: Experimental behaviour of a symmetrically coated fibre as the index of the surrounding medium changes. The solid line shows the fibre transmission when unpolarised light propagates along the fibre and the dotted lines shows the transmission using polarised light. A single wide plasmon dip appears in the spectral transmittance curve [14].

The metallic coating is usually gold [11,13] due to its chemical inertness. palladium/silver alloys, silver and aluminium have also been used [16, 17, 14, 18]. The metal layers can have thicknesses ranging from 8 nm to 70 nm.

These coatings are usually deposited using either sputtering or high vacuum evaporation using a thin layer (~ 2 nm) of either titanium or chrome [19] to assist in the adhesion of the thicker SPR layer. As well as using vacuum evaporation to deposit

coatings, wet chemistry techniques can also be used to deposit functional coatings [21]. These techniques are discussed in sections 6.3.3 and 6.3.4.

Some researchers [20] have improved the sensor sensitivity still further by either inserting dielectric layers beneath or above the metallic layers. Materials used in these cases were either teflon, alumina or titania [20, 14]. Using these additional layers, allows the option of tuning the wavelength of the resonance minima throughout the visible spectrum by adjusting the layers physical thicknesses.

Rotating tooling is ideally used to support the fibre to ensure that the sputtered coating thickness is uniform around the circumference of the fibre, otherwise the coating can be preferentially deposited on one side of the fibre with an associated thickness gradient around the circumference of the fibre (figure 71).

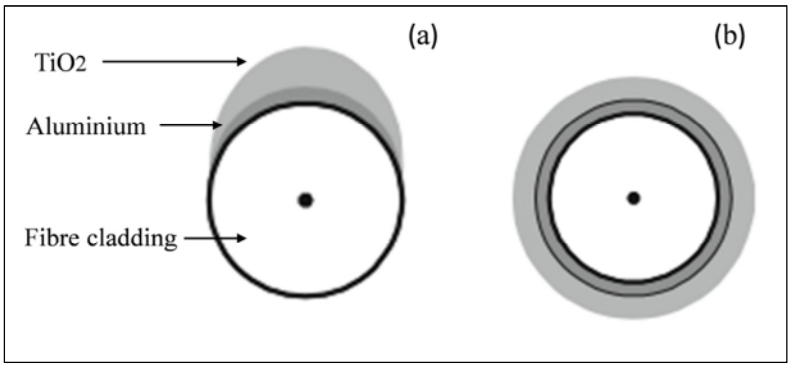

Figure 71: Schematic of the cross-section through a non-uniform coating on a fibre (a) and a uniformly coated fibre (b) [14].

Several methods have been used to produce an improved uniformity fibre coating. The fibre can be rotated about its axis behind a narrow slit shaped aperture during the deposition process [14]. Another approach is to employ triangular shaped tooling [11] with three apertures spaced by 120^{0}. The tooling is then sequentially rotated three times to produce an overlapping uniform coating around the fibre circumference.

When the metallic coatings are uniform in thickness around the circumference of the fibre, the resonance minima will be unique [14] and tends to be deeper with a broad

bandwidth (figure 70), whereas if the thickness is non-uniform it will produce several resonance minima as the condition for surface plasmon resonance now occurs at multiple wavelengths (figure 72).

The solid lines in figures 70 and 72 show the fibre transmission when unpolarised light propagates along the fibre and the dotted lines show the transmission using polarised light. The symmetrically coated fibre shows minimal differences between the different polarisation states confirming the uniformity of the coating.

.

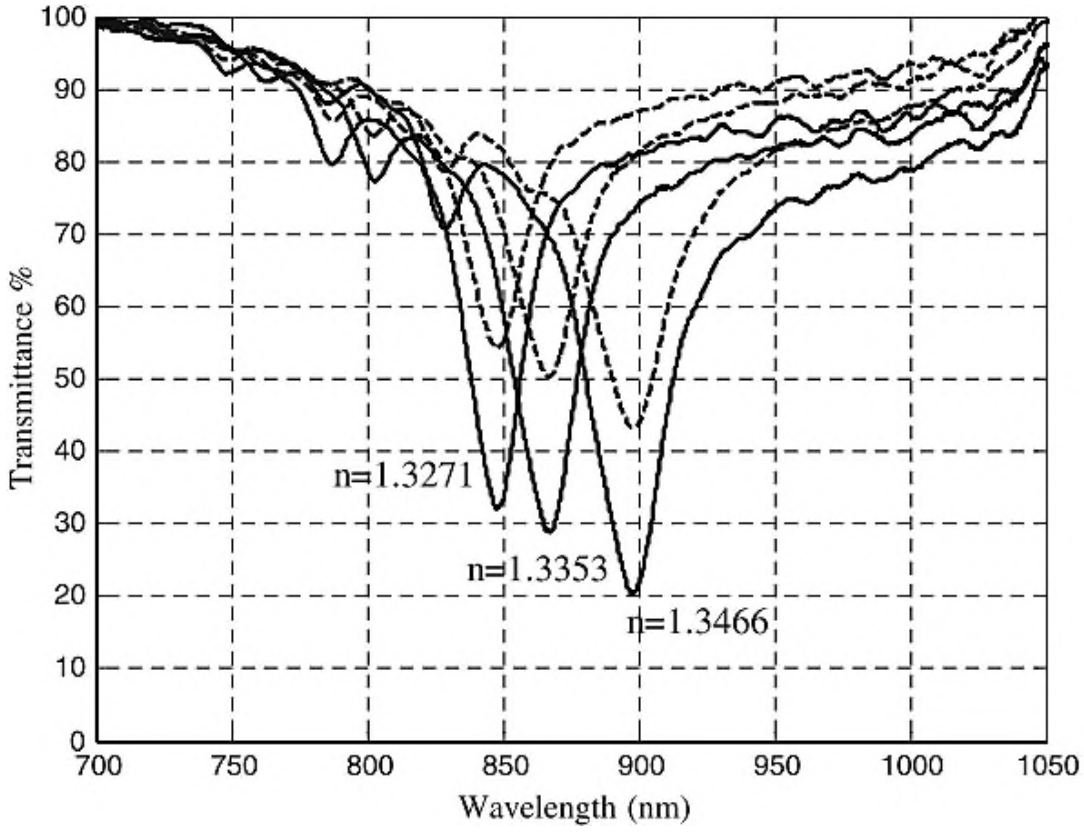

Figure 72: Experimental behaviour of an asymmetrically coated fibre as the index of the surrounding medium changes. The solid line shows the fibre transmission when unpolarised light propagates along the fibre and the dotted lines shows the transmission using polarised light. Multiple plasmon resonances appear [14].

The next section of the thesis describes the experimental results produced by depositing a titanium / gold coating onto a tapered fibre using sputtering techniques.

6.3.2 Sputtered coating experimental results

Given the choice of available sputtering targets, it was decided to deposit titanium at a thickness of 2 ± 1 nm followed by 50 ± 5 nm of gold on the waist and transition regions of a non-adiabatic 10 ± 0.2 mm long taper. The waist diameter was 15 ± 0.5 μm, with a waist length of 3 ± 0.2 mm.

The layer of titanium is a "seed layer" and improves the adhesion of the gold coating to the fibre [22]. The gold coating physical thickness was chosen as it produces a surface plasmon resonance at ~ 800 nm [13]. If a thicker gold coating was used, the spectral resonance shifted to a longer wavelength and its sensitivity would be reduced [13].

The Ti/Au coatings were deposited using a Nordiko sputtering chamber. The fibres were fixed to a stationary tooling plate over the centre of the magnetron target. It is unlikely the gold film thickness was uniform around the circumference of the fibre as the fibres were stationary and sputtering processes have a degree of directionality.

The gold thickness of 50 ± 5 nm was determined by depositing a calibration gold film on glass substrates and measuring their reflectivity and transmission using a Perkin Elmer λ9 spectrophotometer. The measured gold film reflectance and transmission values were then modelled using Filmstar, which is commercial thin film modelling software [http://ftgsoftware.com]. This modelling software has defined gold optical constants data which permits a close match between the measured and theoretical transmission curves by adjusted the theoretical film thickness to a specific value. Given the deposition time of the calibration gold film, the deposition time for the target gold film thickness of 50 nm on the fibre was determined.

The coated taper were placed in a polytetrafluoroethylene (PTFE) trough (figures 73) which allows the taper to be immersed in oils of differing refractive index (1.378 - 1.424) while the transmission of the fibre was measured, see figure 74. The transmission of the fibre measured in air was used as the 100% transmission reference. A weak SPR minima (A) is observable at 680 nm when the refractive index was 1.378. The fibre transmission has been increased to > 100 % at 880 nm as more light has been coupled into the fibre due to the increase in external refractive index from 1.0 to 1.378. When the refractive index was increased to 1.4, the resonance minima "red-shifts" to

780 nm (B) with a greater extinction than at A. As the refractive index increases to 1.424, the resonance minima (C) shifts to a longer wavelength (980 nm). The refractive index sensitivity of this coated taper was 6549 nm /RIU.

The "red shift " of the resonance minima as the refractive index increases has been predicted theoretically by Verma *et al.* in 2008 [10] and observed by other researchers [13, 23, 24]. As the resonance minima shifts to longer wavelengths its extinction increases and broadens as more light is coupled into the external media, this behaviour has also previously been observed by Ju *et al.* in 2013 [13].

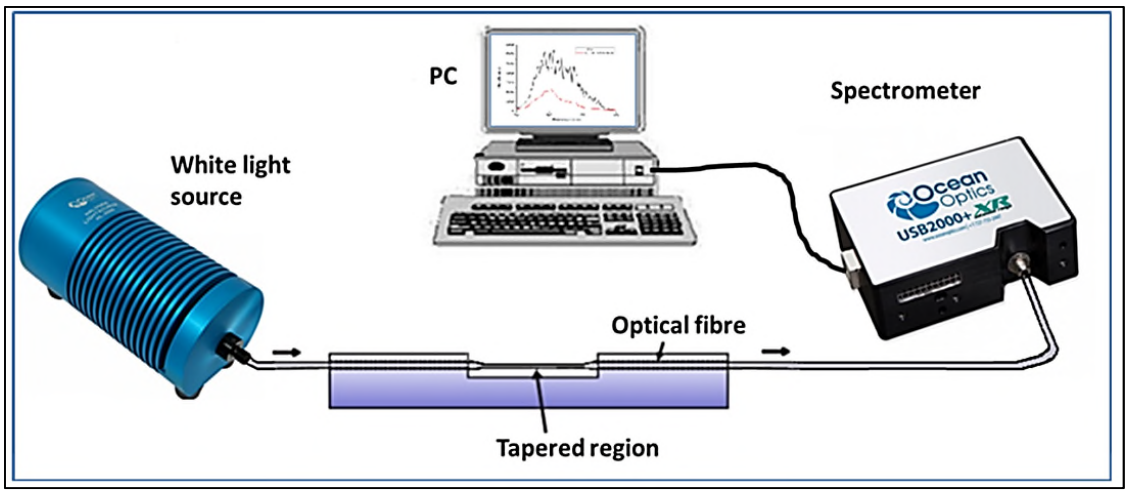

Figure 73: The experimental arrangement used to assess the refractive index sensitivity of the coated tapers. The length of the trough is 20 ± 0.5 mm with a depth of 3 ± 0.25 mm.

As discussed in section 6.3.1, the gold thickness around the taper waist is unlikely to be uniform as the fibre was not rotated during deposition. This will tend to broaden the observed resonance minima as the resonant wavelength will be a function of a graded gold thickness [13]. This effect could be corrected in future work with bespoke tooling which rotates the fibre over the sputtering target during the deposition process. This would reduce the bandwidth of the resonance minima and increase the resolution of this device in a sensing configuration [12].

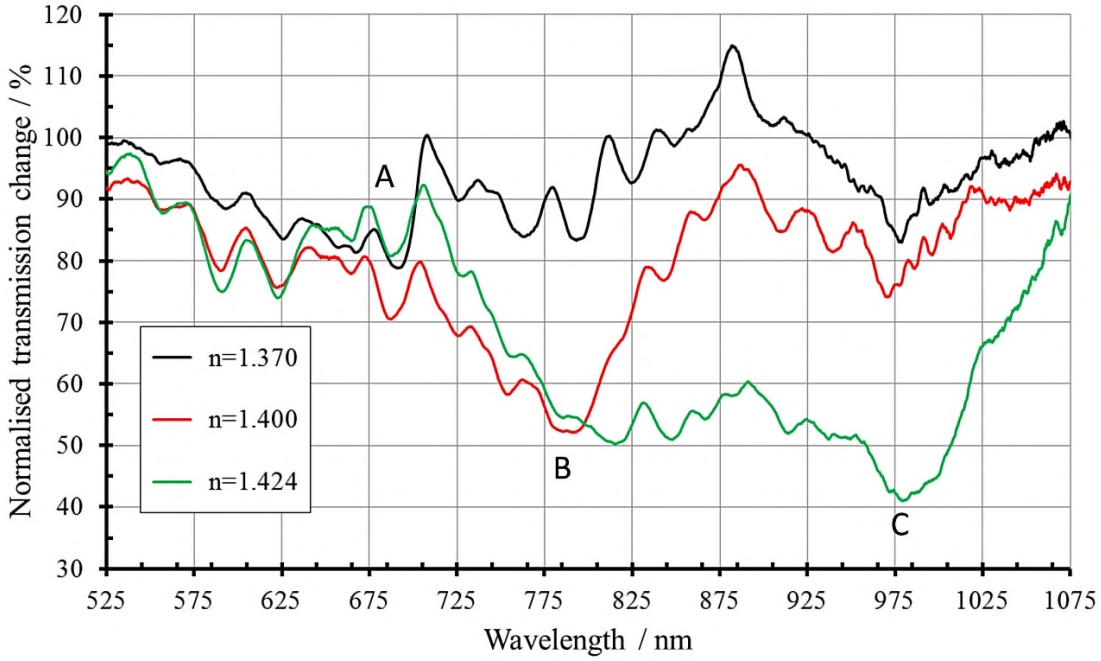

Figure 74: The transmission of a gold coated non-adiabatic taper with a waist diameter of 15 ± 0.5 µm, when immersed in index oils, varying in refractive index from 1.378 to 1.424.

6.3.3 Gold-based nano-coatings on optical tapers

6.3.3.1 Introduction

As well as sputtering technology, other deposition techniques such as dip and spin coating, layer-by-layer (L-b-L) electrostatic self-assembly and Langmuir–Blodgett (LB) deposition have all been employed to deposit functional coatings on optical fibres [25, 26]. Among these techniques, the layer by layer technique which is based on the alternate adsorption of polycations and polyanions onto the optical fibre surface is a powerful surface modification technique. The following sections describe a novel alternative deposition method on tapered fibres based on the L-b-L technique that provides a means to control the porosity and morphology of the thin films as opposed to the other techniques cited which are somewhat less flexible [25].

The following work was done in conjunction with the University of Nottingham [25] with the objective of fabricating a protein sensor. This is a novel use of tapered optical fibre sensors to detect very low protein concentrations. Cranfield University supplied ~ 90 tapers similar to taper B (section 6.2) and Sergiy Korposh and his team from the

University of Nottingham, undertook the L-b-L deposition and the subsequent analysis. Their results are reported in the following section.

6.3.3.1 Experimental results

Tapered non-adiabatic 14 μm tapers were coated with two types of gold based coating for use as a protein sensor. In this work biotin and streptavidin (SV) binding was chosen as the protein sensing model.

The two types of coatings which were investigated were:

a) L-b-L deposition of poly (allylamine hydrochloride) (PAH) and negatively charged SiO_2 nano-particles followed by the deposition of charged gold nano-particles (NPs). For the T2 $_{Au\ NPs}$ sensor, three bilayers of PAH: SiO_2 NPs followed by two bilayers of AuNPs:PSS and a final layer of gold NPs were deposited onto the taper.

b) The sputtered gold sensor (T1 $_{Au\ sputtered}$) had a thickness of 10 nm of gold which was used as a comparison to (a).

The optical transmission of these two coating types are shown in figures 75 and 76. The original spectrum of the $T1_{Au\ sputtered}$ sensor was recorded along with the spectrum after the deposition of the Au film. The Au deposition step results in a significant attenuation of the transmitted signal. The characteristic fringes of the non-adiabatic taper are no longer visible after sputtering the gold thin film. The broad decrease in transmission around 600-750 nm is believed to be the plasmon resonance of the Au film. The disappearance of the characteristic interference fringes is most plausibly a result of the high refractive index of the gold coating which suppresses the excitation of the higher order modes in the tapered region of the optical fibre.

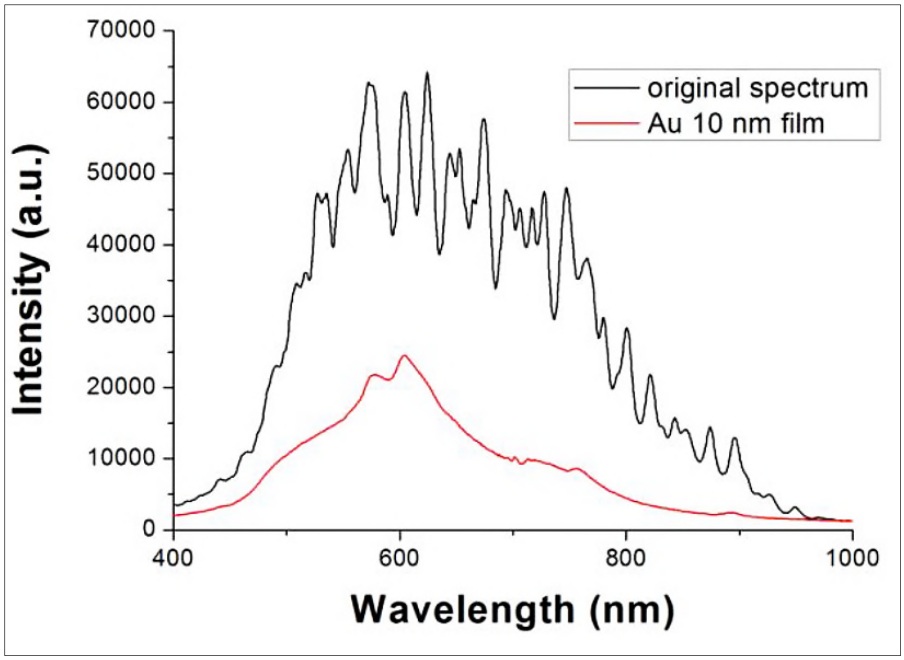

Figure 75: Transmission spectra of a tapered fibre before and after the deposition of the sputtered gold thin film [25].

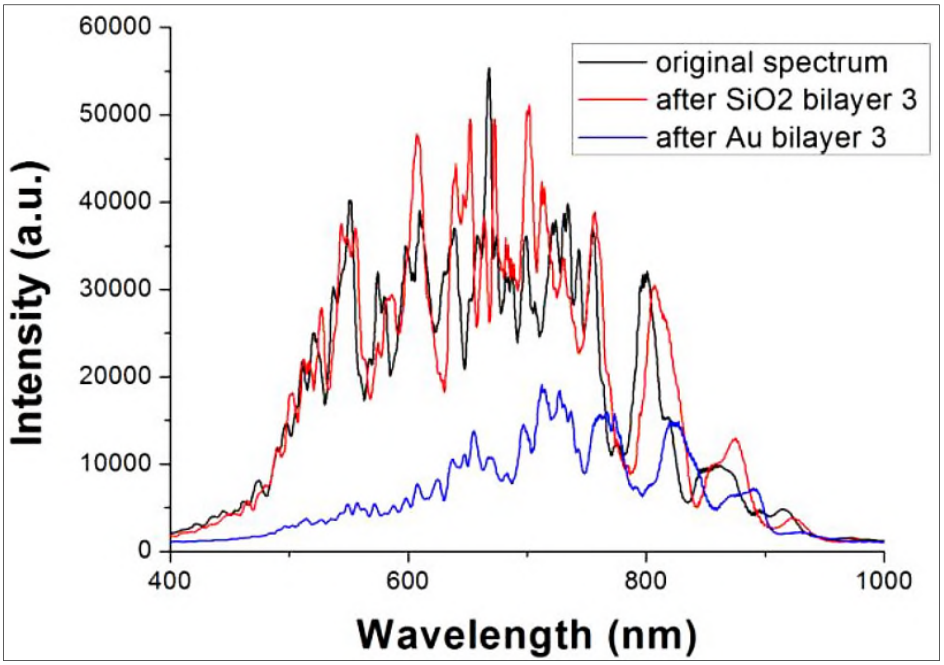

Figure 76: Transmission spectra of a tapered fibre before and after the deposition of gold NPs [25].

The initial L-b-L process steps in figure 76 causes a red shift in the transmission spectrum due to the deposition of the SiO_2 nanoparticles. In contrast to the sputtering process not all of the fringe features disappear after the deposition of the Au NPs. There are however noticeable changes in the region 750-900 nm at the sensor surface due to the effect of the Au NPs.

Both the $T1_{Au\ sputtered}$ and $T2_{\ Au\ NPs}$ sensors were coated with biotin to provide binding sites for the SV molecules. Biotin-SV binding was detected by optical losses in the transmission spectra of the tapered optical fibre. The sensing principle of the devices is explained using evanescent field theory. The higher concentration of SV bound to biotin produces additional signal losses, due to external refractive index (RI) changes. If the external RI is higher than the core RI, then as differences between the external RI and the core RI increase, then the optical losses increase also. $T1_{Au\ sputtered}$ and $T2_{\ Au\ NPs}$ were exposed to SV concentrations ranging from 2.5 nM to 1.33 μM, and their results were monitored and analysed. $T1_{Au\ sputtered}$ and $T2_{\ Au\ NPs}$ exhibited a logarithmic response in terms of optical signal versus SV concentration. The results are shown in figure 77.

Both the $T1_{Au\ sputtered}$ and $T2_{\ Au\ NPs}$ sensors could detect levels of SV below 2.5 nM. $T2_{\ Au\ NPs}$ shows enhanced results in terms of sensitivity and dynamic range, and it could also detect the SV variations from three simultaneous peaks measurements and also wavelength shift based measurements. The L-b-L coating based on Au nanoparticles had a higher surface area than a sputtered Au thin film and so was more efficient in the biotin adhesion process, and therefore in SV concentration detection.

Future work will focus on improving and optimizing the sensor design to achieve a lower limit of detection (LoD) and improved properties in terms of selectivity, dynamic range and sensor response time. The development of these coated sensors demonstrates the concept that tapered optical fibres and their configurations are very suitable to detect not only proteins but also other substances such as volatile organic compounds, gases, relative humidity, with ultra-low LoD values.

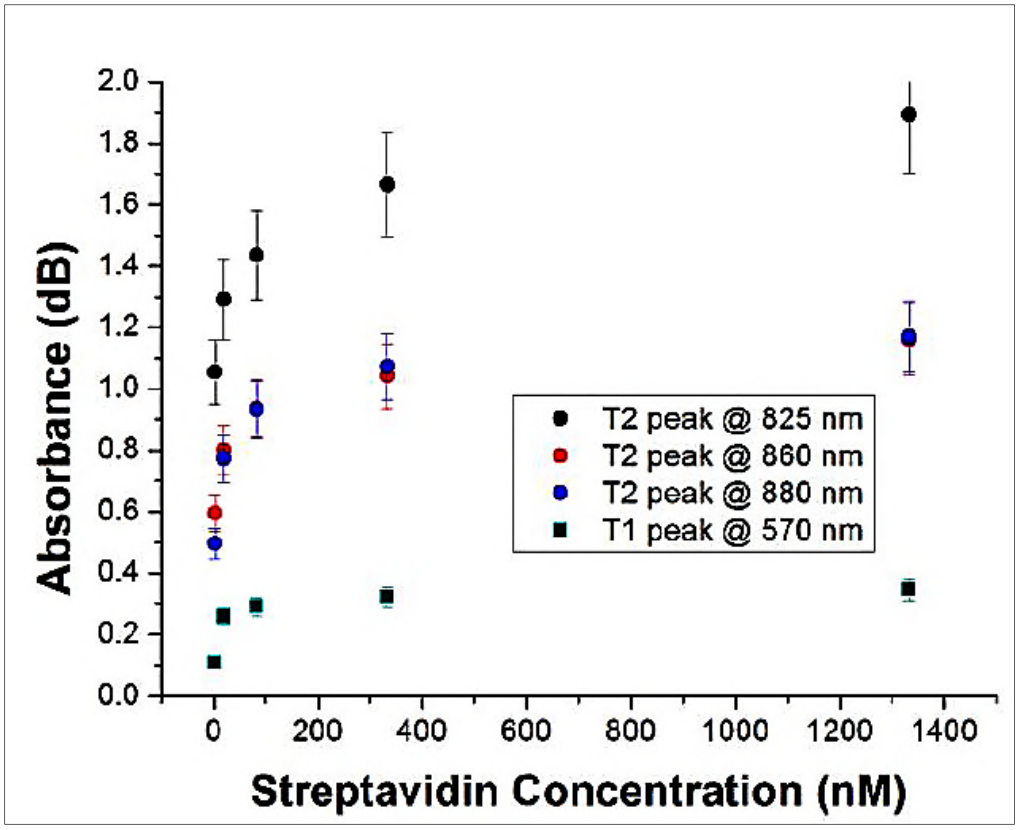

Figure 77: $T1_{Au\ sputtered}$ and $T2_{Au\ NPs}$ transfer functions: normalised absorbance maximum peaks for different SV concentrations [25].

6.3.4 Lossy mode resonance in coated adiabatic tapers

6.3.4.1 Introduction

As well as using the SPR technique as an optical sensor (sections 6.3.2 & 3), a similar phenomenon using lossy mode resonance (LMR) can also be used as an optical sensor. LMR sensors are usually fabricated by removing the cladding from a multimode fibre so accessing the evanescent field of the core [27, 28]. An absorbing coating is then deposited on the fibre core which forms the new cladding. For LMR to occur, the coating permittivity must be positive and its absolute value is higher than the absolute value of its own imaginary part and higher than the absolute value of the material surrounding the absorbing coating [29, 30]. The resonance consists of coupling light from the fibre core to lossy modes guided in the absorbing coating.

If an adiabatic taper is used as the sensing platform then the evanescent field can be accessed without removing the cladding and the fibre transmission will be high with a reduced fringe pattern modulating the response [30, 31].

The next section describes the work undertaken to fabricate a LMR optical sensor. The coating deposition and optical measurements were undertaken by Dr. Divya Tiwari and are reported in the next section.

6.3.4.2 LMR experimental results

A 17 ± 0.5 μm diameter adiabatic taper (0.1 dB insertion loss) was fabricated in SM750 fibre using the tapering process described in section 6.2.1. An adiabatic taper was used for this application to avoid the formation of a channelled spectrum in the transmission characteristic of the fibre. Channelled spectra are usually produced by non-adiabatic tapers. If a channelled spectrum were present, it would inevitably distort the transmission profile of the LMR spectral feature. The taper waist diameter used was chosen to increase the sensitivity of the device [30]. The 17 μm taper was then coated using liquid phase deposition of a nanoscale coating of titanium dioxide (TiO_2) infused with a functional material TMPyP (5,10,15,20 – Tetrakis (1-methyl-4-pyridinio) porphyrin tetra (p-toluenesulfonate)) to provide ammonia sensitivity. The base coating thickness was designed such that it accesses the LMR, which further enhances the sensitivity of the taper to external refractive index changes. The tapers were placed in a PTFE trough as shown in figure 73 and its transmission was recorded.

LMR was observed after ~ 7 hours of deposition when the thickness of the sensitive coated layer is approximately 70-80 nm. The LMR resonance band is identified by observing the transmission spectrum (see figure 78) of the tapered fibre while depositing the nanoscale coating of TMPyP-infused TiO_2. Figure 78 shows the LMR appearing after 7 hours and moving to longer wavelengths with the increase in thickness of the titania coating. The fibre was removed from the chemical solution after the appearance of the LMR band.

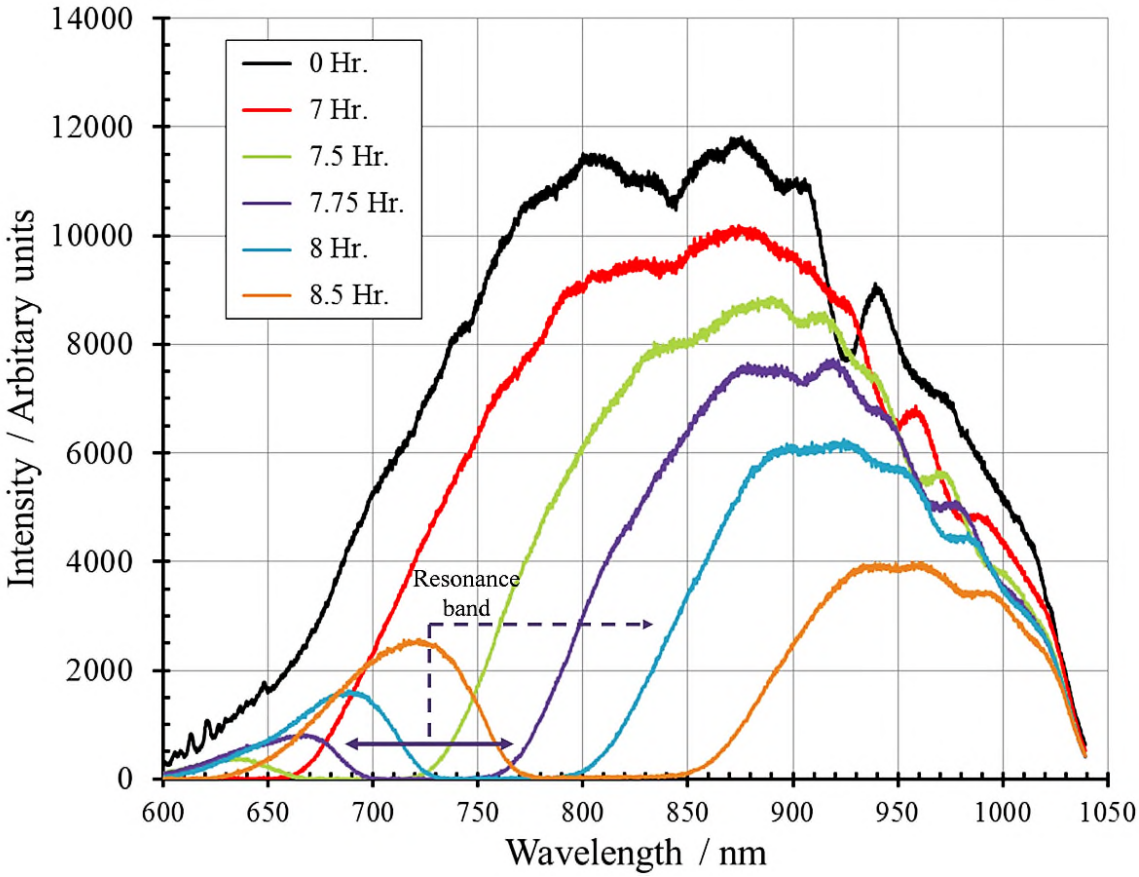

Figure 78: Lossy mode resonance in a TMPyP-infused TiO_2 coated, adiabatic SM750 taper. As the deposition time increases, the resonance minima red shifts.

The tapered fibre coated with the sensitive TMPyP-TiO2 layer was then exposed to varying concentrations of ammonia in water. The transmission spectrum was observed in water and was monitored while exposing it to 0.1, 0.6, 1, and 10 ppm concentrations of ammonia in water. Immersing the coating in a 0.1 ppm ammonia concentration, caused no change in the spectrum. However, when the concentration was increased to 0.6 ppm, the attenuation band showed a red-shift by 0.49 nm, after 1 minute in solution. As the ammonia concentration was further increased to 1 ppm an immediate red-shift in wavelength was observed in 5 seconds which increased to 3 nm within 1 minute and further increased to 3.85 nm after 3 minutes in solution. All samples were immersed in the solution for 3 minutes. After 3 minutes, no further wavelength shift was observed for the differing solutions. The shift in attenuation band to longer wavelengths is continuous and upon exposure to 10 ppm ammonia concentration, a red-shift of 4.9 nm

was observed in 1 minute. The magnitude of the red-shift increases, with concentration. Figure 79 shows the transmission spectra recorded during the experiments.

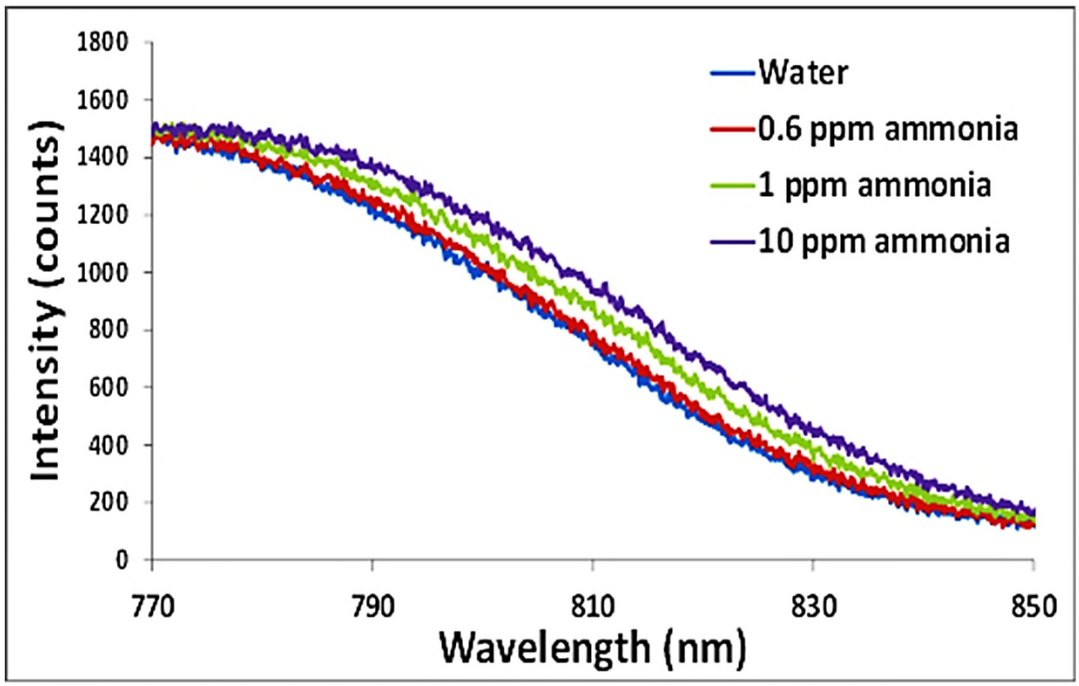

Figure 79: The response of the transmission spectrum of TMPyP-TiO_2 coated tapered optical fibre to immersion in water and varying concentrations of ammonia in water.

It is believed that the observed changes in taper transmission spectrum are due to an increase in refractive index of the coating upon exposure to the ammonia in solution.

6.4 Conclusions

6.4.1 Single tapers

A system for fabricating optical tapers with repeatable physical dimensions has been developed. Single tapers were fabricated with waist diameters down to 5 ± 0.5 μm and with waist lengths of 20 mm using single-mode SMF-28 fibre.

The use of a range of optical techniques to monitor the process of fabricating optical fibre tapers has also been investigated. A camera operating in the near infra-red has been used both to aid fibre alignment and to allow the laser power profile for the process to be easily determined. This is a novel application of this instrument.

Monitoring the transmission spectrum of the fibre during the tapering process allows the operator to ensure that the taper will have the required spectral properties in the wavelength region of interest. The use of an IR camera, together with monitoring the transmission of the fibre, are effective process tools so allowing the taper process to be optimized for specific sensing applications.

FBGs have been used as a novel indicator of the strain experienced by the fibre during the tapering process and have potential utility in optimizing the control of the rotation stages, the laser power profile and in determining the onset of fibre breakage when fabricating very small diameter tapers. In this context, FBGs can be used for developing and optimizing the tapering process but not for routine taper fabrication activities, as for many applications it may not be appropriate to have the FBG in-line with the taper.

Future work could explore the effectiveness of using the IR camera to measure fibre temperature during the process so allowing the laser power to be actively controlled, thereby eliminating the need for unique laser power curves for tapers of differing profiles.

6.4.2 Coated tapers

Single tapers have been coated with a titanium/ gold coating to create a surface plasmon resonance sensor. The refractive index sensitivity of this sensor was 6549 nm /RIU.

Improvements could be made to improve the sensitivity of this device by changing the deposition process so that the gold coating thickness is uniform around the circumference of the fibre.

Using a layer-by-layer deposition technique, gold nano particles have been deposited on a tapered fibre to produce a novel protein sensor. This sensor exhibited greater sensitivity when compared to gold coated tapers deposited using conventional sputtering techniques. Both types of sensors could detect levels of streptavidin (SV) below 2.5 nM.

Lossy mode resonance has been demonstrated on an adiabatic taper which was coated with titanium dioxide (TiO_2) infused with a functional material (TMPyP). As an ammonia sensor, this device was effective at sensing ammonia concentrations in a solution within the range; 0.6 -10 ppm.

6.5 References

[1] T. A. Birks and Y. W. Li, "The shape of fiber tapers," *J. Light. Technol.*, Vol. 10, No. 4, pp. 432–438, 1992.

[2] F. Bayle and J. P. Meunier, "Efficient fabrication of fused-fiber biconical taper structures by a scanned CO_2 laser beam technique.," *Appl. Opt.*, Vol. 44, No. 30, pp. 6402–11, 2005.

[3] FlIR Systems AB, "ThermaCAM ^{TM} SC3000," No. 557 379, 1999.

[4] FLIR Systems AB, "The Ultimate Infrared Handbook for Research & Development Professionals." FLIR Systems Incorporated.

[5] R. Jarzebinska, C. S. Cheung, S. W. James and R. P. Tatam, "Response of the transmission spectrum of tapered optical fibres to the deposition of a nanostructured coating," *Meas. Sci. Technol.*, Vol. 20, No. 3, pp. 1–6, 2009.

[6] J. M. Ward, D. G. O'Shea, B. J. Shortt, M. J. Morrissey, K. Deasy and S. G. Nic Chormaic, "Heat-and-pull rig for fiber taper fabrication," *Rev. Sci. Instrum.*, Vol. 77, No. 8, p. 083105, 2006.

[7] A. J. C. Grellier, "Characterisation of optical fibre tapering using a CO_2 laser," *PhD Thesis*, University of Canterbury, 2000.

[8] J. Lee, C. H. Lee, M. K. Kim and K. T. Kim, "Characteristics of fiber Bragg grating temperature sensor using thermal strain of an external tube", *J. Korean Phys. Soc.*, Vol. 59, No. 51, p. 3188, 2011.

[9] J. Villatoro, D. Monzo and D. Talavera, "High resolution refractive index sensing with cladded multimode tapered optical fibre", *Electron. Lett.*, Vol. 40, No. 2, 2004.

[10] R. K. Verma, A. K. Sharma and B. D. Gupta, "Surface plasmon resonance based tapered fiber optic sensor with different taper profiles," *Opt. Commun.*, Vol. 281, No. 6, pp. 1486–1491, 2008.

[11] T. Wieduwilt, K. Kirsch, J. Dellith, R. Willsch and H. Bartelt, “Optical fiber micro-taper with circular symmetric gold coating for sensor applications based on surface plasmon resonance”, *Plasmonics*, Vol. 8, No. 2, pp. 545–554, 2013.

[12] M. C. Navarrete, N. Díaz-Herrera, A. González-Cano and Ó. Esteban, “Surface plasmon resonance in the visible region in sensors based on tapered optical fibers,” *Sensors Actuators B Chem.*, Vol. 190, pp. 881–885, 2014.

[13] S. Ju, S. Jeong, Y. Kim, P. Jeon, M.-S. Park, H. Jeong, S. Boo, J. H. Jang and W.-T. Han, “Experimental demonstration of surface plasmon resonance enhancement of the tapered optical fiber coated with Au/Ti thin film,” *J. Non. Cryst. Solids*, pp. 1–7, 2013.

[14] M. C. Navarrete, N. Díaz-Herrera, A. González-Cano and Ó. Esteban, “A polarization independent SPR fiber sensor,” *Plasmonics*, Vol. 5, No. 1, pp. 7–12, 2010.

[15] S. Kumar, G. Sharma and V. Singh, “Sensitivity of tapered optical fiber surface plasmon resonance sensors”, *Opt. Fiber Technol.*, Vol. 20, No. 4, pp. 333–335, 2014.

[16] J. Villatoro, D. Monzón-Hernández, E. Mejía and D. Monzo, “Fabrication and modelling of uniform-waist single-mode tapered optical fiber sensors.,” *Appl. Opt.*, Vol. 42, No. 13, pp. 2278 –2283, 2003.

[17] J. Hu, M. Jiang and Z. Lin, “Novel technology for depositing a Pd–Ag alloy film on a tapered optical fibre for hydrogen sensing,” *Jour. of Optics A: Pure & Appl. Optics.*, Vol. 7, pp. 593–598, 2005.

[18] H. Moayyed, I. T. Leite, L. Coelho, J. L. Santos and D. Viegas, “Analysis of phase interrogation in SPR-based sensing supported by tapered optical fibres,” *Fifth European workshop on optical fibre sensors*, Krakow, Poland, *Proc. SPIE*, Vol. 8794, p. 879426 1–5, 2013.

[19] S. K. Srivastava and B. D. Gupta, “A Multi-tapered fiber optic SPR sensor with enhanced sensitivity,” *IEEE Photonics Technol. Lett.*, Vol. 23, No. 13, pp. 923–925, 2011.

[20] R. Jha, R. K. Verma and B. D. Gupta, “Surface plasmon resonance based tapered fiber optic sensor: sensitivity enhancement by introducing a teflon layer between core and metal layer,” *Plasmonics*, Vol. 3, No. 4, pp. 151–156, 2008.

[21] C. Caucheteur, T. Guo, and J. Albert, “Review of plasmonic fiber optic biochemical sensors: improving the limit of detection,” *Anal. Bioanal. Chem.*, Vol. 407, No. 14, pp. 1–15, 2015.

[22] J. C. Hoogvliet and W. P. Van Bennekom, “Gold thin-film electrodes: An EQCM study of the influence of chromium and titanium adhesion layers on the response,” *Electrochim. Acta*, Vol. 47, No. 4, pp. 599–611, 2001.

[23] H. Chen, X. Kou, Z. Yang, W. Ni and J. Wang, “Shape and size dependent refractive index sensitivity of gold nanoparticles,” *Langmuir*, Vol. 24, No. 10, pp. 5233–5237, 2008.

[24] X. Dou, P. Y. Chung, P. Jiang and J. Dai, “Surface plasmon resonance and surface-enhanced Raman scattering sensing enabled by digital versatile discs,” *Appl. Phys. Lett.*, Vol. 100, No. 4, 2012.

[25] A. Urrutia, K. Bojan, L. Marques, K. Mullaney, J. Goicoechea, S. W. James, M. Clark, R. P. Tatam and S. Korposh, “Novel highly sensitive protein sensors based on tapered fibres modified with Au-based nanocoatings”, *Fiber Sensor Technology: Distributed, Multiplexing and Networking Systems, submitted.*

[26] S. W. James and R. P. Tatam, “Fibre optic sensors with nano-structured coatings,” *J. Opt. A Pure Appl. Opt.*, Vol. 8, No. 7, pp. S430–S444, 2006.

[27] F. J. Arregui, I. Del Villar, J. M. Corres, J. Goicoechea, C. R. Zamarreño, C. Elosua, M. Hernaez, P. J. Rivero, A. B. Socorro, A. Urrutia, P. Sanchez, P. Zubiate, D. Lopez, N. De Acha and I. R. Matias, “Fiber-optic Lossy Mode Resonance Sensors,” *Procedia Eng.*, Vol. 87, pp. 3–8, 2014.

[28] P. Sanchez, C. R. Zamarreño, M. Hernaez, I. R. Matias, and F. J. Arregui, “Optical fiber refractometers based on Lossy Mode Resonances by means of SnO_2 sputtered coatings,” *Sensors Actuators, B Chem.*, Vol. 202, pp. 154–159, 2014.

[29] I. Del Villar, M. Hernaez, C. R. Zamarreño, P. Sánchez, C. Fernández-Valdivielso, F. J. Arregui and I. R. Matias, “Design rules for lossy mode resonance based sensors,” *Appl. Opt.*, Vol. 51, No. 19, pp. 4298–4307, 2012.

[30] A. B. Socorro, I. Del Villar, J. M. Corres, I. R. Matias and F. J. Arregui, “Lossy mode resonances dependence on the geometry of a tapered monomode optical fiber,” *Sensors Actuators, A Phys.*, Vol. 180, pp. 25–31, 2012.

[31] I. Del Villar, C. R. Zamarreño, P. Sanchez, M. Hernaez, C. F. Valdivielso, F. J. Arregui and I. R. Matias, “Generation of lossy mode resonances by deposition of high-refractive-index coatings on uncladded multimode optical fibers,” *J. Opt.*, Vol. 12, No. 9, pp. 1–7, 2010.

7 TLPG Experimental Results

7.1 Introduction

The experimental results for the TLPGs which were fabricated are provided in this chapter. The aspects of this work which is novel is the optimization of micro-taper geometry such that compact TLPGs can be fabricated. Cascaded TLPGs were also fabricated and their optical performance is described here also.

7.2 TLPG process development history

7.2.1 CO_2 TLPG system

The optical system that was developed to fabricate single tapers was then adapted so that it could also fabricate periodically spaced micro-tapers. The objective was to reproduce the optical performance of arc-induced TLPGs described in section 2.3.2.3 but using micro-tapers to produce the periodic refractive index modulation. The TLPG process features from tables 2 and 3 are summarised in table 13 together with the proposed features to be investigated in this thesis.

Table 13: CO_2 TLPG process features to be investigated.

Process requirement	Process feature to be examined.	Comments
Laser power	< 10 W, $\leq$ 20 s pulse lengths.	Longer pulses reduce potential timing errors.
Laser power control	Pre-programmed timed laser pulses rather than using a shutter.	A shutter will be used later if required.
Lens type – focal length	Plano-convex cylindrical – 100 mm, line focus perpendicular to fibre axis.	This will give a hot-zone width of < 388 μm (section: 4.3.4).
Fibre type	SM750	CO_2 tapered LPGs operating in the visible spectrum have not been reported to date and allows low cost spectrometers to be used.

Process requirement	Process feature to be examined.	Comments
Micro-tapers	Waist diameters to be ≥ 100 μm.	Objective will be to get repeatable performance on taper length and waist diameter.
Fibre-tensioning	Rotation stages used to pull the taper and maintain tension.	A single weight will not be used to maintain tension during the process as this technique can create asymmetric tapers [6].
Fibre translation method	Rotation stages to translate the fibre.	The impact of duty-cycle on the spectral performance of TLPGs will be explored as it known to be an important feature [1]. To date this parameter has not been investigated for this type of LPG.

7.2.2 Early process

The optimized process for fabricating TLPGs is described in section 5.3. This section summarizes the process changes that were followed to *arrive at the optimized process*. The experimental layout and process that were used in the initial arrangement is shown in figure 44, with the following modifications:

a. The rotation stages rotated about the y-plane.
b. No weight was used to pre-tension the fibre before starting the process. Instead, the stages were powered for 1 s to pull the fibre in opposite directions to apply pretension to the fibre.
c. The fibre was attached to the rotation stages with “Sellotape”.

7.2.3 Initial experimental results

Using the set-up described in sections 7.2.2, a TLPG in which 18 micro-tapers were spaced by 704 μm, was fabricated using SM750 fibre. The average taper waist diameter was 113 μm and the average length of the tapered regions was 229 μm. The average period was 704 μm with a variation of ± 32 μm. The dimensional measurements of the TLPG were made using an Olympus BX51 microscope and are shown in figure 80 and

micrographs of the TLPG are shown in figure 81. (This TLPG is referred to as TLPG-(a) in the following paragraphs).

The normalised transmission of TLPG-(a) is shown in figure 82. Several resonance bands are seen at 642, 670, 681, 911, 978 nm and a broad band centred at 788 nm. The average transmission over the wavelength range 525-1025 nm was ~ 10% and no sharply defined transmission pass-bands and resonance bands were observed as is typically observed in LPGs (section 3.5.3, figure 17). During the fabrication of this TLPG it was decided to limit the number of micro-tapers to 18 as the optical transmission was decreasing significantly as each micro-taper was subsequently formed. The transmission was monitored during the process using a CCD spectrophotometer (Ocean Optics S2000) and a tungsten light source (HL-2000).

Owing to the varying period spacing (± 32 μm) and variations in taper length throughout the TPLG, the duty cycle of each period varied throughout the TLPG. The average duty-cycle of this TLPG was 32.5%, which is significantly lower than the optimal value of 50% which has been suggested by other researchers [1]. It was viewed that variations in the duty-cycle throughout the TLPG, cause the resonance bands to have reduced extinction levels and displaces the location of the resonance bands [1].

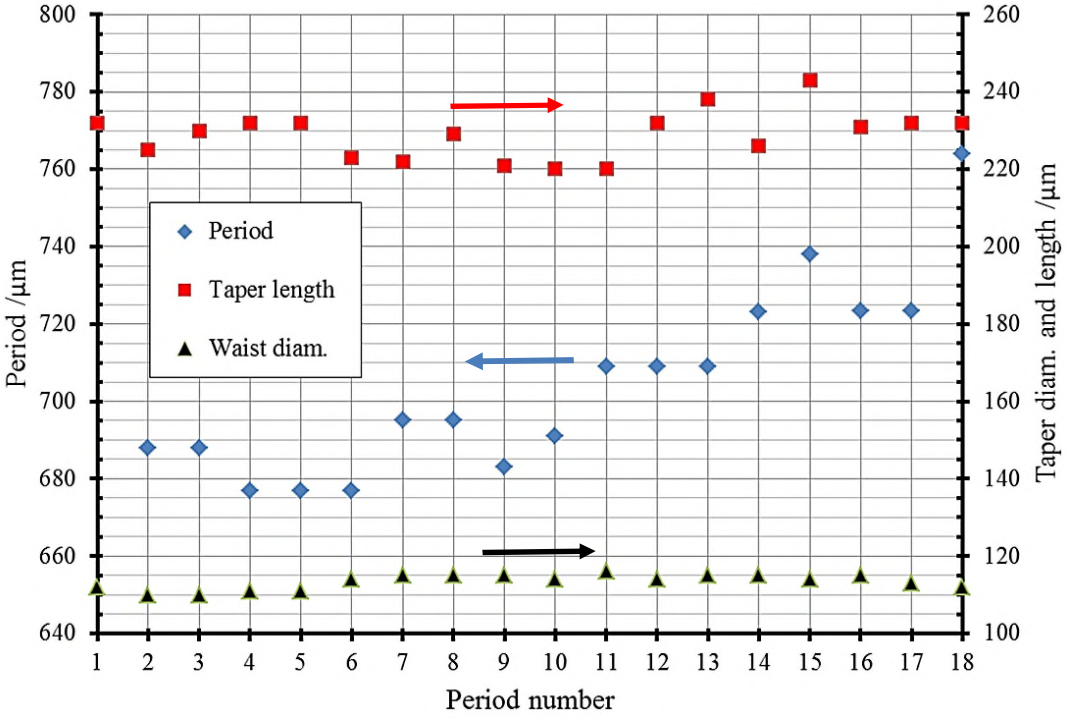

Figure 80: Physical dimensions of an 18 period TLPG-(a) written in SM750 fibre. The average period spacing was 704 µm.

The estimation of duty-cycle percentage is subject to some error as it was not possible to determine the contribution of laser induced refractive index modulation of the fibre and so only the geometrical modulation was determined by measuring the total micro-taper length. The taper length was measured using an Olympus BX51 microscope.

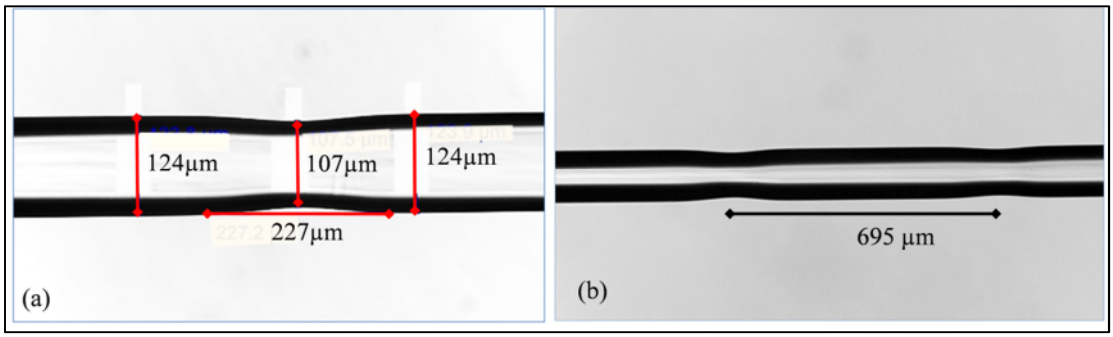

Figure 81: (a) The micrograph of a typical 227 µm long micro-taper, magnification x20 and (b) the micrograph of two micro-tapers separated by 695 µm.

To assess the refractive index sensitivity of this TLPG, it was taped into a PTFE trough, which allowed the grating to be immersed in liquids of differing refractive index. The transmission spectrum was measured using a tungsten light-source and an Ocean Optics CCD spectrophotometer. The transmission of the TLPG, measured in air, was normalised to 100% and the change in normalised transmission was recorded when liquid was added to the trough.

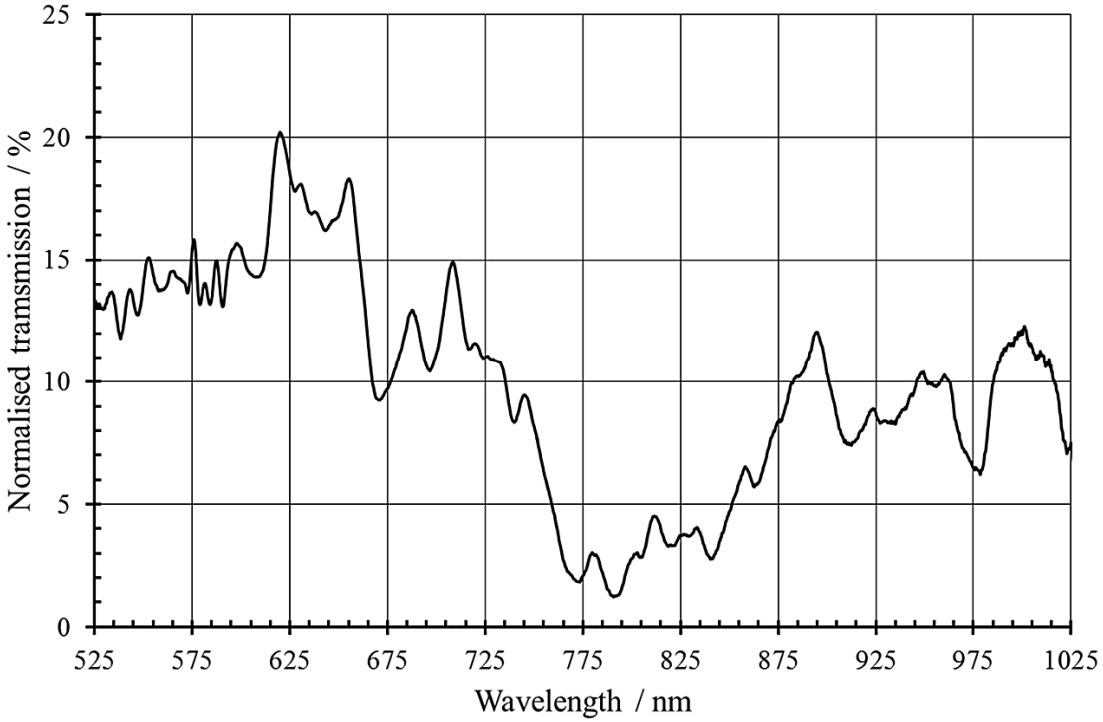

Figure 82: The transmission of an 18 period TLPG-(a), with an average period of 704 μm. SM750 fibre was used.

The TLPG was immersed in distilled water (n= 1.333) followed by isopropyl alcohol (IPA) (n=1.376) and the transmission spectra are shown in figure 83.

For both liquids, the spectra changes in the regions that coincide with the spectral resonance bands of the TLPG. Immersion of the TLPG in these liquids causes the transmission spectra to invert, causing bands of low transmission to have higher transmission and vice versa. Isopropyl alcohol causes a small wavelength shift to longer wavelengths compared to water.

The broad resonance band centred at 788 nm in figure 83 has a high frequency modulation superimposed around this wavelength. It was viewed that the high

frequency modulation may be caused by the progressively increasing grating period observed with this TLPG.

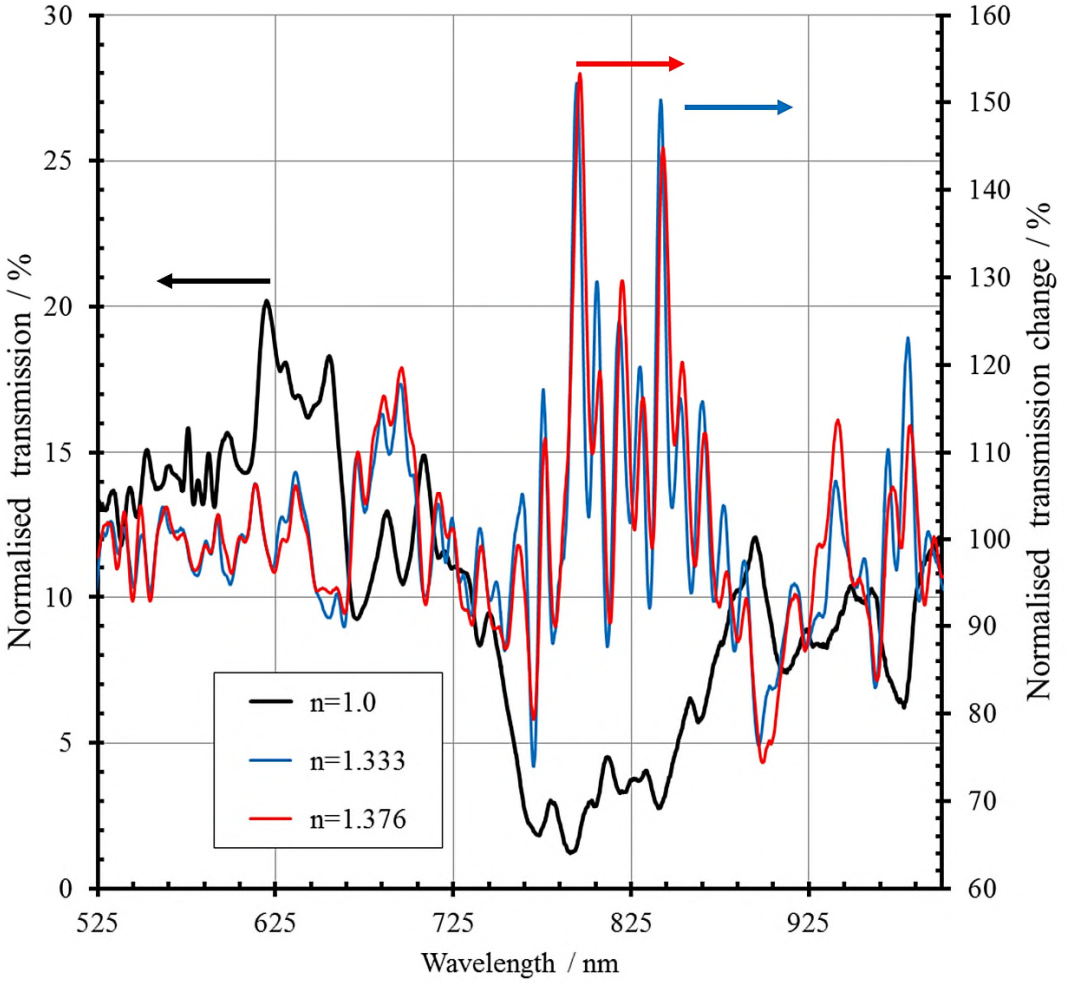

Figure 83: Transmission of an 18 period TLPG-(a) measured in air (n=1) and the normalised transmission change when the TLPG is immersed in water (n=1.333) and followed by I.P.A. (n=1.376).

To assess the repeatability of the TLPG-(a) spectral response, a second TLPG-(b) was fabricated using the same process conditions. This had an average period of 647 ± 21 µm, waist diameter of 114 ± 2 µm and an average taper length of 223 µm. On this occasion, the period spacing was more uniform than that of the previous TLPG-(a). The normalised transmission spectrum (figure 84) of TLPG-(b), exhibited well-defined resonance bands at 780, 680, 660 and 630 nm.

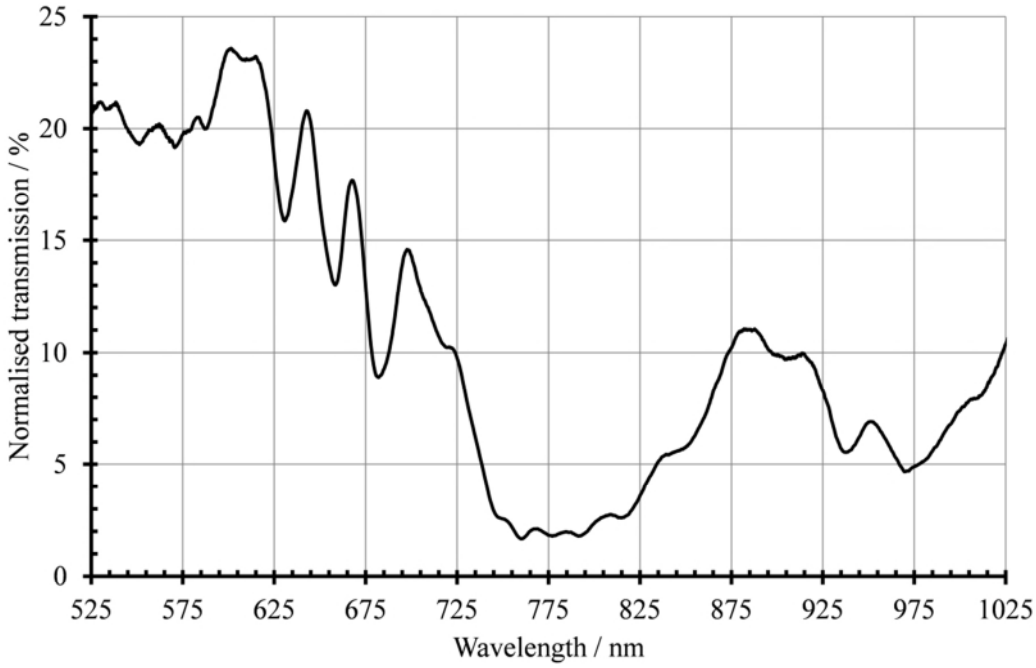

Figure 84: The transmission of an 18 period TLPG-(b) with an average period of 647 μm.

A comparison of the period repeatability between TLPG-(a) and (b) is shown in figure 85. While TLPG-(b) has superior repeatability compared to TLPG-(a), the variability in period spacing increases for both devices from period ~ 10 onwards.

It was viewed that the current process results in TLPGs that are not reproducible in terms of resonance band definition when the period number exceeds ~ 10, due to the increased period spacing variability. It was viewed that this may be caused by variability in the fabrication process which is discussed in the following paragraphs.

It was decided therefore, to limit the number of periods to six to improve the resonance band definition in an attempt to make the transmission spectra of the TLPGs more similar to UV-written LPGs, which are sharply defined.

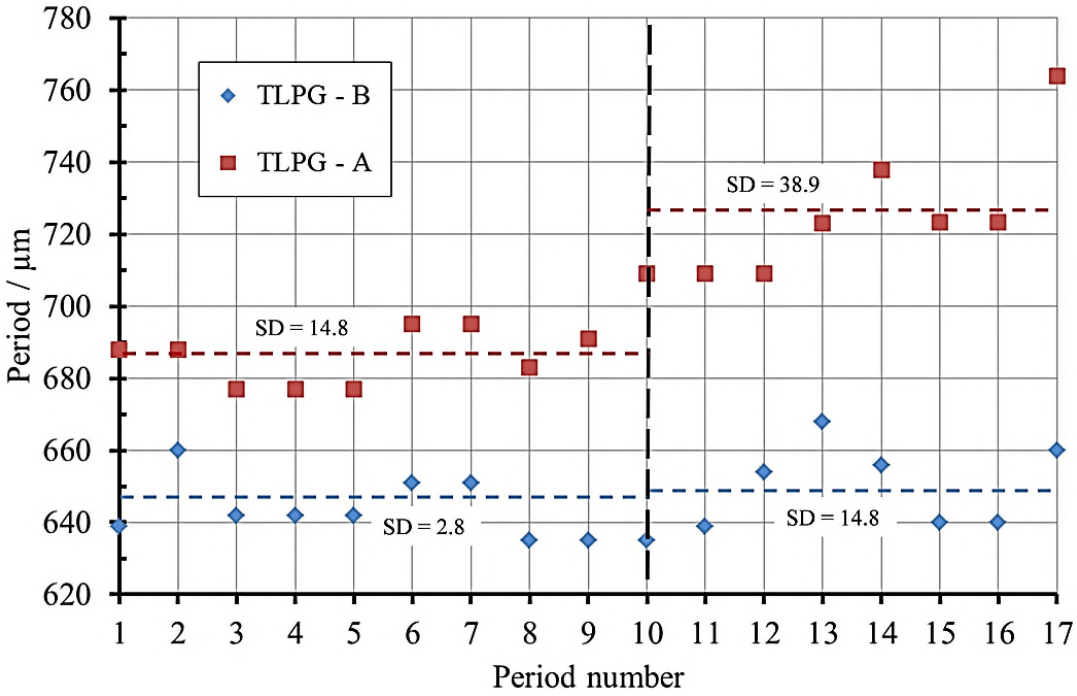

Figure 85: Comparison of the period repeatability between TLPG-(a) and (b) before and after 10 periods. The dotted red and blue lines represent the mean period and the standard deviation (SD) of the period mean is also given.

It was viewed that the variability in grating period may have been due to the use of "Sellotape" to attach the fibre to the stages as it was observed that it could have variable adhesion between reels and also between tapes taken from the same reel. This could lead to the fibre slipping on the stages, impacting on the length of a taper and causing variations in pulling tension or the physical spacing between tapers. The use of "Sellotape" was therefore discontinued and replaced with "Magic" tape (supplied by 3M) as it is known to have a more consistent adhesion in similar application areas [2].

The next TLPG fabricated consisted of 6 periods and "Magic" tape was used to adhere the fibre to the rotation stages. The average diameter of the taper waists was 104 ± 1 µm and the average period spacing was 697 ± 47 µm. The first taper had a diameter of 120 µm and was distorted (figure 86). The transmission spectrum of this TLPG, measured in air and IPA, is shown in figure 87.

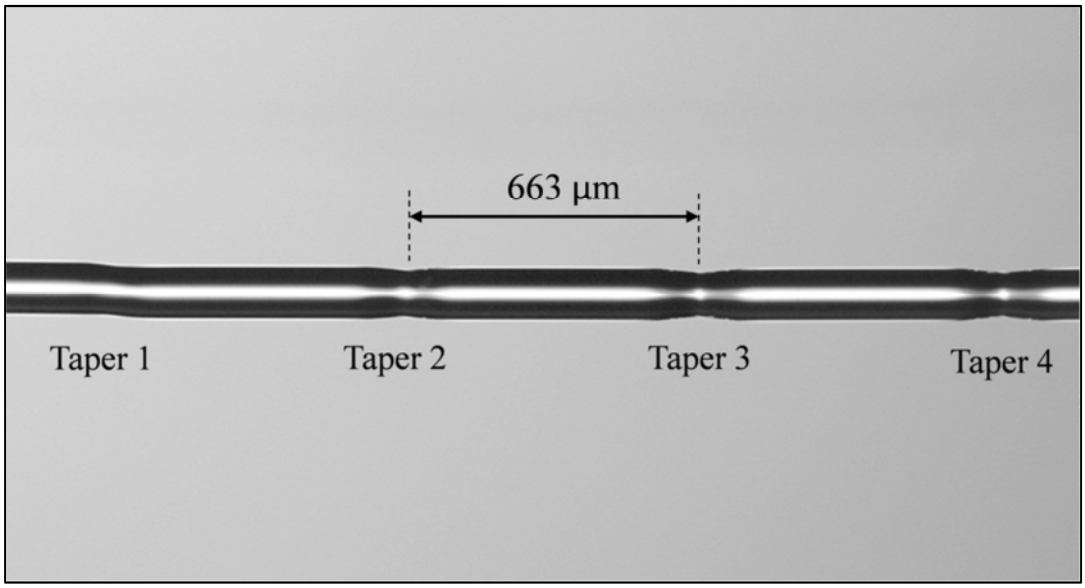

Figure 86: Micro-graph of a 6 period TLPG with an average period of 697 µm and a duty-cycle of 28%. Taper 1 has a distorted profile. SM750 fibre was used.

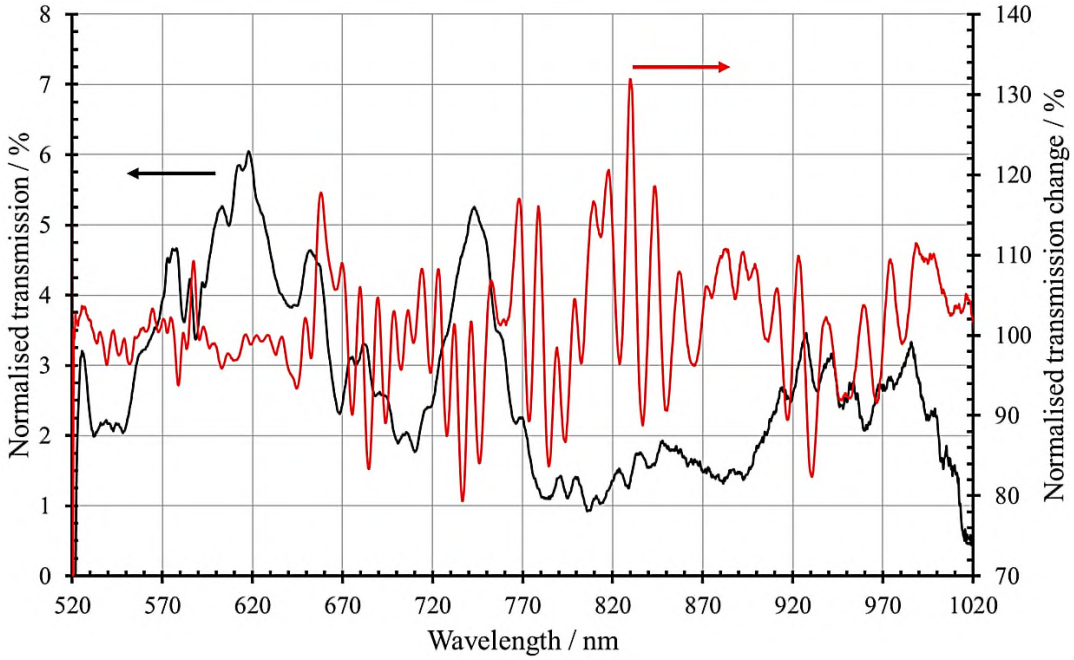

Figure 87: The normalised transmission of a 6-period TLPG with an average period of 697 µm and a duty-cycle of 28%, measured in air (black curve). The normalised transmission change when the TLPG is immersed in IPA is shown as a red curve.

Even though “Magic” tape had been used to attach the fibre to the stages, the spectral performance of the TLPG was still degraded and required further improvement. This 6 period TPLG, confirms that it is possible to fabricate short ~ 3.45 mm [3] TLPGs, as compared to UV- written LPGs, which can have lengths of typically 30 mm. However, a significant number of performance issues needed to be corrected before these short TLPGs had a similar optical performance to a UV-written LPG. These issues are listed below:

i. The first taper caused a significant fibre transmission loss due to its distorted profile.
ii. Subsequent tapers result in a lower transmission loss over a wide spectral range. There are no regions of high transmission coupled with defined attenuating resonance bands, which are usually observed with UV-written LPGs.
iii. Variations in the grating period results in displaced resonance bands which superimpose and forms broader bands which are in turn modulated at a higher frequency.
iv. Variations in duty-cycle between periods broaden the appearance of resonance bands.
v. There was poor spectral repeatability between TLPGs fabricated using the same process even when reducing the number of periods to six.
vi. Tape/fibre slippage may still be causing a variation in the tension of the fibre.
vii. The initial tensioning technique of the fibre was not reproducible using the existing method.

It was viewed that the initial high transmission loss was caused by the distorted profile of the first taper, which coupled a significant amount of light into the fibre cladding. This was confirmed by observing the fibre transmission change when each successive taper was formed. The first taper caused a greater attenuation compared to subsequent tapers.

The 6 period TLPG, had taper waist diameters which were ~ 104 µm compared to ~ 114 µm in the previous TLPG-(b). This reduction in waist diameter resulted in the tapers exhibiting increased loss (section 3.3) as the taper half angle was increased.

To improve the process for making TLPGs and correct the issues listed previously, the following process features were identified as requiring improvement:

1. Laser power stability.
2. Distorted first taper and subsequent taper waist diameter variations between TLPGs.
3. Non-reproducible, initial fibre pre- tensioning.
4. Variations in TLPG grating period.

These topics are discussed in the following sections.

7.2.4 Laser power stability

It was found early in this work that the laser power level critically determines the on-set of tapering. It was also viewed that any variation in laser power during the formation of a micro-taper could impact on both the length of the taper and the waist diameter, especially as a micro-taper is fabricated over a relatively short time interval ~ 16 s.

To determine the typical power variation, the laser power was monitored during six 5.25 W pulses and the power variation is illustrated in figure 88. During each 16 s pulse, the laser power fluctuates and could contribute to variations in taper length and waist diameter. The power variation between the 6 pulses was ± 2.75% and are within the ± 5 % power stability specification for the Synrad 48.2 laser. In this experiment, the laser was brought to the process power (5.25 W) from a cold start.

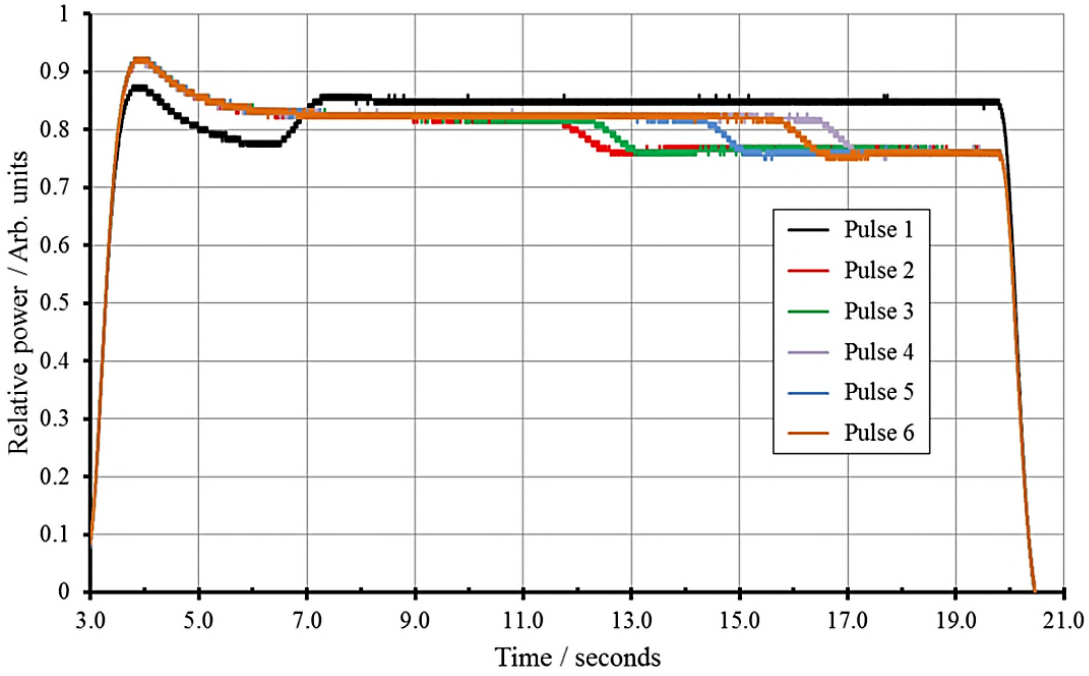

Figure 88: The power recorded during six 16 s laser pulses. Average pulse power was 5.25 W.

It was viewed that to improve the repeatability of the process, the laser power stability should be improved. A series of experiments were undertaken where the laser pwer was allowed to stabilise for 6 minutes at 5% and 10 % duty-cycles, before increasing the duty-cycle to a final duty cycle level of 19% for the micro-taper process. It was found that this technique, improved laser stability to ± 1.1 % between pulses but the power stability was now more variable (± 5%) between repeated TPLGs. This result was inferior to that achieved with operating the laser from a cold start.

Another approach that was explored, consisted of operating the CO_2 laser for 2 hours at a duty cycle of 19% prior to starting the TLPG process. This approach eliminated laser mode-hopping entirely. A second laser shutter was fabricated and inserted between the beam splitter optics and the safety shutter (see section 4.4.1). The second laser shutter was used to time the delivery of power while fabricating the TLPG and was controlled in a LabVIEW environment. It consisted of a small stepper motor which rotated an angled gold coated mirror into the beam. The reflected laser energy was then directed into a beam-dump.

It was found however, that this approach resulted in the laser power varying by ± 5% in a cyclical pattern and made the fabrication of tapers more difficult than when the laser was mode-hopping, as the power variation was greater and over a much longer time span ~ 70 minutes. It was viewed that the cause of this long time span power variation was most likely a combination of power supply instability [4, 5] and instability in the mechanical structure of the resonator. Therefore, it was decided to revert to operating the laser from a cold start as this provided the optimum laser stability for the process in the short term.

For the future, controlling the laser with a feedback loop, is the preferred solution as both mode hopping and long timescale cyclical power variations would be reduced. The laser pulse length would be then be controlled using a mechanical shutter.

7.2.5 Asymmetric first taper, tensioning and waist diameter improvements

In section 7.2.3 it was shown that the first taper could usually be distorted. This caused an initial fibre transmission loss of ≤ 80% from the first taper. It was viewed that the distortion may have been caused by the fibre having mechanical stress induced into it when it was taped to the v-grooves of the rotation stages. When the fibre is then heated to its melting point, the induced stress is relieved by the fibre moving in a direction which minimizes its stress, thereby locally distorting the first taper by creating a ‘kink’ in its shape.

To correct this effect, the rotation stages were mounted on an L-shaped bracket so they rotated about the z-axis instead of the y-axis as shown in figure 89. This allows the fibre to be placed unstrained across the grooves in the stages, prior to taping. In the original configuration, where the stages rotated about the y-axis, the fibre was located in the stage grooves on a vertical surface, so there was the possibility of introducing a twist into the fibre axis during the taping process.

To identify if rotational stress was acting on the fibre, two paper squares were attached to the fibre and their relative orientation were noted. Rotational twist in the fibre could then be corrected after attaching a 6 g weight to the end of the right hand fibre. A weight of 6 g has been used by previous researchers [6]. The weight ensures that a

repeatable tension is placed on the fibre prior to final attachment to the stages. After the fibre was attached to both stages the weight was then removed. A more detailed description of the fibre preparation procedure is given in appendix E of this thesis.

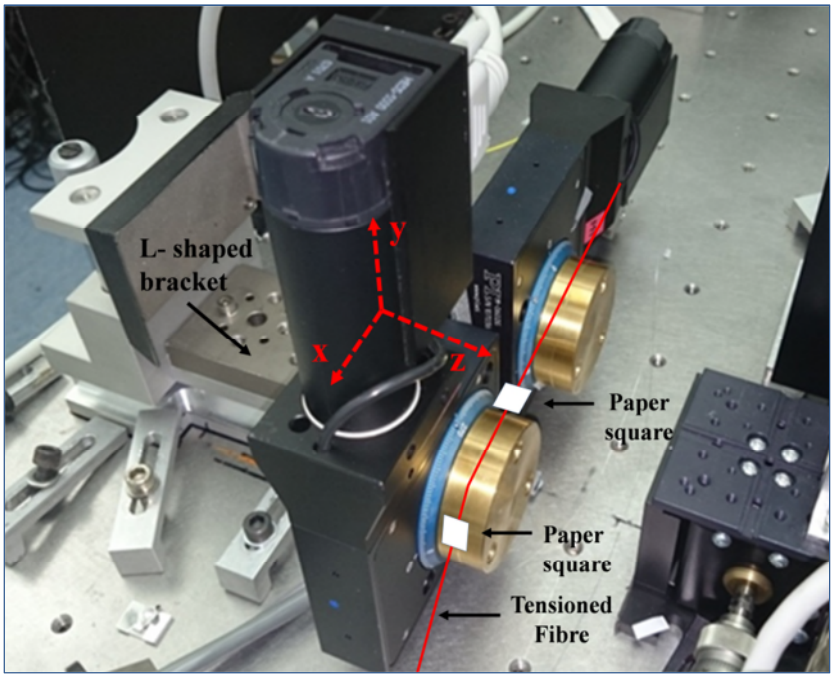

Figure 89: Optimized stage configuration used to fabricate TLPGs, showing the position of the 'paper squares' used to aid fibre alignment, (the red line indicates the location of the fibre).

To reduce the variability in waist diameter and therefore improve the transmission of the TLPGs, a number of experiments were undertaken to increase the diameter of the waist from the current value of ~ 100 µm so the tapers had a smaller taper half-angle (see section 3.3).

Various taper pull-times were trialled from 18 s to 13 s. Decreasing the pull time to 16 s resulted in the waist diameter increasing to 110 µm, accompanied by a corresponding increase in transmission through the taper. A further reduction in the pull-time to 13 s resulted in the waist diameter increasing to 121 µm. At this diameter, a single resonance band was observed at 800 nm and the fibre pass-band transmission increased to ~ 30% . This would suggest that the waist diameter determines the number of cladding modes

which are excited (section 3.5) and suggests that the optimal waist diameter is in the region of ~ 115 µm, with a pull time of 15 s to 16 s. At this waist diameter, higher order modes are excited while still maintaining high light transmission.

Using the new fibre preparation procedure and a taper pull-time of 15 s, a 6 taper TLPG was fabricated. The spectral performance is illustrated in figure 90. The average waist diameter of this TPLG was 117 ± 2 µm, the average period spacing was 418 ± 11 µm and the duty cycle was 54 ± 6 %. The passband transmission at 825 nm is high at ~ 57% and does not substantially degrade when successive tapers are added.

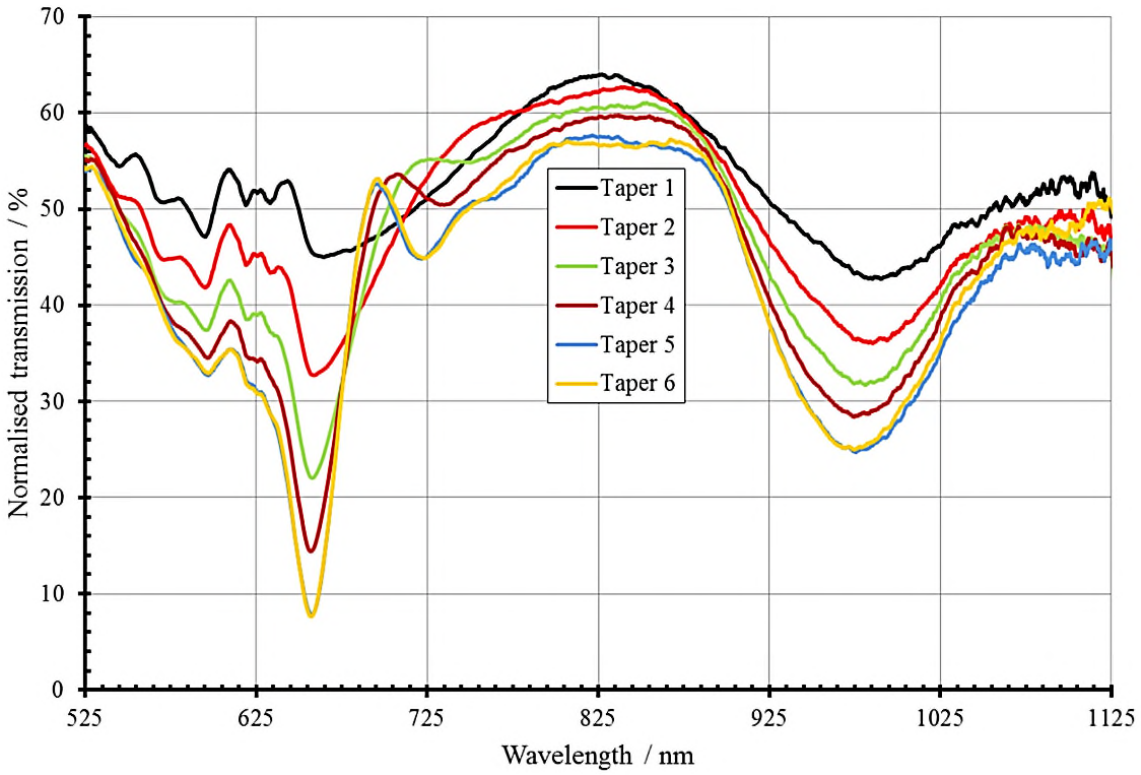

Figure 90: The spectral characteristic of a 6 micro-taper TLPG with a waist diameter of 117 µm and a period of 418 µm, using SM750 fibre.

The development of the resonance bands are shown as the number of micro-tapers increases. Two deep resonance bands are visible at 630 and 980 nm, and weaker bands are located at 721 and 770 nm. There may also be weaker ones present shorter than 630

nm in wavelength but these are difficult to discern with just 6 periods. The duty cycle on this TPLG was targeted at 50%, as it is known from UV- written LPGs that this would produce high pass-band transmission coupled with increased spectral resonance band definition [1]. The TLPG duty-cycle was measured to be 54%: 46% where 54% refers to the taper percentage length and 46% refers to the non-tapered length of fibre. The “kink” on the first taper was substantially reduced and coupled with the increased taper waist diameter, has produced an improvement in light transmission in the pass-band region ~ 825 nm.

The refractive index sensitivity of this TLPG was assessed using the same method described in section 6.3.2. The normalised transmission changes associated with immersing the TLPG sequentially in deionised water, IPA and an index oil of refractive index 1.456 are shown in figure 91. The HF modulation, which was present in figures 83 and 87, is absent in figure 91 and suggests that the improvements in reducing the period spacing variability have been effective at eliminating this feature.

The refractive index sensitivity of this TPLG is 372 nm/ RIU. Increasing the refractive index of the media surrounding the fibre appears to have two effects on the multiple resonance bands observed in the spectra; as the refractive index increases the transmission change increases and shifts the resonance bands to shorter wavelengths. This latter effect has been reported by previous researchers [7] and occurs when the external medium index is just below the cladding index of the fibre.

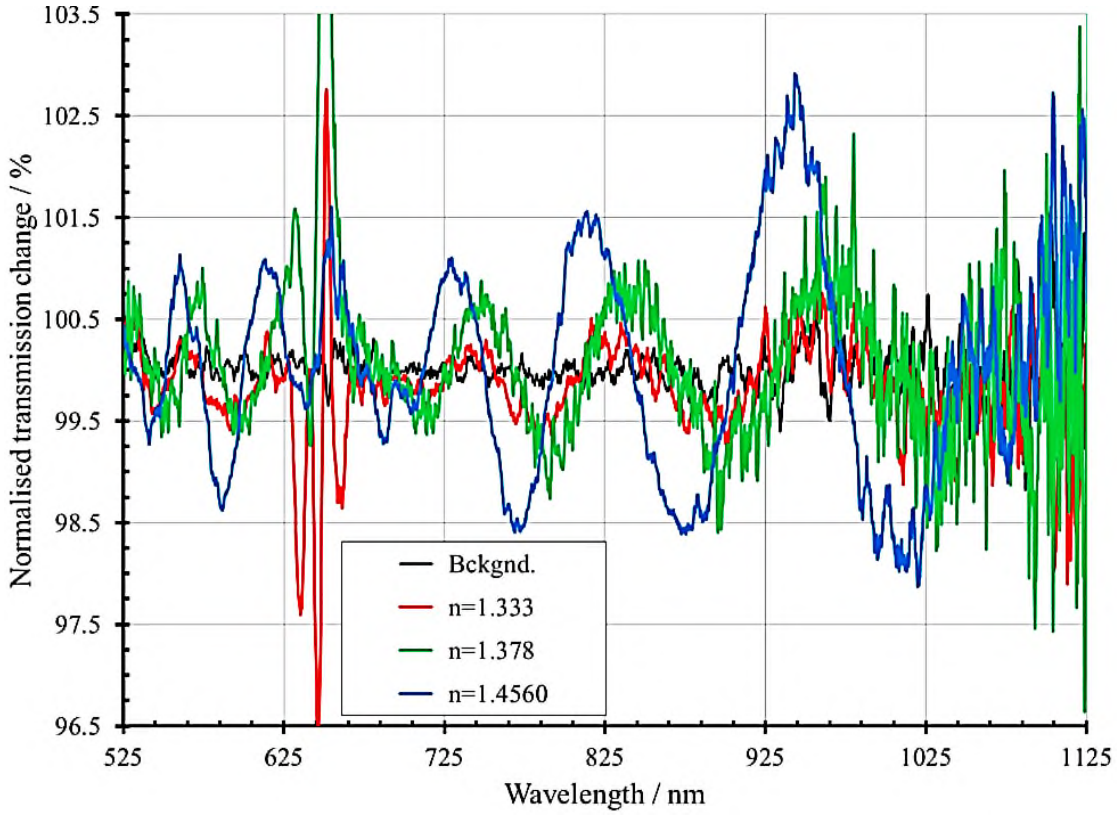

Figure 91: Transmission change of a 6 taper TLPG with a waist diameter of 117µm and a period of 418 µm when it is immersed in liquids with an index ranging from 1.333-1.456. The fibre used was SM750.

7.2.6 TLPG period software change

One of the objectives of this work was to improve the reproducibility and reduce the bandwidth of the resonance bands, as this would improve the performance of the TLPG as a sensor. The relationship between taper length, taper spacing and duty cycle was analysed for several TLPGs and it was found that a variation in taper length in a given period caused a concomitant error in the following period spacing as the fibre translation distance was constant in the current process. With TLPGs it is known that variations in grating spacing would have a greater impact on spectral performance than duty-cycle variations [1], therefore the period spacing should be kept constant.

To improve the TLPG process, the program for calculating the period spacing was modified so that the fibre translation distance between tapers was adjusted to

compensate for variations in taper lengths. To determine the taper length (T_L) the rotation stage encoder scale was used. The fibre translation distance (F_d) was then calculated so that the sum of $T_L + F_d$ was constant for each period of the TLPG.

7.2.7 TLPG period spacing changes

To examine the effects of variations in period and duty-cycle on the spectrum of the TLPGs, three TLPGs were fabricated in SM750 optical fibre. The details of the variations are shown in table 14. Each TLPG comprised of 6 tapers, and the revised method was used for calculating the fibre translation distance as discussed in section 7.2.6.

Table 14: Period and duty-cycle changes for TLPGs.

TLPG reference	Period / μm	Duty-cycle / %	Resonant λs / nm
TLPG (a)	378	55	957,751,700
TLPG (b)	421	45	975,732,675
TLPG (c)	460	41	996,830,796,754,706

The spectral performance of the differing TLPGs is shown in figure 92. As the grating period increases, then the resonant wavelengths increases also, as predicted theoretically by the TLPG resonant wavelength equation (equation 3.19). The transmission level in the pass-band region (~ 775 nm) appears to be influenced by the duty-cycle value, with a duty-cycle of 55% resulting in increased transmission through the TLPG. Cladding mode resonance bands can be observed at wavelengths longer than the fibre cut-off wavelength (660 nm). The resonance bands seen in figure 92, also vary in their extinction level and spectral bandwidth.

The 3-layer cylindrical LPG model discussed in section 3.5.3 was then used to predict the theoretical wavelengths of the 1st and 2nd order resonance bands to model the experimental spectra exhibited by TLPG-(a) and (c) shown in figure 92.

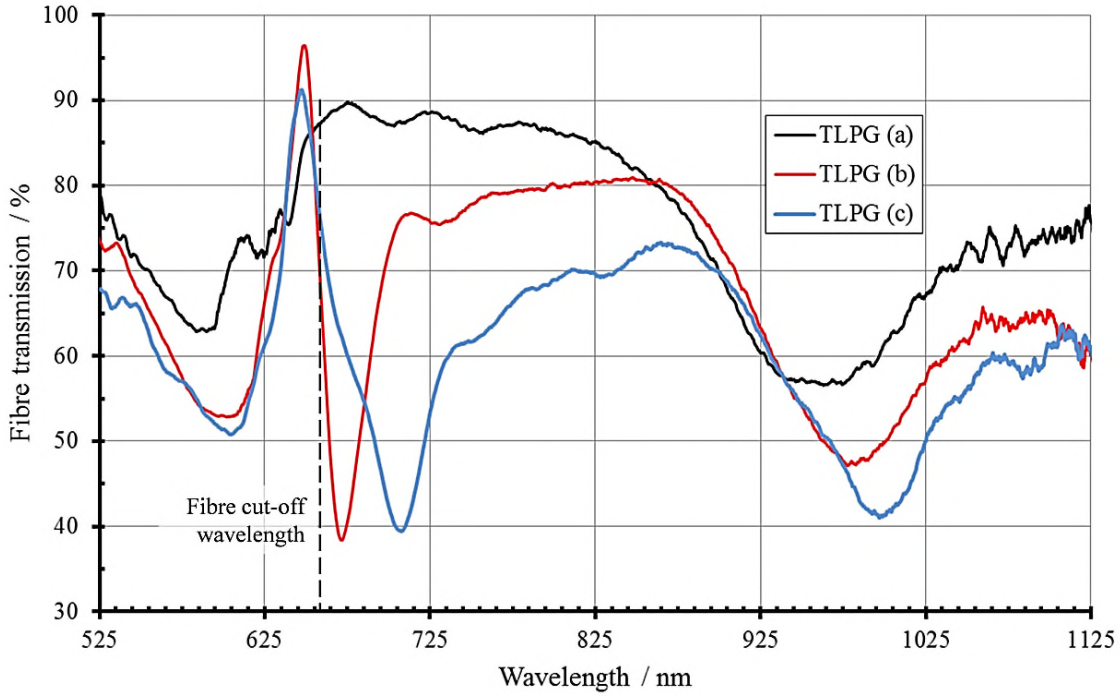

Figure 92: The spectral transmission of six period TLPGs with differing periods and duty-cycles (see table 14 for details). The TLPGs were fabricated in SM750 fibre.

The resonant wavelength cladding modes for SM750 fibre was determined from the phase matching curves for the 1st and 2nd order coupling, shown in figures 93 and 94. These figures were calculated using the 3-layer cylindrical waveguide model of a fibre shown in figure 11, using MATLAB software within Cranfield University [8]. The physical characteristics assumed for the fibre are given in table 5 (section 3.5.3). The phase matching curves should be taken as indicative only, as the LPG model assumes the fibre core is index modulated only. Both the even and odd numbered modes are given, but as discussed in section 3.3, the odd modes will give the greatest extinction values as the overlap integral is more significant for these modes.

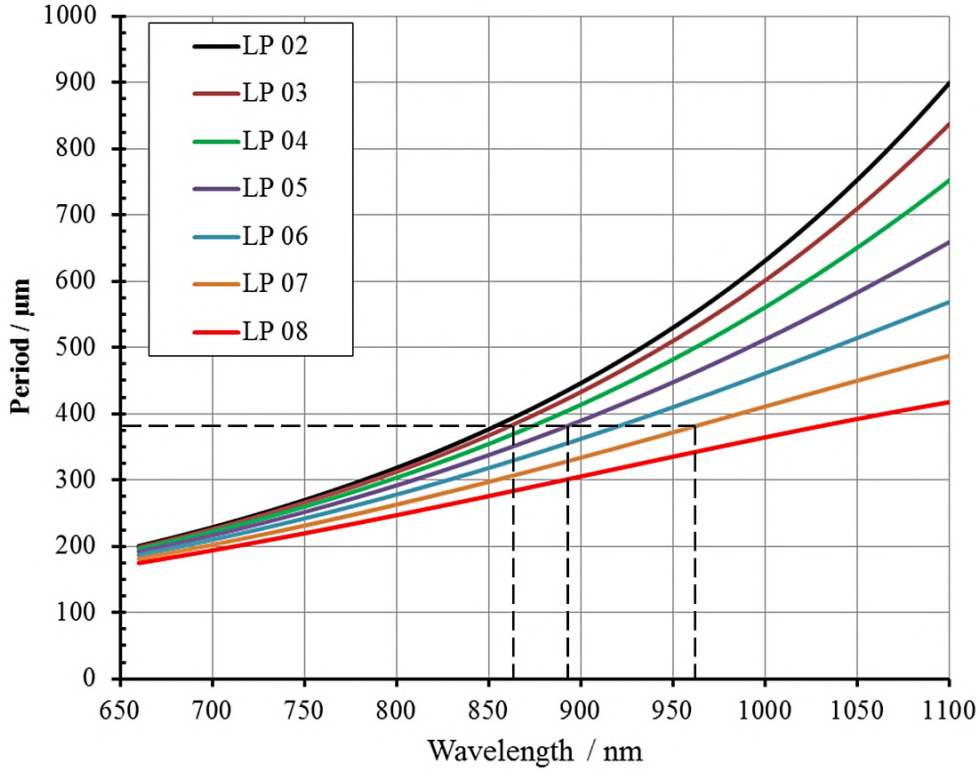

Figure 93: Theoretical curves of LPG resonant wavelengths as a function of period for the 1st order modes [8]. Dashed lines indicate the resonant wavelengths of the odd numbered modes for a period spacing of 378 µm.

The theoretical spectral wavelengths of the 1st and 2nd order odd modes for LPGs with a period spacing of 378 and 460 µm are shown in figures 95 and 96. These periods correspond to TLPGs (a) and (c) respectively. The mode intensities were assigned an arbitrary intensity of 1.

If figures 95 and 96 are compared to figure 92, these theoretical results suggest that the broad resonance band seen at ~ 975 nm (figure 92) may be caused by a superposition of the 1st and 2nd order coupling modes for both TLPGs and the resonance band seen at ~ 680 nm is the superposition of the 2nd order coupling modes.

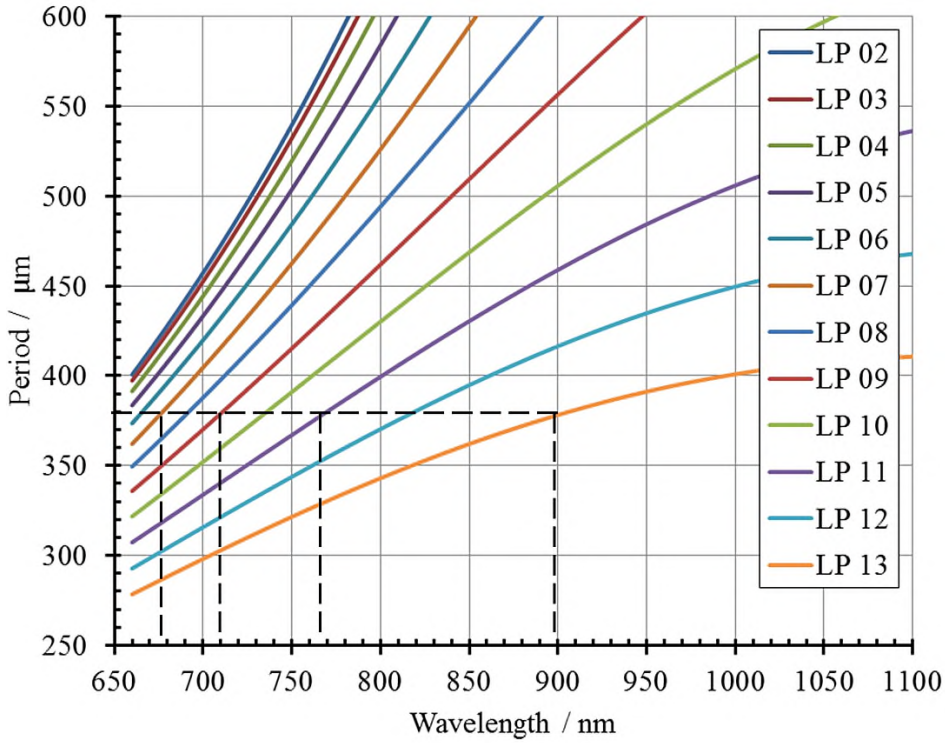

Figure 94: Theoretical curves of LPG resonant wavelengths as a function of period for the 2nd order modes [8]. Dashed lines indicate the resonant wavelengths of the odd numbered modes for a period of 378 µm.

The 3-layer LPG model assumes a weak modal coupling coefficient as the index modulation from UV irradiation is relatively low (section 3.5.5.2). For TLPGs, where the magnitude of the index modulation is greater, the spectral bandwidth of the resonant bands is greater (equation 3-13) and so will superimpose forming the broad resonance bands observed in figure 92.

The 3-layer LPG model was also successful in predicting in figure 92:

i. the presence of the transmission passband centred at ~ 825 nm,
ii. the resonant band shift to longer wavelengths, as the period spacing increases.

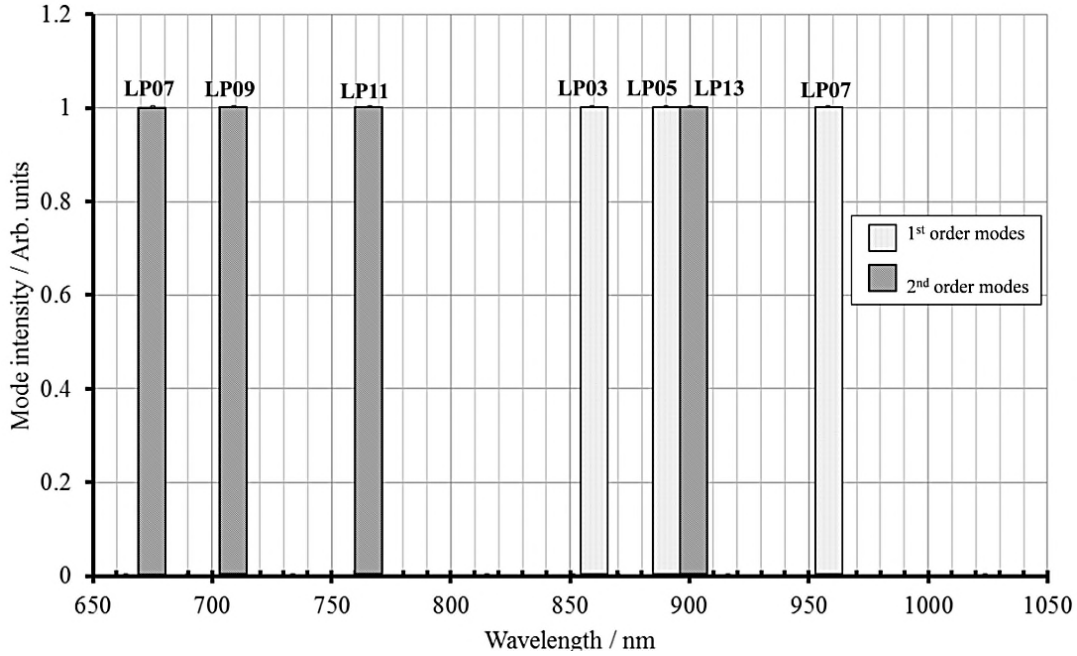

Figure 95: The theoretical wavelength positions of both the 1st order odd modes and the 2nd order odd modes for an LPG with a period of 378 μm**.**

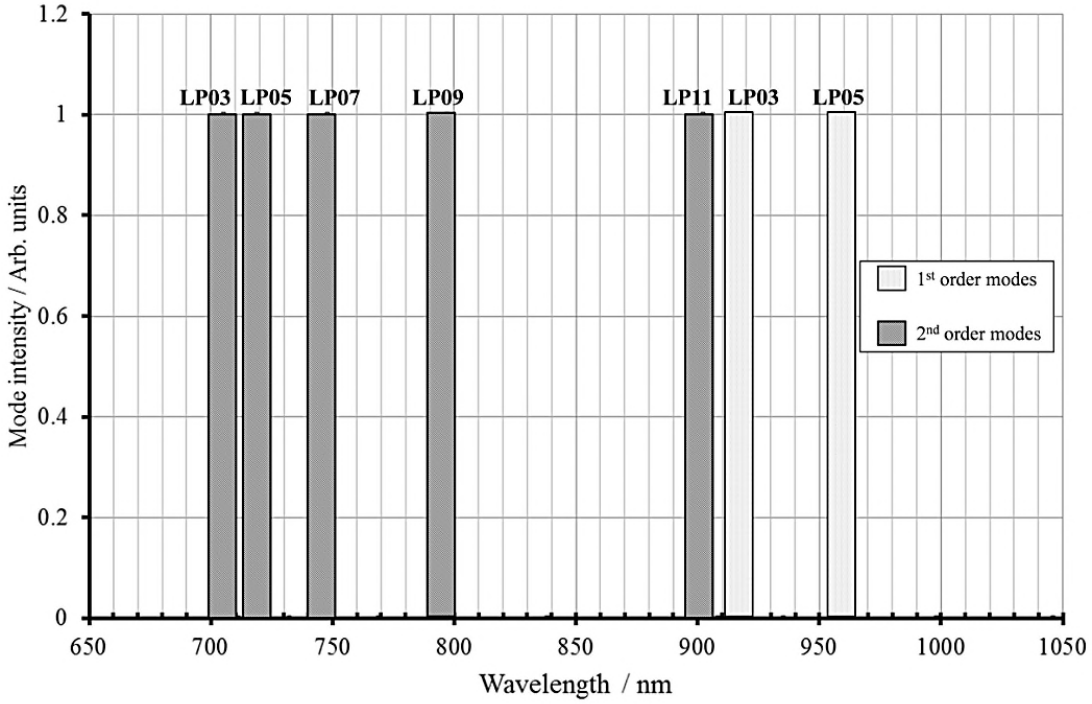

Figure 96: The theoretical wavelength positions for the 1st order odd modes and the 2nd order odd modes for an LPG with a period of 460 μm.

7.3 Cascaded tapered long period gratings

7.3.1 Background

If two TPLGs are separated by a small distance, then a cascaded TPLG is produced. This is essentially a Mach-Zehnder interferometer [9, 10, 11]. The first TLPG couples a portion of the light to cladding modes, which undergo a different path to the remaining light propagating through the core. At the second TLPG, the cladding modes are coupled back into the core and interfere with the core mode. The transmission spectrum of a cascaded TLPG has the usual resonance bands of a TLPG but these are modulated by a sinusoidal channelled spectrum, the frequency of which is dependent on the physical separation between the two TLPGs. If the environment around the fibre between the two TLPGs is modified due to a change in refractive index, then the channelled spectrum is displaced as the phase of the propagating cladding modes are perturbed [11] with respect to the core mode.

Cascaded LPG devices have been used as chemical sensors by several researchers [9, 11] and have used either arc discharge or UV irradiation techniques to create the periodic index perturbation in the core. In both cases, the length of the cascaded LPG sensor was typically greater than 90 mm. As resonance bands were observed using the short TLPGs described in section 6.4, trials were undertaken to identify if a cascaded TLPG could be made with these TLPGs.

7.3.2 Experimental

A cascaded TPLG was formed in SM750 fibre by fabricating a six-period TPLG followed by a one period TPLG. The separation between the two TLPGs was 9 ± 0.5 mm. The tapers comprising the TLPGs had a waist diameter of 119 ± 2 μm. The first TPLG had a period of 447 ± 25 μm with a duty cycle of 42 ± 6 %. The second TPLG had a period of 488 μm with a duty cycle of 42 ± 6 %. The spectral resonance bands for the first TLPG were located at 1000, 700 and 584 nm with a weaker band observable at

780 nm as shown in figure 97-(a). The transmission spectrum of the cascaded TLPG is shown in figure 97-(b).

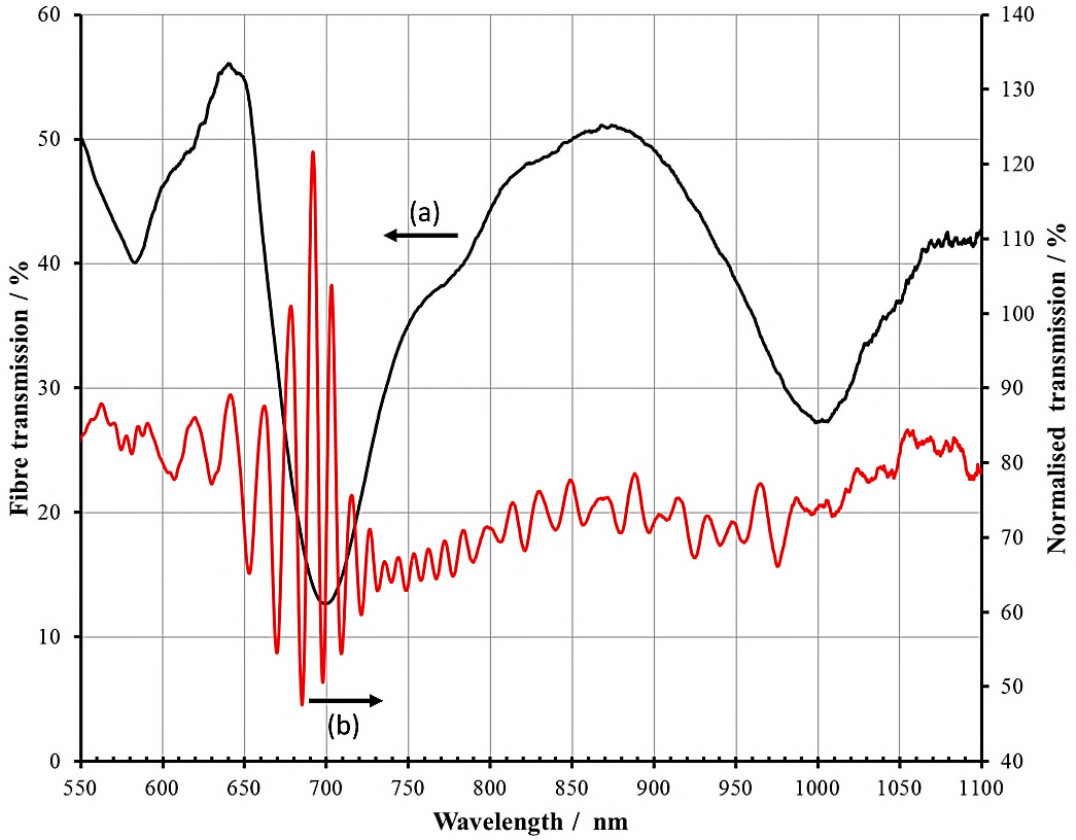

Figure 97: (a) and (b). (a) The optical transmission of a fibre with a six period TLPG (a), and (b) the normalised transmission change of a cascaded TLPG after a one period TLPG (b) is separated from TLPG (a) by 9 mm.

A channelled spectrum centred at 690 nm was observed after the first period of the second TLPG was formed. The second TLPG couples light from the cladding to the core, producing a channelled spectrum within the envelope of the resonance band located at 700 nm. The second TLPG comprised of one period because if two or more periods were used, then the visibility of the channelled spectrum was reduced, most likely due to the inevitable errors in the period spacing of the second TLPG.

7.3.3 Discussion

Cascaded tapered LPGs can be fabricated with overall lengths of ~ 12 mm compared to lengths of ~ 90 mm [13] for UV written LPGs. The length of these devices is determined by both the grating length and the physical separation between them. Because the tapering process produces a strong refractive index modulation of both the fibre core and cladding (section 3.5.5), the extinction of the resonant bands and bandwidths are greater and so the TLPGs can be much shorter than LPGs. The optical path length between the two gratings determines the frequency of the channelled spectrum and as the grating separation increases, the channelled spectrum frequency will increase also [12,13]. For UV written gratings, because the bandwidth of the grating resonance bands are narrower than for TLPGs, observation of a channelled spectrum requires a greater physical separation between the two gratings than for a TLPG device as the bandwidth of the channelled spectrum has to be less than the bandwidth of the individual resonance bands.

Future work could explore the effect of reducing the TLPG separation still further so creating a more compact sensor. The bandwidth of the individual TLPGs could be optimized together with investigating the refractive index sensitivity of this type of sensor and its use as a coated chemical sensor.

7.4 Conclusions

A system has been developed for fabricating TLPGs using a CO_2 laser in the spectral region 525-1100 nm. These gratings have a periodic spacing of around 400 μm and typically had 6 periods. The key advantage of this type of grating over LPGs formed using UV irradiation is their potential high temperature resistance coupled with their compact length (section 2.3). Gratings fabricated by locally tapering a fibre have high coupling coefficients which means that a high optical extinction can be achieved in a relatively few number of periods. The TLPG geometrical properties were optimised for improved spectral performance. The refractive index sensitivity of a 6 period TPLG was measured and found to be 372 nm/ RI.

Cascaded TLPGs can be fabricated with overall lengths of 12 mm compared to lengths of ~ 90 mm [7] for UV written cascaded LPGs.

Future work should concentrate on improving the repeatability of the fabrication system in terms of period spacing and duty-cycle. The spectral definition of the resonance bands of the TLPGs were found to be strongly influenced by the combination of the specific geometry of the tapers and the laser pulse characteristics used. More work should be undertaken on these fundamental aspects to further optimize the TLPG optical performance.

7.5 References

[1] R. Y. N. Wong, E. Chehura, S. E. Staines, S. W. James and R. P. Tatam, "Fabrication considerations for fiber optic long period gratings operating at the phase matching turning point," *Appl. Opt.*, Vol. 53, No. 21, pp. 4669–4674, 2014.

[2] R. Correia, "*Private communication*," Cranfield University, July, 2014.

[3] S. Nam, C. Zhan, J. Lee, C. Hahn, K. Reichard, P. Ruffin, K.-L. Deng and S. Yin, "Bend-insensitive ultra-short long period gratings by the electric arc method and their applications to harsh environment sensing and communication.," *Opt. Express*, Vol. 13, No. 3, pp. 731–7, 2005.

[4] B. Li, Y. Wang, D. Peng and Q. Li, "Power measure and control system for high power laser in real-time," *Proc. SPIE*, vol. 6622, no. 2008, p. 66221B–66221B–6, 2007.

[5] W. Zheng, H. Sugawara, T. Mizushima and W. Klimowych, "Heating power feedback control for CO_2 laser fusion splicers," *Fiber lasers X: Technology, systems and applications*, San Francisco, USA, *Proc. SPIE*, Vol. 8601, pp. 860129–1/7, 2013.

[6] Y. Wang, "Review of long period fiber gratings written by CO_2 laser," *J. Appl. Phys.*, Vol. 108, No. 8, p. 081101, 2010.

[7] S. W. James and R. P. Tatam, "Optical fibre long period grating sensors: characteristics and application", *Meas. Sci. Technol.*, Vol. 14, R49-R62, 2003.

[8] S.W. James, Cranfield University, *Personal communication*, Feb. 2014.

[9] Y. Liu, L. Zhang and I. Bennion, "Phase shifted and cascaded long-period fiber gratings," *Opt. Commun.*, Vol. 164, pp. 27–31, 1999.

[10] P. Pilla, P. Foglia Manzillo, M. Giordano, M. L. Korwin-Pawlowski, W. J. Bock and A. Cusano, "Spectral behavior of thin film coated cascaded tapered long period gratings in multiple configurations.," *Opt. Express*, Vol. 16, No. 13, pp. 9765–80, 2008.

[11] S. Korposh, S. W. James, S.-W. Lee and R. P. Tatam, "Temperature and surrounding refractive index insensitive cascaded long period grating chemical sensor,"

23rd International Conference on Optical Fibre Sensors, Santander, Spain, 2014, Proc. SPIE, Vol. 9157, p. 91574J.

[12] S. W. James, S. Korposh, S.-W. Lee and R. P. Tatam, "A long period grating-based chemical sensor insensitive to the influence of interfering parameters.," *Opt. Express*, Vol. 22, No. 7, pp. 8012–23, 2014.

[13] G. Salceda-delgado, A. Martinez-rios and D. Monzón-hernández, "Tailoring Mach – Zehnder comb-filters based on concatenated tapers," *J. Light. Technol.*, Vol. 31, No. 5, pp. 761–767, 2013.

8 Discussion and suggestions for future work

8.1 Tapers

A system for fabricating adiabatic and non-adiabatic optical tapers with repeatable physical dimensions has been developed. Tapers can be made with waist diameters which are repeatable to ± 0.5 μm. This repeatability value is equal to or better than the measurement accuracy of the microscope used to measure the diameter of the taper waist. Single tapers were fabricated with 5 ± 0.5 μm waist diameters and with waist lengths of 20 mm using single-mode SMF-28 fibre. Many tens of tapers have been supplied to the University of Nottingham with a yield which exceeded 90%.

The aims and objectives of this thesis, stated section 1.2, were to develop the capability to fabricate optical tapers as a repeatable process and to develop the techniques for making tapered long period gratings for use as optical sensors. These aims and objectives have all been met during the course of this work.

A range of optical techniques to monitor the process of fabricating optical fibre tapers has also been investigated. These techniques included; transmission monitoring of the fibre using a spectrophotometer, using an in-line FBG to measure taper strain and the use of an NIR camera to aid fibre alignment and laser power optimization.

There are a number of areas which would benefit from future work:

i. Improved laser power control
ii. Improved control automation
iii. The fabrication of non-exponential taper profiles

During the tapering process, the CO_2 laser mode-hops, which results in small power fluctuations during the fibre heating and pulling process. It may be beneficial for future applications to have fast feedback control of the laser to reduce the mode-hopping effect. This can be implemented in-house by using a proportional integral derivative (PID) control loop in LabVIEW. The output of the laser power meter could sample the power from the laser and form the input to the PID loop. The output of the PID loop would then reduce rapid fluctuations in laser power by adjusting the laser duty cycle

accordingly. Synrad Inc. can supply a closed loop stabilization kit for the 48-2 laser which would limit power fluctuations to better than ± 2%.

With the existing process, when a specific taper profile is produced there is an associated unique laser power profile (figure 39) which has been generated following a number of trial runs. Future work could explore the effectiveness of using an IR camera to measure fibre melting temperature during the process so allowing the laser power to be actively controlled, thereby eliminating the need for unique laser power curves for tapers of differing geometrical profiles.

The current tapering process is semi-automated from a control perspective and would benefit from full-automation at some stage in the future. The laser is controlled via LabVIEW and the rotation stages are controlled via PIMikroMove. It would be beneficial to drive the rotation stages in a LabVIEW environment so the tapering process could be a totally automated.

Tapers which are produced using the existing process described in this thesis, have exponentially shaped transition zones which is a consequence of the stages pulling at a constant velocity and the length of the fibre heated zone being fixed [1]. For the future, using varying velocity profiles for each of the rotation stages and/or varying the length of the heated zone during the process allows the possibility of producing linear [1], asymmetric [2], concave and convex taper transition profiles. There are a number of different applications for these types of tapers:

- Linear-exponential profiles have been used to enhance the sensitivity of SPR sensors [3].
- Asymmetric tapers have been used to shape the spectral output of ultra-short laser pulses [2,4,5].
- Linear profile tapers can be been used for optical tweezers [6].
- FBGs can be written in the transition zones of tapers to produce wideband chirped FBGs [6].

8.2 Tapered long period gratings

A system has been developed for fabricating TLPGs using a CO_2 laser. These gratings had periodicities from 378 μm to 704 μm and typically comprised of between 6 to 18 periods. First and second order resonance bands were observed but discrete mode specific resonances are not clearly defined at this stage of the development. Adding more periods may increase the definition of specific resonance bands. Gratings fabricated by locally micro-tapering a fibre have high coupling coefficients which causes the bandwidth of the modal resonance bands to be larger than typically observed in LPGs formed by UV irradiation. High optical extinctions can be achieved in a relatively few number of periods. The key advantage of this type of grating over LPGs formed using UV irradiation is their potential high temperature resistance coupled with their compact length. Initial work exploring the index sensitivity of these devices has produced promising results. The refractive index sensitivity of a 6 period TPLG was measured at 372 nm/ RI.

The current method for producing TLPGs produces significant manufacturing errors in the formation of the periods. The typical variability obtained with the current process is given in table 15. As TLPGs are spectrally sensitive to errors in the physical dimensions of the repeating periods, then these errors need to be reduced to produce higher resolution TLPGs.

Table 15: Typical physical variation in grating properties

Grating property	**Variation / %**
Taper waist diameter	± 1
Taper length	± 9
Period spacing	± 4
Duty-cycle	± 8

Variations in taper waist diameter affect the repeatability of TLPG transmission and the efficiency with which higher order modes are excited. Random changes in periodic spacing will wavelength shift the position of resonance peaks and reduce resonance band definition; variations in duty-cycle will tend to degrade the extinction efficiency especially when the duty-cycle deviates from the optimum value of 50 %.

There are a number of process areas which could benefit from future work, these are:

i. Method for improved fibre attachment
ii. Improved laser power stability and fast process shuttering.
iii. Symmetric irradiation of the fibre.
iv. Smaller laser spot-sizes and improved control.
v. Automation
vi. Parameter investigation – experimental design techniques.

These areas are discussed in the following paragraphs.

At present the fibre is attached to the stages using adhesive tape allowing the possibility of fibre movement especially after a micro-taper has been fabricated. An improved more reproducible fibre attachment scheme needs to be developed either involving mechanical clamping or perhaps using magnets in conjunction with high stiction surfaces.

The laser power stability improvements to reduce mode-hopping discussed in the previous section are even more applicable for micro-taper formation as the taper pulling times are in the seconds rather than hundreds of seconds time domain.

The beam delivery should be modified so that the fibre is irradiated equally around its circumference rather than single-sided asymmetric irradiation as is currently employed. This could be achieved [7] by employing a second shaped reflector located behind the fibre as shown in figure 98. A target specification for such a reflector has already been developed.

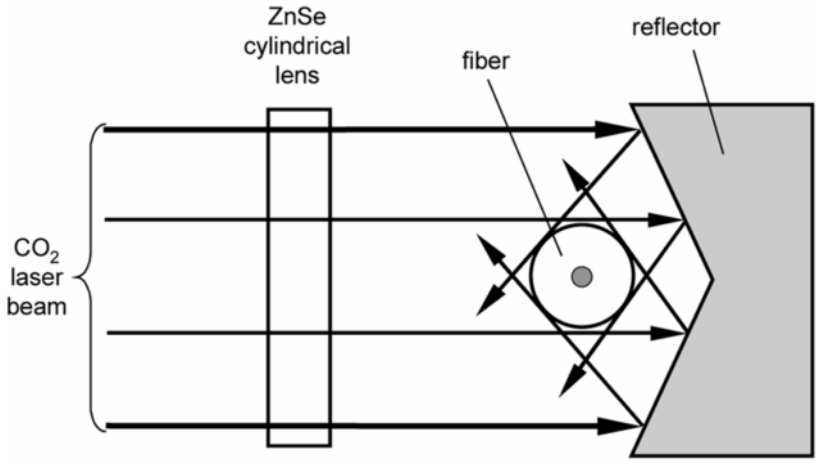

Figure 98: Single incident beam is converted by a reflector into three beams separated in angle by 120^0. The reflector redirects the side portions of the incident beam back to the fiber, thereby creating a more axially uniform illumination of the fibre [7].

The laser beam delivery optics should be modified to reduce the laser spot size to 100 μm and provide flexible control over the spot size. This could produce TLPGs with a period of 175 μm. Spot size control could be achieved by using a beam expanding telescope to change the diameter of the beam before it impinges on a suitable plano-convex lens. If this were used in-conjunction with a galvanometer mirror, then it would be possible to easily vary the TLPG period.

The control of the rotation stages and laser is currently under manual control, migrating to a fully automated control system would both improve process repeatability especially when attempting shorter period gratings.

Once items (i-v) have been implemented, experimental design techniques could be used to efficiently explore the optimal parameters for TLPG fabrication. Process parameters which require detailed investigation are:

i. Laser power/time span/spot size if index modulated LPGs are being investigated
ii. Laser power/time span/spot size/taper geometry and fibre tension if TLPGs are being investigated.

Future work should also concentrate on improving the repeatability of the fabrication system in terms of period spacing and duty-cycle. The optical performance of the gratings produced was found to be strongly influenced by the combination of the specific geometry of the tapers and the laser pulse characteristics used. More work should be undertaken on these fundamental aspects to further optimize the optical performance.

8.3 References

[1] T. A. Birks and Y. W. Li, “The shape of fiber tapers,” *J. Light. Technol.*, vol. 10, no. 4, pp. 432–438, Apr. 1992.

[2] A. S. Paterno, R. Kremer, D. S. Matos, R. Zolet, A. Felipe, and H. J. Kalinowski, “Asymmetric fiber tapers fabricated with a pulsed CO2 laser,” *Proc. SPIE*, vol. 8794, no. 47, pp. 1–4, May 2013.

[3] R. K. Verma, A. K. Sharma, and B. D. Gupta, “Surface plasmon resonance based tapered fiber optic sensor with different taper profiles,” *Opt. Commun.*, vol. 281, no. 6, pp. 1486–1491, Mar. 2008.

[4] S. Pricking and H. Giessen, “Tailoring the soliton and supercontinuum dynamics by engineering the profile of tapered fibers.,” *Opt. Express*, vol. 18, no. 19, pp. 20151–20163, 2010.

[5] S. Pricking and H. Giessen, “Tapering fibers with complex shape.,” *Opt. Express*, vol. 18, no. 4, pp. 3426–37, Feb. 2010.

[6] S. W. Harun, K. S. Lim, C. K. Tio, K. Dimyati and H. Ahmad, “Theoretical analysis and fabrication of tapered fiber,” *Opt. - Int. J. Light Electron Opt.*, Vol. 124, No. 6, pp. 538–543, 2012.

[7] V. Grubsky and J. Feinberg, “Fabrication of Axially Symmetric Long-Period Gratings with a Carbon Dioxide Laser,” *IEEE Photonics Technol. Lett.*, Vol. 18, No. 21, pp. 2296–2298, 2006.

List of publications

Peer – reviewed journals

1. K. Mullaney, R. Correia, S. Staines, S.W. James and R. P. Tatam, "Monitoring techniques for the manufacture of tapered optical fibres", *Applied Optics*, 54(28): 8531-8536, 2015**.**

2. A. Urrutia, K. Bojan, L. Marques, K. Mullaney, J. Goicoechea, S. James, M. Clark, R. Tatam and S. Korposh, "Novel highly sensitive protein sensors based on tapered fibres modified with Au-based nano-coatings", *Journal of Sensors*, Volume 2016, 2016.

3. D. Tiwari, K. Mullaney, S. Korposh, S. W. James, S.-W. Lee and R. P. Tatam, "An ammonia sensor based on lossy mode resonances on a tapered optical fibre coated with porphyrin-incorporated titanium dioxide", *Sensors & Actuators: B. Chemical, submitted.*

Conferences

1. K. Mullaney, "The development of a CO_2 laser based system for the fabrication of tapered optical fibres", Oral presentation at the *Student conference on Photonic Technologies*, Birmingham, U.K., 2013.

2. D. Tiwari, K. Mullaney, S. Korposh, S. W. James, S.-W. Lee and R. P. Tatam, "Ammonia sensing using lossy mode resonances in a tapered optical fibre coated with porphyrin-incorporated titanium dioxide", *Sixth European Workshop on Optical Fibre Sensors (EWOFS 2016),* Limerick, Ireland, 2016.

APPENDICES

Appendix A CO_2 Laser controller LabVIEW code.

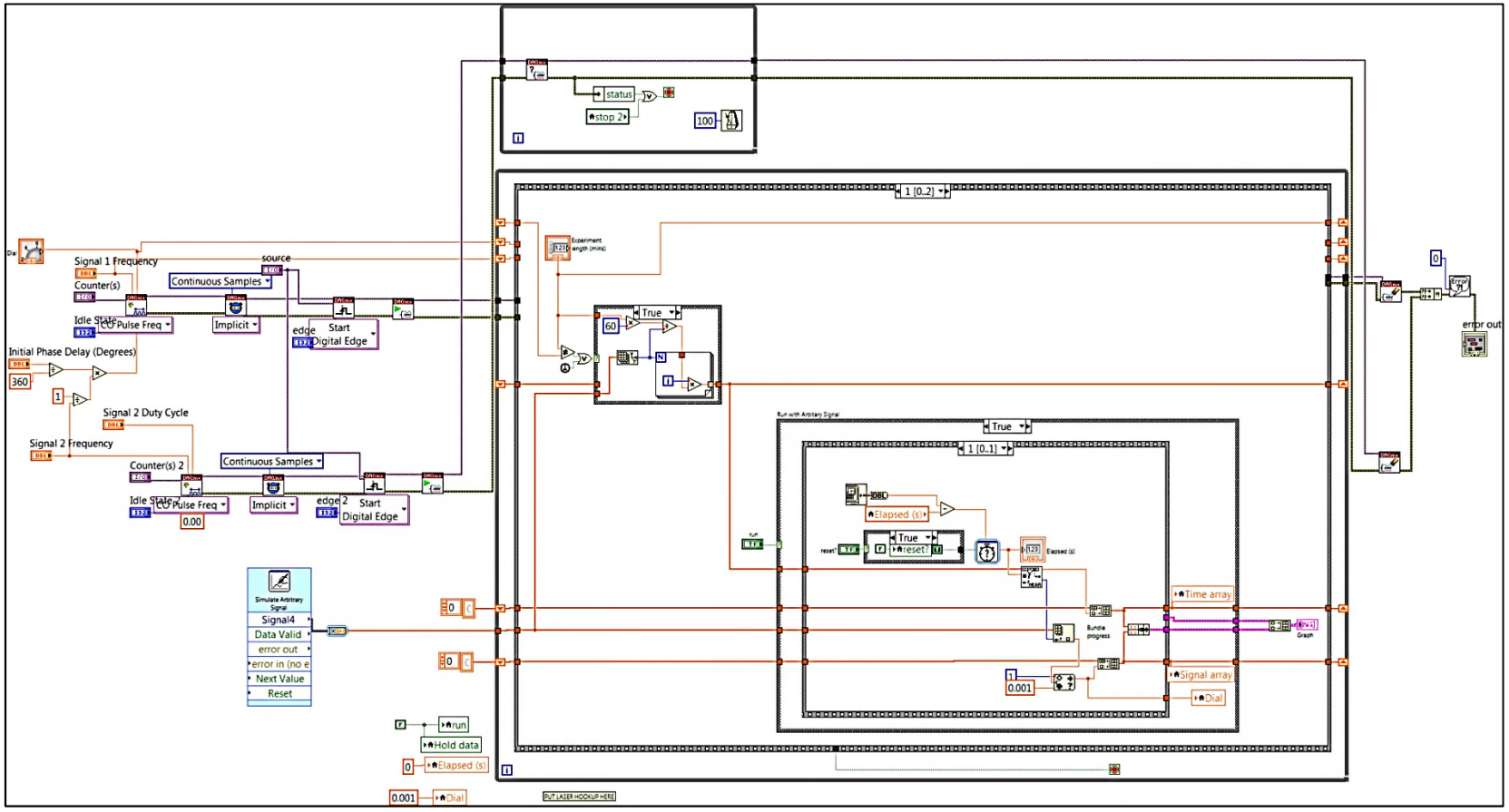

Appendix B Galvanometer mirror controller LabVIEW code.

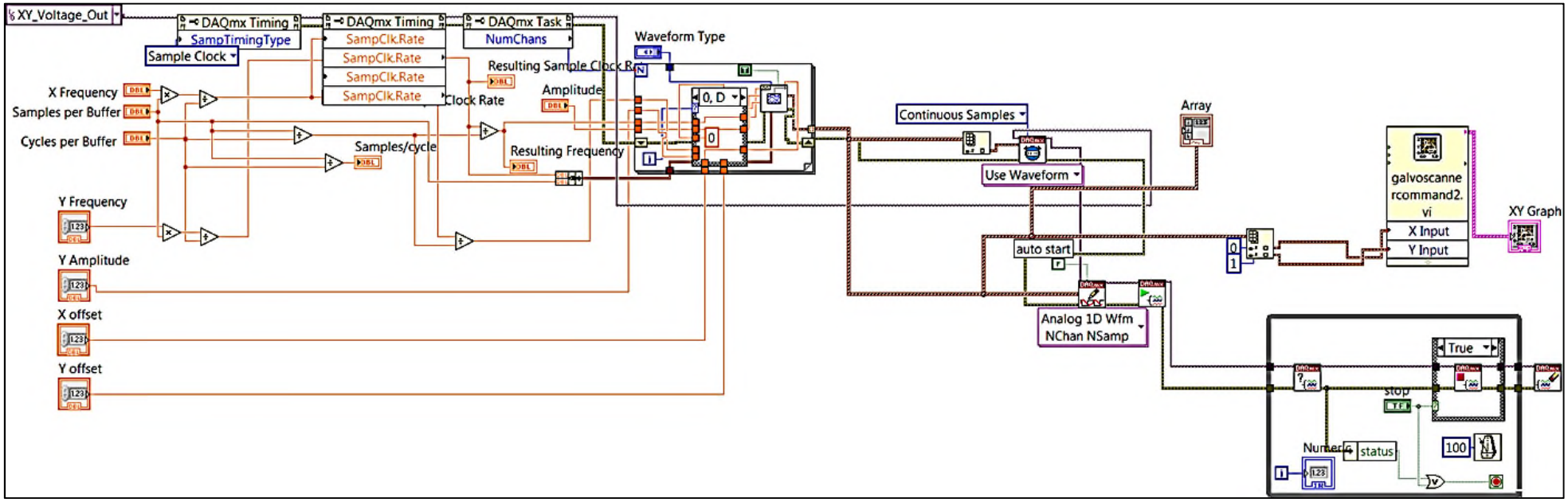

Appendix C Taper rig alignment process

C.1 Introduction

This appendix describes the process of aligning the components of the taper rig. This sequence should be followed if any of the components are removed and replaced.

The CO_2 laser used in this equipment is a Class 4 laser, therefore applicable departmental procedures should be adhered to when working on the CO_2 and the HeNe alignment lasers.

C.2 Alignment steps

The process for aligning the components illustrated in figure 99 is given below:

i. The CO_2 laser is secured to the optical table and adjusted so that it is horizontal in the x and z planes using a spirit level.

ii. The galvanometer mirror assembly is mounted such that it is horizontal in the x and z planes and the HeNe beam is incident on the centre-line of the mirror as specified by the mirror engineering drawing (Ref. D05616 – Rev A). The distance from the laser output window to the mirror rotation axis is > 300 mm.

iii. The HeNe laser spot is projected onto a paper screen 2.0 m from the nominal lens position.

iv. The HeNe laser spot centre on the screen was marked with a pencil and a “light brown spot” was then burnt on the paper screen with the CO_2 laser at a duty cycle of ~ 15 %. The HeNe laser screw fixings on the combiner are then adjusted until the HeNe spot and the CO_2 burn spots perfectly overlap. Care should be taken to ensure this is achieved.

v. The scanning mirror is then activated with a triangular waveform at 100 Hz and an asymmetric burn pattern may be observed on the paper screen. This typically appears as a variation in the intensity of the “light brown” burn pattern. Some experimentation may be required to fine tune the laser duty cycle so maximum colouration contrast is achieved.

vi. The scanning mirror is then adjusted along the z- axis using the micrometer adjustment until the CO_2 beam impinges exactly on the axis of rotation of the mirror this will produces a symmetric burn profile on the paper. The micrometer should be adjusted in 100 µm intervals when undertaking this adjustment.

vii. The adjustable fibre stage is then located in position and adjusted and fixed until it is level in the x and z planes and perpendicular to the laser beam axis.

viii. A stripped, cleaned fibre is then attached to the stage using “Magic tape” and the height adjusted in the y-plane so a HeNe laser diffraction pattern is observed ***above and below*** the fibre. The mirror is stationary during this step.

ix. The 100 mm focal length ZnSe lens is then inserted between the galvanometer mirror and the fibre such that it was 108 mm from the fibre. This latter dimension is the effective focal length of the lens. The distance from the exit aperture of the laser to the lens location must be in excess of 0.6 m.

x. The lens mount upper surface is adjusted in the z and x planes using a spirit level to ensure the mount was parallel to the surface of the optical table.

xi. With the galvanometer mirror scanning a distance of 10 mm along the fibre using the triangular 100 Hz waveform, the lens height is then adjusted until a uniform rectangular diffraction is observed above and below the fibre using the HeNe laser. The lens was then rotated about its optical axis (z) until an equal diffraction pattern was observed above and below the fibre. This will appear as a symmetric rectangular band above and below the fibre plane with a uniform brightness. Care will be required to achieve this, as it is a fine adjustment.

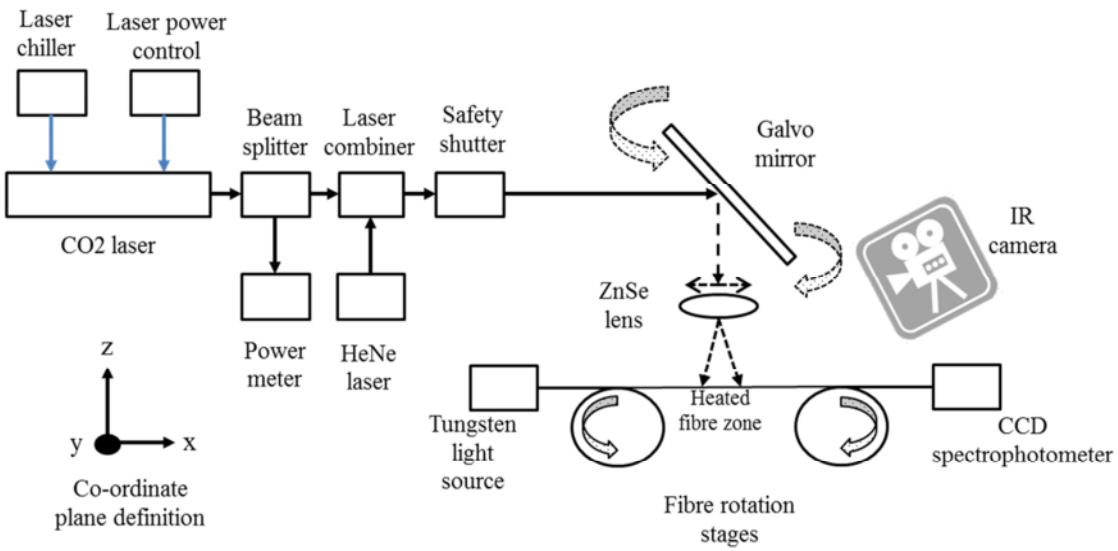

Figure 99: Experimental layout of taper rig.

Appendix D Process for fabricating single tapers.

D.1 Introduction

This appendix describes the process for fabricating single tapers in optical fibres with an unjacketed diameter of ~ 125 μm. It assumes the taper rig has been in aligned in accordance with appendix C - Taper rig alignment process.

The CO_2 laser used in this equipment is a Class 4 laser therefore applicable departmental procedures should be adhered to when working on the CO_2 and the HeNe alignment lasers.

It assumes that the operator has a knowledge of: LabVIEW, PIMikroMove software, Acquire camera control software and the software interface to operate the Ocean Optics spectrophotometer.

Using the parameters stated in this appendix, tapers down to 5 μm waist diameters can be made with various taper lengths depending on the application.

D.1.1 Equipment switch on

1. Switch on the laser water chiller. Ensure the chiller temperature is set to 18 ^{0}C.
2. Allow the chiller to function for one hour, prior to powering the Synrad 48-2 CO_2 laser.
3. Switch on the power supply for the laser. Then reset/switch the keylock on the laser so the green LED is illuminated. The red LED should not be illuminated at this stage.
4. Switch on the power supply for the laser shutter and the room warning signage. Ensure off lights are activated.

5. Switch on the power supply for the mirror scanner and the NIR camera. Ensure indicator lights illuminate on the power supply and the camera head.

6. Switch on the Ocean optics spectrophotometer, if it is required to monitor fibre transmission properties during the tapering process.

7. Ensure the personal computer is switched on.

D.1.2 Software Parameter Entry

Ensure the following programs on the computer are running:

- LabVIEW laser controller.
- Galvonometer mirror controller.
- NIR camera, Acquire control software.
- Spectrophotometer, Ocean optics software.
- PIMikromove software.

Laser controller.

The laser controller GUI is shown in figure 100. The laser power, as a function of time, is fully programmable from this interface. The meaning of the various parameter fields numbered L1 to L9 is detailed below.

L1: Once the LabVIEW program has been started, pressing "**start"** powers and sends the required driving signals to the laser.

L2: If pause is pressed, the automatic ramping function of the program is disabled and the laser operates continously at its current settings.

L3: If "stop" is pressed then all driving signals to the laser are reset to zero and the laser is switched off.

L4: Convert the programmed ramp total length in seconds to minutes and enter the value into this field.

L5: The length of time in minutes that the laser will be powered, should be inserted in here.

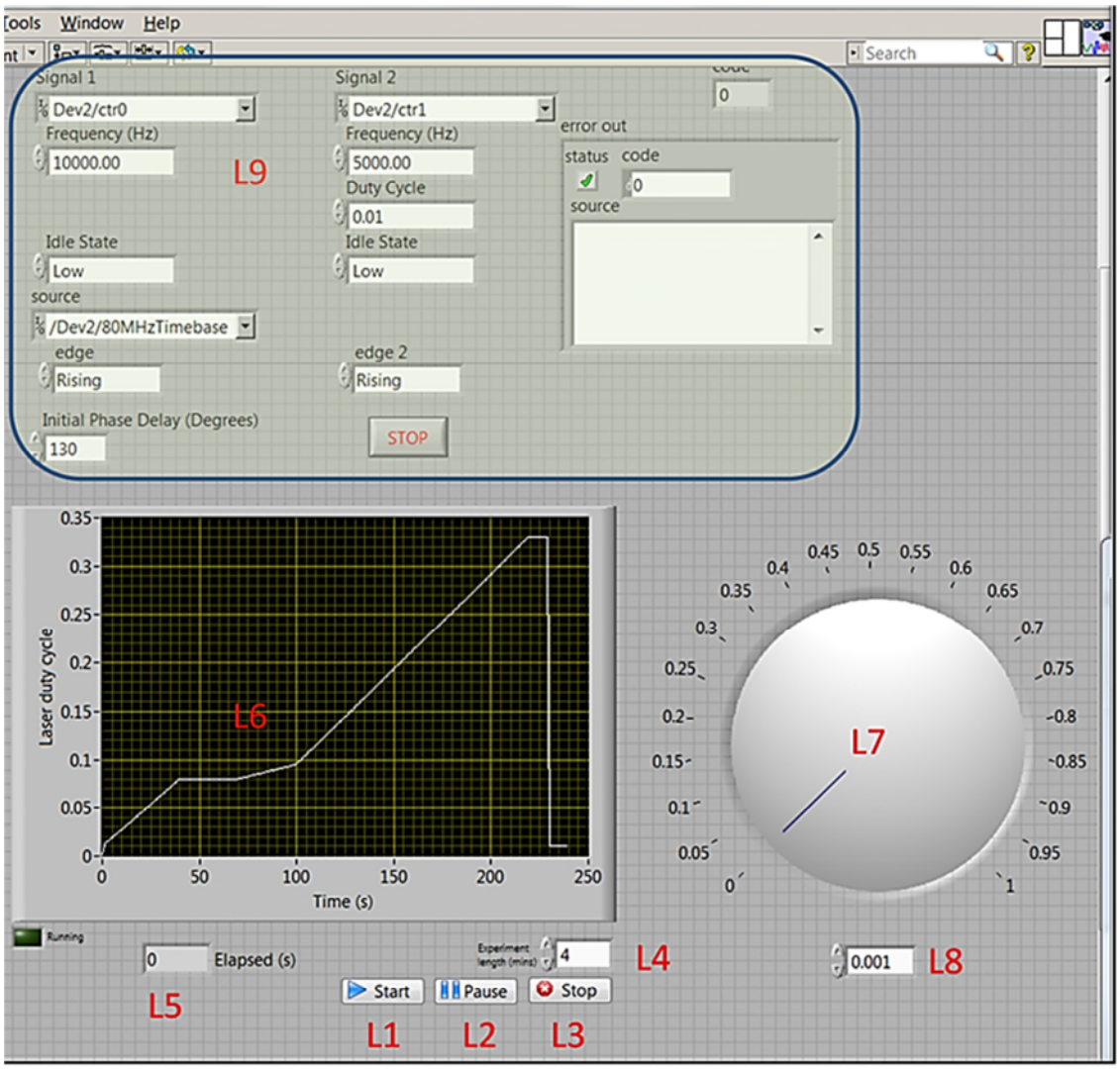

Figure 100: User interface for the CO_2 laser controller. L1 to L9 are parameter fields which allows the laser to be programmed to have specific characteristics.

L6: This display shows the programmed laser duty cycle as a function of time. When the “start” button is pressed, a red line progresses along the white line and indicates the specific duty cycle at a specific time.

Any duty cycle profile can be programmed using the “simulate arbitrary waveform function”. This function can be changed by clicking on this function in the “LabVIEW wiring diagram” and following the prompted instructions.

L7: This control knob becomes usable once the pause button is activated. It allows the laser duty cycle to be manually varied from zero to 100 %. This feature is used when initially identifying the optimum ramp profile for a specific taper geometry.

L8: This display indicates the current laser duty cycle as a digital value.

L9: The grey call-out box, defines the “tickle” and PWM driving frequencies, repetition rates and phase separation. These parameters were selected when the laser parameters were initially established, ***under normal circumstances these values do not need to be changed.***

Galvonometer mirror controller

The galvanometer mirror GUI is shown in figure 101. The mirror motion is fully programmable from this interface. The significance of the various parameter fields numbered G1 to G6 is detailed below.

G1: This parameter defines the rotational amplitude of the galvanometer mirror. A value of 700 equates to a scan distance along the fibre of 8 mm. A value of 388 equates to a scan distance along the fibre of 4.5 mm. (These parameters are typically entered as 0.7 or 0.388).

G2: This parameter defines the scanning frequency in Hz, a typical value is 100 Hz. This value should not be changed for the current taper processes.

G3: This parameter allows the user to translate the centre-point of the mirror motion along the fibre if required. Currently, the default value is zero.

G4: This parameter does not need to be adjusted.

G5: Defines the waveform type. The default is triangular, other options are square, saw-tooth and sinusoidal. Triangular should be used for exponential taper transition zones.

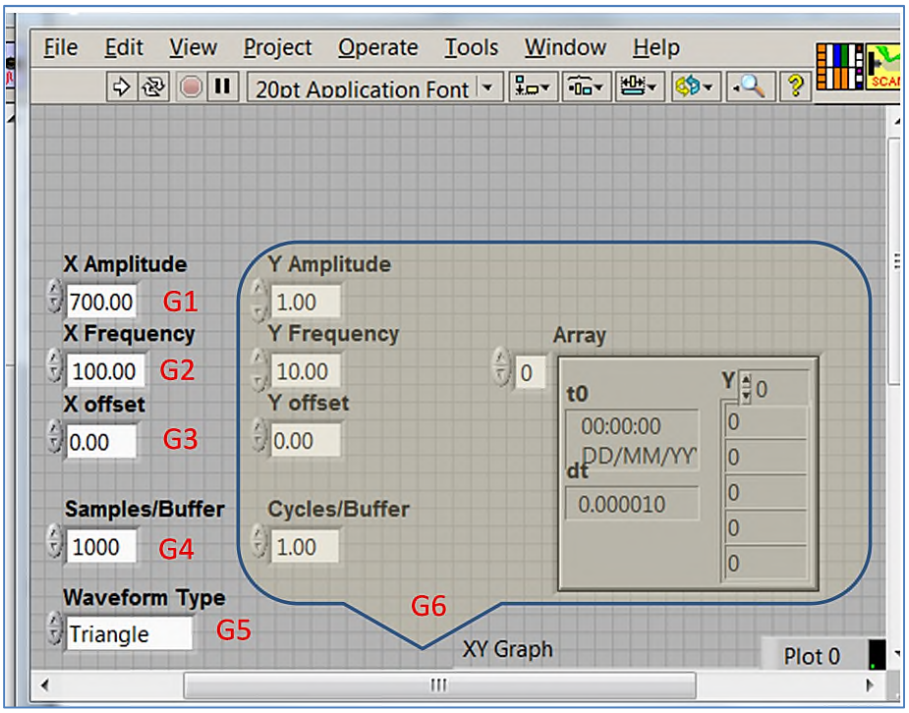

Figure 101: GUI for the galvonometer mirror controller. G1- G6 are parameter fields which allows the galvanometer to be programmed to have specific characteristics.

G6: These parameter fields can be used if a second mirror is used with the system, at present these are not used.

PIMikromove software.

The rotation stages GUI is shown in figure 102. The left and right rotational stage motion is fully programmable from this interface. The significance of the various parameter fields numbered P1 to P7 is detailed below:

P1/P2: Reference the left and right rotation stages respectively. M-060.DG is the stage reference number.

P3: “Target” is where the stage is being programmed ***to move to***.

P4: “Position” is the current position.

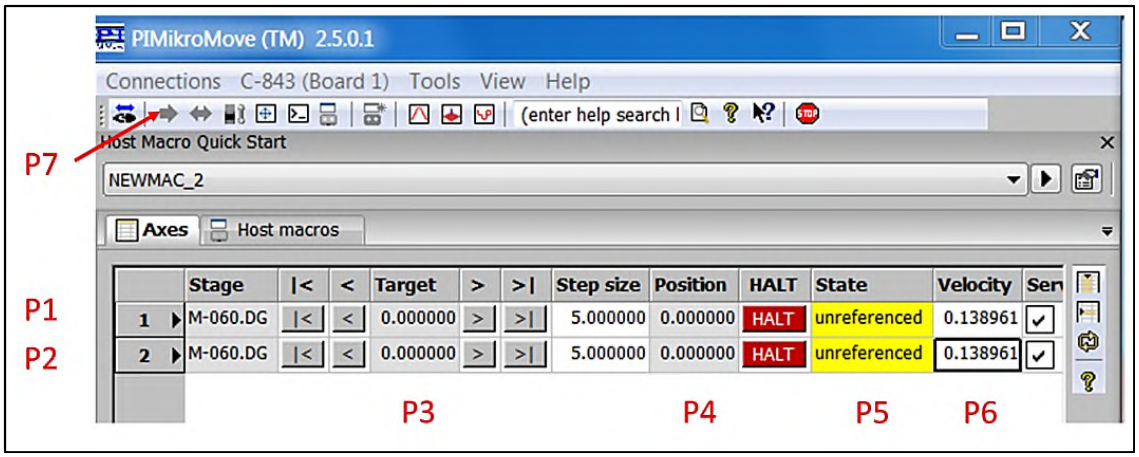

Figure 102: Main User interface for the PIMikroMove rotation stages. P1 to P7 are parameter fields which allows the rotation stages to be programmed to have specific characteristics.

P5: “State” indicates whether the stages have been base- lined.

P6: “Velocity” this allows the relative velocity to be specified. The value 0.138961, is equivalent to a tangential velocity of 0.06089 mm s^{-1} for the individual stages being used. ***This currently the default value for the stage velocity for tapering processes and should not be changed.***

P7: Click on this icon to start the stages in motion.

P8: Before the stages can be used they need to be referenced to a datum start point.

In figure 102 they are unreferenced, so they are referenced to a start point. This is achieved by right clicking on either the stage references in figure 102, this will bring up the command box in figure 103. Click on “automatic” P8 in the text box, and the stages will move to the reference datum point of zero. When this occurs the stage status will change from unreferenced to “on target” see figure 104.

P9/P10: To move the stages in a specific direction then press P7, this will bring up the text box below in figure 104. If “- 45” is inserted in the left stage 1, then the stage will rotate 45 degrees in an ***anticlockwise direction***. If 45 is inserted in the right stage 2, then the stage will rotate 45 degrees in a ***clockwise direction***. These values are the current parameter settings for making single tapers.

P11: Pressing the “start” box in figure 104, will start both stages rotating in opposite directions to position -45 and 45 at velocities of 0.06089 mm s^{-1}.

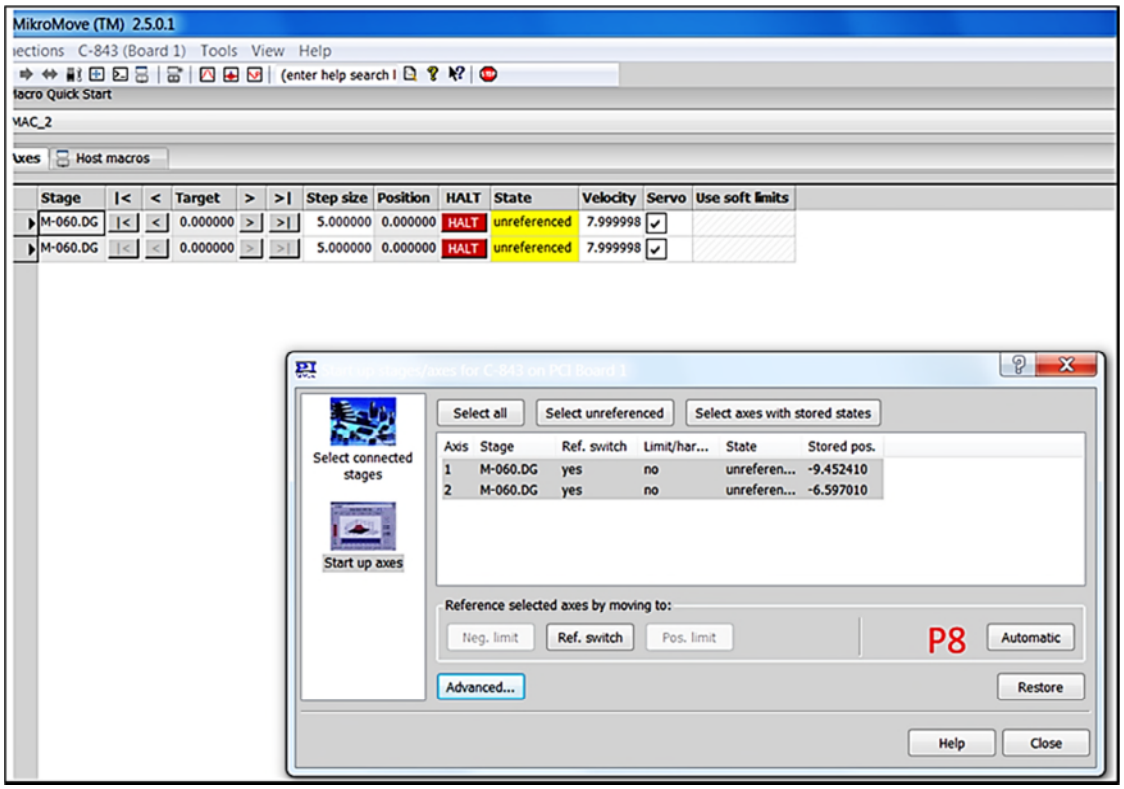

Figure 103: User interface for base lining or referencing the stages before use. P8 shows the location of the automatic button.

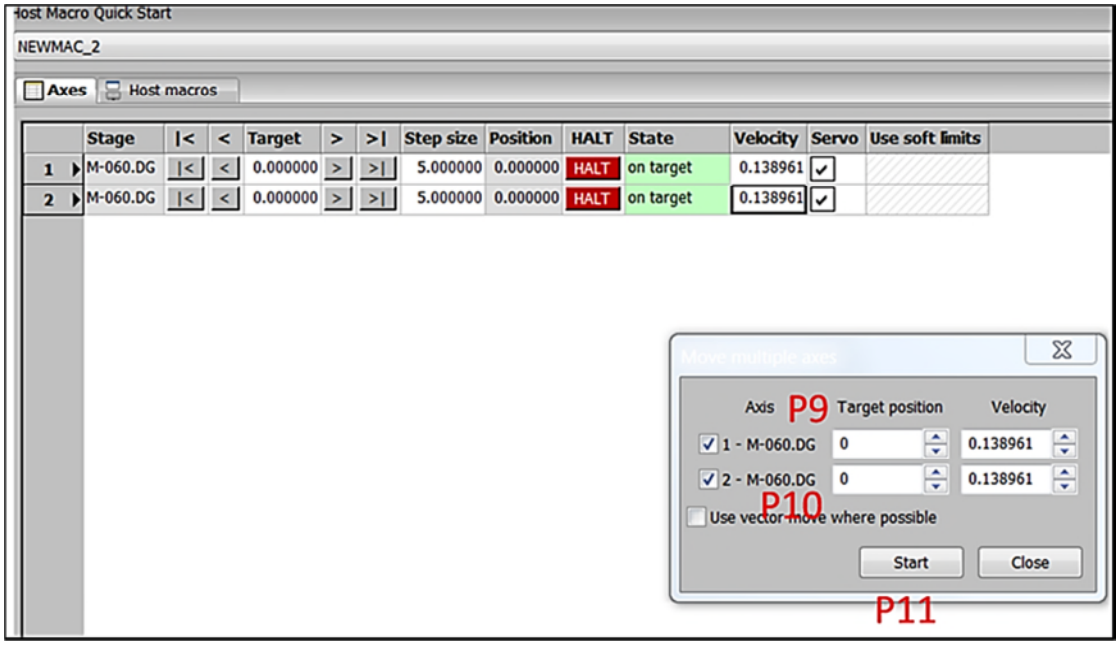

Figure 104: User interface for programming the stages and starting rotational motion. P9 – P11 indicate the locations of the fields/buttons which need to be used.

D.2 Fibre preparation and mounting

a. Cut the fibre to length, ensuring its unjacketed diameter is ~ 124 microns.
b. Cleave both ends, ensure light transmission is acceptable using Ocean Optics spectrophotometer.
c. Using fibre strippers, remove a section (~ 20 mm) of fibre jacket in the centre of the length of fibre.
d. Clean the fibre section to be tapered with fresh “Texwipe” tissue soaked in fresh Isopropyl alcohol.
e. Using one fresh tissue per wipe, clean at least five times. Inspect under 20X magnification to ensure stripped fibre is defect free.
f. Hang the fibre in a location so the taper is not contaminated with dust, prior to mounting on the stages.

D.3 Taper process

a. Switch on equipment and programs as defined in section D.1.
b. Depending on the shape of tapers required the following parameters are entered into the mirror controller and the laser controller:
   - For long thin tapers use: 700 scan, “signal 3” power profile.
   - Short thin tapers use: 388 scan, “signal 4” power profile.
c. Ensure the v-grooves on the stage faces are cleaned with alcohol/tissue where the fibre is to be placed.
d. Ensure the stages are referenced and are on target, see P8 in section D1.
e. Cut two 15 mm pieces of “Magic tape” and place temporarily on the top surface of the two stages.
f. Place one end of the fibre in the left hand stage v-groove, locate in position and fix with one piece of magic tape. Do not roll the fibre when attaching tape as this induces rotational stress into it. Applying very slight tension and not rotating fibre, locate in right hand v-groove, and attach with tape.
g. If required fix fibre connectors and attach the two free fibre ends to a tungsten light source and Ocean Optics spectrophotometer to measure fibre transmission.
h. Ensure the fibre is visible in the NIR camera.
i. Switch off the air-conditioning to the clean room.
j. Turn of the room lights.
k. Switch on the laser by switching on the laser LabVIEW program.
l. Ensure the laser green LED light is illuminated and the red LED is faintly illuminated. (The red light gets progressively brighter as the duty cycle increases to ~ 95%.
m. Open the laser safety shutter.
n. Press “start” on the laser controller.
o. At 50 s, adjust the micrometer on the stage mount for maximum camera brightness.
p. At 102 s elapsed time, press “start” on the stages command box, to start pulling the fibre.
q. After for example 170 s elapsed time, stop the stages.
r. Press stop on the laser controller within a few seconds of stopping the stages.

s. Close the laser safety shutter.
t. Turn on the room lights.
u. Switch the air-conditioning back on.
v. Generate a calibration curve of taper waist diameter versus process pulling time to determine required pull time for a specific target waist diameter. An exponential function can be used to generate the calibration curve to fit to the data points.

D.4 Fibre removal

a. Supporting the right hand fibre, remove the magic tape, ensuring no strain is placed on the taper, ***otherwise it will break***. Repeat for the left hand fibre and remove.
b. With the tapered fibre hanging vertically downwards place the fibre in a suitable holder to support it.

D.5 Equipment switch off

a. Switch off all equipment.
b. Ensure all lasers are switched off.

Appendix E Process for fabricating tapered long period gratings.

E.1 Introduction

This appendix describes the process for fabricating tapered long period Bragg gratings (TLPGs) in SM750 optical fibre with an unjacketed diameter of ~ 124 μm. It assumes the taper rig has been in aligned in accordance with appendix C. When fabricating TLPGs the taper rig is configured differently as described below:

a. The ZnSe cylindrical lens should be rotated in the lens holder by 90^0 to produce a narrow focussed spot perpendicular to the plane of the fibre.
b. The rotation stages are mounted on an L-shaped bracket such that they rotate about the z-axis (see figure 105).

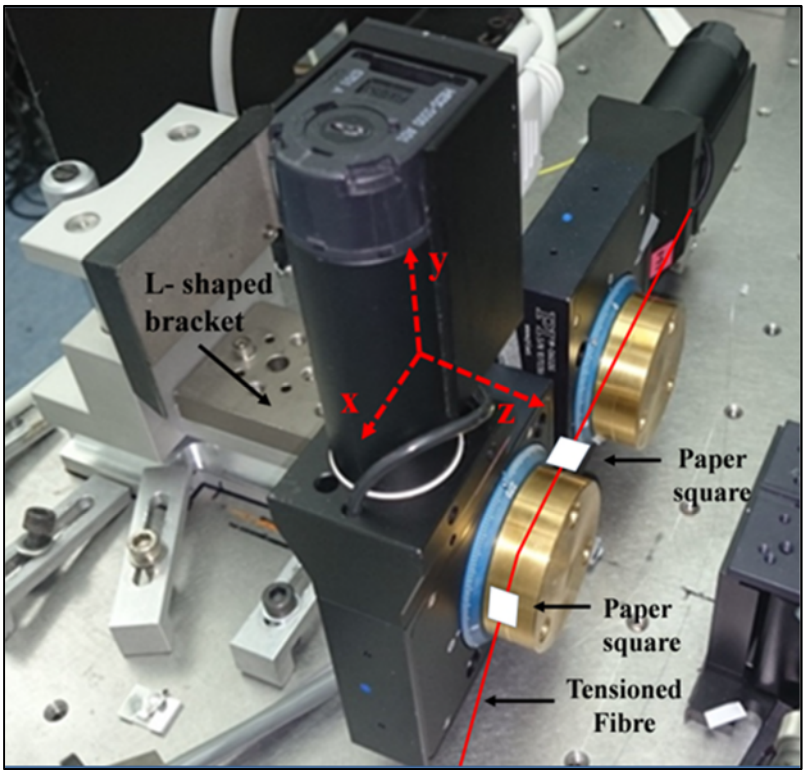

Figure 105: Physical orientation of the rotation stages when fabricating TLPGs.

The CO_2 laser used in this equipment is a Class 4 laser therefore applicable departmental procedures should be adhered to when working on the CO_2 and the HeNe alignment laser.

This appendix assumes that the operator has a working knowledge of: LabVIEW, PIMikroMove software and the software interface to operate the Ocean Optics spectrophotometer.

Using the parameters given in this appendix, TLPGs with a grating period of 400 μm and up to 30 periods can be fabricated depending on the application.

E.1.1 Equipment switch on

i. Switch on the laser water chiller. Ensure the chiller temperature is set to 18.0 ^{0}C.

ii. Allow the chiller to function for one hour, prior to powering the Synrad 48-2 laser.

iii. Switch on the power supply for the laser. Then reset/switch the keylock on the laser so the green LED is illuminated. The red LED should not be illuminated at this stage.

iv. Switch on the power supply for the laser shutter and the room warning signage. Ensure off lights are activated.

v. Switch on the power supply for the NIR camera. Confirm status lights illuminate on the power supply and the camera head.

vi. Switch on the Ocean optics spectrophotometer to monitor fibre transmission properties during the TLPG process.

vii. Switch on the personal computer.

E.1.2 Software Parameter Entry

Ensure the following programs on the computer are activated:

- LabVIEW laser controller.
- NIR camera, (Acquire control software).
- Spectrophotometer (Ocean optics software).
- Rotation stages (PIMikromove software).

LabVIEW laser controller

The laser controller graphical user interface (GUI) is shown in figure 106. The laser power as a function of time is programmable using this interface. The definition of the various parameter fields numbered L1 to L9 is detailed below.

L1: Once the program has been activated, pressing "**start",** powers and sends the required driving signals to the laser.

L2: If "**pause**" is pressed, the automatic ramping function of the program is disabled and the laser maintains its current settings.

L3: If "**stop**" is pressed, then driving signals to the laser are reset to zero and the laser is switched off.

L4: The programmed ramp total time in minutes is entered into this field.

L5: Once the **"start"** button has been pressed, this display indicates the length of time in seconds that the laser has been functioning.

L6: This display shows the programmed laser duty cycle as a function of elapsed time.

Any duty cycle profile can be programmed using the "simulate arbitrary waveform function". This function can be changed by clicking on this function in the "LabVIEW wiring diagram" and following the prompted instructions. Once the "start" button is pressed, a red line progresses along the white line and indicates the specific duty cycle value at a specific time.

L7: This control knob becomes activated once the paused button is activated. It allows the laser duty cycle to be manually varied from zero to 100 %. This feature is used when identifying the optimum ramp profile for a specific taper geometry.

L8: This display indicates the current laser duty cycle as a digital value.

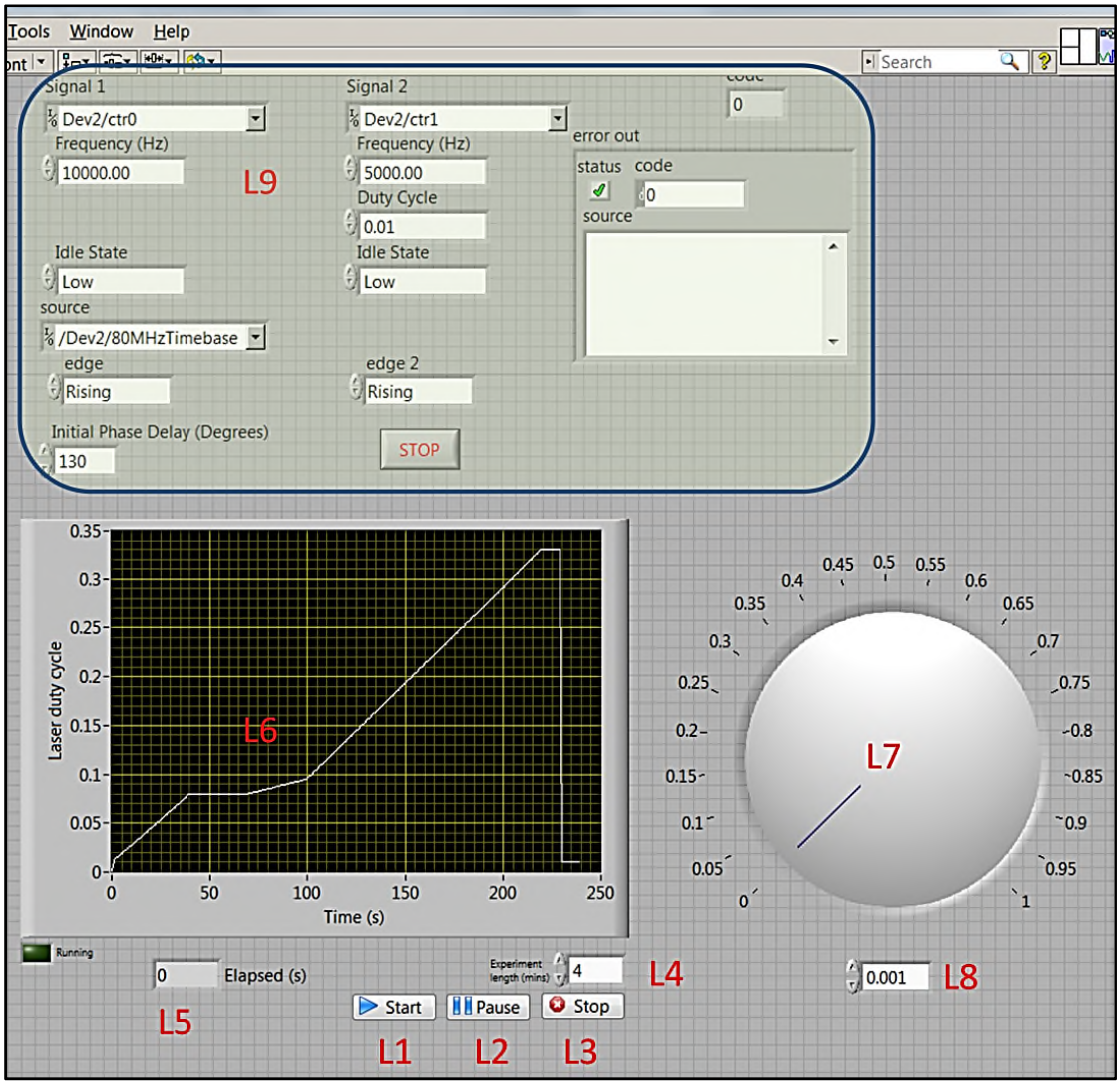

Figure 106: GUI for the CO_2 laser controller. L1 to L9 are parameter fields which allows the laser to be programmed to have specific characteristics.

L9: The light grey call-out box in figure 106, defines the “tickle” and PWM driving frequencies, duty-cycle and phase separation. These parameters were selected when the

laser was initially set-up, ***under normal circumstances these values do not need to be changed.***

Galvonometer mirror controller

The galvanometer mirror controller GUI is shown in figure 107. The mirror motion is fully programmable using this interface. The definition of the various parameter fields numbered G1 to G6 is detailed below.

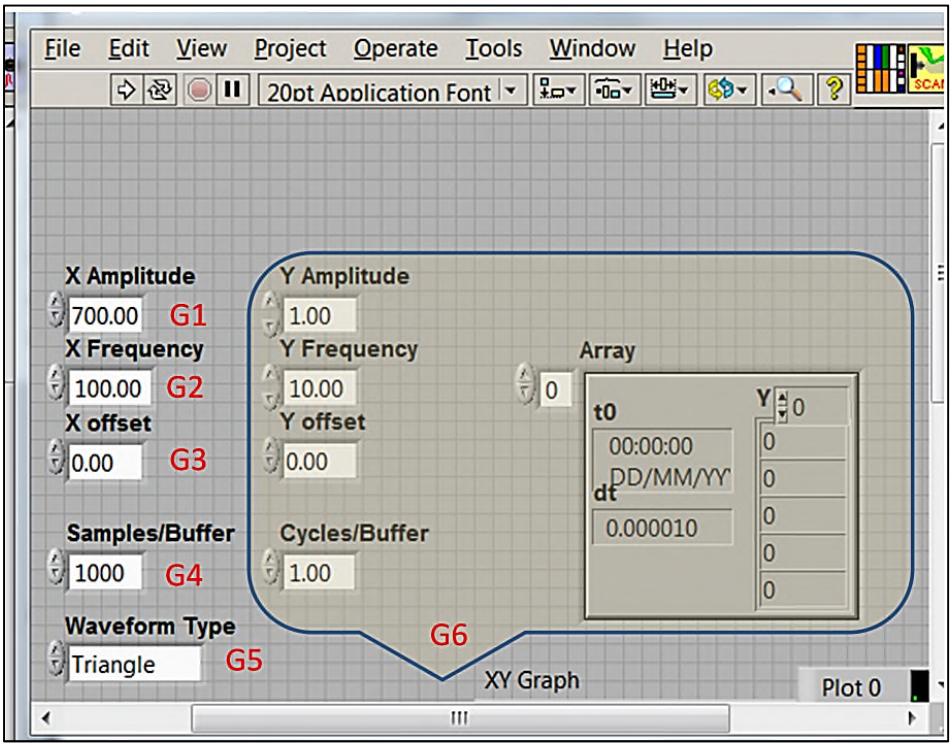

Figure 107: User interface for the galvo-nometer mirror controller. G1- G6 are parameter fields which allows the galvanometer to be programmed to have specific characteristics.

G1: This parameter defines the scanning amplitude of the galvanometer mirror. A value of 700 equates to a scan distance along the fibre of 8 mm (these parameter is typically entered as 0.7). When producing micro-tapers for TLPGs, no scan is used, and 0.00 is entered as the scan distance.

G2: This parameter defines the scanning frequency in Hz, a typical value is 100 Hz. This value should not be changed.

G3: This parameter allows the user to translate the centre-point of the mirror motion up and down the fibre if required. The default value is zero.

G4: This parameter should not be changed.

G5: Defines the scanning waveform type. The default is triangular; other options are square, saw-tooth and sinusoidal waveforms.

G6: These parameter fields can be used if a second mirror is used with the system.

Stage control software.

The rotation stages GUI is shown in figure 108. The left and right rotational stage motion is fully programmable from this interface. The definition of the parameter fields numbered P1 to P7 is detailed below:

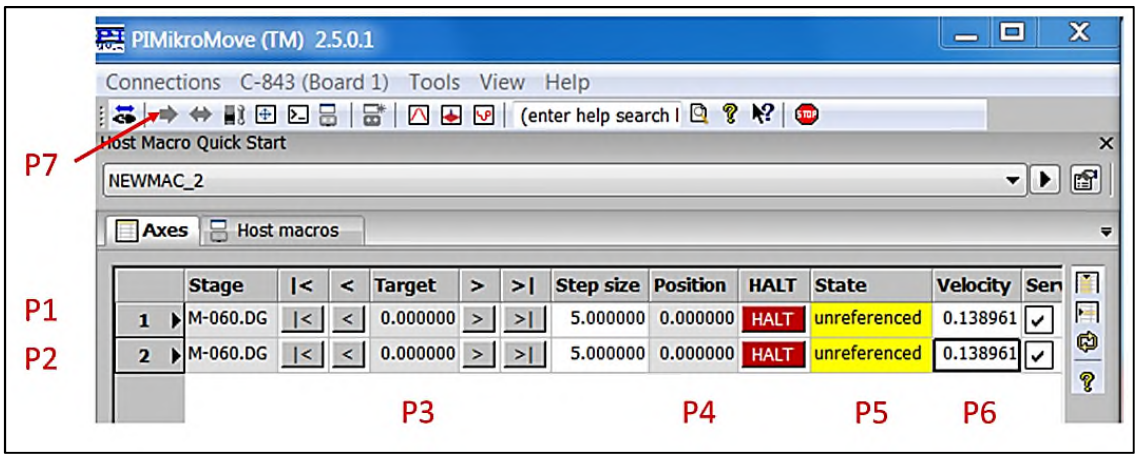

Figure 108: User interface for the PIMikroMove rotation stages. P1 to P7 are parameter fields which allows the rotation stages to be programmed to have specific characteristics.

P1/P2: Reference the left and right rotation stages respectively. M-060.DG is the stage reference number.

P3: “**Target”** is where the stage is being programmed ***to move to***.

P4: “**Position”** is the current stage position.

P5: “**State”** indicates if the stages have been base-lined.

P6: “**Velocity**” allows the stage relative velocity to be defined. A value of 0.0138961 is equivalent to a tangential velocity of 0.006089 mm s^{-1} for each individual stage. ***This currently the default value for the stage velocity for micro-tapering processes and should not be changed.***

P7: This icon is pressed to start the stages rotating.

P8: Before the stages are used, they are referenced to a start point.

In figure 109 the stages are unreferenced, This is achieved by right clicking on either the stage references in figure 109, this will bring up the command box in figure 109 below. Click on the “**automatic**” P8 in the text box, and the stages will move to the reference datum point of zero. When this occurs the stage status will change from “unreferenced” to “on target”, see figure 110.

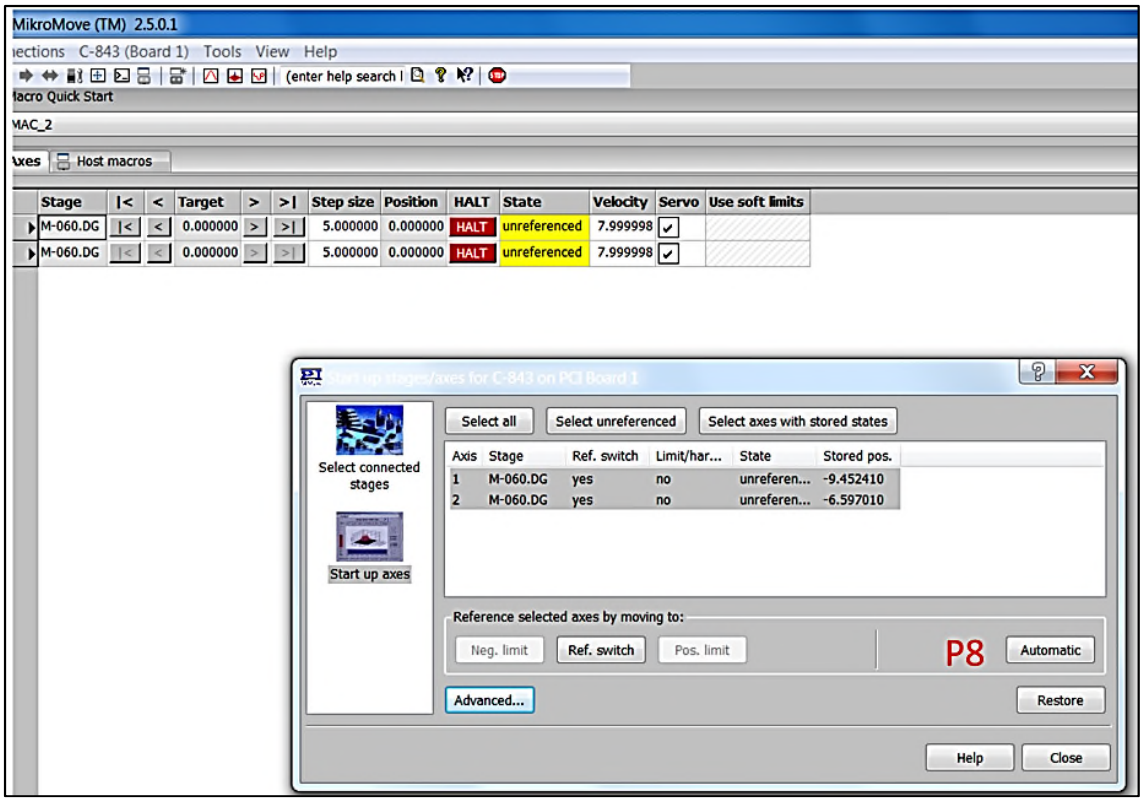

Figure 109**:** User interface for referencing the stages before use. P8 shows the location of the automatic button.

P9/P10: To move the stages in a specific direction then press P9 (figure 110). If "- 45" is inserted in the left stage 1, then the stage will rotate 45 degrees in an ***anticlockwise direction***. If 45 is inserted in the right stage 2, then the stage will rotate 45 degrees in a ***clockwise direction***. These values are the current parameter settings for making micro-tapers.

P11: Pressing the "start" box in figure 110, will start both stages rotating in opposite directions to position -45 and 45 at a velocity of 0.006089 mm s^{-1}.

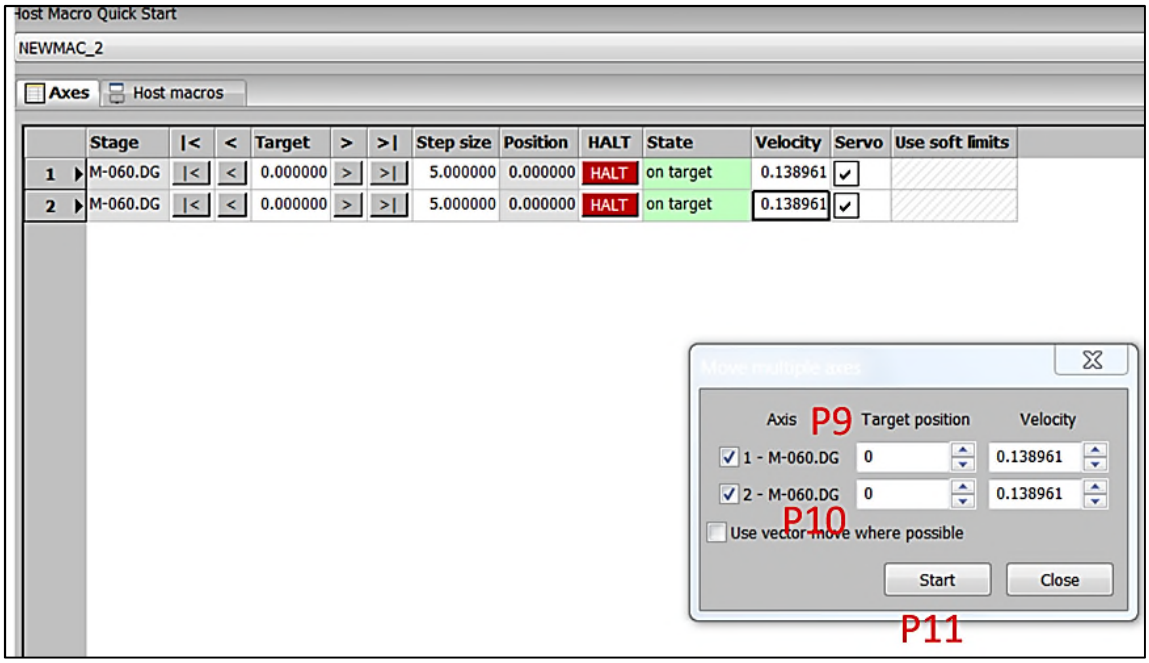

Figure 110: GUI for programming the stages and starting rotational motion. P9 – P11 indicate the locations of the fields/buttons which need to be activated.

E.2 Fibre preparation and mounting.

a. Cut the fibre to length, and ensure its unjacketed diameter is ~ 124 microns.
b. Cut and cleave both ends and ensure light transmission is acceptable using the Ocean Optics spectrophotometer.
c. Using fibre strippers, remove a section (~ 10 mm) of fibre jacket in the centre of the length of fibre.
d. Clean the section to be micro-tapered with new “Texwipe” tissue soaked in fresh Isopropyl alcohol (old alcohol can become contaminated with water which will then contaminate the fibre surface).
e. Using one fresh tissue per wipe, wipe at least five times. Inspect under 20X magnification to ensure the fibre is defect free.
f. Hang fibre from a vertical clean surface, fixing tape above the exposed section, ensuring the fibre hangs freely down.

g. Attach a small piece of square card (8x3 mm) to the fibre with magic tape, on the jacket below the region which has been stripped, ensure its flat.
h. Repeat (g) above , but ~ 250 mm below the first card.
i. Ensure both cards are in same plane, when the fibre is free hanging.
j. Lay fibre across stages ***unstressed***, ensuring first card is just after the right hand stage – the card must be planar to the table (figure 105).
k. Use 2 “post-it notes” to temporarily locate the left hand fibre side, then use “Magic tape” to fix the fibre into the left hand v-groove.
l. Remove “post-it notes”.
m. Locate fibre in right hand v-groove. Ensure the fibre is not twisted by observing the cards relative orientation.
n. Attach the ~ 6 g weight with tape to the free hanging end of the fibre.
o. Ensure both cards are in the same plane, correct if required.
p. Attach the fibre with “Magic tape”, ensure the tape is rubbed along the fibre axis, not across it.
q. Carefully remove the weight.
r. Attach fibre connectors and confirm the fibre transmission is satisfactory.

E.3 Taper process

a. When making micro-tapers the following parameters are entered into the laser controller and the mirror controller:
   “0.0” mirror scan, “signal 6” laser power profile (see figure 46), stage velocity “0.013896”.
b. Ensure the v-grooves on the stage faces are cleaned with alcohol/tissue where the fibre is to be placed.
c. Ensure the stages are referenced and are on target, see P8 in section E.1.
d. Mount fibre as detailed in the preceding section.
e. Switch on the laser by activating the laser LabVIEW program.

f. Ensure the laser green LED light is illuminated and the red LED is faintly illuminated. (The red LED gets progressively brighter as the duty cycle increases).

g. Open the laser safety shutter.

h. Press “start” on the laser ramper.

i. When 51 seconds is reached on the ramp profile, with -45, 45 programmed on the stages, start stretching the fibre. When 67 seconds is reached, stop the stages and record and input the stage 1 and stage 2 actual position values into the spreadsheet shown in figure 111.

	A	B	C	D	E	F	G	H	I	J
1								target taper length	0.477	
2								stage global offset	0.9	
3								stage local offset		
4										
5	TLPG Element no.	Stage 1 actual pos.	Stage 2 actual pos.	Stage 1, calc. new pos.	Stage 2, calc. new pos.	Cumulative difference	Element difference			Stage local offset
6	1			-1.377	-1.377	0	0	0	0.477	1.377
7	2			-1.377	-1.377	0	0	0	0.477	1.377
8	3			-1.377	-1.377	0	0	0	0.477	1.377
9	4			-1.377	-1.377	0	0	0	0.477	1.377
10	5			-1.377	-1.377	0	0	0	0.477	1.377
11	6					0				

Figure 111: Spreadsheet used to calculate stage positions when fabricating TLPGs.

j. These values are inserted into B6 and C6 of the spreadsheet. The spreadsheet then calculates the new stage starting positions for the next element (no. 2). These values are displayed in cells D6 and E6. This data is then entered in to the PIMikroMove parameter field (figure 110) and the stages both then move to the new starting position for element 2.

k. Repeat steps h to j , until the desired number of elements are fabricated. Figure 112 shows a typical example of the spreadsheet after 6 elements of the TLPG have been fabricated. This example had a period of 447 μm with an average micro-taper length of 190 μm.

l. Press stop on the laser controller after stopping the stages.

m. Close the laser safety shutter.

							target taper length	0.477	
							stage global offset	0.96	
							stage local offset		
Element	Stage 1 actual	Stage 2 actual	Stage 1 minus local offset	Stage 2 minus local offset	Cumulative difference	element difference			stage local offset
1	-0.237919	0.240834	-1.196166	-0.717413	-0.478753	-0.478753	0.478753	-0.001753	0.958247
2	-1.435046	-0.475596	-2.391349	-1.431899	-0.95945	-0.480697	0.480697	-0.003697	0.956303
3	-2.63023	-1.190083	-3.586533	-2.146386	-1.440147	-0.480697	0.480697	-0.003697	0.956303
4	-3.824927	-1.905177	-4.782324	-2.862574	-1.91975	-0.479603	0.479603	-0.002603	0.957397
5	-5.021204	-2.620635	-5.977385	-3.576816	-2.400569	-0.480819	0.480819	-0.003819	0.956181
6	-6.214323	-3.336944			-2.877379				

Figure 112: Completed spreadsheet, after 6 elements of a TLPG have been fabricated.

E.4 Fibre removal

a) Supporting the right hand fibre, remove the magic tape, ensuring no strain is placed on the TLPG. Repeat for the left hand fibre and remove.
b) With the TLPG hanging vertically, place the fibre in a suitable holder to support it.

E.5 Equipment switch-off

a) Switch off all equipment.
b) Ensure all lasers are switched off.